UNIVERSITÀ DEGLI STUDI DI PADOVA

Head Office: Università degli Studi di Padova

Department of Chemical Sciences

Ph.D. COURSE IN: SCIENCE ENGINEERING OF MATERIALS AND NANOSTRUCTURES
SERIES XXXV

PLASMA ELECTROLYTIC POLISHING AND VIBROTUMBLING AS INNOVATIVE SURFACE TREATMENTS FOR SUPERCONDUCTING RADIOFREQUENCY CAVITIES

Coordinator: Prof. Giovanni Mattei
Supervisor: Dott. Cristian Pira
Co-Supervisor: Prof. Davide De Salvador

Ph.D. student: Eduard Chyhyrynets

Acknowledgements

My PhD journey took place during a crucial period of my life, with all its ups and downs. Over the course of almost four years, a lot has changed, and practically all the consequences are still being felt.

Trust and belief in my ideas were the most valuable things that I had the luck to obtain from my direct supervisor – Cristian Pira. He remained steadfast in his support until the end of the dissertation activity, with time enhancing the value of my work and incorporating it deeply into the various research projects and collaborations. His support and guidance were always present, resulting in productive partnerships.

My success would not be possible without the people who contributed with their opinions, suggestions, discussion, and practical help. I would like to begin with Fabrizio Stivanello, who will always remain for me a voice of logic and common sense in applied chemistry. I also had the great pleasure of tutoring Roberta Caforio when we worked systematically on the PEP R&D together. I extend my sincere thanks to Vanessa Garcia, whose unparalleled support, helpful contributions, and ingenious suggestions will always be recognized by me. Vanessa is more than the best colleague I have worked with; she became a part of my Venezuelan family. Several people I have had the luck to work closely with and each of them has contributed to the result I obtained: Oscar Azzolini, Katherine Ballen, Luca Lazzaroni, Luca Zanotto, Davide Ford, Oleksandr Hryhorenko, Krystsina Shynkarova and Andrii Tsymbaliuk, with whom we shared the long path through the hills of challenges and had a long conversation about all the possible theories.

I would also like to extend my gratitude to Giorgio Keppel, who as chief of the service was always trying to fulfil my needs and has never declined any of my constructive advice. To me, Silvia Martin will be someone who extended a great amount of assistance, particularly helpful and undoubtfully important to me.

The completion of my dissertation would not have been possible without the support and nurturing of my beloved wife, mother of my son, friend, and colleague, Alisa Kotliarenko. She provided me with encouragement and patience throughout the duration of the PhD. Alisa offered me as much time as it was possible to write the dissertation, while she dealt with everything else. I am deeply indebted to the sacrifice she made every weekend in the last months for me to pursue the PhD degree. And this year it is going to be my turn to fully support her with her path, as she did for me. Люблю і ціную тебе.

Lastly, I would like to mention my family, that always stand behind me, supporting and helping me in the most difficult times. My mother navigated me through the academic world, my father gave me unconditional, unequivocal, and loving support, and to my son, Lukas, who showed me that we always have much more time than we normally take advantage of.

Last year was particularly difficult, and I would like to express my deepest gratitude to the Armed Forces of Ukraine that saved my family's life in March 2022 in Irpin. As of today, they continue to save Ukraine's territory, culture, and people during this unjust war.

Abstract

Superconducting radio frequency (SRF) cavities performances strongly depend on the surface preparation. For that reason, surface treatments represent an important aspect in the development of future accelerators. The state of art of the Nb cavity production relies on 60-years' experience in superconducting radiofrequency (SRF) cavities field dealing with this material. Nb is a type II superconductor and high critical temperature natural material. A copper substrate may be used for the deposition of a superconducting (SC) layer to reduce costs and improve mechanical stability comparing to the bulk niobium technology.

The conventional protocol of substrates surface preparation includes chemical and electrochemical polishing techniques, and may include as well mechanical processing, such as chemical barrel polishing (CBP) and grinding. Harsh and corrosive solutions are typically used for chemical preparation: concentrated HF and H_2SO_4 acids for Nb, and H_3PO_4 with Butanol mixtures for Cu.

Vibro-tumbling (VT) technique is a variation of the vibratory and mass-finishing process. Usually, the systems are composed of an eccentric motor that provides the vibration motion at a certain frequency. The rotation of the cavity with the abrasive media and vibration allows uniform abrasion of the internal surface given by a step motor.

A VT system has been refurbished and updated. A series of experiments were conducted on both Cu and Nb prototype cavities varying frequency, abrasive, media, volume. A study was done on the two types of substrates: elliptical 6 GHz cavities and coupons, placed in the dummy 6 GHz cavities. A two-step protocol was developed that involves an initial erosion step using ceramic abrasive, which achieves a peak rate of 24 µm/min. This is followed by a finishing step that utilizes coconut shell abrasive to produce the desired surface quality. Surface morphology and roughness, erosion rates and other parameters were studied, and a final protocol was implemented into the continuous workflow of the National Legnaro Laboratories Cu 6 GHz cavity production.

In this dissertation, an innovative treatment – Plasma Electrolytic Polishing (PEP) has been studied to substitute the conventional treatments and possibly eliminate the need for mechanical preparation. Plasma electrolytic polishing is an evolution of electropolishing. The PEP uses diluted water-based salt solutions, able to achieve low roughness values of ≤100 nm. The smoothing of the surface is superior comparing to the standard treatments at the parity of the removal thickness. This is made possible by implementing a different working regime, which involves high voltage DC anodic polarization, a high temperature bath, and the formation of a uniform, stable vapor-gas layer (VGL) over the anode surface. The presence of this VGL enables the ignition of the plasma, resulting in the desired polishing. The stable VGL and plasma

discharges allow the levelling of the surface. "At present, there is no commonly accepted theory regarding the mechanism of the PEP technique. While various hypotheses have been put forward, none have been conclusively proven or widely accepted."

In this research work, 4 unique solutions were developed for Nb and Cu PEP processing. The process parameters behaviour was characterised by parameters such as voltage, temperature, and solution composition. Surface morphology and roughness, erosion rates, current efficiency were obtained and discussed. Experiments were conducted on the planar samples, and more complex geometries like dummy 6 GHz cavities, Quadrupole resonator (QPR) samples. 3d printed coupons were studied as well, and polished with PEP.

The planar samples were a key tool for preliminary study of the PEP process and later for solutions optimisation and characterisation of final surface quality (linear profilometer, optical and electron microscopy). Dummy 6 GHz cavities substrates were used to simulate the elliptical geometry of the cavities during the PEP process and to analyse the possibility of PEP application in cavity preparation. QPR sample is a test instrument for characterisation of surface resistance with accuracy in the nano-ohm range. Thus, the polishing of QPR samples by PEP was done for future comparison with conventional treatments.

Content

Introduction

Sustainable development requires continuous research and optimization of existing technologies. Recently, there has been a focus on optimizing economic aspects that were previously overlooked. The need for such optimization arises not only from economic or political considerations, but also from industry and fundamental scientific requirements. Superconductive radiofrequencies cavities are operating with materials (metals, alloys, and chemical compounds) that reach a critical temperature, T_c, at which they become superconductive. Currently, there are more than 100 particle accelerators worldwide in use, (excluding the ones used for medical or industrial purpose only), and the total number may overreach tens of thousands [1]. A particle accelerator is a scientific instrument designed to increase the kinetic energy of subatomic particles, such as electrons, protons, or ions, to extremely high levels. Accelerators can be meters long (typically for medical application) or kilometres long – like LHC, 27 km of circular accelerator.

The state-of-the-art material used in the production of Superconducting Radiofrequency (SRF) cavities is Niobium. The production of these resonant cavities requires careful attention and superior surface treatments to achieve the required performance. Industries have demonstrated that existing methods and technologies can deliver high-quality surfaces on Niobium cavities, approaching the theoretical limits of the Niobium superconductor. However, other promising superconductors are also of interest, although their production is not always straightforward due to their mechanical and physical properties. A known approach of superconductor (SC) layer (thin film) sputtered over the copper substrate might be a path for future accelerators, that greatly contribute both to the final performance and the economic aspect. Nevertheless, surface treatments, particularly surface polishing, remain a crucial step that greatly affects the final performance of SRF cavities, whether they are made of bulk Niobium or a SC thin-film on copper.

In this work two new methods were introduced in the superconductive cavity surface treatments preparation protocol: Vibro-tumbling (VT) and Plasma Electrolytic Polishing (PEP).

The goal of this work is to investigate innovative treatments that could be applied in the SRF field. The first part of the study focuses on Vibro-tumbling (VT) as a potential alternative to traditional centrifugal barrel polishing or mechanical grinding methods. The second part of the dissertation is devoted to Plasma Electrolytic Polishing (PEP), an advanced chemical polishing technique that offers superior removing rates and the lowest industrial roughness values. The optimisation of the VT and a deep research and development of the practical aspects of the Nb and Cu PEP were done. Four original solutions for PEP were developed, studied and optimised. The polishing substrates in this work included dummy 6 GHz cavities, planar coupons, quadrupole resonators and 3d printed samples. The rectangular samples were used for R&D stage and later for characterisation of the surface morphology, roughness and for a comparison with standard treatments. Complex geometry substrates were also

polished to evaluate the possibility of applying PEP to cavities and to address potential issues during the process.

The dissertation is organized as follows:

- Chapter 1 introduces SRF technology and resonant cavities.
- Chapter 2 describes the current state of the art in SRF cavity production and preparation.
- Chapter 3 presents a literature review of the Plasma Electrolytic Polishing (PEP) technique and its current state of the art.
- Chapter 4 describes the characterisation techniques that were applied, the experimental instrumentation used, and provides examples of data calculation.
- Chapter 5 provides a description of the Vibro-tumbling (VT) system, including its parameter optimisation and the ultimate protocol for mechanical preparation of Cu 6 GHz cavities.
- Chapter 6 describes the PEP configuration that was built, including its parameter optimisation, experimental data, and discussion for Nb and Cu processing.

PART I
Theoretical part

1 SRF Technology

In this chapter, a brief introduction to particle accelerators and SRF technology is presented. The first paragraph is devoted to particle accelerators in industry and science. The second paragraph describes the materials of interest and superconductivity. The third paragraph explains the current state of production for single cavities at various sites. Finally, the last paragraph highlights the requirements for both Nb and Cu substrates.

Particle accelerator is a powerful tool for both the fundamental and practical research in sciences. It also has found many technical and industrial field applications. Nowadays, more than 30.000 different types of accelerators are working around the world. Only few of this number are complex machines with energies about 1 GeV [2], [3].

1.1 Fundamentals of SRF technology for particle accelerators

Ideally, particle accelerator should provide high accelerating electric field E_{acc} with minimal energy consumption in a radio-frequency (RF) resonator cavity shape. Usual values of the E_{acc} are in the range of $10 - 10^2$ MV/m, and it is limited by the cavity materials. So the only way to increase the energy performance of accelerated particles is to extensively use additional cavities, sometimes numbering in the tens of thousands [4]. The need to reduce power consumption in such machines led to the introduction of superconducting RF resonating (SRF) cavities more than 60 years ago [5]. This idea has come almost immediately after the development of the Bardeen-Cooper-Schrieffer (BCS) theory, which explained microscopic mechanism of superconductivity, extremely low power losses in superconductors under low-frequency electromagnetic fields [4]. The BCS theory explains at quantum mechanical level how superconductivity originates. At its core, it demonstrates how a set of fermions (electrons) can interact through a lattice deformation (phonon) to generate an ensemble of bosons (cooper pairs) [6].

The SRF cavities have significantly lower dissipation than the normal-conductor cavities (e.g., Cu). The RF dissipation is characterized by the quality factor [7], which is one of the most important parameters in the SRF technology is proportional to the ratio of the mean electromagnetic energy to the mean dissipated power:

$$Q = \frac{\omega \mu_0 \int_V |H(r)|^2 dV}{\oint_A R_s |H(r)|^2 dA}, \tag{1.1}$$

where, ω is a frequency, $|H(r)|^2$ – energy density, V – volume, A – surface area and R_s – surface resistance, caused by the RF dissipation in the cavity walls. Q is proportional to the ratio of the stored energy divided by the energy lost by dissipation.

The formula (1.1) can be rewritten:

$$Q = \frac{\omega_0 U}{P_d} = \frac{\omega_0}{\Delta \omega_0} = \frac{G}{R_s} \qquad (1.2)$$

$$\text{where } G = \frac{\omega_0 \mu_0 \int_V |H(r)|^2 dV}{\oint_A |H(r)|^2 dA} \qquad (1.3)$$

P_d represents the dissipated power in the cavity walls, while the factor G is a geometrical constant that varies with the cavity shape, resonant mode and R_s considered.

Practically, R_s defines the main parameter of merit of any SRF cavity. A simple comparison of the R_s and Q for both normal and superconducting RF cavities results in a five orders of magnitude gain. Taking in consideration normal conducting case of Nb at T = 10 K, normal state resistivity of $\rho_n = 10^{-8} \Omega m$, at the RF frequency of $f = 1.3 \, GHz$, and superconducting grade Nb cavity at T = 2 K. Resulting surface resistance will be $R_s = 7 \, m\Omega$ and $R_s = 20 \, n\Omega$ for normal and superconductor respectively, yielding in : $Q_{nc} \sim \frac{Q_0}{R_s} \cong 10^5$ vs $Q_{sc} \sim \frac{Q_0}{R_s} \cong 2 \cdot 10^{10}$ [4]. Comparing SRF vs Normal conducting RF cavities, SC cavities have higher quality factor Q_0, consequently smaller heat dissipation, allowing them constantly running, see Table 1.1.

Table 1.1 – A brief comparison between the normal and superconductor Cu and Nb respectively [8]

Normal Conductor: Cu	Superconductor: Nb
Dissipation because of Joule effect: to avoid melting of the structures it is necessary to keep the average injected power low; most of it will be lost through heating of the cavities.	A better yield: the overvoltage coefficient is between 10 000 and 100 000 times bigger than for copper; less thermal dissipation on surfaces, almost all the power of the klystron transfers to the beam
Long duty cycles are not possible with high gradient accelerators; low efficiency, and very powerful klystrons are needed to power the cavities.	Need to cool down to 2 K (-271 °C); the amount of electricity needed to deliver the necessary cryogenic power considerably lowers the - in principle – much higher efficiency.
Less sensitive to field emission phenomena (dark current) ; other sources of losses prevail.	Very sensitive to defects, like field emission and surface conditions.
Penetration depth of field ~ 0.5-1 μm	Penetration depth of field ~40 nm
More complex cavity shapes: conditioning is difficult	Simpler and more open cavity shapes: less problems with alignment

Such a small surface resistance at temperature T below the Tc is due to the RF heating of the smaller density of unpaired electrons yielding from the dissociation of the Cooper pairs [9], [10]:

$$R_{BCS} = \left(\frac{Af^2}{T}\right) exp\left(-\frac{1.76 \, T_c}{T}\right), \qquad (1.3)$$

where, factor A is material purity dependent. The BCS surface resistance increases significantly with the Temperature increase, that's determine the efficiency of the SRF cavities is best at lowest temperatures and has to be chosen considering power losses and operational costs to

determine optimum values. At the same time, in the low field $R_s(T, f)$ generally follows different dependence:

$$R_s(T) = R_{BCS}(T) + R_i, \qquad (1.3)$$

For which $R_s(T)$ does not drops at $T \to 0$ but tends to a certain value independent of the temperature R_i [11] (see **Figure 1.1**). R_i is temperature independent but depends on the material property and magnetic flux trapping during transition to the superconducting state. It is also important to mention that R_s depends on the surface preparation, and in case of some defects (micro or macro scale) or even other non-superconducting contaminants might significantly contribute to the R_s.
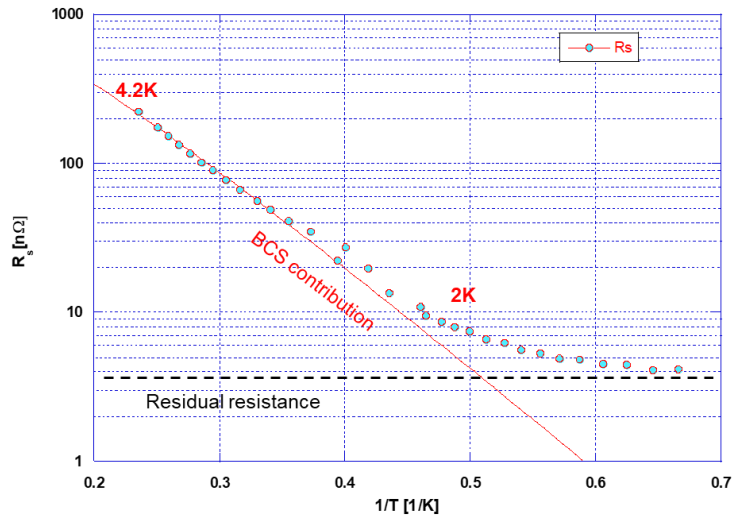

Figure 1.1: R_s behavior vs $1/T$ showing the BCS and R_i contributions [6]

Exponential behaviour of the equation 1.2 between the R_{BCS} with T_c led to the assumption, that ideal material of choice for the SRF technology can be with highest T_c. However the current SRF material is Niobium with a relatively low $T_c = 9{,}2\ K$, comparing to other superconductors like Nb3Sn $(T_c = 18{,}2\ K)$, MgB2 $(T_c = 40\ K)$, cuprates $(T_c \sim 30 - 170\ K)$ and FeSe $(T_c \sim 100\ K)$. See other superconducting materials on **Figure 1.2** and Table 1.2.

Table 1.2 – Common superconductors and their critical temperature

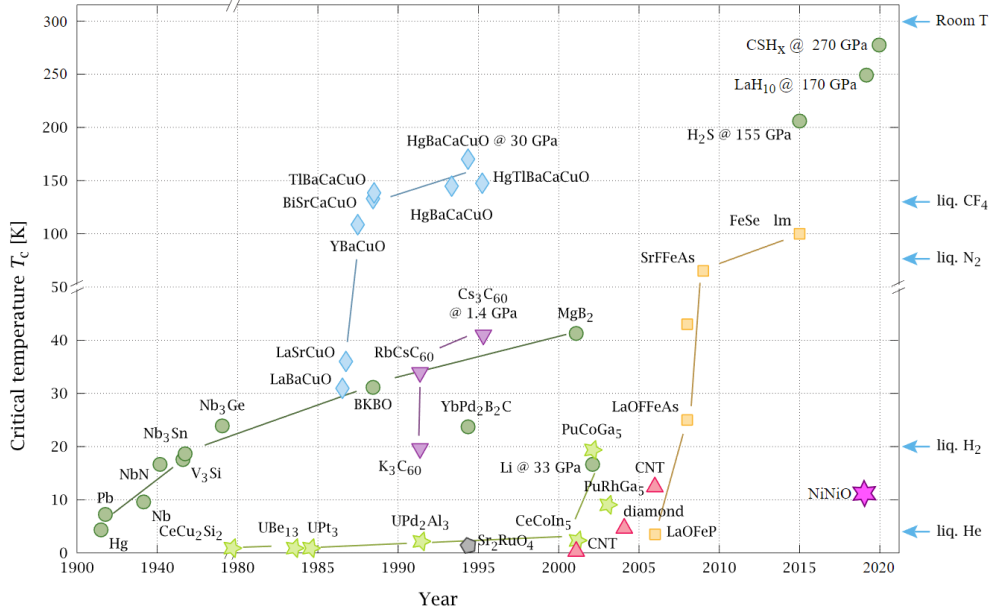| Material	Ti	Al	Hg	Sn	Pb	Nb	NbTi	NbN	NbTiN	Nb3Sn	Nb3Al	MgB$_2$
T$_c$ [K]	0.4	1.14	4.2	3.72	7.9	9.2	10	16.2	17.3	18.3	18.7	40

Figure 1.2: Superconductors transition temperature Tc versus their year of discovery
[12]

The important aspects of superconductors are also related to the technological aspects. According to the Gurevich a list of requisite for the superconductor for SRF application [4]:

1. Low R_s (including low residual resistance R_i);
2. An s-wave Cooper pairing state with a full superconducting gap on the entire Fermi surface.
3. A high lower critical magnetic field H_{c1};
4. A high superheating magnetic field;
5. High thermal conductivity (for the power dissipation inside the walls of cavity);
6. Grain boundaries transparent to high rf screening currents in polycrystalline cavities;
7. Relatively simple chemical composition, so that the material can avoid contamination with non-superconducting compounds;
8. Good mechanical properties and malleability to minimize crack formation during cavity manufacturing (forging, deep drawing, etc.).

As a result, Niobium is the metal that satisfy most of the requirements and provide an optimal compromise among other superconductors. After four decades of the Nb technology progression it was achieved a significant gain in the accelerating gradient for elliptical cavities from 3 MV/m up to the 40-50 MV/m, close to the material limits [8], [13]. For a characterisation of a single SRF cavity it is commonly used graphics where the Quality factors plot vs peak RF field (B_p) or peak electric field ($E_p = 0,43B_p$) or the accelerating field ($E_{acc} = 0,29B_p$). Using the conversion coefficient for a particular SRF cavity geometry it is possible to replot the graphic with one of the selected parameters. The $Q(B_p)$ curves (see **Figure 1.3**) normally has three distinct regions: 1) low fields, where the $Q(B_p)$

8

remain unchanged or increases with the increase of B_p, 2) intermediate fields where the $Q(B_p)$ decreases by a factor of 2 (so called medium-field Q-slope), 3) high fields, where $Q(B_p)$ decrease gradually or even drops significantly; around the breakdown field B_b (a field after which a superconducting state is no longer present).

It was described that high temperature annealing of 600-800 C° for few hours with the further low-temperature baking of 120 C° for 24h led both to the increase of the $Q(B_p)$ and the breakdown field, moreover it eliminates the high field Q-slope [14]–[16].
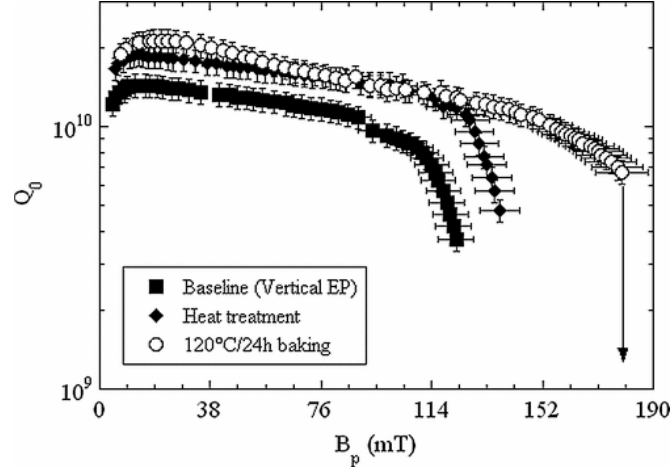

Figure 1.3: Q_0 vs B_p graph for the fine grain ILC single-ceel cavity "AES0001" after the baseline (squares) and after the heat treatments (triangles) at 800°C-3 h and 400 °C-h. Circles are the data after additional in situ baking at 120 °C for 24 h [15].

The surface resistance results from the RF dissipation in a very thin layer of ~ 40-100 nm, that is determined by the London penetration depth λ over which a low-frequency magnetic field penetrates in a superconductor surface. For the cavity-grade Niobium it is around ~40 nm [4].

$$\lambda_L = \sqrt{\frac{m}{\mu_0 n_s q^2}} \tag{1.4}$$

where m is the carrier's mass, q is the carrier's charge, and n_s is the density of superconducting electrons.

From the Gorter and Casimir two-fluid model, appears that London penetration depth is dependent on the density of the superconducting electrons, that practically means a dependence on the temperature:

$$\lambda_L(T) = \lambda_0 \left(1 - \left(\frac{T}{T_c}\right)^4\right)^{-\frac{1}{2}} \tag{1.5}$$

This means, that the performance of the SRF cavities depends heavily on the top few tens of nanometres of the surface. Consequently, surface treatments are playing a significant role in the SRF.

1.1 Particle accelerators facility

The particle accelerators are the complex machines that can accelerate charged particles using electromagnetic fields to higher energies in a well aligned beam. One of the main scopes of the particle accelerators were the research on the particle physics. Most extreme particle accelerators can speed up protons, ions and electrons up to the speed of light and > 10 TeV energies. Nowadays, more than 30 000 accelerators for different purpose, shape and complexity are operating around the world. Applications can vary from purely industrial to fundamental physics research, including medicine as well. All the accelerators can be classified based on how the acceleration is done and shape of the facility. Two main shapes are known: linear and circular.

The first acceleration of electrons by SRF technology was accomplished with Pb plated cavities at SLAC linac in 1965 [17]. Since 1970s [18], the lead-plated cavities have been replaced with cavities made of Niobium. The first elliptical cavities were developed in the late 1970s and early 1980s, and the TESLA (TeV-Energy Superconducting Linear Accelerator) cavity was proposed in 1992 [19], [20].

Some of the most well-known accelerators in history include the Stanford Linear Accelerator Center (SLAC), which produced the first evidence of quarks in the late 1960s. The Continuous Electron Beam Accelerator Facility (CEBAF), located at JLab, was a ground-breaking accelerator that used superconducting radio frequency (SRF) cavities to accelerate electrons to energies of up to 12 GeV [21].

The world's highest-energy particle accelerator, the Tevatron, located at Fermilab in the United States was a proton-antiproton collider that operated from 1983 to 2011 until the opening of the Large Hadron Collider (LHC) in 2008. The Tevatron played a crucial role in the discovery of the top quark in 1995, which helped to confirm the Standard Model of particle physics [22]. In Europe, the Large Electron-Positron Collider (LEP) at CERN was the largest accelerator of its time, operating from 1989 to 2000. It was followed by the LHC, which is currently the most powerful accelerator in the world and has been instrumental in the discovery of the Higgs boson [23], [24].

In the field of X-ray free-electron lasers (XFELs), the Linac Coherent Light Source (LCLS) at SLAC was the first facility to generate high-intensity, ultra-short X-ray pulses, revolutionizing the field of X-ray science. Its successor, the LCLS-II, is expected to generate even more intense X-ray pulses. Another notable XFEL facility is the European XFEL in Germany, which is one of the most advanced XFELs in the world and has been used to study a wide range of materials and biological systems [25], [26].

1.2 Niobium and Superconductivity

The superconductivity was discovered in 1911 by H.Kamerlingh Onnes in Leiden, that was followed by the first liquefaction of helium, allowing him to reach temperatures of a few Kelvin

degrees. As a result, Kamerlingh observed that the resistivity of some metals (such as Hg, Pb, and Sn) decreased to zero under the critical temperature (which was lower than 10 K). Later, many other metals were found to be superconducting as well. Nowadays, superconductivity is a key element not only for particle acceleration (magnets, cavities...), but also for social needs of transport (Maglev trains) [61]. Among the transport applications, superconductors are used for industrial (SQUID sensors, cables) and medical applications (magnetic resonance imaging).

The performance of superconducting cavities for particle acceleration applications is characterized by two parameters (**Figure 1.4**) [8]:
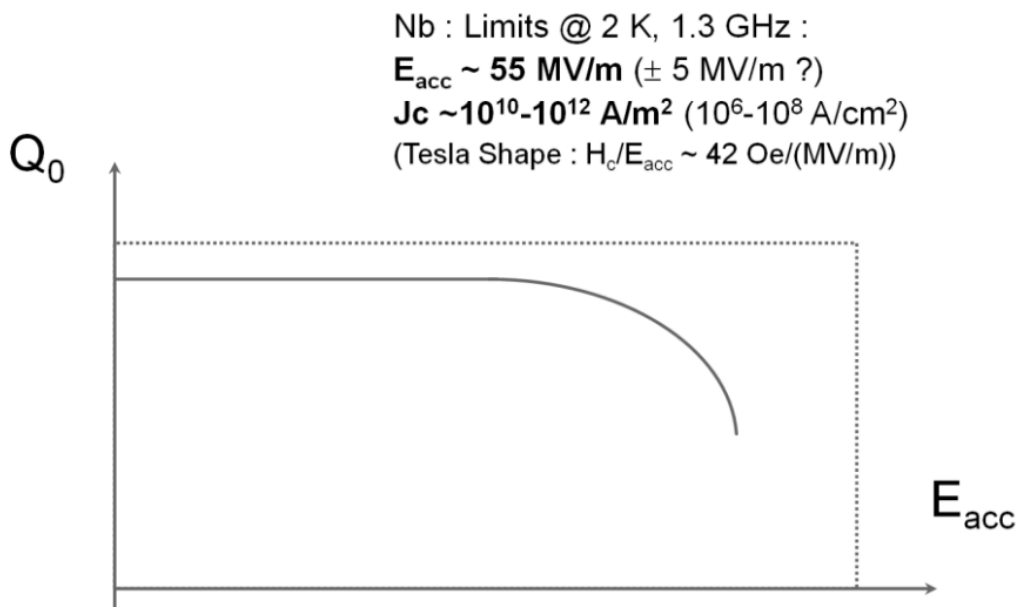

Figure 1.4: Simplified performance of RF Niobium cavities

- The accelerating field E_{acc}, as seen by a particle traversing the cavity (sometimes called «gradient»).
- The quality factor Q_0, which measures the ability to store the electromagnetic energy.

Superconducting properties of the Niobium metal is listed below in the Table 1.3.

Table 1.3 – Superconducting properties of niobium

Parameter	Sign	Value
Critical temperature	T_c	9.25 K
Energy gap	Δ	1.5 meV
London penetration depth	λ_L	40 nm
Coherence length	ξ	35 nm
Lower critical field	H_{c1}	180 mT
Superheating field	H_{sh}	240 mT
Upper critical field	H_{c2}	280 mT

Niobium has the highest pure metal critical temperature. A list of other alloys based on Nb were discovered as well, reaching Tc up to 40 K. More complex compounds can have relatively "high" critical temperatures (see **Figure 1.2**). The superconducting state can be lost once the temperature Tc will be lost or if the external magnetic field is too high.

1.3   SRF resonators

RF cavities are a central element of both circular or linear accelerators. A relatively simple resonant cavity can be described as a cylindrical pillbox cavity (see **Figure 1.5**). A detailed explanation of such resonant structure is available in [27], [28]. The electric field direction is along the cavity's profile and the magnetic field around their inner walls. Both electric and magnetic fields are alternating and the direction change. The alternating electric field produces alternating magnetic fields. The cavity restricts the electromagnetic fields by shielding currents with surface, which results in losses or simply heating. Such losses can be significantly reduced by using superconducting materials, as described earlier [29].

RF waves are injected in the cavity through the power coupler. Different shape of such cavities may enable more heavy ions / protons acceleration, for e.g., non-elliptical shapes as quarter-wave. Multi-cell elliptical cavities (see **Figure 1.6**) are used in XFEL and LHC facility, instead for ALPI accelerator quarter-wave resonator structure is used. Single-cell elliptical shapes are normally used for R&D, more rarely finds accelerators applications [28]. Common shapes of cavities and their frequency with particle velocity regions are presented below (see **Figure 1.7**).
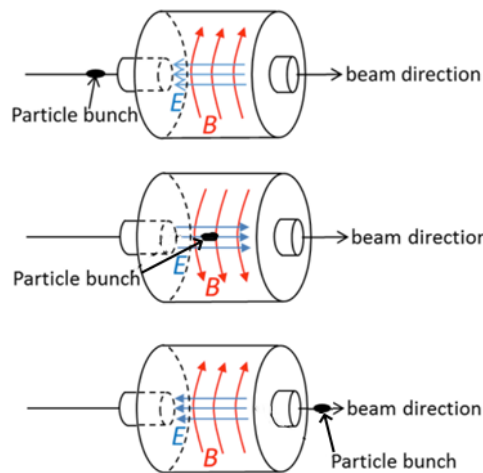

Figure 1.5: Electromagnetic fields in a pillbox cavity during acceleration, a scheme of three distinct phases [29]
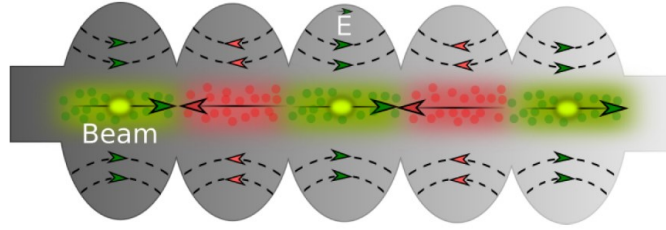
Figure 1.6: Sketch of multi-cell elliptical superconducting RF cavity [30]

Superconducting radiofrequency (SRF) cavities are one of the key technologies in many accelerators: LBNF/DUNE [31], LHC [17], HL-LHC [18], EIC [32], ILC [33], FCC-ee [34], CepC [35], ALPI [36], ISOLDE [37], ATLAS [38], SNS [39], CEBAF [40], LCLS-II [41], KEK-B [42], PIP-II [43], ESS [44].

Different types of cavities have been developed in the last few decades of years. The variation of such cavities can be related to the velocity of the accelerated particles v in respect to the light velocity c, or simply to the beta factor (β):
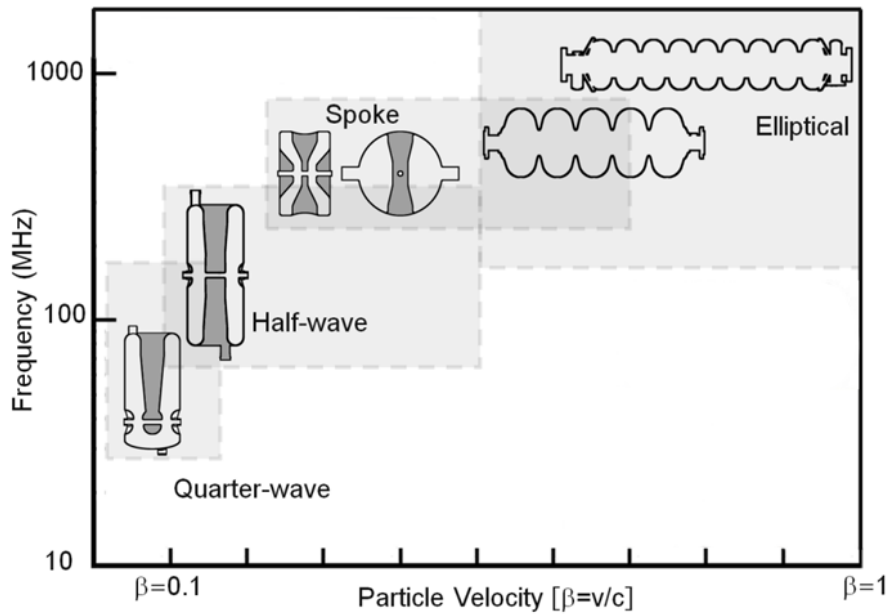
$$\beta = v/c \tag{1.6}$$

Figure 1.7: A scheme of various shape SRF cavities [45]

Three types of cavities can be distinguished: high – β, medium – β, and low – β. The high – β structures are used for acceleration of electrons, positrons, or high-energy protons. The medium – β can accelerate protons and ions with energies lower that 1 GeV. Finally, the low – β cavities are used exclusively for acceleration of heavy ions [28].

1.4 Surface requirements for Niobium SRF Cavities

The overall state of art of the cavity production is a major challenge for the SRF accelerator field. As mentioned earlier, macro, and microscopic defects (scratches, inclusion and contaminations, pull-outs etc.) could cause sever decrease of the SRF performance, causing Q-quench. Removing a certain thickness of the damaged layer is required with the variations depending on supplier of the Nb material.

For superconducting metals, such as Nb, exist parameter that can determine its quality and material purity: residual resistivity ratio (RRR). Electrical resistivity of metals at low temperatures is related to the impurity concentrations. The residual resistivity at T=0K is caused mainly by scattering of electrons by impurities. RRR is given:

$$RRR = \frac{\rho_{295K}}{\rho_{4.2K}} \tag{1.7}$$

Any impurities contribute additionally to the resistivity even in the lowers concentrations (see **Figure 1.8**) [8]:

Impurity	$\partial\rho/\partial C$ (nΩ.m/At ppm)
N	0.52
O	0.45
C	0.43
H	0.08
Ti	0.096
Ta	0.025

Figure 1.8: Low temperature resistivity contribution of the main contaminants

Normally, Niobium has a layer of oxide, that forms at the ambient conditions, the thickness is around 5-10 nanometres. Due to the fact, that RF waves are penetrating on few tens of the nanometres into the bulk material, leads the necessity that among this thickness superconducting properties has to be excellent. Oxide layer in the end works as a protective layer, inhibiting the absorption and diffusion of various gasses and impurities.

The smoothness of inner surfaces of niobium cavities required to achieve high gradient E_{acc} > 30 MV/m according to Saito [46] has to be below Rz equals to 2 μm. This requirement is easily reached by the currently used electropolishing process which removes more than 100 μm of material. After this process a roughness of Rz <0.303 μm can be reached [47]. Xu et al., instead, see a difference in performance as a consequence of surface topology, rather than the resulting roughness after the EP or BCP treatment [48].

Unfortunately, there were no systematic study on the precise requirements for the cu substrate, as it was done for the bulk and superficial Niobium. It is naturally, that Nb deposited via PVD over the Cu substrate will reproduce the microstructure of the surface, thus the non-uniformities, defects, pits, scratches etc. Those problem may lead to the local heated spots, affecting the SC properties of the film [49].

1.5 Limitations

The performance of the SRF resonant cavities are limited in the ideal case by the theoretical performance (ideal performance, see **Figure 1.9**). In this case the line is almost horizontal, however in the real world, the performance is constrained by limiting factors. A brief overview of such phenomena: thermal instability, field emission, multipacting and hydrogen Q-disease are discussed below.
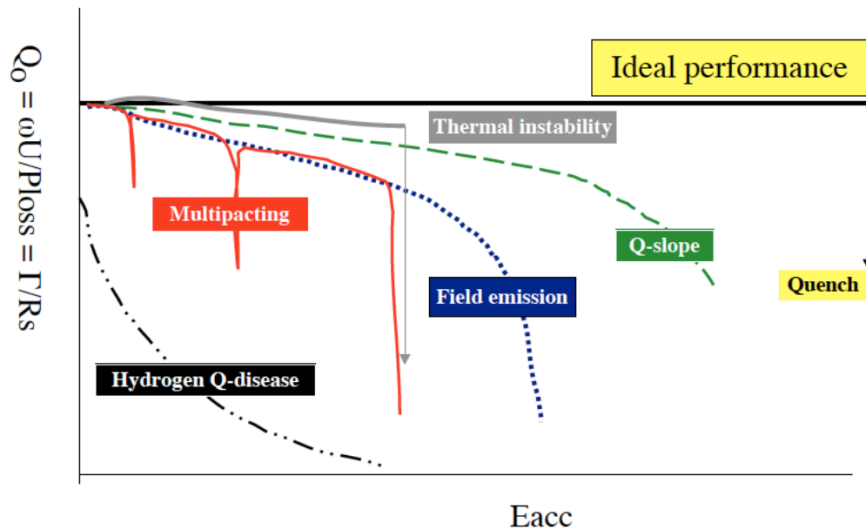

Figure 1.9: Principal limitation in the performance of the SRF cavities [50]

Thermal instability

Thermal breakdown (also known as thermal instability) is associated with the presence of defects in the superconductor, thus provoking a local quench, increasing the temperature, and spreading in the cavity. Such defects are of submillimetre-size dimensions causing high RF losses. Once the local defect exceeds the Tc superconducting transition temperature, RF losses are increased significantly. A growing local region become a normal conducting yielding to the rapid loss of the previously stored energy [28], [29], [51]. This limiting factor can be detected by temperature mapping of the SRF cavity, placing temperature sensors all over the cavity. A solution for this issue is consisted of the increase superconductor thermal conductivity, for e.g., using 300 RRR quality grade of Niobium. The main advantage of requiring an RRR (residual resistance ratio) of 300 is that it improves the

cleanliness of the material fabrication process, reducing the occurrence of inclusion defects that would otherwise require thermal stabilization.

Q-Slope

The most common limiting factor of the SRF cavity performance is known as a Q-slope. Three regions can be distinguished: low, medium, and high field Q-slope. The low field Q-slope is primarily present in the bulk niobium cavities, causing a small increment in the quality factor followed by quenching. The origin of this factor was initially linked to the oxide layer present on the surface of the SRF cavity walls. These oxide accumulations behave as quasiparticles that reduce surface resistance at low fields due to the mismatch in absorption rates in the RF field [28]. However, no tests so far have clearly associated significant RF losses with typical surface oxides. Fluxoid losses and hydride losses tend to dominate the current bulk Nb R_s performance limitations [52]. Low-field Q-sloped can be improved slightly by low-temperature baking (100-120 C° for 48-60 hours).

In the middle field Q-slope region, the quality factor reduction is mild, and it is usually attributed to a combination of factors such as surface heating, non-linear BCS resistance, and losses due to frozen-in flux.

Multipacting

The nature of this limiting effect relates to the release of the electrons from the cavity surface and then are accelerated by the RF fields. This produces a cascade effect, as the electrons hitting the cavity surface produce secondary electrons. When the secondary electron hit the same spot, the absorbed RF energy heats the surface and eventually creates a local hot spot. The most effective way to decrease the multipacting effect is to apply improvements in the cavity design and reduction of surface Secondary Electron Yield (SEY) via careful surface treatments. However, completely avoid this factor is not possible. An example of such design is elliptical cavities, in which the electromagnetic field configuration guide the electron to impact close to the equator, and thus reducing the number of impacts [29], [51].

Field emission

Another well-known phenomenon that limits the accelerating field from reaching higher values is field emission. It normally appears once the gradient reaches 10-20 MV/m [28]. In such a situation, field emission can take place, and the Q-factor starts to fall exponentially. Field emission is generated by impurities, such as powders, which are the emitters. Electrons may be ejected from the cavity surface and accelerated by RF fields impacting the cavity surface. Due to these effects, x-rays can be produced during the cavity operation, which can heat the cavity wall. Similarly to multipacting, this phenomenon adsorbs a huge portion of the RF power. As the microparticles are primarily the source of emission, it is strictly necessary to follow the cleanliness procedures during final surface preparation and assembly procedures. Besides clean room operation, high-pressure rinsing with distilled water of the internal wall surfaces is a powerful tool to avoid field emission.

Hydrogen Q-disease

The presence of hydrogen in the niobium structure can sufficiently limit its performance. In case of slow cooling down, hydrogen precipitation can take place around the 100-150 K. The increase of the hydrogen presence can occur during production, processing, and chemical treatments. A solution to avoid the hydrides formation is to cool down rapidly. Additionally, a greater way to cure the cavity is the high temperature ultra-high vacuum (UHV) baking at 800 C°, that is already is a part of a standard protocol (see chapter 2.1.1 in detail) [53]. Alternatively, a 600°C bake for 10 hours can be used to achieve the same reduction in hydrogen content, with less softening of the Nb due to annealing.

2 Surface treatments for SRF cavities

This second chapter is devoted to the detailed description of various surface treatments, paying a special attention to those that are applied in the SRF technology (in particular for European XFEL, ALPI, and LCLS-II). Some relatively innovative possible approaches for SRF are also mentioned.

After more than 60 years of development of Niobium SRF technology, the surface treatments have been studied in various aspects yielding to a generally common protocol of a single cavity production starting from the forming and through various steps of mechanical, chemical and electrochemical treatments resulting in the high SC performance. Even though the protocol might be seen similar for various facilities, it is different depending on the requirements placed, material of choice, cavity shape.

As the scope of the dissertation was devoted to the exploration of new innovative surface treatments for the SRF technology, some of them are described below including alternative forming methods, innovative approaches in mechanical surface preparation, and non-conventional electrochemical treatments and others.

2.1   Existing protocols

For every accelerator a well-defined protocol was developed and consisted of the production and preparation processing of the SRF cavities. The protocols are typically optimized during periods of time, thanks to the discoveries and advancements that have been obtained by the SRF community over the years.

The substrate surface plays a key role in their RF performance, consequently the complete protocol of production must include surface treatments achieving commissioned requirements for the SRF cavities, generally regarding the certain values of Accelerating gradient *Eacc*, Quality factor Q_0. Some of the surface requirements are described below in the chapter 1.4.

The forming process is the first procedure that has two main scopes: obtaining a desired shape and attempting to minimize surface defects [47], [54]. Even though the surface damages are still present, and chemical (electrochemical) treatments are mandatory to decrease the irregularities of the surface to come up with the requirements, mechanical treatments are still used.

Surface treatment protocols exist for both copper and niobium SRF cavities, which typically involve the removal of at least 100-200 μm of material to eliminate surface imperfections caused by

the forming process. While the Niobium chemistry is less studied, its 50+ year history in SRF has led to a well-defined protocol. In contrast, Cu chemistry has been studied over the years, some of the aspects are even hundreds of years old, but the approach of using a copper substrate with a superconducting layer is still less common, leading to more uncertainty in treatment protocols and the absence of standard requirements for copper substrates prior to the deposition of the superconducting layer.

Initially, all the Nb cavities were produced by deep drawing and electron beam welding of sub-parts (see chapter 2.2.1). More recently, attempts have been made to switch to the seamless technology to avoid producing additional critical defects (see chapter 2.2.2), resulting in the elimination of some of the initial treatments in protocols (such as EBW, mounting, etc.). Further advancements have led to surface modification technologies, such as nitrogen doping, allowing to achieve higher performance.

Among all the treatments it is noted the High Pressure rinsing (HPR), that is an important step to get rid of powders and contaminants attached to the surface, that may be a cause of severe degradation of the RF performance. It was also implemented and showed the importance of HPR not only before the assembling of the cavity into the helium tank, but also after the bulk electropolishing (for more details see chapter 2.5.2.3).

Currently innovative treatments (such as pulse-reverse EP, EP with the usage of ionic liquids, magneto electropolishing, plasma electrolytic polishing, vibro-tumbling and others) have not been yet implemented in the protocols of the cavity production (treatment) of any facility, only proof of concepts were demonstrated with the final RF measurements. The scientific community considers E-XFEL protocol as a state of art for the preparation of niobium bulk cavities and often cites it as a guideline for the surface preparation. Nowadays, with guidance from the laboratories, vendors have significantly improved their fabrication and processing standards to meet the higher standards required for projects such as LCLS-II, ESS, PIP-II, and SNS-PPU. Meanwhile, the ALPI protocol can be considered as a state of art for the copper substrate preparation for Nb/Cu SRF technology.

2.1.1   Protocol for European XFEL (Germany)

In 2017 an electron linac, based on SC technology having a high accelerating gradient of 25 MV/m has been placed in operation at DESY, namely European X-FEL [16]. In collaboration with 17 international institutes, E-XFEL has shown excellent scientific collaborations across borders. The purpose of the facility is to produce extremely brilliant and short pulses of spatially coherent x-rays of 0.1 nm. A pulsed beam of 0.7 ms with a repetition rate of 10 Hz is accelerated to 17.5 GeV by 768 1.3 GHz SRF cavities of 1,7 km length. The fundamental technology of this project has been developed by the international TESLA collaborations.

The main challenge for XFEL was the industrialization of the cavity production [26]. A production protocol was adapted from the experience of the DESY laboratory and FLASH from the

TESLA collaboration. A resulting adopted protocol include two paths: purely electrochemical or with additional buffered chemical polishing of a niobium – Flash BCP. A scheme is presented below (see **Figure 2.1**).

At a manufacturer Niobium is moulded into an ingot. A series of remelting in an ultra-high vacuum electron-beam furnace allows purification of the Nb ingot. In this process lighter contaminants evaporate. Four to six melting steps are normally needed to reach the RRR 300 [8]. The composition and cleanliness must be maintained during all treatments and forming procedures. Niobium sheets are sliced from the ingot, followed by a sequence of forging, rolling, polishing and annealing. Besides inspection of mechanical parameters, the quality control of the manufactured sheets with regard to purity and RRR is done by eddy-current scanning of the niobium sheets [55]. The ≥ 300 RRR requirement is needed mainly for the high thermal-conductivity needed for the SRF conditions.

The structural part of the final elliptical cavity is a half-cell. Nb half-cells are formed via deep drawing the sheets with a set of forms, followed by trimming the edges at the equator and iris side. Additionally, some procedures (like coning) are applied to the half-cells to provide a certain curvature and resonant RF.

The absence of structural defects and impurities of various kind is one of the key requirements for the high-quality factor and high accelerating field. This can be achieved through the above-mentioned protocol, removing the 110-140 µm in average of the thickness of internal surface with electropolishing. Most of the defects come from sheet rolling and half-cell deep drawing.

Following, the next treatment includes annealing at 800 C° (also called heat treatment). At this stage niobium metal undergoes partial recrystallisation, thus elastic deformation is destressed. Additionally, migrated hydrogen from electropolishing bake out of the bulk niobium. During the baking, in case the furnace vacuum quality is insufficient, residual gases might contaminate the upper layers of niobium. In such a case, additional electropolishing or buffered chemical polishing is required to get rid of it.

In case of a buffered chemical polishing a standard solution of three acids is used: Hydrofluoric acid (HF), Nitric acid (HNO_3), Phosphoric acid (H_3PO_4). The mixture of 1:1:2 respectively volume ration composition is used. Hydrofluoric acid is used to remove the oxide of Niobium, that is consequently forming inside the oxidizing agent – Nitric acid. Such mixture of two acids with niobium metal yield a strong exothermic reaction, and might lead to the removal rates of up 30 µm/min. Meanwhile huge volumes of gasses are produced. To address this, a buffering agent is added: Phosphoric acid, that limits the heating and removal rate. Additionally, the mixture is cooled down to 15 C°. Such improvement yields in lowering of Hydrogen diffusion into the bulk metal. And the resulting removing rate reaches 1 µm/min.
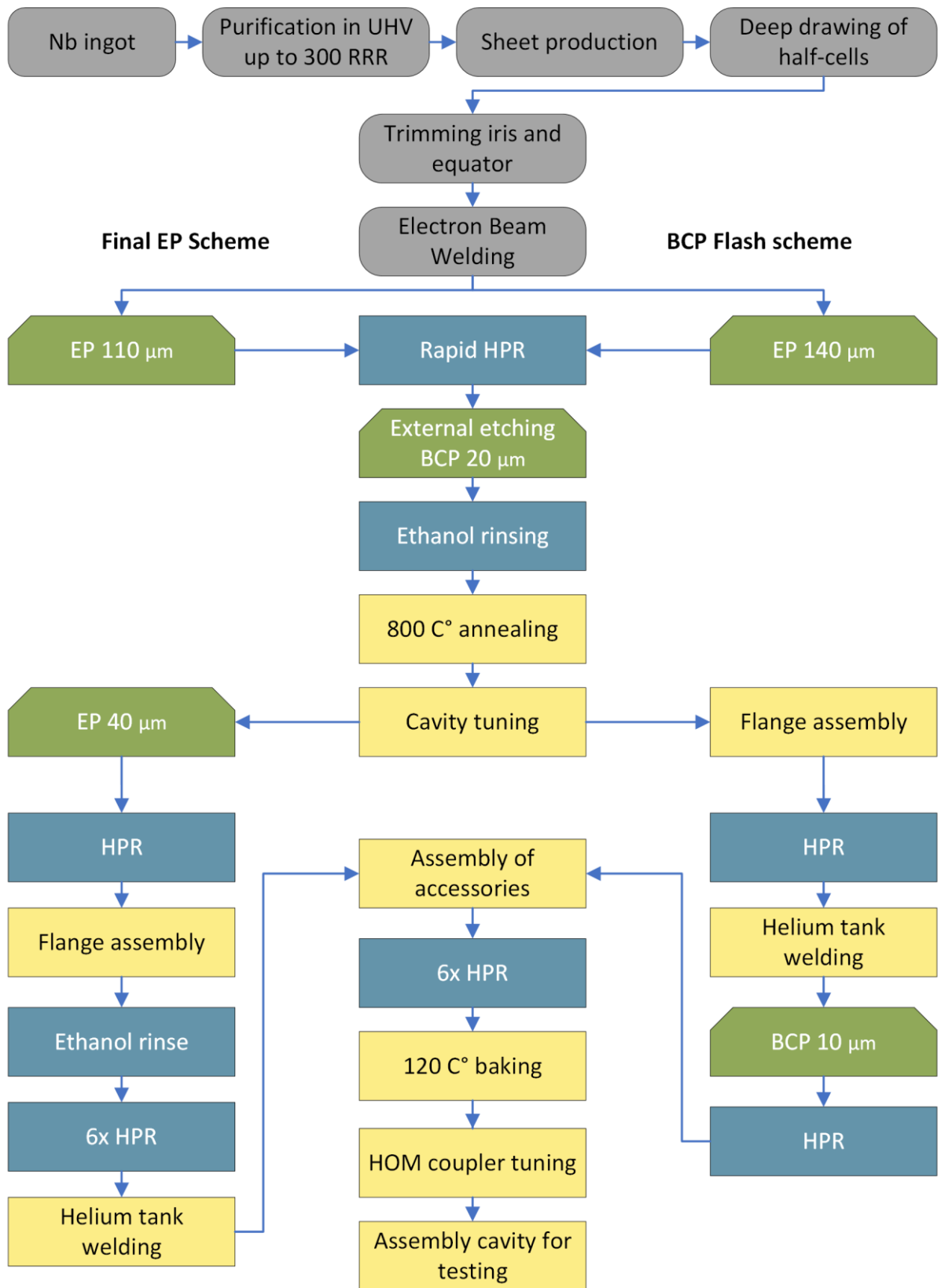
Figure 2.1: Cavity preparation scheme for European XFEL facility

Electropolishing is a widely used chemical method to smooth the surface both in industry and the SRF field. Similarly, as in BCP, the niobium metal is oxidised with sulfuric acid and applied anodic polarisation. Meanwhile, hydrofluoric acid dissolves the niobium oxide. Working voltage is set around 17 V. During electropolishing, the niobium surface is dissolved by an electrochemical reaction that creates a layer of niobium oxide, which is then removed by a chemical reduction reaction. In the case of diffusion-limited conditions, the etching rate is determined by the rate at which the reducing agent diffuses through the oxide layer to reach the niobium surface. This creates a self-limiting process, where the etching rate is slower at areas of the surface that are more oxidized. This self-limiting process is what creates the levelling effect [56], [57].

During electropolishing, sulfuric acid can contaminate the internal surface of the niobium cavity with sulphur-based compounds. To remove these contaminants, the cavity is rinsed with ethanol. The sulphur contamination can be attributed to excessive polarization at the aluminium cathode, resulting in high local current density and temperature at the Nb cavity wall [57]–[59].

Due to the mechanism, the resulting roughness after EP is lower than after BCP, this might explain why the EP treated cavities shows slightly higher accelerating gradients [60]–[62].

High Pressure Rinsing (HPR) of cavities with ultra-pure distilled water decrease the presence by 99% of residual particles, thus eliminating the chance of field emission [108]. A cleaning tube with nozzles is inserted inside cavity volume. Through the series of nozzles, high pressure (100 bar) ultrapure water jets are directed onto the inner cavity surface [109]. Water efficiently removes dust and particles from the inner surface of the cavity. The standard XFEL fabrication scheme has a repetition of the HPR for four times to diminish the particle amount inside the cavity. It is reported that HPR has been proven to be the most effective retreatment in the XFEL production scheme [61].

After the final chemical treatment, including additional HPR and ethanol rinsing, the helium vessel is welded onto the cavity. All other parts of a performance test are assembled in a clean room.

XFEL protocol scheme does not foresee the application of any mechanical polishing scheme. And naturally, the state of art of this scheme refers only Niobium metal (that will be discussed in detail later).

2.1.2   Protocol for ALPI (Italy)

A different SRF technology that relies on copper substrate sputtered with SC layer is also a choice for some applications, for instance linac ALPI, the HIE-ISOLDE upgrade project at CERN. Such a different approach undoubtedly cannot rely on the niobium chemistry surface preparation scheme that is well developed. Luckily, the copper chemistry is less complicated, allowing to achieve low-roughness surface morphology with either chemical or electrochemical polishing methods.

For the ALPI three types of cavities were used, lead plated, niobium plated and bulk niobium cavities. In this dissertation, all the information regarding the ALPI protocol is referring to the Nb/Cu approach.

A developed protocol in the 90s years [63] and slightly updated later in the 2019 for the upgrade of the ALPI linac described in details [64]. A protocol describes the mechanical, chemical and electrochemical polishing and other surface treatments for the preparation of the quarter-wave resonator (see **Figure 2.2**).

The forming steps had in principle two main routes: deep drawing or turning machining (extrusion). In the case of deep drawing there the bulk cavity is being produced in one step, achieving excellent superficial quality. Additionally, some brazing and extrusion were also applied to form features. In the case of turning route, the quarter-wave resonator shape is extruded with the turning machine, similarly additional brazing might be applied, depending on the generation of the cavity. In both cases, the treatments were done externally by private company.

After the forming of the cavity, it was processed with a tumbling machine for at least 72h. The time can be extended, in case of the presence of some noticeable issues on the surface. The final protocol contained two steps (in the contrary even 4 steps) of tumbling. The first was meant to "cut" the surface and uniform it. While the second step was a finishing treatment to prepare the surface for the electropolishing. Two different abrasives were used in the presence of distilled water.

A mechanically polished cavity undergoes the fast ultrasound cleaning and then the electropolishing takes place. The solution used for the EP of Cu QWR: Phosphoric acid 85% and n-Butanol 99%, with the volume ratio of 55:45. Generally the cavity is electropolished for at least 1 hour, that may be estimated to remove approximately about 20 μm. The working voltage is selected with the custom written software, choosing the value that corresponds to the maximum resistance on the plateau of the voltage-current curve. After the electropolishing, a cavity is inserted in the cleaning bath to eliminate eventual chemical products, and then the rapid HPR is applied.

After the electropolishing, the second chemical way to prepare the surface applied – SUBU polishing. A 4-component solution, composed of Sulfamic acid (5 g/L), Ammonium Citrate (1 g/L), n-Butanol 99% (50 mL/L), Hydrogen peroxide 30% (50 mL/L). Preheated solution up to the 72 ± 2 C° and agitation is required to obtain desired surface. The treatment is limited to 2-3 minutes, resulting in the 2-4 μm total removal rate.

A passivation step after the SUBU treatment is applied, to preserve the heated copper surface with the active chemical residuals. Practically by immersing the cavity into the passivation solution it dilutes the surface and cools at the same time. Finally copper sulphamate is formed, that preserves oxidation. A thin layer evaporates later during baking in the vacuum conditions.

A high-pressure rinsing is fundamental to ensure the cleanliness of the surface before the sputtering and after the successful Nb deposition before the RF test. In case of low performance, or

any other issues, a cavity may undergo a repetition of the treatment protocol starting from the stripping process, that involves dissolution of the Nb layer selectively.
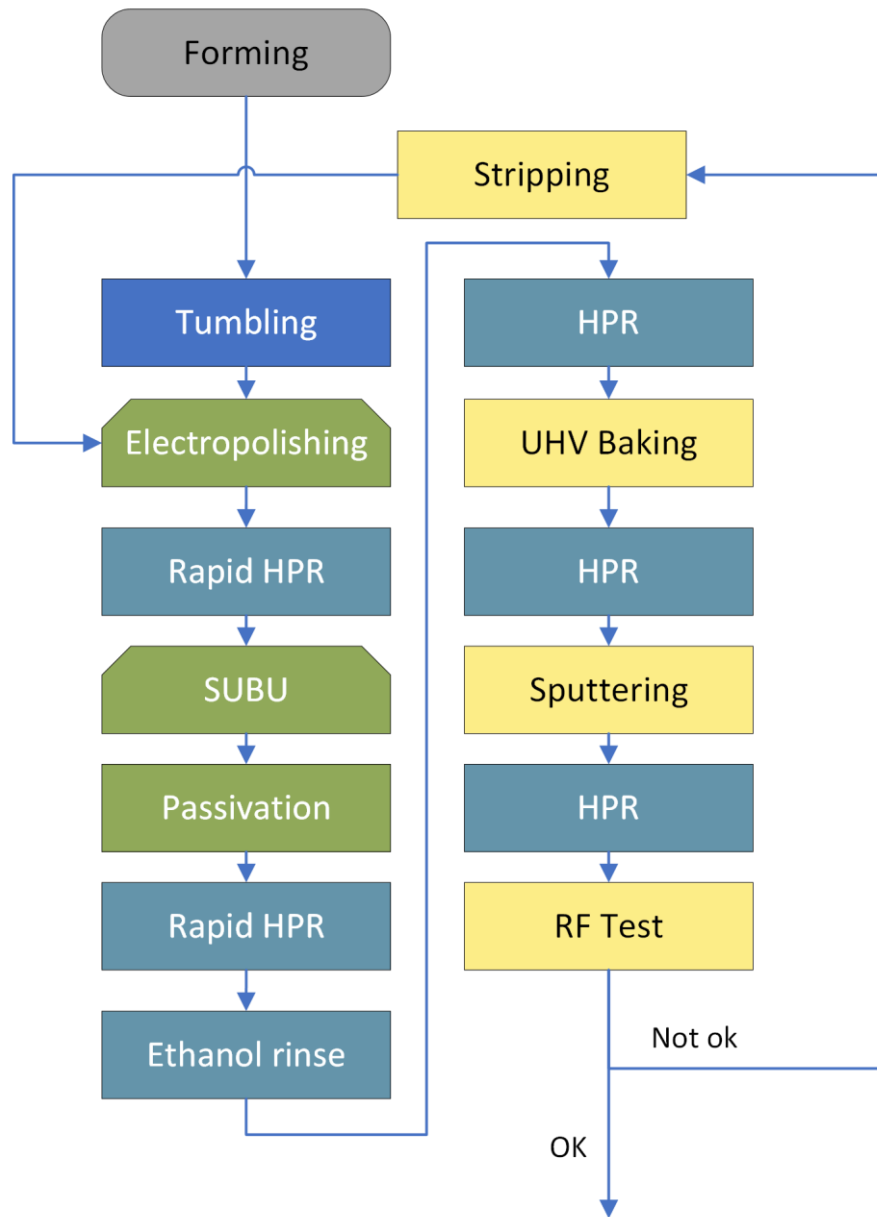

Figure 2.2: The ALPI accelerator Nb/Cu cavities preparation scheme

2.1.3   Protocol for LCLS-II (USA)

The Linac Coherent Light Source II (LCLS-II) accelerator is a free-electron laser (FEL) facility located at the SLAC National Accelerator Laboratory in California, USA. It is a next-generation X-ray laser that produces ultrafast pulses of intense X-rays with unprecedented brightness and coherence.

The LCLS-II is designed to operate at a repetition rate of up to one million pulses per second, which is 8,000 times faster than the original LCLS facility. The LCLS-II uses a total of 280 cavities arranged in 35 cryomodules, which are connected in series to form a continuous accelerator structure

[65]. The main novel aspect of the cavity preparation protocol for the LCLS-II accelerator is the use of a new surface treatment process called Nitrogen Doping. This process involves exposing the inner surface of the niobium cavities to a flow of nitrogen gas at high temperatures and pressures, which creates a thin layer of nitrogen-doped niobium on the surface. This is typically done between 600-1000°C at a pressure of some tens of millitorr. The process results in two effects - the formation of a niobium-nitride phase on the surface of the niobium, and nitrogen diffusion into the bulk of the niobium, which can extend up to 40-50 μm for the LCLS-II recipe [41], [66].

However, the nitride layer formed on the surface is quite lossy and can result in a Q_0's on the order of 1×10^8 if not removed. Therefore, after the doping phase in the furnace, the first few microns of the surface are removed via EP, which produces very smooth surfaces. It should be noted that the success of the doping process is dependent on the substrate being electropolished before nitrogen doping, to ensure a smooth starting surface.

The full cavity preparation method involves the following steps (see a **Figure 2.3**)[65]:
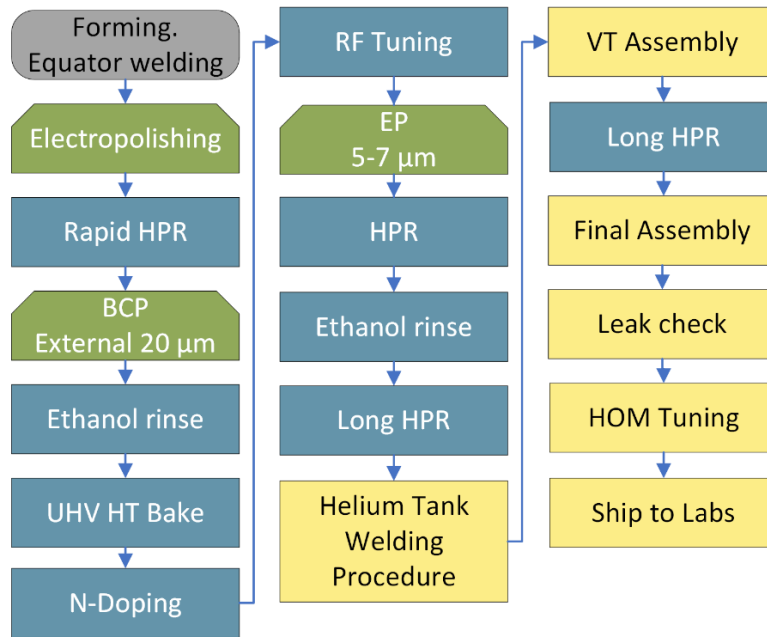
Figure 2.3: The LCLS-II accelerator Nb/Cu cavities preparation scheme

- Bulk electropolishing of 140 (200) μm.
- Degas in UHV furnace in vacuum at 800 ∘C (900 ∘C) for 3 hours.
- Nitrogen-doping in 26 mTorr of nitrogen gas for 2 minutes at 800 ∘C.
- Annealing in vacuum for 6 minutes at 800 ∘C.
- Light electropolishing of 5-7 μm.

As in other protocols described earlier, surface preparation remains a crucial part of the protocol. Therefore, Electropolishing is still used both before and after the N-doping process, together with all the rest of the advanced protocol steps.

2.2　Production methods

2.2.1　Deep drawing and Electron beam welding

Complex shape objects production (e.g., elliptical cavities) is not a trivial task for the industry, as the elliptical shape and closed geometry limits accessibility of many machining and forming methods. In the end, the most convenient way to produce such geometries in the beginning of the SRF technology development became a deep drawing with the electron beam welding approach (see a scheme **Figure 2.4**). The idea behind such technology is based on the assembly of simpler geometries, which eventually form the desired shape. For e.g., a nine-cell cavity is formed from a series of half-cells and other objects (like HOM coupler, beam-pipe, input-port, flanges and others)

Half-Cells parts are produced by physical pressure (stamping) into the shapes using male and female dies. The dies are normally done from anodised aluminium. This step is important because the resonant frequency of a cavity is being formed here. The resulting frequency may be changed later with other treatments by a small margin. In order to avoid possible surface defects, the processing has to ensure the absence of dents, blisters, scratches and contaminants. The Nb sheet has to have certain mechanical properties and be treated prior with the heating process – annealing at 750-800℃ in the ultra-high vacuum conditions for 1-2 h.
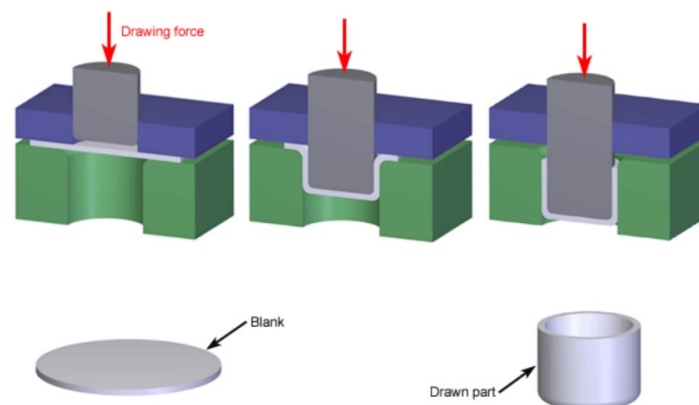
Figure 2.4: Deep drawing scheme

Two half-cells are joined at the iris with an Electron Beam Welding (EBW) (see **Figure 2.5**) to form a dumb-bell. Then there is a welding of the stiffening ring. Welding may lead to a small deformation of the cell, which has to be addressed. This linkage is performed under vacuum conditions by applying an electron beam and melting together the half cells to close the resonant structure. The welded line part of the elliptical cavity represents the most critical sector for the final RF performance. In such complex way a half-cell cavity is produced. Specifically, a difficult process is in fact a welding of half-cells between each other on the equator. Quite delicate process is complexed as well with the choice of welding parameters and intermediate cleaning steps to achieve a complete penetration of

the obtained joint. A reproducibility of a final performance is also a challenge, since during processing tight mechanical and electrical tolerances should be taken into consideration [67]. The dumb-bells are inspected visually to detect possible defects and contaminant imprints, in such cases a grinding may be applied (see in details paragraph 2.3.1.3) [67].
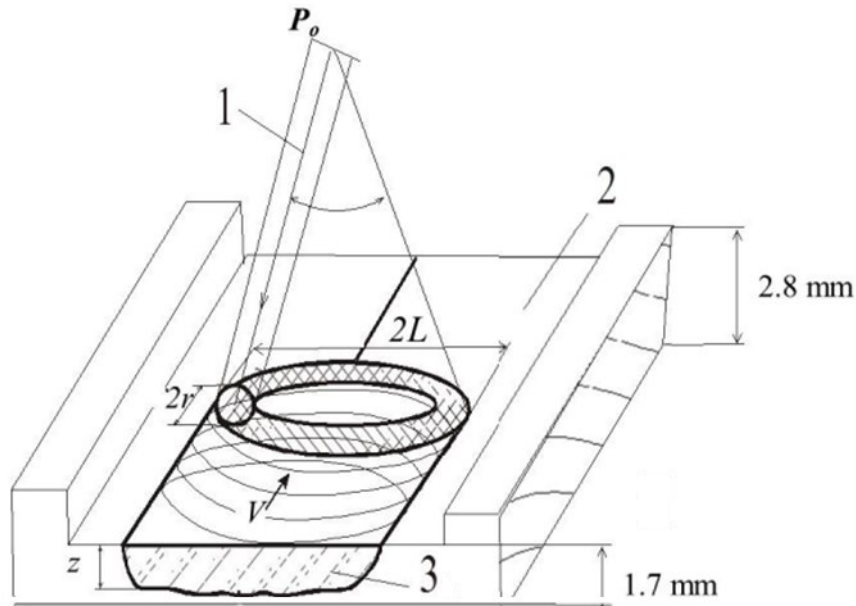

Figure 2.5: A schematic of the EBW of niobium sheets: 1, the electron beam (P_0, power of beam; r, radius of slightly defocused beam on the surface; L, scanning amplitude; V, beam velocity); 2, Nb sheets; 3, melting zone (z, depth of the melting zone)

For the last 40 year, a significant improvement and developments has been achieved [68], [69]. Simultaneously, the quality of industrial niobium increased, by elimination of undesired contaminants such as Ta, W and more difficult ones: carbon, oxygen and nitrogen. The development of Ultra-High Vacuum (UHV) technology contributes as well to the purity of Nb material. As a results, some companies are already in the grade to produce enough quantities of niobium of RRR 300 quality.

In the case of Cu, the internal surface quality may be an issue for such approach, for example, high temperature might cause voids and bubbles like defects, optically invisible. Naturally, the seamless technology for Cu/Nb approach is not only theoretically better but shows a superiority to the EBW cavities in practice. E.g., for HIE ISOLDE (High Intensity and Energy Isotope Separator On-Line Device) it was studied the effect of EBW of the Cu QWR [51]. Until now, no superiority over EBW cavities of the seamless approach has been demonstrated for bulk Nb cavity production.

Summary: deep drawing and eventual EBW has become a standard formation path for the Niobium cavities, despite the complexity of the protocol required for the SRF cavities production, it is good industrialised, has proven within years and - what is important, has enabled to achieve close to theoretical limits of Niobium SC performance.

The forming process of resonator has to be economically appropriate and enough easy to be industrialised, ideally without additional problematics to the technology. The production of a series of cavities made of Nb may require millions of euros. Any possible enhancement is considered beneficial. Thus, seamless technologies are at a constant search and developments. Nowadays, more and more attention is brough by spinning, hydroforming and electroforming technologies, that are finding it application mostly in the SC thin film approach (see details in the next chapter 2.2.2). For the bulk niobium deep drawing and EBW has become a standard and well explored way of production.

2.2.2 *Alternative methods*

New accelerators require well-industrialized mass production of multi-cell superconducting cavities. According to Palmieri [70], considering the crude cost of production a TESLA type cavity consists of two main parts: material and fabrication costs respectively. Taking a 20.000 cavity production and estimate weight of a single cavity of 25 kg, roughly 500 tons of Niobium metal is needed. Moreover, the requirement of 300 RRR size the available market. Additionally, waste is not considered but takes place. In case of fabrication cost analysis, equipment, tooling and manpower constitute the main expenses. A 9-cell cavity, for example, requires 19 EBW in critical only regions. Some of the welding might be done simultaneously in one vacuum run, that means that UHV must be established multiple times. Thus, may require tens of years for the 20.000 cavities production with such assumptions. All these pretty simple approximations led to the alternative' ideas that potentially may decrease the time of production, provide seamless production technology or significantly decrease the costs. In the next sub-chapters the most notable alternative paths for the production of both bulk niobium or copper substrate for the SRF technology are presented.

2.2.2.1　Spinning technology

Spinning is a chip-less production method of forming axially symmetrical hollow objects. By the point deformation of a roller disk, almost any shape can be obtained under the axial or radial motion (see **Figure 2.6**). The spinning is also characterised as a tension-compressing forming process, as the tangential compressive and radial tensile stresses are obtained similarly as in deep drawing. Any cold-forming material can be used for the spinning method being able to achieve elongations more than 1000% [70].

In 1994 Palmieri have come to the manufacturing of the Nb and Cu elliptical cavities via spinning technique [71].The processing is industrially simple and, does not require ultra-high vacuum. A planar disk sheet of oxygen-free High thermal conductivity copper OFHC (or high purity 300 RRR Nb) is pressed into a rotating mandrel with a conical frustrum shape. The formation of the cylindrical cut-off part is done by substitution of the mandrel shape. The mandrels have a possibility to be collapsed and then extracted in the end of processing [72]. The final quality depends on the tenacity and viscosity of the applied lubricant: animal fat and soaps are considered less contaminant [70].
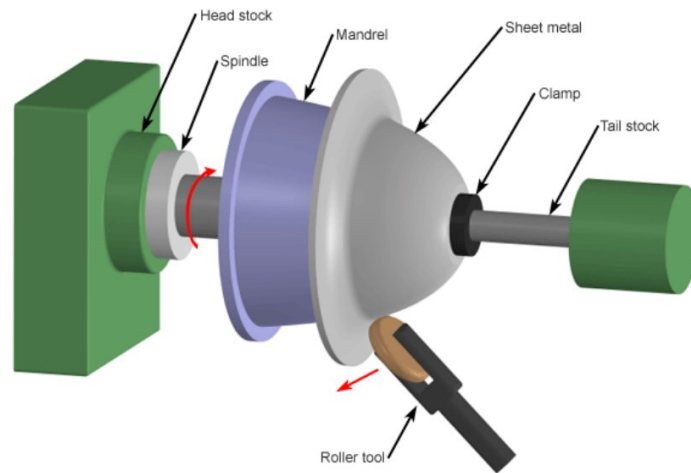
Figure 2.6: Spinning method [73]

Multi-cell cavities can be spun either starting from the circular blank sheet or from the tube. In the last case spinning is easier and the cavity wall thickness guarantees more uniform values. Spinning from the sheet blank is started from the formation of the conical preform and then into a cavity shape. Cell by cell, the material is shaped in a frustrum that decreases the wall thickness and changes shape as more cells are spun.

As it was mentioned before, the absence of the defects plays a significant role in the resulting performance of the resonant cavity, thus elimination of the EBW processing is a valuable step for the production technology. According to the authors, the spinning technology is at least 5 times cheaper than its competitor [74]. The production of the seamless single-cell and multi-cells 400 MHz, 1.3 GHz, 6 GHz has been successfully obtained and industrialised with Piccoli Sr.L (see **Figure 2.7**).

Figure 2.7: Spinning formed resonant copper cavities: 500 MHz, 1.3 GHz, 6 GHz

Summary: very promising approach that has found its application (HIE-ISOLDE, ALPI accelerators) providing a relatively fast way to produce seamless resonating structure of various elliptical forms including complex 9-cell cavities. As an advantage can be as well listed simple industrialisation, economic gain. However, the process is mostly relied on the operator (but automatization is still possible) and his skills, mood etc. A characteristic defect left after the mandrel extraction inside the cell is the main drawback, that normally is addressed via mechanical treatments and electropolishing.

2.2.2.2   Additive manufacturing

Additive manufacturing is a modern technology, which in theory can produce complex geometries, including closed cylindrical ones without the need of welding. Such innovative, emerging technology can be implemented in SRF protocols once current limitations are overcome. The limitation of such approach can be listed as: higher cost per cavity production, mainly for the clean precursor powder, the rate of stamping and scalability for the industry. As for the quality, it is often observed more roughness surface structure, due to the limitation of various techniques of AM. However, advanced surface treatments may polish the surface to the desired state, and thus, the community is yet to check the overall limitation and margins of such approach.

P. Figola et. al has demonstrated printed with powder-bed fusion AM technology prototype 3.9 GHz cavity design that was measured resulting in lower performance [75]. F. Motschmann has started a study on the possibility of improvements of the purity of the Selective Laser Melting (SLM) printed Nb to reach standards of the SRF technology. The purifying is done by vacuum firing and Ti-getter-heat treatments [76] resulting in values more than 100 RRR. The technique of interest AM can become not only for the SRF technology, but also for the RF applications [77]. Gerard R. has gathered the information with the latest advancements of such applications. Samples for Quadrupole Resonator, 6 GHz (half-cell) and complete seamless 6 GHz cavities were produced in Nb.

Recently, in the framework of IFAST project the DIAM group [78] started the study on the AM technology application into the SRF field. Together with INFN LNL and Rosler the research is ongoing. Till now it has been shown the possibility of Cu 99,99% density printing together with the polishing studies achieving the < 1 μm Ra roughness, suitable for the EP (see **Figure 2.8**). More details are presented in the chapter 6.7.4 dedicated to the 3d printed samples experiments.

Figure 2.8: 6 GHz samples printed for the IFAST collaboration research

Summary: relatively modern way of additive approach for the formation has opened a new possible path for fabrication of the resonant cavities. Current status of the technology allows to print both Nb and Cu with a density close to the 100%. A high price for the production is one of the drawbacks. (machines, powders, time). Additional attention must be paid for the surface preparation, as the technique does not allow to provide roughness lower than few µm. Till now, there is no information on the possible SC performance (E_{acc}, Q_0), so the application is still quite immature.

2.2.2.3   Electroforming

Galvanoplastic is a well-known technique in the electrochemistry (more specifically in electrodeposition technologies), and it is as well noted in seamless cavity production [79]. At the same time only. Copper may be deposited from the classic water-based solutions; in the case of Niobium, electroforming might be enabled in the bath of melted Nb salts or with another physical approach (e.g., Organometallic CVD) [80], [81].

Such approach was studied back then in 90s and has recently obtained a new application at CERN [82], [83]. To minimize any possible sources of defects, it was proposed to form the Cu substrate on the sacrificial mandrel with a further deposition of the superconductive layer. Aluminium metal is proposed as a mandrel, that is relevantly easy to dissolve, and Cu as a material for the substrate.

A technology of thick electrodeposition normally relies on surfactants and additives of organic base to enhance the structure formation or electro impulse regime. In the case of recent CERN approach this problem is not considered, as the Cu thin film is deposited via Physical Vapour Deposition (PVD) and the rest of the thick layer is not required to be as good as the PVD film.

The proposed technology will consist of series of steps (see **Figure 2.9**):

1. The formation of the Al mandrel
2. Copper PVD onto the mandrel
3. Copper electroforming via electrolysis
4. Dissolution of the Aluminium.
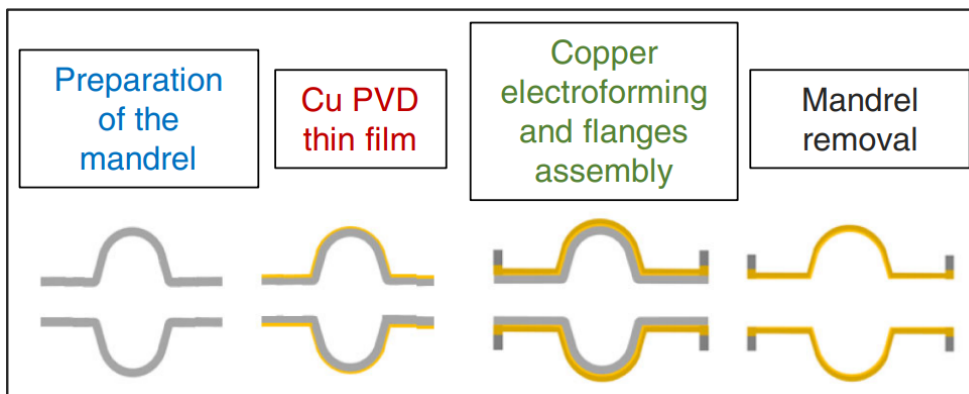
Figure 2.9: The main steps of the production process: preparation of the mandrel, copper thin film coating by DC magnetron sputtering, the electroforming of the cavity, and the removal of the mandrel

It is reported [83], [84] that electroformed cavities are having similar or better mechanical and cryogenic properties than OFE copper. Unfortunately, it was reported the non-uniformity of the copper thickness distribution along the cavity.

Summary: electroforming cannot be described as something completely new, however it is still promising, being able to deliver internal surface with a high quality, not less than a forming shape. However, the need to have a good starting mandrel is also a limiting factor; moreover, it is also noted quite long electrodeposition, and the need of the dissolution of the initial mandrel.

2.2.2.4 Hydroforming

Another attempt to get a seamless elliptical shape resonant cavity was firstly shown by Cornell University and later by CERN [85], [86]. Later additional studies showed the advancements in

2015,16 years [87], [88]. Basically, the process contains several steps shown in the **Figure 2.10**. Starting from the initial Nb tube with a good formability. The iris parts are formed by Neckin process, by pludging the two counter rollers meanwhile the tube is rotated. After the complete of all Necking parts, the annealing is required. The next part is the equator, and it is formed by hydroforming using the external dies; in that case the internal diameter is increased from 130 to 160 mm. The external hydraulic pressure is applied to the Nb cylinder, meanwhile the swagging it axially. It is reported that internal pressure is raising up to the 25 MPa.
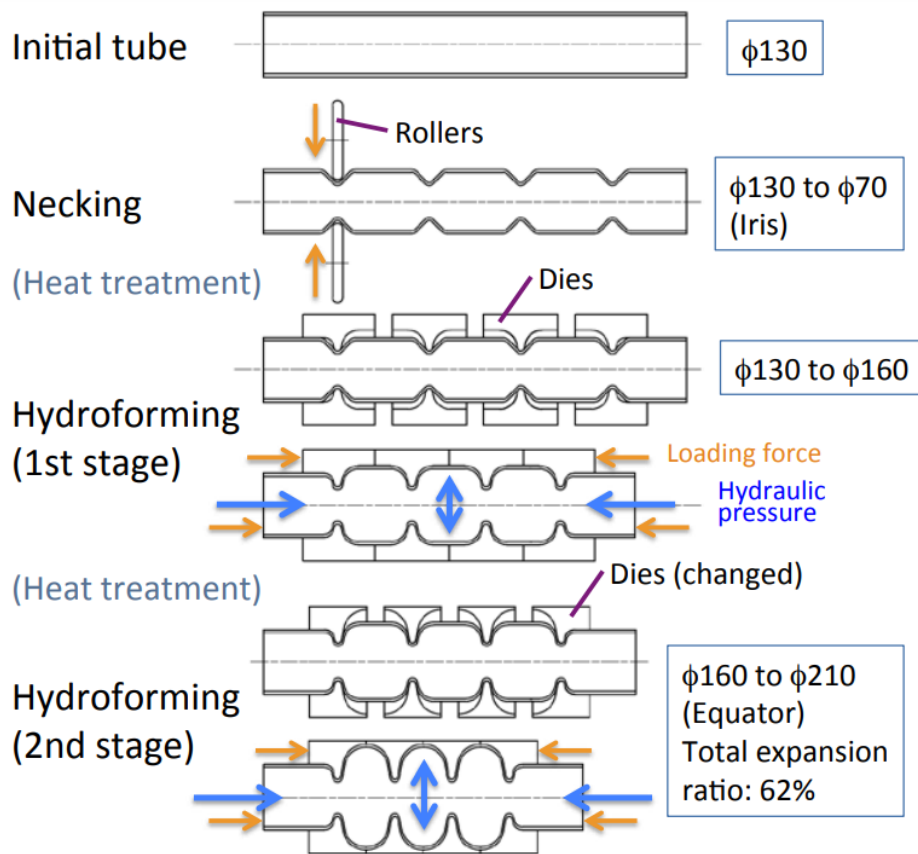
Figure 2.10: Process of necking and hydroforming.

A series of private companies has invested in the research of electro hydro-forming technique to produce seamless shape resonators. Unfortunately, the complexity and difficulties they have encountered led the industry to focalise on the welding of the two half-cell together. A continuous optimisation of the process is going at various research institutions: JLab, DESY, and others [67], [89].

Summary: quite classical approach has shown as a promising path for the seamless technology. According to Palmieri [74] Hydroforming has three minor drawbacks (see as well **Figure 2.11**):

1. The hydroforming machine is suitable only for the cavity shaper for which it has been designed. A different cavity geometry requires new machine design.

2. The thickness uniformity of the starting tube required for hydroforming is vital. Even a small variation in the tube wall could affect the resistance of the wall portion under pressure and consequently fracture meanwhile bulging.

3. Only the outside shape of a cell can be precisely formed. The accuracy and reproducibility of the inside structure exposed to the RF fields depend on the wall thickness, that naturally changes with hydroforming.
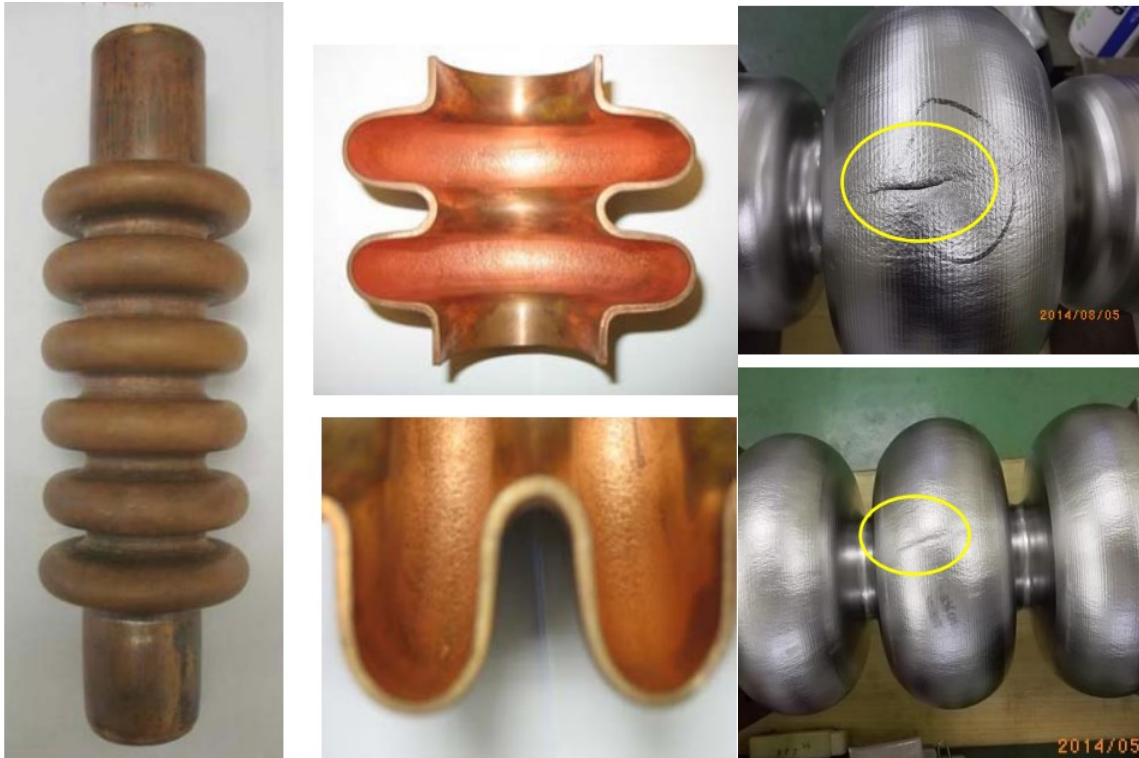
Figure 2.11: Hydroformed Cu and Nb cavities that may present some difficulties [90]

However, the main limitation for such technology is the absolute need of multiple forming steps with intermediate annealing, which increases the complexity of the process [91], [92]

2.3 Mechanical preparations

The problematic defects and contaminations are the key reasons why the mechanical treatments can be applied to the SRF substrate. The superior technologies of production discussed below, often cannot produce absolute defect-free surface, resulting in the need of some preparation steps before more fine chemical polishing. In case of EBW welding, such regions require additional curing, such as mechanical polishing. Some examples of the defects found are presented below (see **Figure 2.12**).

The mechanical polishing is basically the first and one of the important steps for the cavity preparation, which is aimed to remove visual defects, scratches, residuals etc.

A high productive mechanical polishing is a key step of the continuous research and development phase but also not less important at the production stage. It can be a key to push the limit of studies involving other materials than SC Nb for RF application.
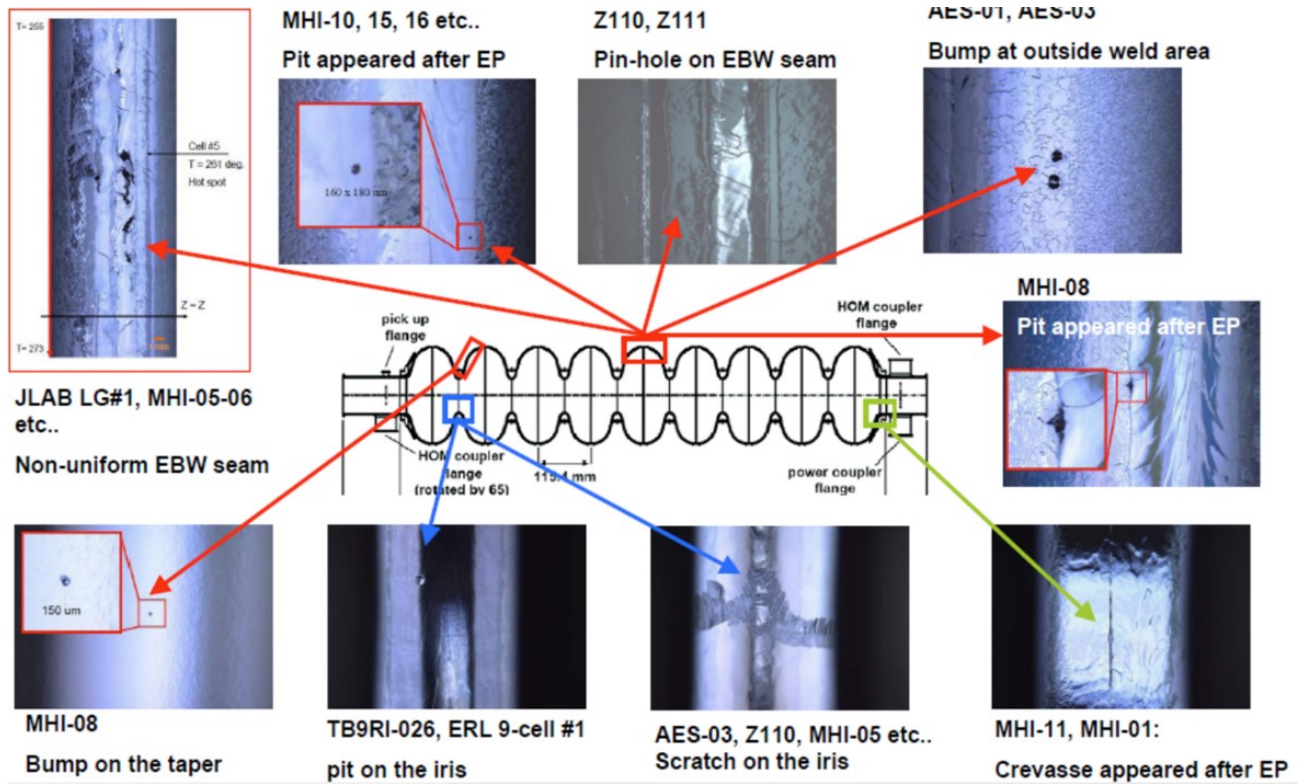
Figure 2.12: Geometrical defects found by optical inspection in the 1.3 GHz 9-cell cavity [93]

2.3.1 Protocolled treatments

2.3.1.1 Tumbling

A second example of mass finishing mechanical treatment process is presented by tumbling, that has widely found its application in the industry and only a limited application in the superconductivity field. The principle that stands behind it is the use of abrasive for polishing and smoothening a surface during rotation, translation and inversion movements (see **Figure 2.13**) [73]. Optimal parameters for a specific material to be treated are determined by the weight of the materials, speed of rotation, quantity and level of both abrasive, presence or absence of liquids and additives. The polishing procedure for the superconductive resonators can be also done without a barrel by putting the media inside the resonator, and providing a rotation, causing the mechanical impact onto the internal surface. Such a particular setup has been used at LNL (see **Figure 2.14**) successfully treating the QWR resonators.
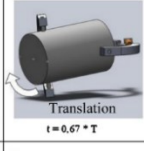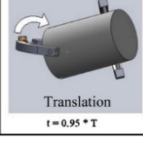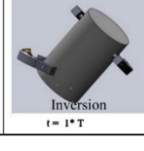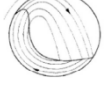
Figure 2.13: Turbula motion made with Solidworks® and Flow mode in a rotary drum according to Mellmann [94]

One step treatment is being used at LNL to treat QWR, in particular putting abrasive in the form of pyramids, soap and distilled water mixture, that is being placed for 48h of continuous treatments.

Figure 2.14: A tumbling system at the Legnaro National Laboratories of INFN

Summary: tumbling is a simple technology, that has been applied more than 20 years ago, and it is able to deliver uniform surface treatment for the future chemical polishing. However, it requires significant amount of time and thus is not able to completely elimination of deep defects.

2.3.1.2   Centrifugal barrel polishing

Centrifugal barrel polishing has become a standard treatment for the elliptical resonators in industry starting from 1990s. The first report on successful usage of the CBP onto SRF substrates

belongs to the KEK (High Energy Accelerator Research Organisation) Kenji Saito & Tamawo Higuchi. The proposed technology was steadily studied and approached in many other laboratories: Jefferson Lab, Fermi Lab and Cornell University in the US, Deutsches Elektronen-Synchrotron in Germany, Laboratori Nazionali di Legnaro in Italy, and Raja Ramanna Centre for Advanced Technology in India. A scheme of a standard CBP machine is presented below (see **Figure 2.15**):
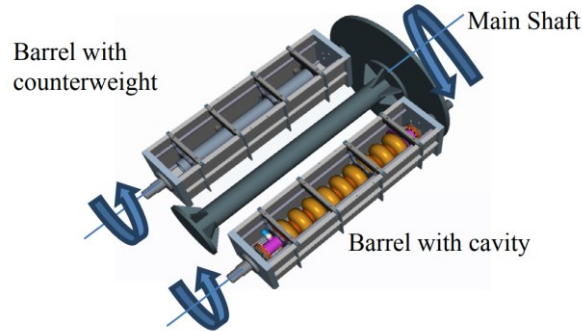

Figure 2.15: A scheme of the CBP machining of a 9-cell Tesla – type cavity [95]

The principle of the polishing is achieved by mechanical actions, that take place inside a closed environment (barrel), where a relatively cheap and ecological friendly abrasive is inserted. The barrel is subjected to the rotation around its own axis. In a meanwhile, the cavity is being forced to rotate in opposite directions, so that creating an outward force of inner (see **Figure 2.16**) [96]. It is similar to the tumbling processing, with the difference, that in case of tumbling, it involves only one rotation around axis, and so considerably longer treatments time. CBP can use similar recipes that are availible for tumbling.
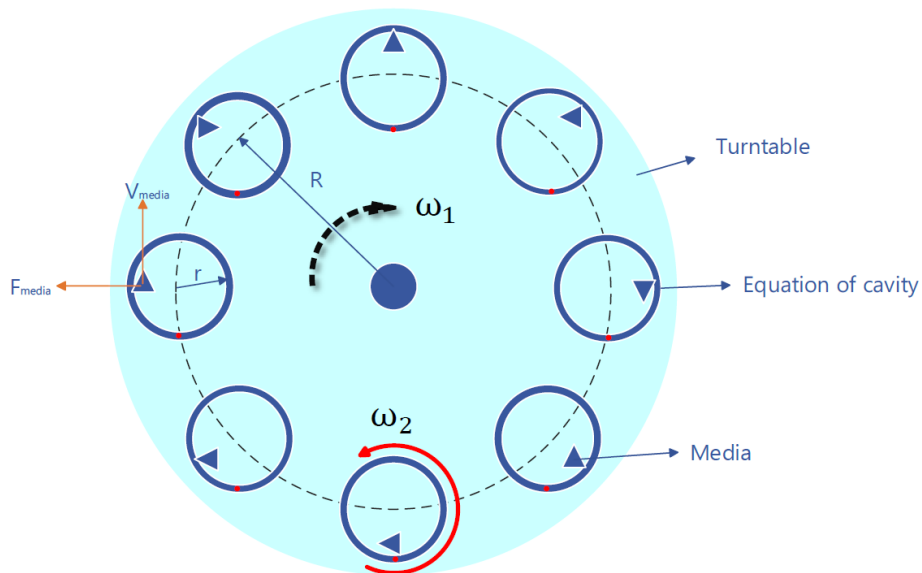

Figure 2.16: a scheme of the forces in the CBP. The red point (•) is the reference point of the position where the angular velocity (ω_2) of the barrel related to the turntable equals to 0 [73]

The tangential velocity of the sliding media on the walls of the cavity is calculated as in the equation:

$$V_{media} = (\omega_1 + \omega_2) \cdot r \tag{2.1}$$

Where ω_1 is the angular speed of the turntable, ω_2 is the angular speed of the cavity in the relation to the turntable and r is the radius of the cavity elliptical shape. The centrifugal force of the media is calculated as:

$$F_{media} = \frac{mV_{media}^2}{R+r}, \tag{2.2}$$

Where m is a weigh of a single particle of the media and R is the radius of the trajectory of the cavity.

A CBP system was built at INFN-LNL, which was able to maintain $w_2=0$, that were achieving relative high erosion rate [96], [97].

The filling of the cavity with abrasive in CBP processing are usually done up to the 50% of the volume of different media. The media can be used similarly as in other mechanical polishing abrasive technologies, in wet or dry conditions. However, the addition of water with surfactants can enhance the process in terms of final quality by cooling the cavity and continuous cleaning of the surface, preventing formation of the powder, which can decrease the etching rate.

Available media on the market are mainly done for tumbling, vibratory finishing machines that are commercialised the most. Moreover, speaking of Nb as a substrate to polish, the industry has little experience with its mechanical properties (soft and work hardens easily). Anyway, CBP can achieve nanometres scale roughness, that is absolutely suitable for post-processing with chemistry.

Typically, ceramics, abrasive cones made of various metal oxides (Al_2O_3, SiO_2, etc.), and carbides are used. These abrasives can achieve up to microns of material removal in an hour [97].

Summary: CBP is a powerful technique for the repairing defects presented in complex geometries like 9-cell cavities. Such mechanical polishing offers a list of advantages, like non-toxic chemicals processing, uniform polishing, smooth surface finishing, ease of industrialisation. Unfortunately, low erosion rate yields in long time of treatments (few-days). CBP cannot completely substitute further chemical treatments.

2.3.1.3   Grinding

Grinding is used to remove production defects, marks, and deep imperfections. Polishing can be referred to as a process that smooths out the defects after rough grinding. Grinding uses fixed abrasive particles that are bonded to the platen or a piece of hard paper. In contrast, polishing uses abrasive particles on paper that are surrounded by lubricant and can move freely over the surface.

Grinding mechanical polishing is a treatment, that uses a grinding tip, abrasive paper as a tool to roughly remove upper layers of a metal. It has found its application in the industry, as quick

and potent way to remove defects or apply local polishing. However, its usage is limited in the superconductive community, since most likely the grinding can produce additional stress to the upper layers, possibly leave higher quantities of abrasive as a contaminant. At LNL it has found its usage as a tool to treat inner surface of 6 GHz cavities, that were produced by spinning, and being able to remove relatively sufficient quantities of material, thus levelling the surface and removing the signs of mandrel, that can typically be found inside the cell (see **Figure 2.17**).

The brushing can remove micro-cracks and smooth the surface, thanks to the Scotch Brite cross shaped rotating tool, no contaminations is being added. As a part of the procedure, two dimensions of the abrasive is used, to ensure steadily lowering of the roughness down to 1-1,5 µm [29].
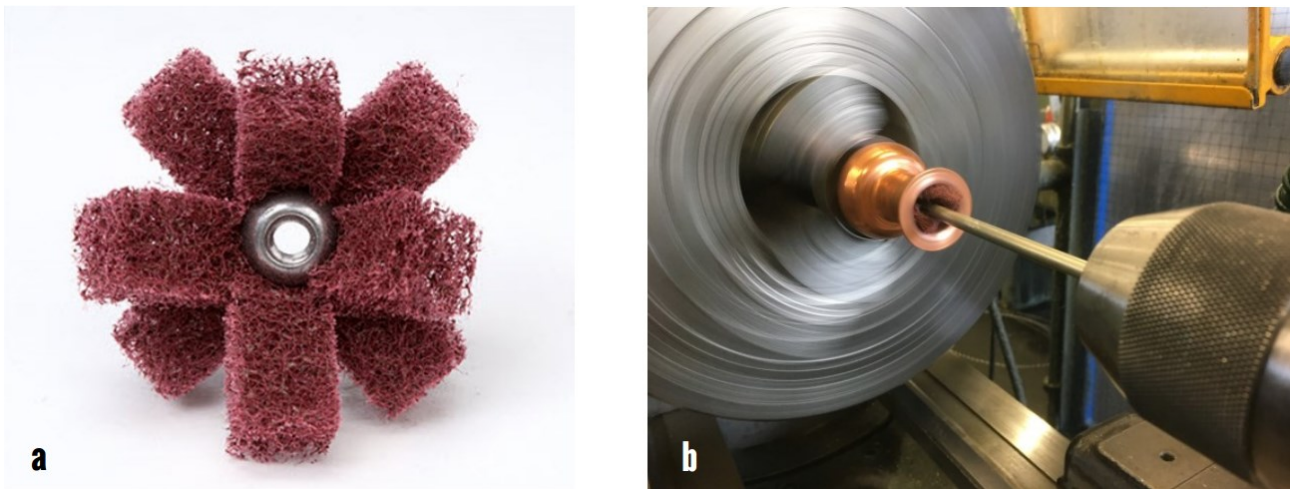

Figure 2.17: a) Scotch Brite™ cross shaped abrasive. b) Mechanical grinding of the 6 GHz monocell. The cavity is rotating while the operator press with the cross shaped abrasive tool on the internal cavity surface [29]

Even though the grinding is a potent way to remove the surface impurities and defects, some of them, mostly the deep ones might remain.

Summary: well-known in industry, the grinding is a relatively fast and potent tool to treat mostly locally (in case of big resonating structures as 9-cell cavities), are used only in the case of verified need to cure a half-cell. In case of 6 GHz, it is practically applied to all internal surfaces, resulting in uniform, but scratched surface. The main advantage is the possibility to apply for a fast curing the resonator, to avoid long treatments (as centrifugal barrel polishing or vibro-tumbling).

2.3.2   Other mechanical treatments

2.3.2.1   Vibro-Tumbling

A particular case of a tumbling, that still uses mass-finishing approaches, that is accomplished with additional vibrational force is called Vibro-Tumbling. First time described by Guolong in 2013 [96], it was used the classical industrial approach, that consisted of the application of an eccentric vibro-motor and connected to the transformer, that variates the working frequency (see **Figure 2.18**).

As a result, a high frequency of up to 400 Hz was achieved at LNL. The limiting performance issue in the case of relatively small 6 GHz cavities is always the volume of the abrasive, that does not permit a flow of abrasives, and a limited quantity of liquid. As a result, relatively higher removing rates were achieved, respect to the CBP and Tumbling methods. However, only in 2019 [98] it was possible, completely avoiding grinding mechanical polishing, which was a standard treatment in the deck of treatments for 6 GHz cavities, thus allowing for a more uniform and less defective surface that is ready for the final micro-roughness levelling. Until now, the application of that technology was limited to the LNL laboratory and small-form factor cavities. Additionally, it seems to be the only working solution to smooth the internal surface of the cavities that were 3D printed.
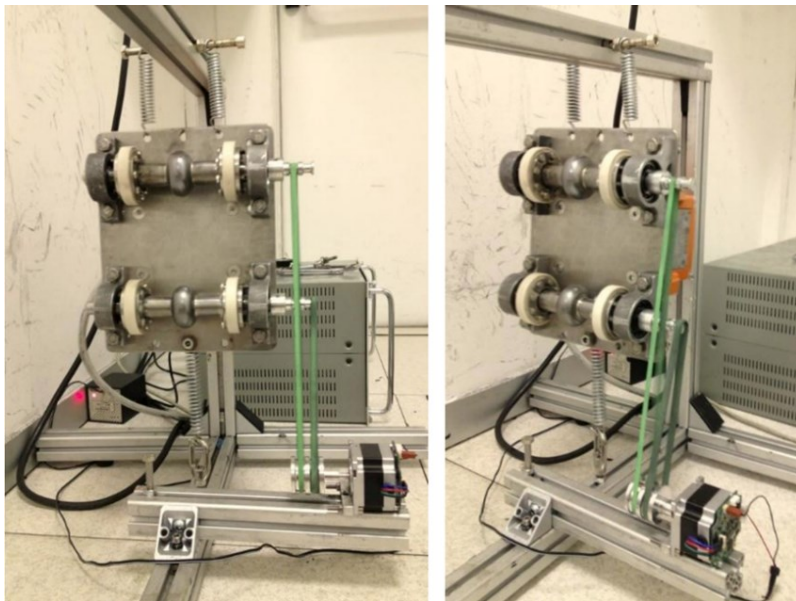

Figure 2.18: A photo view of the first generation vibro-tumbling machine built LNL [96]

Summary: A vibro-tumbling is a new-generation of tumbling and CBP approaches, resulting in significantly increased erosion rates and uniformity. Despite the vibratory finishing isa a well-known industrial method, till now it has found its application exclusively at LNL facility for the 6 GHz cavity. The drawback is mainly concerning the limited application and the inability to cure pitting-like defects.

2.3.2.2 Metallographic polishing

Metallographic polishing is a case of mechanical polishing where the normal and tangential forces are induced by a constant pressure of the workpiece onto the rotating disk with loaded abrasives. It consists of three consequent sub-process (see **Figure 2.19**) that can be named as grinding, lapping, polishing with a final scope to relieve the bulk surface of the substrate for further examination (see figure 3.7 of the visual representation of every process included in the metallographic polishing and the abrasive used [99]). Different metals with its hardness and ductility properties require define

and different type of processing accordingly. Moreover, metallographic polishing should not leave additional defects and stresses, or more precisely minimise them.

The first part of the procedure is grinding, that is a rough method to remove upper layer of defects (inclusions, scratched, voids). The abrasive size at this stage typically varies from tens to hundreds of micrometres. The following step – lapping, is in fact a process that uses lower grain sizes (typically from few to tens of micrometres). The main scope is to reduce previously created defects and damaged layers but also to planarize the sample and naturally decrease the roughness. The final step is devoted to the fine polishing that uses down to the tens and hundreds of nanometres scale abrasive. As a result of consequence decrease of abrasive scale, the removal processes as well are diminishing. Hence, the polishing step is able to produce a scratch free, glass-like reflective surface.
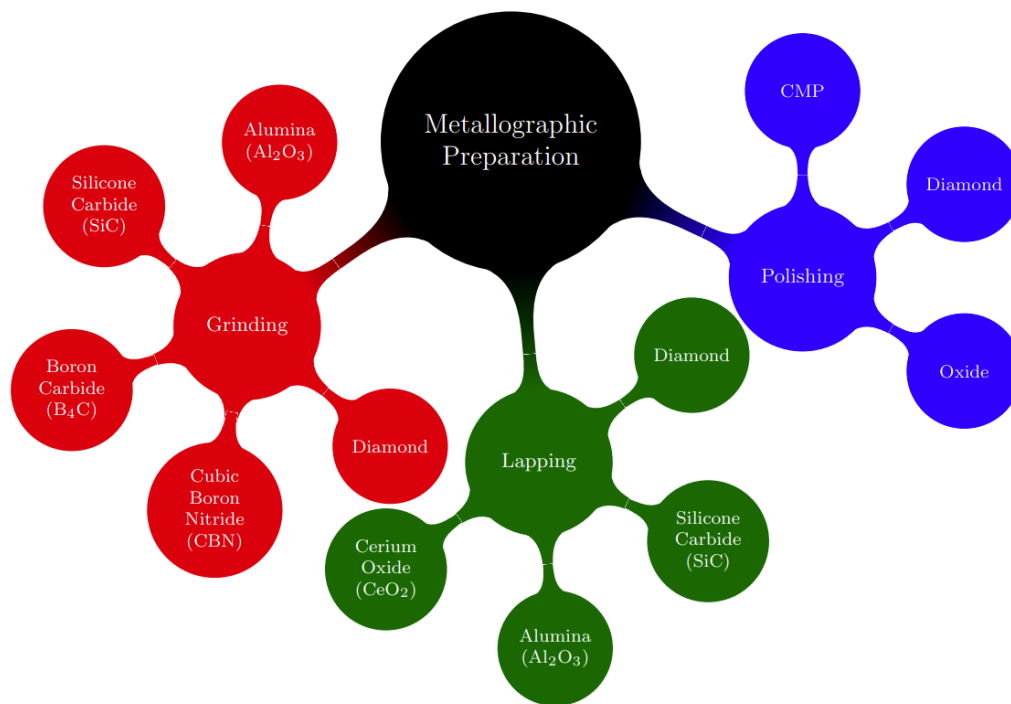

Figure 2.19: A scheme of metallographic preparation with a division on main steps: grinding, lapping and polishing three families: diamonds, oxides (silica, alumina, cerium, chromium, ferric) and chemical-mechanical polishing (CMP) [99]

The CMP technique is exclusively used to treat planar surfaces, which limits its application in the SRF field. However, as it has been studied and developed for years in the scientific community, many valuable achievements and recipes are already available. To solve this problem of application, a proposal was made by a group [99], [100], to apply metallographic polishing to the Nb (Cu) forming sheets prior to the formation of the elliptical shape. After the formation, a light chemistry is needed to ensure the low roughness and contamination of the upper layers. According to their publication, the so-called damaged layer, will not be formed deeply, and a light EP will eventually remove all the remaining defects.

Polishing and CMP

Chemical-mechanical polishing also known as Chemical-mechanical Planarization is a process of a surface levelling and polishing that uses a combination of synergetic actions of mechanical and chemical processes (see **Figure 2.20**). A diluted solution of etchant is used as a media, ensuring activation of the surface. The technique is used mostly for ductile materials, refractory and transition metals, multiphase alloys and coatings. The process uses an abrasive and a chemical slurry (colloidal solution with a low-dispersion particles) with a combination of a polishing pad.
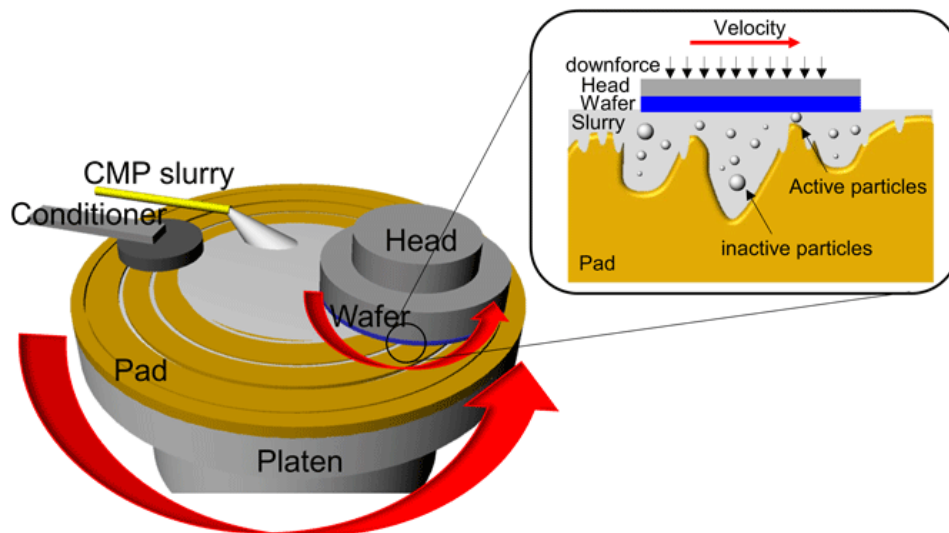
Figure 2.20: A schematic view of the CMP [101]

An advanced version of CMP is Chemical-Mechanical Electro Polishing (CMEP), which uses both mechanical and chemical actions similar to CMP. Additionally, it utilizes the phenomenon of electrochemical dissolution, which occurs when a positive charge is applied to the treated surface and a negative charge (the cathode) is applied to the rotational pad with a cloth saturated electrolyte system connected to a DC power supply. The use of an alternate current mode with a relatively low frequency may further improve the polishing quality for a selected metal system. Currently, it is predominantly used in the semiconductor industry and finds significant application as a sample preparation technique for metallographic studies.

Summary: metallographic polishing is a well-known polishing method in materials science and semiconductor industry. However, it was not applied in the SRF field due to the requirement of planarity. Nevertheless, the proposed approach of forming a cavity after MP could be used for the fabrication of elliptical cavities, leading to a decreased reliance on chemical polishing. The advantages of metallographic polishing include easy technology with a high erosion rate, exceptional uniform polishing, and a clean surface processing. However, the presence of minor and limited damages cannot completely replace the chemical phase of preparation [102].

2.4   Chemical and Electrochemical treatments

The chemical treatment of surfaces has been used since the 19th century, with electrochemical treatments becoming an increasingly important part of the field with further development and study. Such treatments allow the modification of a metallic surface with a minimal risk of defecting the surface. Any mechanical imperfection is excluded to be produced at all, thus making this path a primary in most fields of industry – medical, semiconductor, automotive, precise metals, and others.

Chemical and electrochemical treatments are commonly unavoidable treatments in the SRF substrate preparation protocols, taking a specific aim to remove any possible impurities, contaminations and defects producing a perfect surface. A certain level of a desired surface quality can be achieved only after mechanical polishing steps, since one of the main limitation properties for the chemical and electrochemical polishing is a starting value of a roughness of the substrate to be treated. A second major difference between industrial polishing and SRF preparation treatment arrives in the need to remove hundreds of micrometres of surface, ensuring the first requirements mentioned above.

Meanwhile, chemical polishing methods have found their application. However, a commonly agreed-upon superiority of electrochemical polishing has been found, resulting not only in lower roughness, but also in higher quality factor and accelerating gradient. In this chapter it will be provided literature review on the chemical polishing treatments (Buffered Chemical Polishing (BCP) and "SUBU").

2.4.1   Bulk Nb chemical treatments

Chemical polishing is often used as a quick method of achieving visible results, rather than as a means of preparing a perfect surface. However, in cases where it is difficult to obtain a deformation-free surface by other means, such as with very soft metals or when other difficulties arise, it may provide the best method of preliminary or final preparation. Refractory metals, such as Zr, Hf, Nb, Ta, and V, are often subjected to chemical polishing after mechanical polishing to improve their polarized light response or to remove minor deformation. Such treatments are relatively easy to apply, as they typically only require placing a substrate into the working solution to achieve a relatively uniform surface attack. Chemical polishing solutions must decrease micro-roughness, improve reflectivity, and remove some upper layers. In industry, these solutions are typically not used to remove more than 1-2 μm, as the tolerances may be significantly compromised, which would prevent, for example, a fillet from functioning properly. However, these methods are very useful for complex geometries where the surface is difficult to treat using other methods, such as electropolishing. Although chemical polishing can smooth the surface, the polishing level is typically lower than that achieved by electropolishing the same metal.

A list of available commercial and scientific solution for a list of metals is given below in Table 2.1 [103].

Table 2.1 – Some common chemical solution of Cu polishing

Formula of the bath	Temperature	Time	Agitation
25 mL H_3PO_4 85% 25mL glacial acetic acid 25 mL HNO_3 65%	55-80 °C	2-4 min	Yes
65 mL glacial acetic acid 27 ml H3PO4 85% 6 mL HNO_3	60 °C	1 min	
30 mL HNO_3 65% 10 mL HCl 32% 10 mL H_3PO_4 86% 50 mL glacial acetic acid	70-80 °C	1-2 min	Yes
35 mL H_2O 40 mL HNO_3 25 g CrO_3			

2.4.1.1   Buffered Chemical Polishing

A well-known solution in SRF community for niobium polishing is called Buffered Chemical Polishing (BCP). The name was given to control niobium etching and it was studied in-depth in references [104], [105] (see Table 2.2). BCP is a relatively easy way to remove 50-200 μm thickness of the damaged surface, and this recipe is used exclusively in some laboratories [106], with no usage of electropolishing. However, while electropolishing solutions can brighten and smooth the surface simultaneously, BCP provides etching with a resulting rough and bright surface.

Table 2.2 – Available polishing recipes for Nb substrate

Bath Name	Formula of the bath	Concentration ratio	Temperature	Removing speed
CP	HF Hydrofluoric acid (48%) HNO_3 Nitric acid (65%)	1:1	15-25°C	2 um/min
BCP	HF Hydrofluoric acid (48%) HNO_3 Nitric acid (65%) H_3PO_4 Phosphoric acid (85%)	1:1:1 1:1:2 1:1:4	15-25°C	0,8 um/min 0,6 um/min 0,2 um/min

The mechanism of niobium polishing has been extensively studied and can be summarized by three main reactions: oxidation of niobium (2.3 and 2.4) and subsequent dissolution in hydrofluoric acid through various reactions (2.5, 2.6). The formation of semi-stable species, such as H_2NbOF, , has also been observed. These species undergo hydrolysis and further dissolution in hydrofluoric acid to form NbO_2F (2.8).

$$2Nb + 5NO_3^- = Nb_2O_5 + 5NO_2 + 5e^- \tag{2.3}$$

$$6Nb + 10HNO_3 = 3Nb_2O_5 + 10NO \uparrow + 5H_2O \tag{2.4}$$

$$Nb_2O_5 + 10HF = 2\ NbF_5 + 5H_2O \tag{2.5}$$

$$Nb_2O_5 + 6HF \Rightarrow H_2NbOF_{5(soluble)} \tag{2.6}$$

$$NbO_2F \cdot \frac{1}{2}H_2O + 4HF \Rightarrow H_2NbOF_5 + 1.5H_2O \qquad (2.7)$$

$$Nb_2O_5 + HF = H_2NbOF_{5(aq)} + HNbF_{6(aq)} + NbF_{5(aq)} + H_6NbO_2F_{7(aq)} + H_2NbF_{7(aq)} + H_2O \qquad (2.8)$$
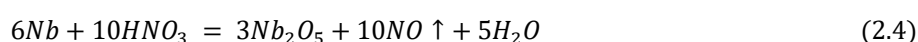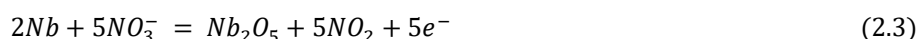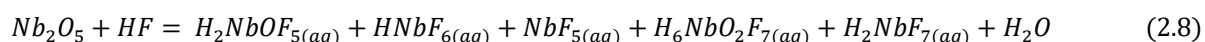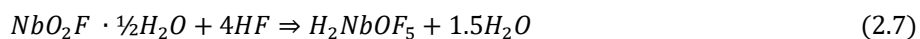
Empirical observations have shown the presence of the so-called layer of products, which, like the viscous layer in electropolishing, limits the dissolution of the metal and determines the smoothing. However, there has been discussion about an alternative solution where classical phosphoric acid is substituted with sulfuric acid, as in electropolishing. It has also been proven that there is a direct connection between the etching rate and processes such as diffusion and convection. Empirically, it has been shown, that a buffer is needed to prevent pitting, similar to SUBU, using concentrated and viscous acids such as phosphoric or sulfuric acids. By adding a buffer component, the etching rate is steadily decreased due to the high viscosity and lowering of the relative concentrations of the active components (hydrofluoric and nitric acids). Roughness profiles of fine-grained niobium on distances of 0.1-100 μm have been reported to be higher by at least an order of magnitude compared to electropolishing [107]. Differential etching of niobium based on crystallographic orientation has also been observed. Notably, large or single-crystal grain niobium structures have been shown to produce much lower roughness profiles [55, p. 201], [108], [109]. Another empirical study showed, that electropolished niobium can sustain higher field peaks than chemically treated niobium [48], [110]. This could be due to differences in roughness or other factors.

For relatively small parts cleaning the BCP consisted of immersing the substrates into the acid mixture for a certain amount of time with provided cooling and agitation if needed. In case of large cavity etching, a closed system with acid mixture circulation is required (see examples on the **Figure 2.21**). At Jefferson lab, a vertical stand is used, where the tank is cooled down to the 10 C° and then the cavity is pumped from the bottom. The acid temperature should be kept below 15 C° to reduce the hydrogen contamination, which can cause severe degradation of the performance (see chapter 1.5). The non-uniformity of the polishing between the top and bottom part of the cavity is addressed by flipping the cavity during the second cycle of the BCP. The etching is finished with the thorough rinsing with de-ionised water and followed by high pressure rinsing to remove the residuals after etching.

Figure 2.21: BCP facilities at different laboratories [111]

2.4.1.2   Electropolishing of Nb

Electropolishing is a well-known technique, that finds its use in various fields to achieve gloss and mirror like surface of the metal part. The main advantage of this technique is that the surface is treated chemically, so that there is no propagation of possible defects as in mechanical treatments. Basically, the process is a local case of electrolysis, in which the anode – is a working piece to be treated, and the counter-electrode is a cathode, that normally is following the shape of a treated piece. There are many studies of the process since it was discovered back then in 1930. From that moment, most of the known metals were successfully electropolished via many recipes. A general view of the current (current density) vs voltage curve is shown below (see **Figure 2.22**). At least 4 zones can be identified: 1) active dissolution (*etching*), 2) *passivation*, 3) *polishing*, 4) oxygen evolution (consequently for some metals *pitting* formation).
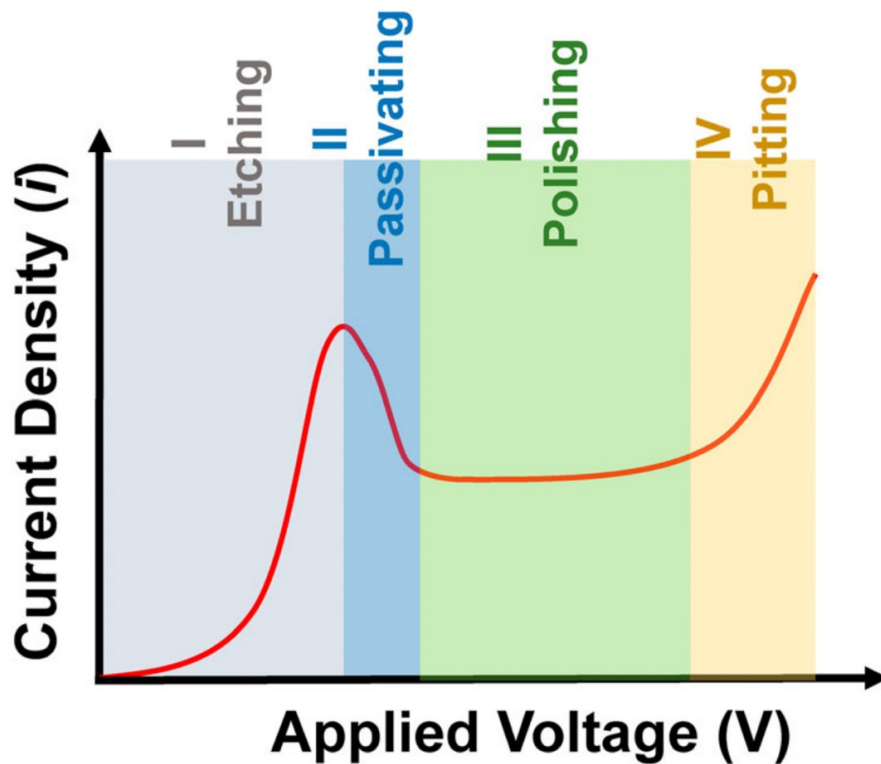
Figure 2.22: A typical voltampere diagram of the EP process

During the process, as in all electrolysis-based process, there at least two reactions that take place on each of the electrode's surfaces. The oxidation-based reactions are evolving on the surface of the anode, that is in case of electropolishing – dissolution of metal into the soluble compound. The reduction process on the counter electrode, can be represented by the reduction of the metal ion in the form of deposition.

W.C. Elmore was the first to propose the theoretical aspects of the electropolishing process [112], [113]. Later, the new theoretical aspects of the mechanism of electropolishing was risen by J.

47

Edwards [114]. Carl Wagner has done a mathematical study which corresponded to the theory proposed by Edwards [115]. Additional contributions by Overbeek [116] and Grahme [117] on the double-layer and general theories presented by Bockris [118] and Brying [119] focused on the processes that take place at the anode and cathode during the electropolishing. A recent study of the EP of Cu in phosphoric solutions and Nb in $HF:H_2SO_4$ showed the acceptor species are the limiting factor of the process, that diffuses to the surface [57].

Electropolishing of Niobium was originally developed at Siemens in 1971 [120], and it was brough to the attention of SRF community by Saito in 1997 [121]. As a main solution it was proposed a solution based on hydrofluoric acid 48% and sulfuric acid 98% in the volume ratio of 1:9. A common sense of understanding the reactions that take place are listed below:

$$2Nb + 5H_2O \rightarrow Nb_2O_5 + 10H^+ + 10e^- \tag{2.9}$$

$$Nb_2O_5 + HF \rightarrow H_2NbOF_{5(aq)} + HNbF_{6(aq)} + NbF_{5(aq)} + H_6NbO_2F_{7(aq)} + H_2NbF_{7(aq)} + H_2O \tag{2.10}$$

$$NbF_5 + (SO_3, H_2O) \rightarrow NbF_3(SO_3F)_2 \cdot 2H_2O_{(aq)} + Nb_2O(SO_4)_{4(aq)} + S_2O_5F_2 \tag{2.11}$$

$$2H^+ + 2e^- \rightarrow H_2 \uparrow \tag{2.12}$$
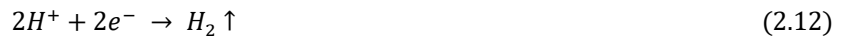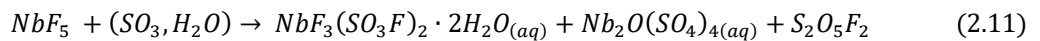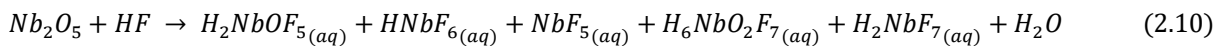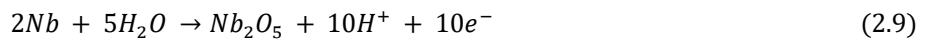
The process of the electropolishing has been adapted in a horizontal scheme at KEK (see **Figure 2.23**) with the following parameters see Table 2.3:
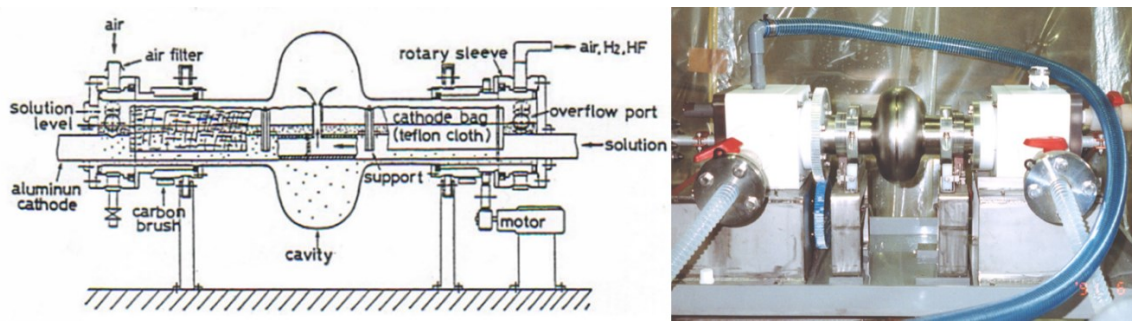
Figure 2.23: A scheme and a photo of the general EP horizontal configuration [46]

Table 2.3 – Parameters of Horizontal EP (HEP) configuration [111]

EP Solution	1 part HF (48%), 9 parts H_2SO_4 (98%)
Temperature	20-40 °C
Voltage	10-25 V
Current density	10 – 50 mA/cm²
Acid flowrate	60 l/min
Rotation	0.4 – 1 rpm , 1-9 rpm
Polishing rate	~0.5 μm/min

Other laboratories as well have built their own variations of horizontal EP configuration (see **Figure 2.24**) together with optimisation of the process state-of-art. At KEK vertical EP process was as well studied, however the H_2 bubbles was leaving the traces on the cavity surface [122]. The HEP has proven with a good SRF performance of almost 800 Nb elliptical 1.3 GHz cavities used in the European

XFEL. Horizontal configuration requires a massive and expensive setup to rotate the cavity with the solution and to finally raise the cavity in vertical position for an acid drainage and cleaning procedures. In HEP configuration the nitrogen fluxing is required to purify the internal volume from the extensive production hydrogen gas. This is possible, by the half-cell solution filling of the cavity, leaving a space for gases.
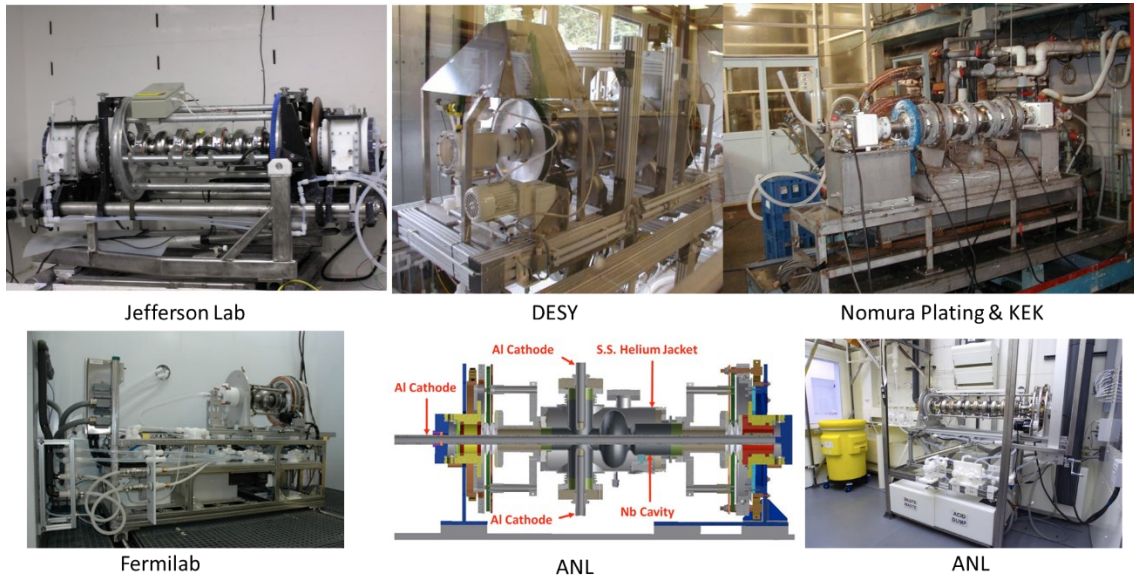

Figure 2.24: Horizontal EP setups for elliptical cavities at different laboratories [123]–[125]

An example of the newly commissioned horizontal EP system for electropolishing can be represented by the Jlab's structure (see **Figure 2.25**), that followed the lessons of SRF community providing reliable and well-controlled processing of the Nb cavities. Such system allows either 20 or 5 C° temperatures operating modes. The cooling is applied both on the circulating electrolyte acid mixture and cavity via water-cooling heat-exchanger, resulting in unformal removal [126].

Figure 2.25: New improved horizontal EP system at Jlab [126]

One of the main interests of the R&D of electropolishing was the temperature factor. The efforts were paid on precise temperature control to achieve a continuous large current oscillation

during the process. A so called "cold" EP was established in 2014 at Fermilab, when the cell surface was maintained at 16 C°. Lower temperatures as well produce less hydrogen gas, consequently less concentration of hydrogen may be adsorbed by the niobium cavity. This method enables achieving continuous large current oscillations during the process, and thus providing the uniform erosion in the cell. More than 2 hundreds of processes were applied on single cell cavities at Fermilab since that time. The key benefits of cold processing are: 1) low water concentration in the electrolyte, 2) low electrolyte flow [127]. Lower temperature decreases the diffusion and reaction rates, resulting in lower current density of the process. This can allow lower working voltage values, maintaining the polishing quality [128]. The cold temperature (13 C°) EP in most cases similar or even better than standard (22 C°) EP in low to middle voltage range (3-10 V) in terms of roughness. However, the situation changes, once the higher voltage is applied due to the pitting production in case of cold EP [129]. At Fermilab extra cold EP (-4 C°) is under investigation, resulting in even lower polishing rate down to the 2-3 μm/h [130].

A Vertical Electropolishing (VEP) is relatively simple and cost-effective way how to polish elliptical cavity. However, the VEP configuration provides nonuniform polishing rates and bubble traces are noted on the cavity surface. The reason for such issues are the hydrogen bubbles production that maybe trapped locally on the complex geometry, thus isolating it from the solution, yielding to the mate or defective surface quality [131]. Those difficulties were steadily addressed with the "ninja cathode" development [132]. VEP facilities were as well adopted in the other labs [133], [134] (see **Figure 2.26**). Cavity flipping (see **Figure 2.27**) during the VEP of 9-cell cavity was studied and tested at KEK with a promising result in terms of uniform polishing.
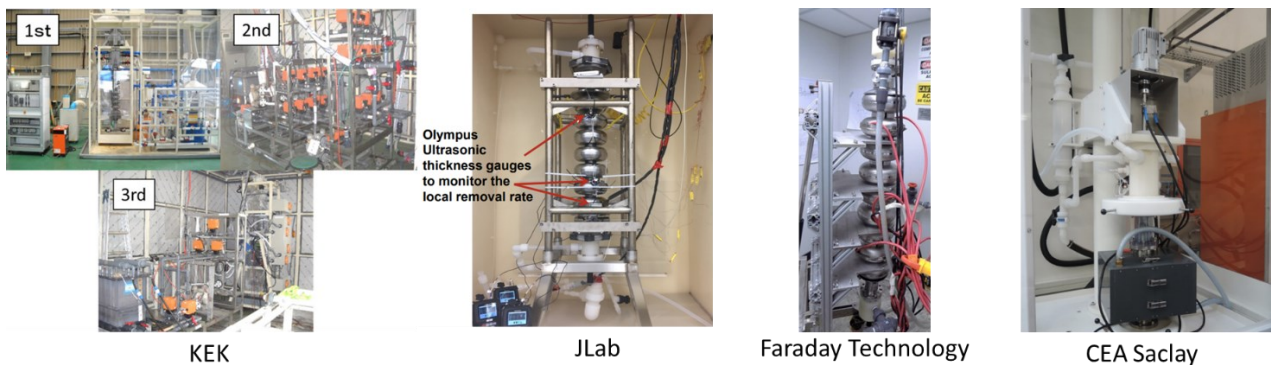

Figure 2.26: Variations of VEP setups at different laboratories

In the vertical configuration buffered electropolishing (BEP) was also studied in a joint collaboration between Peking University and Jefferson laboratory. The electrolyte of the buffered EP consisted of HF(48%),H_2SO_4 98%, and Lactic acid 85% with the volume ratio of 4:5:11 [135], [136]. The solution provides significantly higher etching rates of up to the 4 μm/min and 50 nm roughness. However, the lactic acid may be explosive in certain conditions, increasing the risks of unexpected incidents.

After the electropolishing it is necessary to do ultrasound cleaning and ethanol thorough rinsing to clean the sulphur-based precipitant from the sulphuric acid. Such ethanol cleaning can be avoided in case of low cathode current density [58]. Such contamination is the major source of field emission.
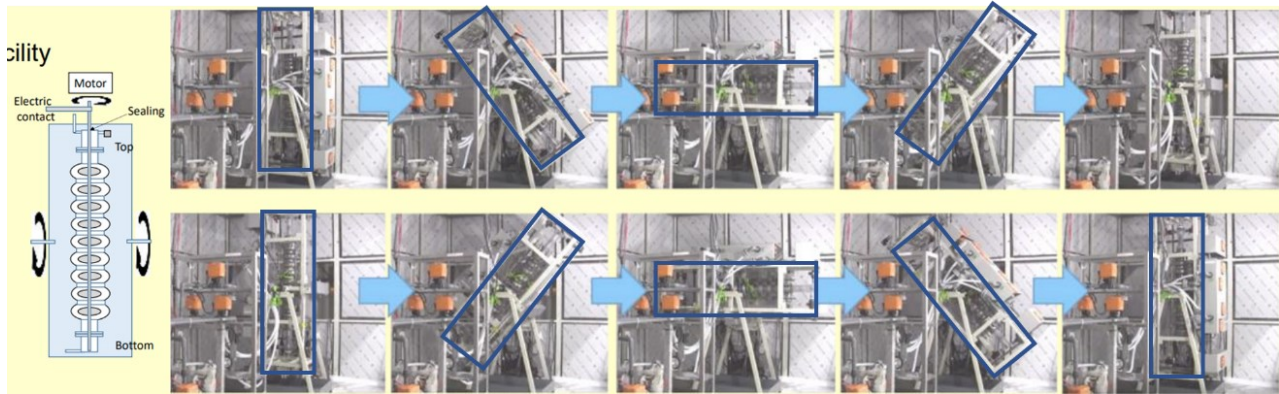

Figure 2.27: Cavity flipping process during VEP of 9-cell Nb resonator [137]

Summary: The temperature of the electropolishing needs to be reduced, that consequently diminish erosion rate and help to reduce parasitic etching and sulphur production. Some of the defects, pitting for e.g., cannot be removed by EP, unless the removing thickness is not bigger that the dimensions of the defect. Both horizontal and vertical configurations are used for the elliptical cavities' preparation, with a prevalence on the HEP.

2.4.2 Copper chemical treatments for Nb/Cu

As a metal Copper has very different chemical behaviour, and naturally the chemical protocols are different in some aspects. Unlike the Niobium, the Copper treatments were studied more in various fields. Instead, the SRF community had the possibility to use the various field experience directly applying it to the protocols of substrate preparation. Currently, the Cu/Nb path has not establish a united way of surface preparation, yet. Similar to niobium, the copper can be polished both by chemical and electrochemical means.

2.4.2.1 Electropolishing of Cu

The current attributes of the modern EP has established, probably, thanks to Jacquet that has done the first systematic study on the EP and has received a patent in the 1930s [138], [139] As a result of the developments, three processes were studied: nickel EP in perchloric-acetic acid, copper in the phosphoric-ether and molybdenum is sulfuric acid electrolytic baths. His publication in 1935 and 1936 drove to a huge wave of interest around the world and quickly spread among other institutions [140]–[144]. The basis of the fundamentals facts that has established Jacquet remained water or alcohol solution of concentrated acids: phosphoric, sulfuric, acetic and perchloric. After almost a century of development solutions of copper electropolishing still rely mostly on the phosphoric acid (see Table 2.4).

Table 2.4 – Electropolishing solution for Cu in the literature

Solution	Current density	Temperature	Working voltage	Reference
Anhydrous orthophosphoric acid H_3PO_4	n/a	25°C	n/a	Jacquet [140]
Orthophosphoric acid solution (Non-agitated Solution) H_3PO_4	0.2 to 1.5 A/dm²	–5.6°C to 53°C	0.7 to 0.9 V	Jacquet [143]
Orthophosphoric acid/water solution H_3PO_4	0.0625 A/cm²	25°C	0.8 to 1.2 V	Allen [145]
Phosphoric acid H_3PO_4/water solution with/without glycerol, ethylene glycol	2 to 4.2 mA/cm²	17 to 25°C	0.25 to 1.5 V	Walton [146]
Phosphoric acid/copper phosphate/water solution	50 to 1000 mA/cm²	25°C	0.2 to 0.8 V	Glarum and Marshall [147]
Orthophosphoric acid/sulphuric acid/water solution	0.1 A/cm²	25°C	1.8 to 2.2 V	Perryman [148]
H_3PO_4: 6, 8, 10, 12M Solvent: Alcohol Ethylene glycol Glycerol		25°C		Taha [149]
H_3PO_4: 6–14M Solvent: Water Tert-butanol		25°C		El-Subruiti and Ahmed [150]
H_3PO_4: 55% Soluble starch, Ethylene glycol, Methanol	5-25 A/dm²	25°C	1,5 V	Awad [151]
H_3PO_4: 98% Formaldehyde, Acetaldehyde, Paraldehyde, Benzaldehyde, Salicylaldehyde, Anisaldehyde, and Tolualdehyde		25°C – 40		Elmalah [152]
H_3PO_4: 8M Proline, Cysteine, Phenyl alanine, Alanine, Hisitidine and Glycine				Rahman [153]
H_3PO_4: 8M Nonionic surfactant, Sodium dodecyl sulphate, Cationic surfactant				Taha [154]

Due to the limited quantity of the accelerators based on the thin film onto the copper substrate technology, copper electropolishing R&D in the framework of SRF field was not deeply studied. The ALPI accelerator and HIE-ISOLDE are implemented the chemical preparation path for copper substrate.

Traditionally, in the literature of copper, electropolishing is done at room temperature, some literature suggested the use of low temperatures of the process motivating that in such situation the viscosity will be increased, and hence the resulting quality would be better, considering the effect of the viscous layer. In addition, the width of the plateau will be increased. However, in practice, higher temperatures of the solution improves both the smoothness and reflectivity of the copper [155]. Not only the roughness is lower in case of higher temperatures, as well Palmieri reported lower density of pitting, that are caused by oxygen bubbles. Palmieri suggested the 50 C° temperature, as at the 60 C° formation of the pyrophosphate can take place in the place where the oxygen bubbles nucleate.

The lock of the minimal differential conductance at Legnaro was suggested as a way to find stable conditions of the electropolishing [105]. The goal was to minimise the parasitic gas production on the anode (oxygen evolution). The result is achieved by monitoring and computing simultaneously

two curves: I – V and dI/dV – V. The working voltage is selected on the second minimum of the differential conductance curve, that corresponds to the maximum resistance of the viscous layer.
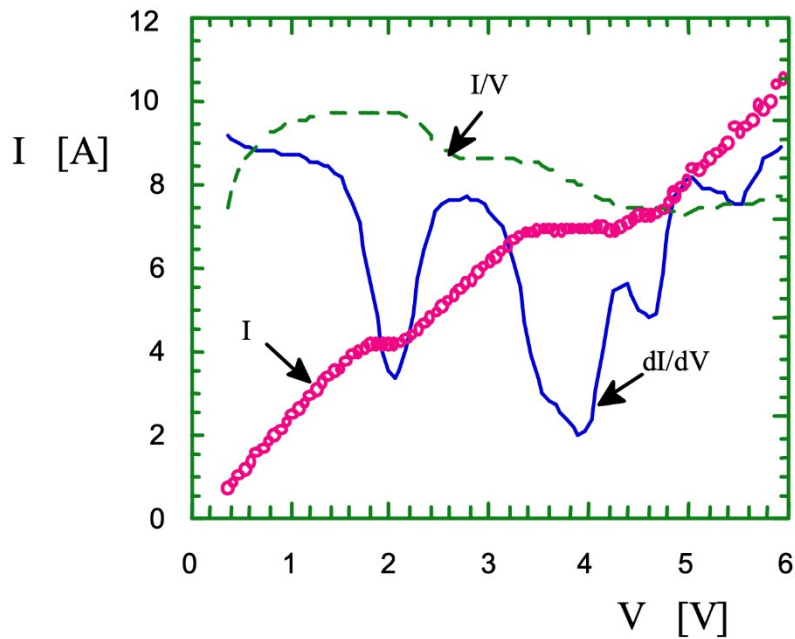

Figure 2.28: Current; Current/Voltage; dI/dV vs voltage characteristics of the standard EP of Cu [105]

The ultimate recipe used at Legnaro laboratory consists of bicomponent solution of phosphoric acid (75-85%) and n-Butanol in the volume ratio of 3:2. This viscous solution has a long lifetime of usage and may be used for months with a non-frequent correction with the butanol, that evaporates with the time. The electropolishing of the quarter wave resonator (QWR) is done in the vertical position in the bath of the electropolishing solution. The cathode is inserted inside the resonator before the EP starts. The average removal thickness is not exceeding 30 μm with a treatment time of no longer than 2 h. Longer treatments might produce pyrophosphate formation.

2.4.2.2 «SUBU» chemical polishing bath

A SUBU bath chemical etching method (**Figure 2.29**) was developed for LEP2 at CERN for 500 and 350 MHz cavities [156]. Two solutions were developed (see Table 2.5), with a selected speed, that variated only with a concentration between each other. The need of development of such solution was described by the volumes needed to treat such a big surface area – around 600 litres. A classical solution of etching-polishing was also producing toxic gases and the reaction were exothermic, producing heat.

Role of the components:

Sulfamic acid is a derivative of the sulfuric acid, and similarly as cyanide it forms soluble metal complexes. It is also very soluble in water (41.91 g/100 mL (70 °C)) as well as its salts, with a moderate hydrolysis with a final formation of sulphuric acid. A single acid at 20 g/L and at 70 C has

53

no effect on the Cu. On the other hand, with a presence of an oxidant, it corrodes the copper by forming a copper sulfamate and allows the release of hydrogen.

Table 2.5 – CERN developed SUBU Cu chemical polishing solutions

Bath Name	Formula of the bath	Concentration	Temperature	Agitation	Removing speed, μm/min
SUBU 5	Sulfamic Acid Ammonium Citrate n-butanol Hydrogen Peroxide	5 g/L 1 g/L 50 mL/L 50 mL/L	70 ±2°C	Yes	1.5
SUBU 20	Sulfamic Acid - H_3NSO_3 Ammonium Citrate - $C_6H_{17}N_3O_7$. n-butanol - C_4H_9OH Hydrogen Peroxide – H_2O_2	20 g/L 1 g/L 50 mL/L 50 mL/L			5

Figure 2.29: SUBU treatment processing at LNL facility

Hydrogen Peroxide: The decomposition of hydrogen peroxide allows oxidising metal surface, and thus the copper to dissolve. From a certain concentration of an active oxygen, that is a limiting factor, a copper oxide layer is being formed, that is instantly dissolved by sulfamic acid. A combination of both sulfamic acid and hydrogen peroxide allows continuous process of copper removal.

n-Butanol – is an organic solvent, used as a moderator of the solution. The main effect is the increment of the wettability of the metal surface and decrease of the etching rate of the polishing solution. Wettability (or surface tensions) plays a key role in the final quality of the copper surface, as it can negatively affects the adhesion of the oxygen bubbles, that are formed from hydrogen peroxide. In case of continuous contact of a bubble with a metallic surface, pitting might appear on the surface, where the local etching rate is increased dramatically. To prevent this effect, the agitation of the

solution is highly recommended, as a way to help the oxygen to detach from the surface, but also to increase the mass transport process.

Ammonium citrate – is a commonly used salt in copper polishing solutions. The main purpose of the small quantity of this salt it the prevention of a brown layer formation, due to the limited mass-transport effect. Ammonium citrate permits many chemical complexes to form, and so prevent partial oxidation.

2.4.3   Other non-conventional treatments

The recent advancements in various applied (but also theoretical) fields are moving forward the state of art of current protocols. New (or less studied) technologies might be useful in some specific cases, and this is the reason of the lack of information. It is also often connected with a complexity of application, that makes all the benefits are more negligible with respect to the classical processes. In this sub-chapter, selected innovative treatments will be discussed, that may find their application in the SRF field of substrate preparation but did not take part in the research of this thesis. By "innovative" we mean a technology that may use conventional physical (chemical) phenomena in a specific (non-standard) way or under different conditions. The main reason of this sub-chapter is to demonstrate and spread the information about those technologies and by that enhance the usage and eventually the level of development.

2.4.3.1   Electropolishing in Ionic Liquids

Ionic liquids (IL) (or deep eutectic solvents) are molten salts with melting points below or near 100 °C. IL consists only of cations and anions and is a type of ionic solvent, composed of a mixture with a melting point lower than both the individual components (see **Figure 2.30**). The charge on these ions is delocalized or shielded by side groups, which is one of reasons why the melting points of ionic liquids are exceptionally low.
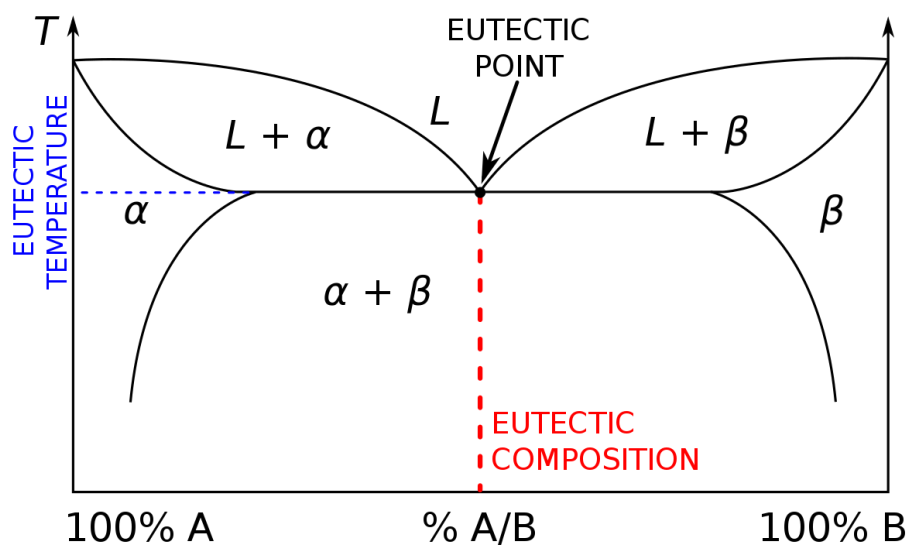
Figure 2.30: Eutectic phase diagram general scheme [157]

The first mentions of the ionic liquids can be traced back then in 1914 by Walden [158]. He studied physical properties of ethylammonium nitrate, that has a melting point of 12 $^\circ$C. The interest of ionic liquids later in 1940 as a electrolytes for electrical batteries and electroplating of Aluminium [159]–[161]. In the 1970-80s Osteryoung and Hussey et al [162], [163], conducted research on organic chloride-aluminium chloride ambient temperature ionic liquids and the first major review of room temperature ionic liquids was written by Hussey [164], [165].

The first generation of deep eutectic solvent were based on quaternary ammonium salts with hydrogen substituted groups (for e.g., amines, carboxylic acids). Four types are commonly known as eutectic solvents [166]:

The classical electrochemistry was developed and mean for the water solution of electrolytes. Thus, the presence of positive ions (H$^+$, H$_3$O$^+$) and negative (OH$^-$) inside such solution determined the acidity (pH level) values. Having water ions in the solution enable the oxygen evolution through (2.13 and 2.14) and hydrogen reduction (2.15 and 4.16) depending on the pH value:

$$2H_2O = O_2 \uparrow + 4H^+ + 4e^- \; [\text{pH} \leq 7] \tag{2.13}$$

$$4OH^- = O_2 \uparrow + 2H_2O + 4e^- \; [\text{pH} > 7] \tag{2.14}$$

$$2H^+ + 2e^- = H_2 \uparrow [\text{pH} < 7] \tag{2.15}$$

$$2H_2O + 2e = H_2 \uparrow + 2OH^- \; [\text{pH} \geq 7] \tag{2.16}$$

The most remarkable advantage of ionic liquids is their large electrochemical windows (> 5V) which gives access to elements that cannot be electrodeposited from aqueous or organic solutions such as for example, Al, Mg, Ti and Ta, at moderate temperatures[167], [168].

The usage of ionic liquids enables electrodeposition of some metals that is thermodynamically was not possible in water solutions, due to the presence of reactions (3,4). Similarly, in EP (1,2) will not be present, and thus may allow electro dissolution of metals, that has more negative reaction potential (comparing to 3,4). With the use of ionic liquids, it was possible to electrodeposit Zn and its alloys with a high current density [169].

Similarly, the wide electrochemical windows of ionic liquids have given access to the electropolishing of metals and semiconductors at ambient temperature, which were previously achieved only from high temperature molten salts [170].

From the ecological perspective, ionic liquids are environmentally greener than other media. When used in electrolysis processes, harsh aqueous electrolytes create quantities of metal-based, corrosive waste solutions, whereas in IL electrolytes the metal will precipitate and be easily separated and recovered. Most of the ionic liquids are non-toxic and non- flammable. In addition, their very low vapor pressures permit the usage in open galvanic baths without releasing toxic vapours, which, in sequence, reduces the amount of volatile organic compounds released into the atmosphere [170].

The characteristics of such technology are extremely interesting, and IL still needs to be studied and optimised. However, due to considerable lack of appreciation and fundamental research, the use of IL in chemical industry and other fields has not yet become common [171].

The attempts to use the IL as a solution for EP of Nb has been noticed in the last decades. Tarek et. al [172] have tried (2-hydroxyethyl-trimethylammonium) chloride (CC), ethylene glycol (EG), urea (UA), ammonium fluoride (AF) ratio of CC:2AU:2EG:1AF. This recipe achieved polishing of Nb down to the 22 nm surface roughness.

At Legnaro National Laboratories, a series of studies has been gradually studying the possibility of application of IL for the Nb EP [173]–[178]. The first solutions contained Choline Chloride and Urea heated up to 150°C with addition of additives: Ammonium Sulphate, Ammonium Persulfate, Sulfamic Acid.

Important milestones have been achieved using the choline chloride and urea at 4:1 ratio with Sulfamic acid 30 g/l and other solution Choline Chloride and Urea at 3:1 ratio and Ammonium Chloride 10 g/l. The highest removing rate of Nb has reached 12 times higher than with conventional EP. Later attempts to automatise the process of cylindrical 6 GHz cavity were introduced [179]. It was also noted the importance of nitrogen flow to avoid passivation, the choice of working current density (higher values may allow bubble production and increase of the resulting roughness).

Summarized advantageous list of the IL usage according to Valente-Feliciano [180]:

1. Non-aqueous
2. Non-volatile
3. Non-toxic
4. Highly conducting
5. Improved current efficiencies
6. Recyclable
7. Decrease hydrogen evolution
8. Decreased emissions
9. Iron Residue Recovery
10. Costs comparable to organic solvents
11. Bacterial growth inhibition
12. Micro finish enhancement
13. Reduced occurrence of intergranular (preferential etching)
14. Reflective finish
15. Polished surface can withstand cleaning and autoclaving
16. Any size metal can be electropolished

Excellent results were obtained on the planar samples using the IL technology. However, the high viscosity of the solution made a scaling process onto the 6 GHz cavities a challenge.

Unfortunately, a limited quantity of processing was done on the elliptical cavities, resulting in just one RF performance measurement published (see **Figure 2.31**) [175]. The results show comparable performance to the standard EP.

Due to the non-satisfactory results, the study and further development of such technology had been interrupted.
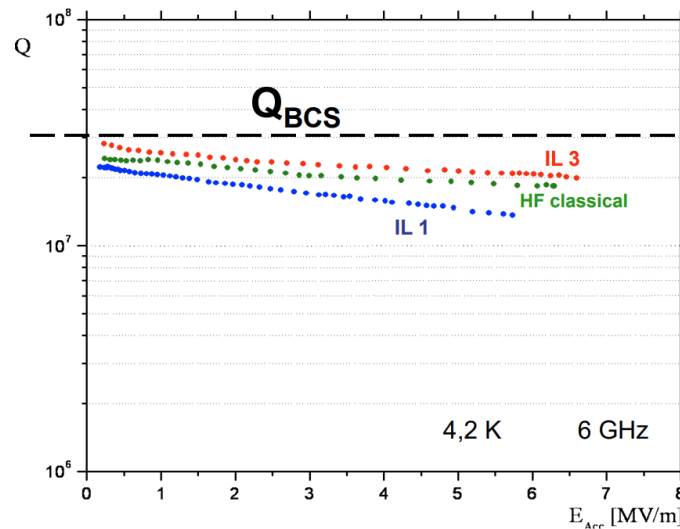
Figure 2.31: RF performance at 4,2 K of the 6 GHz Nb cavities measured at Legnaro and polished by classical EP (in green) and IL EP in Choline chloride: Urea ratio 4:1 with Sulfamic acid 30 g/l at 120°C [175]

Summary: a powerful approach, IL did not succeed in the scaling from the planar samples to the elliptical cavities EP, even though some results were published and looked promising. High current densities (0,3 A/cm^2, [179]) are one of the advantages, that outperform the standard EP polishing rates. The lack of optimisation and systematic studies on the complex geometries EP leaves this approach at the current state.

2.4.3.2   Pulse, pulse/reverse EP

A different approach of current application in the EP is known as the Pulse or Pulse/Reverse (i.e., bipolar EP) electropolishing. In which in case of Pulse EP, the polarity is fixed, and the polarization is being applied in the form of waving for a short time (typically ms.). In case of Pulse Reverse EP (see **Figure 2.32**), the polarisation is still applied for a short time of ms, additionally reversing the polarity of power supply is prompted. Between the pulses, naturally there is a pause (time-off) period. Such modes can enhance the processes of electrolysis. Short pulses of DC power supply may decrease the overall heating of the system, increase the mass-transport rate, thus improve the quality of the technology. Reversing the polarity may activate passivated anodic surface, by that activation the "continuous" process of dissolution of metal will take place. The pulse EP may allow release reaction by-products at each off-current interval, thus employing a lower average electric current density compared to conventional EP. During the off-current interval, the growth of reaction

gas bubbles and their accumulation at the surface of the workpiece can be limited, thus improving the surface finish [181].

In some particular cases, even allowing the dissolution of metals like Niobium in water solutions of H_2SO_4 5-10% that do not contain any Fluoride ions [182], [183]. Moreover, such approach can significantly decrease economical waste using the bipolar power supply. More systematic studies on the solution composition, surface roughness and working pulses values (cathodic) were published by Tian H. et. al [184].

On **Figure 2.32** the typical pulse reverse waveform is shown where T_{AA} is the anodic time, T_C is the cathodic time, I_{AA} is the anodic current density, I_C is the cathodic current density, $\bar{I}_A$ is the average current density, and T is the cycle time.
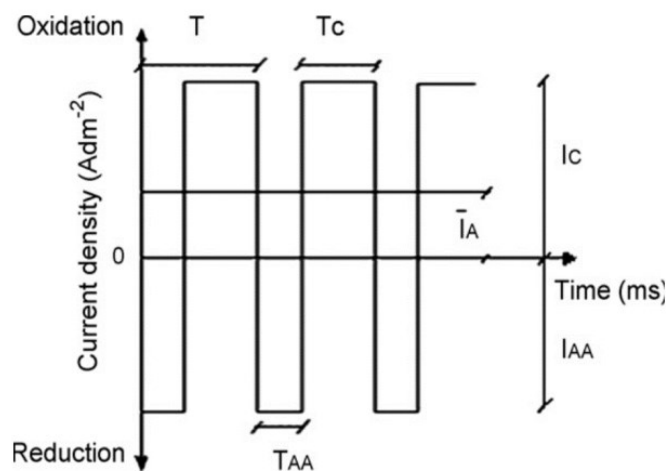
Figure 2.32: A typical pulse reverse waveform [178]

While the pulse/pulse reverse waveform contains off-times and cathodic pulses (e.g., non-productive), the material removal speeds during pulse/pulse reverse EP is usually higher than or equal to those obtained with the use of direct current [185].

A typical current curve for a modulated waveform of the Bi-polar Electropolishing (BPEP) is shown below for 10 and 37 % of sulphuric acid (**Figure 2.33**A). A systematic study shows superiority of roughness values for 10% solution in the low voltage modes (**Figure 2.33**B).
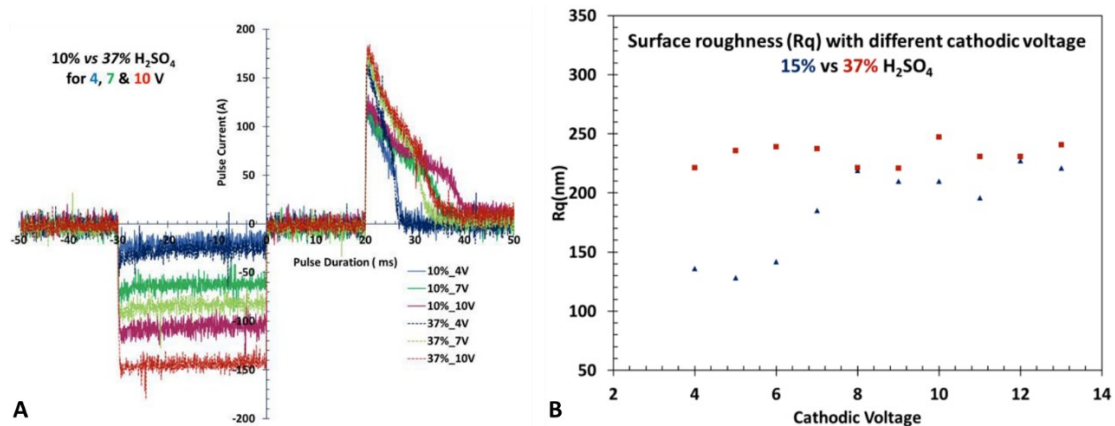
Figure 2.33: A) Current curves during BPEP of a single cell cavity, B) Surface roughness study on the samples done in 10% and 37% of H_2SO_4 [184]

A study and application of BPEP of a collaboration between Jefferson Lab and Faraday Technology Inc., has led to the RF performance measurements of cavities. The summary of the results is shown below on the **Figure 2.34**. Notably, the performance is identical to the standard Nb electropolishing one, allowing to achieve 25 MV/m accelerating field, where the multipacting takes place. Further HPR and mild 120 C° baking can extend the accelerating field up to the 32 MV/m [184], [186].
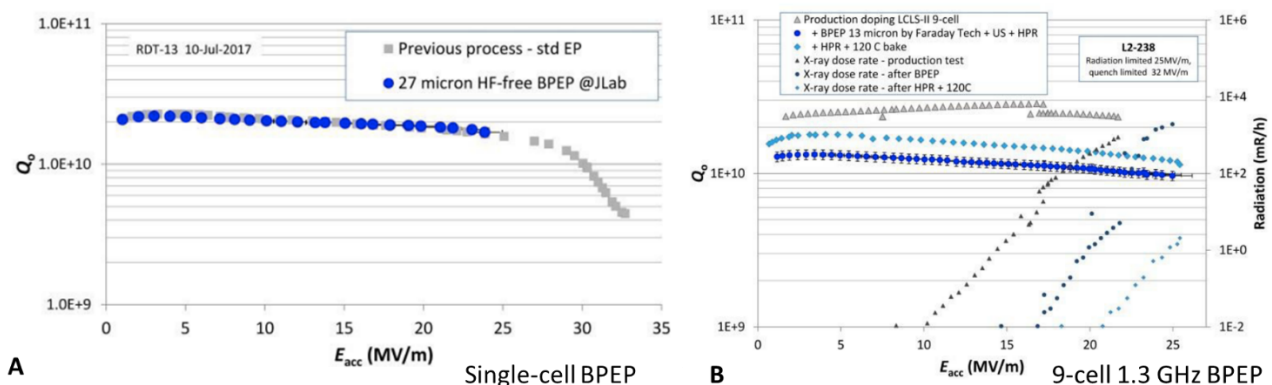
Figure 2.34: RF performance of Nb cavities processed with BPEP in 10% H_2SO_4 for A) single cell, B) 9-cell 1.3 GHz Nb cavities [184], [186]

Summary: BPEP is a great candidate for a substitution of the harsh Fluoric acid-based acid electrolytes used in EP of Nb. The process adaption requires relatively easy upgrade of current setups. A width range of parameters (concentration, temperature, waveform properties) leaves a possibility for further optimisation. The erosion rate of the technology is claimed to be in the range of 0,15 – 1,3 µm/h, that is equal or greatly higher than standard EP values.

2.4.3.3   Magnetoelectropolishing

It is known, that one of the ways to increase the speed of electrochemical reactions is the application of the magnetic field. Such effect of the static magnetic field on the process of

electrodeposition of Cu in water solution was firstly studied by Hinds [187]. The effect is explained by field-induced convection. The tangential fluid velocity is induced by the field resulting in the formation of the hydrodynamic boundary film at the metallic surface. And thus, it decreases the diffusion layer thickness resulting in the increase of the mass transport rate. Magnetic fields can be created by using the permanent magnets or electromagnets. The possible schematic view of the magnetoelectropolishing is shown below on the **Figure 2.35**.
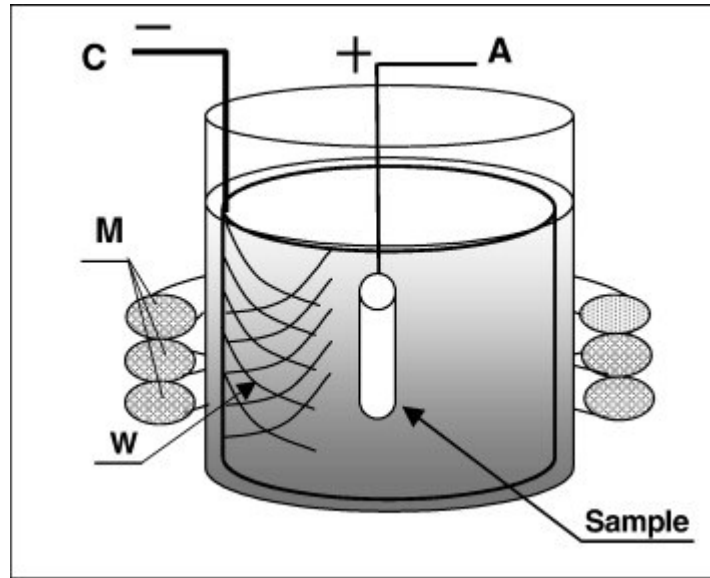
Figure 2.35: Magnetoelectropolishing system schematic: A — anode, K — cathode, M — magnet or electromagnet, W — steel wire of cylindrical shape

A magnetic field can work either slowing or accelerating the dissolution rate. The change of the electrochemical rate reaction is purely determined by physical phenomenon – strength of the magnetic field, and thus the rate does not depend on the magnetic properties of the metal or the chemical composition of the electrolyte.

A new process was then developed and patented by Rokicki [188]. In-deep study was continued by a series of researches to evaluate the advantages and disadvantages of the present technology, in the meantime theories and mechanisms of electropolishing was continuously being studied [189]–[191]. Studies shown some characteristics of the MEP over the conventional EP: lower surface roughness, more advantageous surface film composition, increased nano hardness, increased corrosion resistance, improvement of the biocompatibility of some alloys. All of beneficial evidence were then correlated with the MEP process tested on a list of common metals and alloys: AISI 304, 304L, 316, 316L, 430, LDX 2101, 2205, Co-Cr alloys, Ti, Nitinol, Ti-alloys, Nb [192].

Hryniewicz [193], [194] has studied the influence of the externally applied static magnetic field on the MEP process. It was shown, that in case of MEP with a constant potential over the oxygen evolution, application of magnetic field leads to the decrease of the working current densities, and vice-versa, in the case of constant potential below the oxygen production, application of the magnetic

field lead to an increase of a working current density. Hryniewicz et. al as well compared conventional EP with MEP and MP (mechanical polishing). After EP of the 319L stainless steel, the presence of metallic Fe and Cr was completely removed by formation of the oxide and hydroxide compounds (confirmed via XPS analysis). In case of MEP, it was shown advantageous increase of the Cr:Fe ratio on the surface [195]–[197], much higher than after EP. As a result, the sample has higher corrosion resistance after MEP. The same trend is relevant for the Ti comparison between EP and MEP, resulting in better corrosion resistance and mechanical properties after the MEP. Additionally, the corrosion resistance of the sample after MEP is 5 times higher than after MP [198], [199].

It is worth to mention that Hryniewicz et. al. have already proposed MEP for the SRF needs and it was tested with a novel solution composted of 70% of methanesulfonic acid and 49% hydrofluoric acid in the 3:1 volume ratio [200]. Later a deeper study on the hydrogen embrittlement of the proposed solution and MEP approach [201] was conducted. The MEP samples showed a lowest content of hydrogen comparing to the non-treated (AR) and electropolished (EP) samples (see **Figure 2.36**).
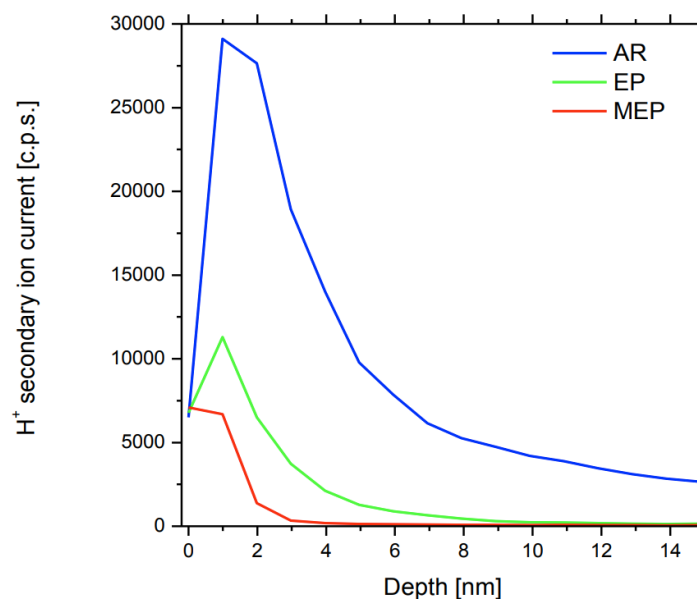
Figure 2.36: Comprasion curves for concentration of Hydrogen for As Received (AR), Electropolsihed (EP), and Magnetoelectropolished (MEP) Nb samples [200]

Summary: a series of results presented by the Hryniewicz looks promising, as potential enhancing of the conventional electropolishing. The resulting performance and quality in some cases are noticeable better for the MEP versus EP. The drawback of course is the additional complications of already not trivial EP and somewhat unclear resulting benefit for the current state of art of SRF technology.

2.5 Cleaning and other treatments

2.5.1 *Overview and importance*

The cleaning processes are fundamental in the SRF industry, as they try to reach more cleaner state of the surface and bulk material. The term "clean" by itself is indefinite in meaning and has different meanings in different contexts. "Clean" in terms of bacteria is not necessarily the same as "clean" in terms of chemical or particulate matter (for e.g., see **Figure 2.37**). Cleanliness is related to the product considered; it is not an absolute measure. If a mechanism or system must be free of contamination to function reliably, measures of contamination control must be taken (see example **Figure 2.38**). The purpose of such an effort is to reduce or manage - contamination at the desired level.
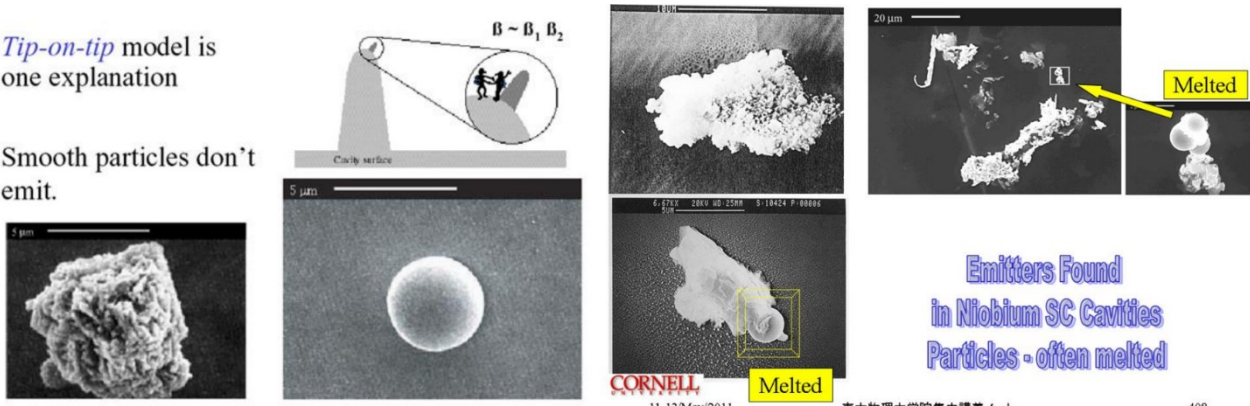
Figure 2.37: Particles and contaminations found on SRF surfaces [202]

Superconductive cavities are quite sensitive objects to deal with. Moreover, their performance is dependent on the cleanliness: Q-value, break-down field, electron loading behaviour are not usually reproducible to that. There are studies and confirmations, that contamination is the key of those negative effects [203]. See Table 2.6 that highlights the possible sources and types of contaminations.

According to Kneisel, all contaminations may be classified in 4 general categories:

1. Particulates - dust, chips, fibers.
2. Chemical contamination - gases, liquids, inorganic compounds, organic compounds.
3. Biological contamination - bacteria, viruses, fungi, spores.
4. Radioactive contamination.

Each of these contaminants can be present in gases (particularly air), liquids (particularly water) or at surfaces.

Contaminants in liquids are:

- Non-volatile residues like skin oils, solder fluxes, cutting fluids, cleaning solvents, plasticizers, lubricants.

- Other liquids in suspension or solution.
- Absorbed gases.
- Particulate matter.
- Viable and non-viable microbiological matter.

In gases we can find:

- Hydrocarbons residues from cleaning agents, lubricants.
- Water.
- Absorbed or mixed-in gases.
- Particulates - corrosion, rust, flakes from wear.
- Microbial matter.

Table 2.6 – A table of sources and types of contamination from different media [204]

Facilities	People	Tool Generated	Fluids	Product generated
Air conditioning debris	Clothing debris (lint, fibres etc.)	Brooms, mops and dusters	Cleaning chemicals	Aluminum particles
Construction material (sheet rock, saw dust etc.)	Spittle	Vibrations	Floor finished or coatings	Cleanroom debris
Paint and coatings	Cosmetics and perfume	Lubricants and emissions	Bacteria, organics and moisture	Quartz flakes
Room air and vapors	Hair	Friction and wear particles	Pasticizers (outgasses)	Silicon chips
Spills and leaks	Skin flakes and oil		Deionized water	
Walls, floors and ceilings			Particulates floating in air	

Superconducting RF cavities, nowadays, are treated with various physical and chemical treatments, and in particular encounter acids, water-solutions, solvents, nitrogen gas. Finally, in the assembly phase, the contact with gasses/air is inevitable and of course, during the lifetime of any single cavity, contamination takes place, and can be only reduced, and not completely eliminated. A strong factor of contamination is the clean environment, that is why the SRF technology usually operates at least in the ISO5 (or higher) cleanroom conditions.

The other way to reduce possible contaminations is to use chemicals that are classified as "For Analysis". Naturally, reduction of the treatment steps is an effective step to eliminate additional sources of contaminations.

Additionally, to verify the cleaning techniques some analysis might be done:

1. Total organic carbon (TOC) content measurements.
2. Visual inspection and white poly wipe.
3. Water break free test.
4. Clean gas spray & particle count.
5. Surface particle counts.

6. UV light inspection.
7. Residual gas analysis.
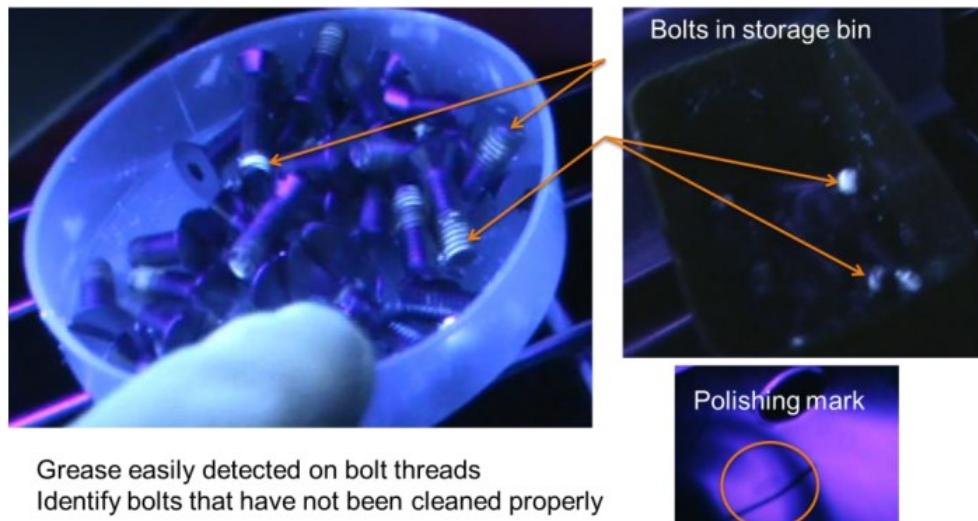
Figure 2.38: Residual presence of grease on the screws via luminescence methods [205]

2.5.2 Conventional treatments

2.5.2.1 Annealing, temperature treatments, doping.

Heat treatments play a significant role in the Nb and Cu preparation for the SRF technology. Standard fabrication and chemical treatment procedures result in high concentration of the interstitial impurities and lattice defects. That will contribute to the RF losses by vortex pinning and vortex penetration. The so called Q-disease can be linked to the formation of the $NbH_{0,7}$ hydride. More precisely, the solubility limit of interstitial hydrogen in niobium is $C_{Hmax1}=4,104$ at. ppm at $T_1=300K$ and decreases drastically to $C_{Hmax2}=5$ at. ppm at $T_2=100K$. Heat treatment under vacuum conditions of SRF bulk Nb cavities reduces the interstitial hydrogen concentration C_H to less than the onset $C_{Hmax}=5$ at. ppm, resulting in a healing of the resonator from Q-disease.

Nb as a material is characterized to be a "getter" of the gasses, especially Hydrogen. A heat treatment can release the surface and bulk volumes of the Nb gas contaminations, generally 750-800 C° is applied for at least 3h. The heat treatments are then followed by a 20-40 µm amount of material removal again with EP or BCP, typically done to remove surface 'contaminants' which might be introduced during the furnace treatment. In case of LCLS-II HE, the standard amount of removed thickness is only 5 µm, followed by heating at 800 C° for 3h with additional 2 min low pressure nitrogen exposure [206].

Another advancement can be achieved if the Nb surface can be doped with nitrogen or even titanium, and more recently oxygen [207] during the high temperature treatment. This can be explained by a reduction of the residual resistance by preventing the formation of the hydrides and reduction of the BCS surface resistance [208].

The last treatment of the cavities consists in a mild baking at 120°C for 48 hrs. This treatment permits the decrease of the thermal dissipation and increases the quality factor at higher fields. This is an important effect for superconductivity (see **Figure 2.39**).
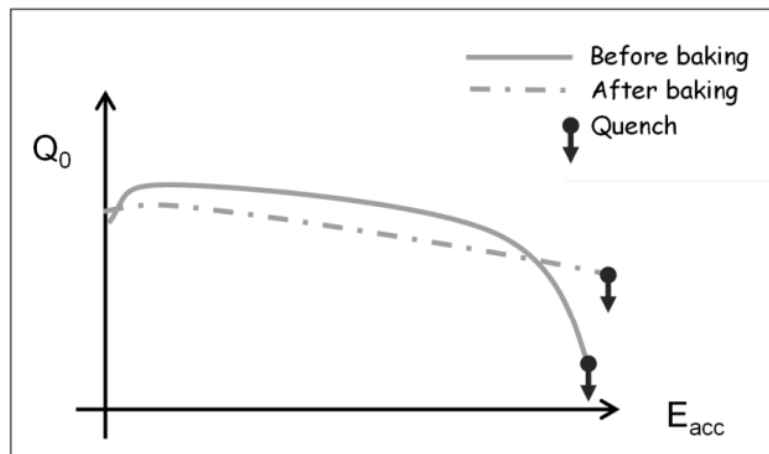
Figure 2.39: Diagram of the effect of moderate baking -120°C, 48h – on the dissipations at high field (logarithmic scale of Q_0) [8]

It is important to mention that another process during the heat treatment takes place: the recrystallization. Recrystallization temperature will decrease with increasing purity: it ranges from 900-1000°C for commercial Nb (RRR < 100) to ~ 800°C for RRR ~ 300 and is expected to be around 750°C for RRR>400. Recrystallization leads to the reduction of dislocation density as well. Recrystallization is suggested before any forming step because it helps with the removal of the effects of cold working and obtain smaller grains.

2.5.2.2 Ultrasound cleaning

Ultrasonic cleaning is one of the most powerful cleaning techniques. Residual polishing compounds can be completely removed, even from very fine cracks, pores of porous or fractured samples, or at the interfaces between the specimen and the mounting material. The ultrasonic cleaning removes even very persistent dirty residues. Naturally, ultrasound cleaning is a fundamental step between chemical and electrochemical treatments because it can efficiently (see **Figure 2.40**) dissolve chemical residuals, that can be hidden from the visual appearance. The ultrasound is widely used in industry for removing contamination from all forms of hard surfaces, such as metals, plastics, and ceramics. Its unique properties can be channelled to clean items of all shapes, sizes, and technical complexity, reaching holes and cavities that are impossible to obtain using ordinary cleaning methods.

In ultrasonic cleaning, as the frequency decreases, the cavitation bubbles get larger (and the number of bubbles decreases). Larger (more energetic) bubbles are more effective on larger particles [209].

This technique utilizes a digital generator powering transducers immersed in a container of hot water. The piezo-electric transducers vibrate at a frequency of around 40 KHz creating millions of

tiny bubbles that form and implode. These sound waves generate zones of high and low pressure throughout the liquid. In the zones of negative pressure, the boiling point decreases and microscopic vacuum bubbles are formed. As the sound waves move, this same zone becomes one of positive pressure, thereby causing the bubbles to implode. This is called cavitation and is the basis for ultrasonic cleaning. Cavitation exerts enormous pressures (approximately 700 bar) and temperatures (approximately 1000 °C on a microscopic scale). These pressures and temperatures loosen contaminants and perform the actual scrubbing of the ultrasonic cleaning process[210], [211].
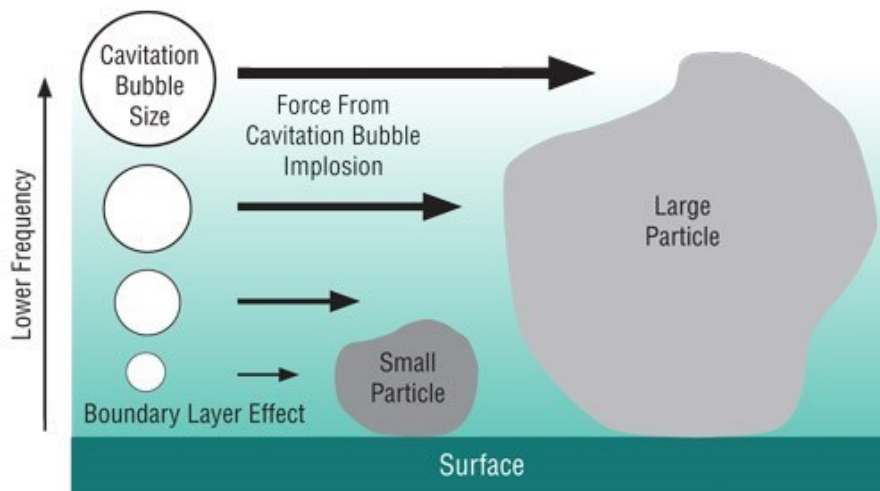
Figure 2.40: Dependency on the efficiency of ultrasonic cleaning with different particle size

The process is capable of cleaning from residual oils and grease by adding soap extracts, such as commercial surfactant GP 17.40 SUP or Rodastel30. The usage of soap is advantageous over classical organic solvents, since only afterwards ethanol rinsing is needed. Easier manipulation and complex geometry surfaces, as well, are not a problem for such approach.

2.5.2.3   High Pressure Rinsing

The High Pressure Water Rinsing (HPWR or HPR) is commonly used as an intermediate and final cleaning method to remove residuals and most of the smallest particles. It has been proved the necessity of the usage of HPWR by reaching higher accelerating gradients supressing Field Emission [212].

Some principles are summarised by Sertore [125]:

- HPWR must be applied as a final step in cavity assembly to remove chemical polishing solution residuals and other particle from the internal surface
- The water-jet must be in a constant movement, to prevent a Nb surface damaging in a certain spot

- The motion of the cavity should respect the jets (a spiral trajectory, that will accomplish a complete cleaning of Nb cavity surface).
- The cavity must be grounded, to prevent electrical charging.
- Ultra-pure nitrogen protection gas injection coaxial with the water has to be prepared, reducing the risk of particles to enter the closed geometry.

The HPWR process can be described as well as a recovery treatment, after which a degraded performance can be reset. Sertore has shown an example [125], when during the 120 C° baking an unexpected grow of pressure occurred, resulted in the particles injection – contamination of the cavity. Thus, the performance drop of the cavity has been noted (see **Figure 2.41**, black markers), that eventually with a HPWR process was possible to recover to adequate values (see **Figure 2.41**, green markers).
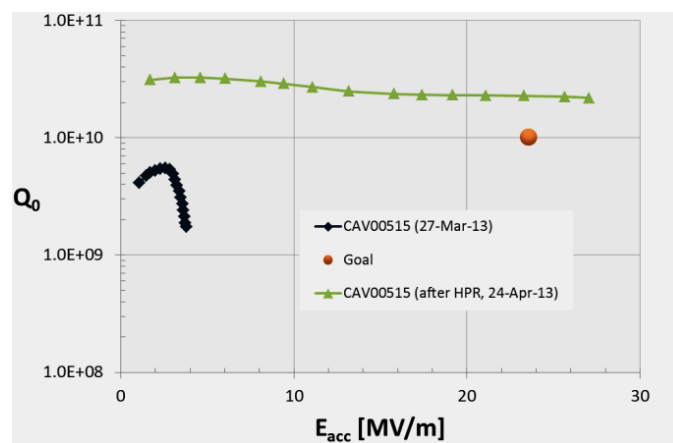
Figure 2.41: RF performance recovery with HPWR [125]

Many laboratories have adapted various systems configuration for HPWR of different shapes, including the elliptical cavities (see **Figure 2.42**). At LNL, the HPWR system was built (see **Figure 2.43**) to clean either the 6 GHz cavity or more bigger surfaces (by using a water-gun manually). A 100-bar distilled water jet is applied against the surface to be treated. A close system uses angle nozzle for the cleaning of internal surface with the possibility to manually change the position and gradually clean the surface from cut-off – cell – cut-off.

It was then studied in a series of works, analysing the pressure, distance, nozzle dimensions and other effective parameters in the process of HPWR [[213]–[215]]. It is also possible the oxidation caused by force at surface, such negative effect can be avoided by enabling absolute continuous motions of the spraying head. A small misalignment in small-pack configuration, such as 6 GHz cavities, may create two circles [213], [215].

DESY
HPR Cabinet

CEA
HPR Cabinet

FRIB
Automated HPR

KEK
Horizontal HPR
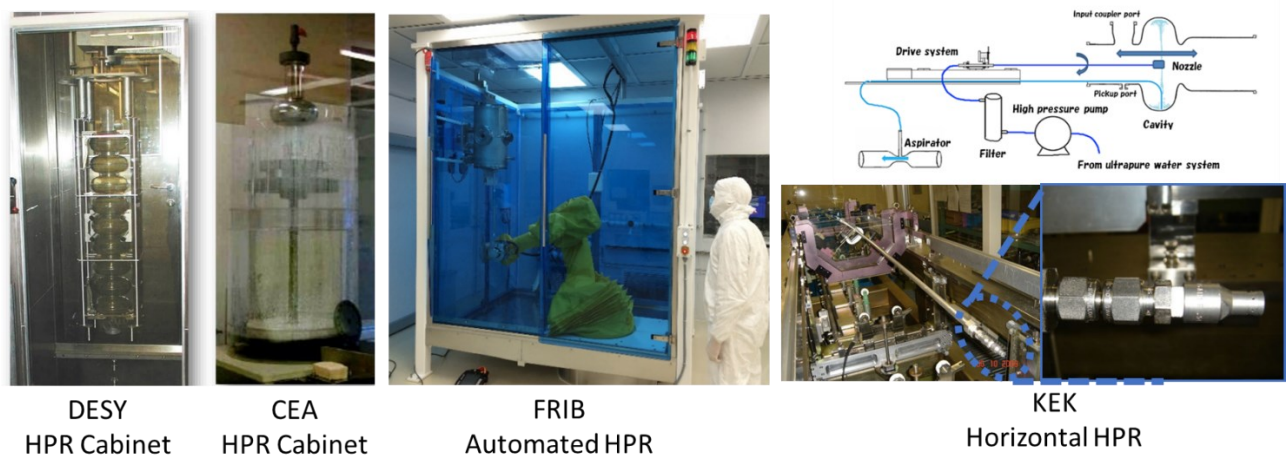
Figure 2.42: HPWR facility at different laboratories [125], [216]–[218]
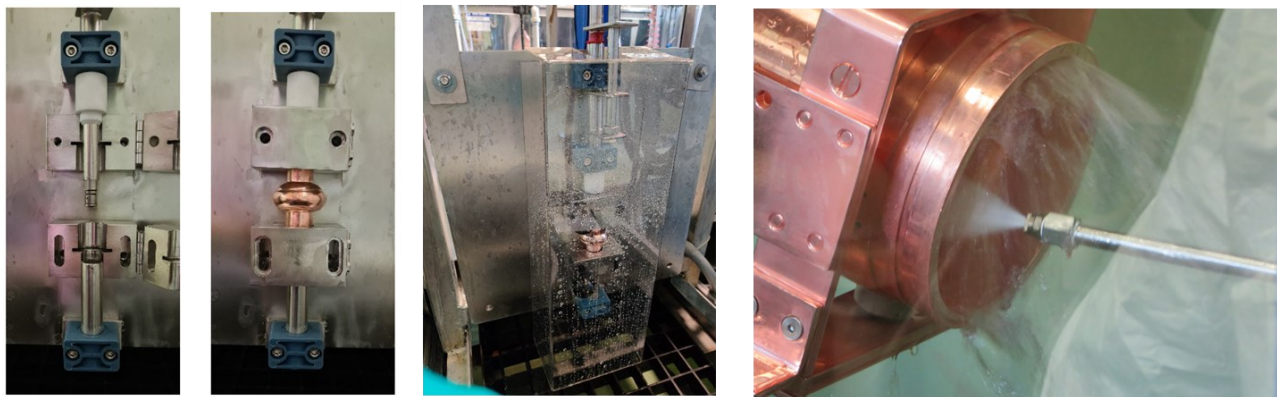
Figure 2.43: HPR system for 6 GHz cavities, before mounting (left) with cavity mounted and during processing(middle), manual processing surfaces with water gun (right)

2.5.3 Innovative treatments

2.5.3.1 Plasma cleaning

Plasma cleaning or Plasma Etching (PE) has been initially developed for the manufacturing of the integrated circuits and surface preparation of the Josephson junctions [219]–[222]. Plasma Etching can remove plastic, silicon, or other non-metallic material using plasma created by exciting ions in a gas, usually oxygen and CF_4 (see **Figure 2.44**). The excited ions collide with the material at the atomic level and remove it without the need for chemical etchants. Plasma processing is a fast-rising surface treatment technology for superconducting radio frequency (SRF) cavities. It is usually applied in the lasting steps of protocol, because plasma can interact with the impurities contamination and tiny burrs, resulting in an etched clean and smooth RF surface.
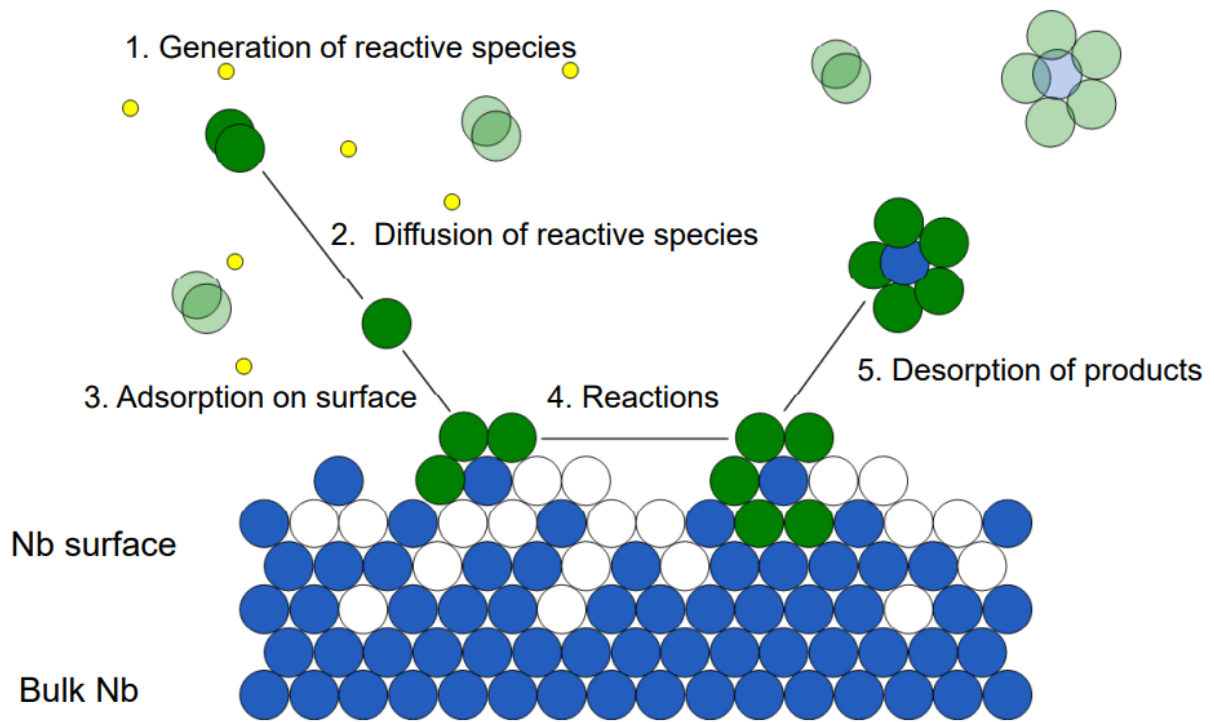
Figure 2.44: Plasma etching process scheme at microscopic level [223]

The process is done by ignition of the plasma (from the reactive gas) that will generate high energy ions that will bombard the surface, and gradually remove atom per atom. Practically treated surface is sputtered out and deposited on the surface of the chamber or evacuated with the pump. PE includes physical and chemical reactions: chemical approach uses corrosive gases to produce volatile compounds to get rid of upper surface layer, and physical sputtering relies on ion bombardment to sputter the surface atoms [224]. It was demonstrated that an etching rate of 1.5-1.7 µm/min can be reached when Cl_2 was used as the reactive agent [225]. The surface finish produced by plasma etching appears to be comparable to that by BCP.

$$2Nb_{(s)} + 5Cl_{2(g)} = 2NbCl_{5(g)} \tag{2.17}$$

PE starts with the creation of charged ions from the reactive gas by electrical discharge. Then the diffusion process takes place and attract ions toward the surface to be cleaned. Therefore, the surface is etched (e.g., atoms are ejected).

Many researches were already published about the PE, as well as more related to the SRF application [226]–[230]. It was reported a direct connection between the removal rate and gas pressure, applied power, reactive gas concentration. Among the chemical reactions, electron and ion collision physical phenomena take place (see Table 2.7).

Table 2.7 - A list of plasma reactions that may take place [224]

Reaction	Formula	Type	$\Delta\varepsilon$(eV)
1	$e + Ar = e + Ar$	Elastic	0
2	$e + Ar = e + Ar^*$	Excitation	11.5
3	$e + Ar^* = e + Ar$	Super-elastic	-11.5
4	$e + Ar = 2e + Ar^+$	Ionization	15.8
5	$e + Ar^* = 2e + Ar^+$	Ionization	4.24
6	$Ar^* + Ar^* = e + Ar + Ar^+$	Penning ionization	-
7	$Ar^* + Ar^* = Ar + Ar$	Metastable quenching	-

In 2017 first cryogenic RF test of PE were presented on the one-cell cavity (see **Figure 2.46**) [227]. A great deal of force has been spent to adjust this technique specifically for Niobium by defining the gas concentration, pressure, voltage, power density and geometrical characteristics of the cathode (due to anisotropy) to obtain the optimum characteristics of the polishing process. An oxygen gas is used as a reactive component that decomposes in the plasma into the atomic oxygen, which in turn breaks hydrocarbons connections, and eventually yields to produce residuals in form of CO, CO_2, H_2O, H_2 (see **Figure 2.45**). A "standard" recipe uses a mix of inert gas (argon or neon) with a few percent of oxygen gas [231].
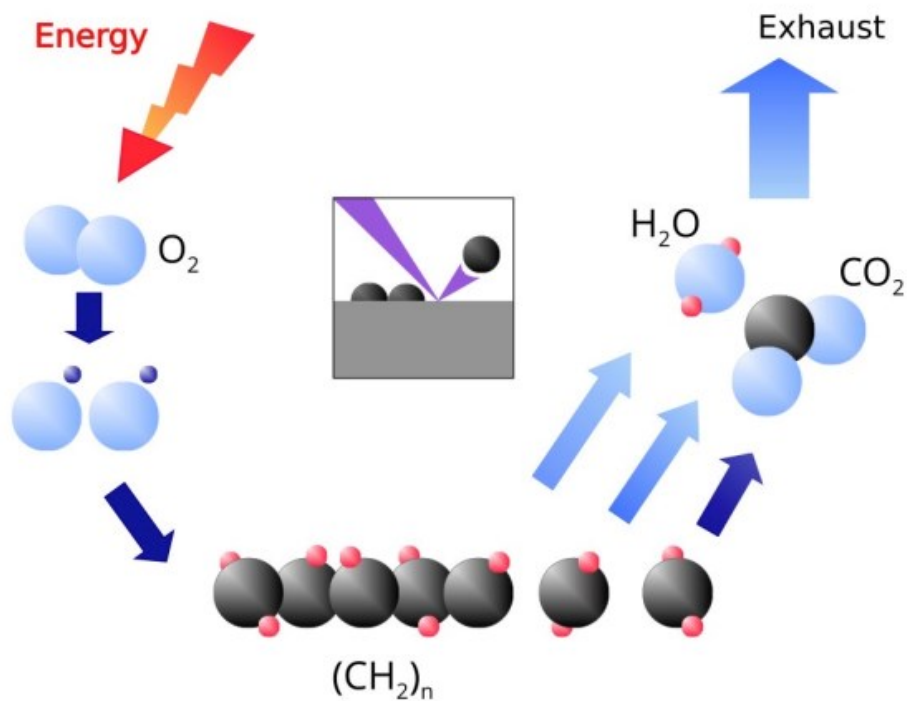
Figure 2.45: A schematic mechanism of PE
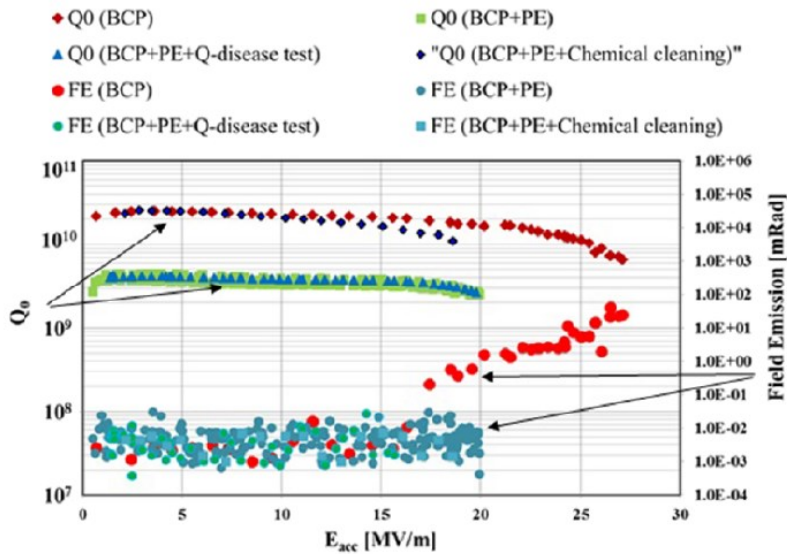
Figure 2.46: The RF performance measurement of the plasma treated single cell cavity (made from bulk Nb) [227]. Quality factor Q_0 and field emission (FE) are plotted versus accelerating gradient E_{acc}

It is evident that plasma treated surface showed lower performance (lower Q-factor) for almost an order of magnitude, as stated by authors due to the surface contamination by the cathode material - stainless steel. With a chemical cleaning as BCP treatment, it was possible to recover the initial performance. This led to the conclusion that only niobium cathode should be considered in the plasma cleaning process.

At JLab a performance improvement was demonstrated (see **Figure 2.47**) on the cavity with the different PE recipe, that involves initial 1% of Oxygen gas treatment, with a following 20% O_2 concentration etching.
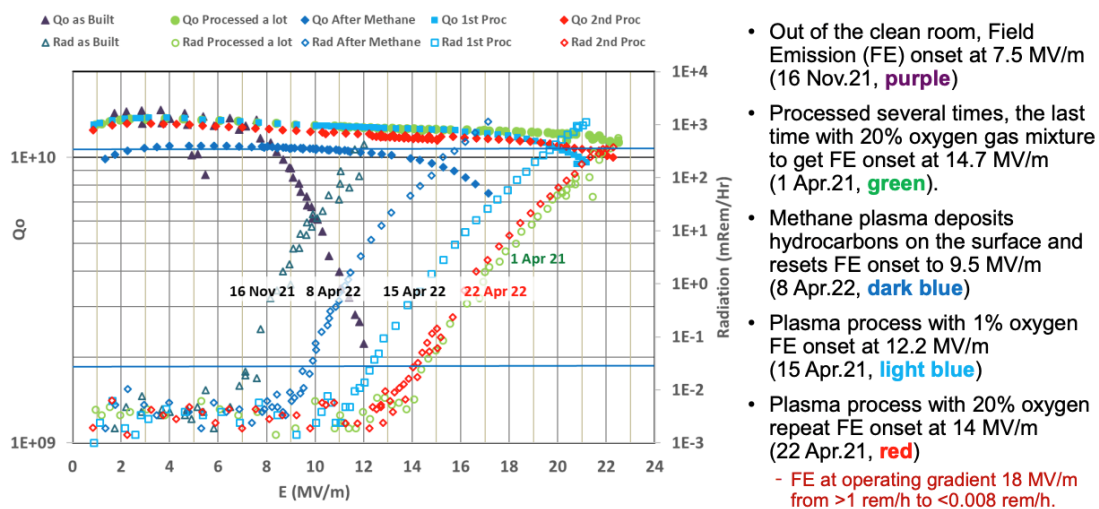
Figure 2.47: Plasma cleaning treatments and its impact on the cavity performance [232]

Summary: Plasma Etching technique is a powerful tool for mitigating the multipacting and field emission Q-disease for elliptical cavities, that has been demonstrated by JLab and Fermilab.

2.5.3.2   Laser polishing

Another promising technique that is considered to be applied in the SRF technology – Laser Polishing (LP) (see **Figure 2.48**). The use of lasers to smooth metal surfaces began to be reported in the 1970s and several processing strategies have evolved since [233]. Many applications were found of the LP in the industry, including the stainless steel polishing and removal if the surface machining patterns with the CO_2 lasers [234]. Pulsed laser micropolishing (also known as PLμP) was seen as an alternative to the CMP of the Nickel [235] allowing the surface roughness reduction and corrosion resistance improvement, similarly as it was found with LP of stainless steel [236]. A medical application has been found for the titanium LP where the surface contamination was reduced and oxide formation was reported [237].
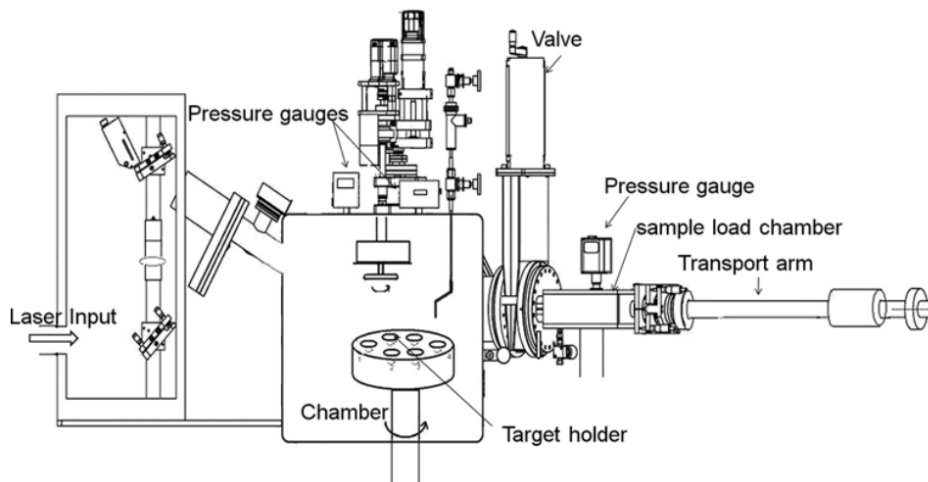
Figure 2.48: Schematic of laser treating apparatus [238]

There is a list of advantages over conventional treatments: chemistry-free technique, no surface contact, simultaneous surface monitoring possible. LP is a promising alternative to the chemical and mechanical polishing methods, which is feasible to be scaled for a large quantity of production. However, it is convincible to apply it not as a substitute for EP/BCP, but as a final step in the preparation of cavities. It is reported the possibility to decrease the roughness from initial tens of micrometres down to the several hundreds of nanometres [239]. L. Zhao has reported a smooth topography of the niobium, similar to that obtained by EP [240]. Although, it is rather difficult to remove any surface defect using only laser polishing. The common approach can be the multi-pulse illumination using a fixed laser fluence [241].

A completely physical method to modify the surface can improve the surface, decrease roughness. An optical concentrated beam is focalised onto the surface thus melting it. Partial melting of the surface is being prioritised, rather than a complete formation of a full liquid surface layer. This

can ensure the absence of hydrodynamic effects (e.g., formation of ripples). The resulting smoothening is a total sum of melt duration and the quantity of the pulses and its power.

Examined comparison of different chemical and mechanical treatments on the Nb surface with further laser polishing has been reported by Zhao et. al. [238]. It is as well reported that sharp edges are removed, as well as the step at grain boundaries. However, over-treating can result in larger surface waviness [240]. A good overview of the possibilities, advancements and difficulties of the LP for the SRF application is published by Zhao Liang [242].

An interesting approach was introduced by Medvids. A LP of the thin film of Nb over the Cu substrate, rather than classical substrate preparation way. Normally, Nb films are not treated neither chemically, nor physically in the SRF technology. However, based on the results, it is feasible the improvements of the surface roughness, and potential increase of the first flux penetration field [243]–[246]. Additionally it was demonstrated the possibility of adhesion improvement in the Nb/Cu structures and an increase of the crystalline structure of the Nb [246].

Summary: LP remains immature in terms of SRF application technology. However, preliminary study has demonstrated already some improvements in the surface roughness, adhesion of SC films on the Cu substrate. The technology needs a systematic study on the material of interest and a continuation of the engineering development of possible implementation of laser polishing of internal surface of an elliptical cavity.

3 Plasma Electrolytic Polishing. Literature review

The third chapter is describing the Plasma Electrolytic Polishing technology, as a main study of this dissertation. In the sub-chapters' literature review, possible mechanism and theories proposed by other scientists, available open list of electrolytic solutions is presented with a discussion.

3.1 Scientific context

Plasma Electrolytic Polishing (PEP) is an innovative process that can reach high gloss, low roughness surface quality using aqueous solutions of salts (more rarely acids, bases). PEP was nominated as one of the most promising alternatives to discover among other technologies of chemical and electrochemical polishing in the accelerator R&D roadmap [247]. Therefore, the European strategy for particle physics suggests the developing of new polishing methods that do not use concentrated acids (in particular hydrofluoric acid), in order to conduct the cavity production in the more sustainable way.

Currently, nothing related to the PEP in SRF field can be found in literature, although it was noted in the scientific communication that some laboratories tested this technology and cavity polishing [102]. The main difficulties can be listed as complex solution research and development for Nb and Cu metal treatments and cavity polishing system implementation. In this PhD dissertation, these limitations were addressed by developing original chemical recipes of PEP specifically for Nb and Cu. A polishing of elliptical geometries is presented in the experimental part as well.

3.2 Introduction

Plasma technology is based on the physical properties of matter in different states. When energy is applied to a solid, it can transition to a liquid state, and further energy can cause it to transition to a gaseous state. In case it is possible to apply even more energy, the gas can be ionized, and can be transformed into energy-rich plasma condition, the fourth state of matter. Among the Plasma Electrolytic Polishing (PEP), other plasma enhanced technologies exists as well (see **Figure 3.1**), such as plasma electrolytic oxidation (PEO), plasma electrolytic saturation (PES) and its variations (plasma electrolytic carburising (PEC), plasma electrolytic nitriding (PEN) etc).
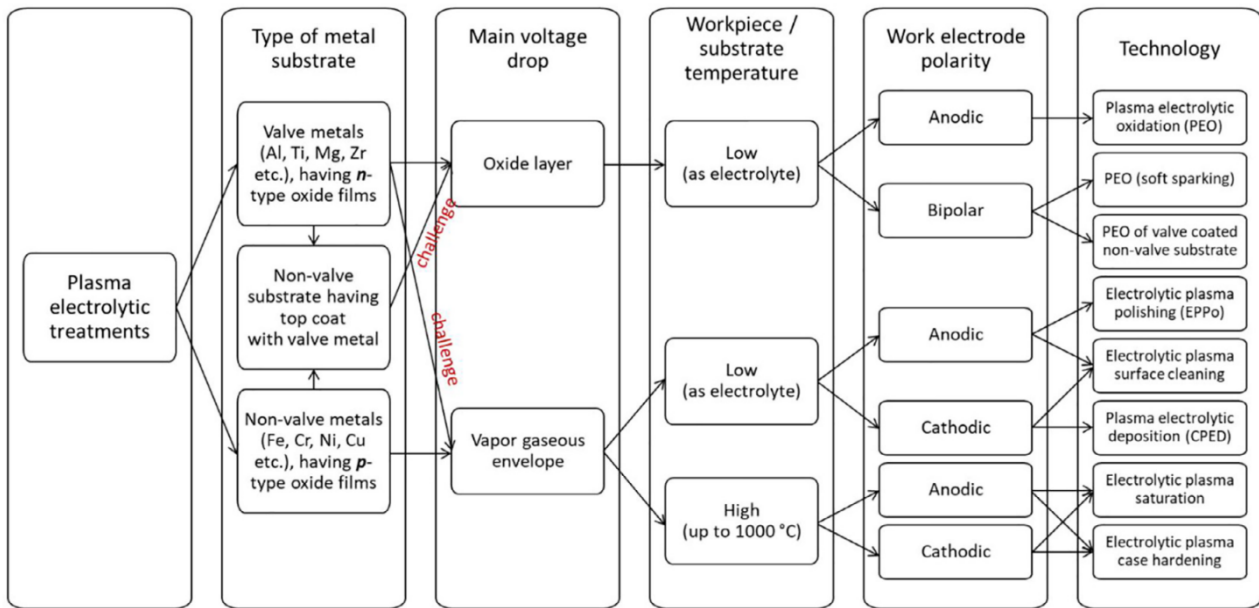
Figure 3.1: Plasma electrolytic treatments proposed classification [248]

PEP is commonly associated with electrolytic process since it shares the same electrochemical process – anodic dissolution of metal. Similarly, two electrodes are immersed into low-conductive electrolytic bath and are circuited with a direct current power supply (see **Figure 3.2**). The main practical difference is the usage of higher voltages and high current density regimes in comparison to EP. This leads to a different, almost not well-studied phenomenon at the metal surface – gas, vapour layer – electrolyte interface. Classical electrolysis is described with cathodic and anodic reactions, that can take place at the electrodes. In case of PEP, it can be divided into cataphoresis, plasma-chemical reactions, diffusion and heating [249]. PEP is primarily determined by the anodic dissolution process and plasma-chemical reactions. Plasma electrolytic polishing can treat almost any shape and any metal without a standard pre-treatment. Low roughness (Ra < 0,02 μm) and well controllable removing rates enable PEP to be used in precision metal industry. It is often mentioned the necessity of the greater surface ratio between anode and cathode: 1 to 10, to ensure the required current density regime for the plasma ignition at the anode surface.

Normally, by PEP it is considered anodic polarisation mode. However, some researchers noted the cathodic PEP, in which similarly, surface area of the cathode must be smaller than anode. Under such conditions high current densities occurring, solution evaporation and boiling taking place. The metal can reach 1000 ℃ in cathodic treatment, where often can co-exist carburizing and nitrocarburizing. Similarly, as in pulsed EP, AC and pulsed/pulsed reversed bipolar PEP can be also realised, where periodically anode and cathode can be reversed, thus combining the benefit of both treatments. This opens a way to variate even more the process, with a significant drawback of complexing the optimisation of the parameters [250]–[254].

76
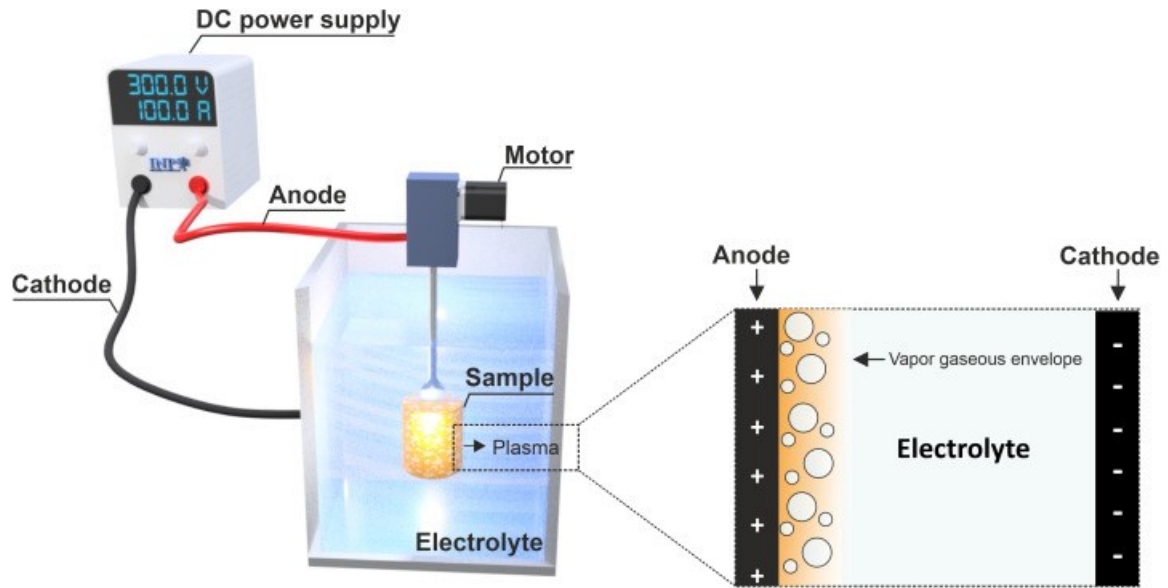
Figure 3.2: Schematic view of an electrolytic cell for PEP

Due to the terminological issues and simultaneous paperwork production from different research group, some miscalling as well still exists. Electro impulse polishing, Electrolytic plasma polishing and others, together with acronyms (EPP, PEP, EIP, PP).

During the process, a vapour-gas layer is formed around the anode electrode, that is a necessary condition for the plasma ignition. This in fact provides a possibility of ionization of the gasses, and subsequent establishment of first the transition period and finally the polishing regime. During the process, the anode pieces can reach temperatures higher than the solution temperature [255]. That is likely to the low conductivity of the solution, and Joule effect on the anode surface. According to the Joule's law resulting heat energy W is proportional to the I current, R electrical resistance and the time τ.

$$W = I^2 R \tau \tag{3.1}$$

The limitation of the PEP technology is determined by its properties described earlier. Similarly, to EP, can be applied only to the metal parts. While PEP can be used for removing burrs and residuals after mechanical processing, a longer treatment can lead to rounding of edges and corners, resulting in a loss of dimensional precision and accuracy of the treated object. Significantly, high area surfaces will require greater power supplies and power source output. A production of heat, gases and vapours requires adequate aspiration system, to ensure the security risk and allow proper cooling. Lastly, even though the complex geometries are possible to treat, naturally small cavities and holes are not activated during the standard PEP.

The current flow can be described with volt-amper characteristic curve (current-voltage relationship). Having two electrodes in the conductive bath, with a significant surface area ratio

between cathode and anode determine various phases (or regimes) of the process, that can be traced on the graph (see **Figure 3.3**).
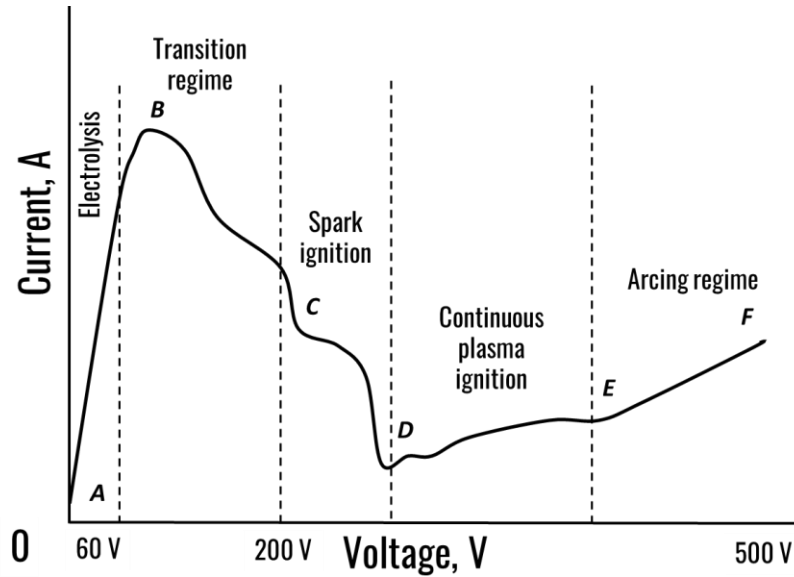
Figure 3.3: Current voltage characteristics of the Niobium PEP

The first sector AB represents classical electrolysis, in which the transportation of the ions of metal and gas production takes place, depending on the electrolyte composition, nature of electrodes, and is described with thermodynamics and kinetics laws of electrochemistry. This process takes places up to the tens of Volts with current densities of 0,01 – 1,5 A/cm². Normally the shape of the slope is linear, due to the nature of processes occurring, and with higher applied voltage with a fixed resistance, the current will increase respectively.

Transition (switching) part of the curve BD is describing the phenomena, when around the anode occurs the formation of the non-stable gas layer periodically, with a certain frequency of about 100 GHz [256], that leads to oscillation of the current, due to the non-stable resistance in the gas-phase layer between the anode and electrolyte. There is also a formation of the reactive gas, that is continuously exploding locally, leading to the instability of the Vapour-Gas Layer (VGL). More specifically, it is noted that in some cases, CD region can be described as a place of partial spark ignition once all the requirements are met.

The following region DE can be defined as a region, where the vapour-gas phase is established in the stable mode and relatively low oscillation of the current density. Here the PEP is taking place in most cases. The current density is decreased down to the 0,2 – 1 A/cm². The character of the curve in this part is descending, that is related to the negative value of the differential resistance:

$$R_{dif} = \frac{dU}{dI} < 0, \tag{3.2}$$

The sloping can be explained as a rise of the circuit resistance with an increment of applied voltage and the increase of the resistance is explained by the steadily increase of the thickness of VGL and the formation of the film on the anode, that has high resistivity [255].

Integral VGE around the anode can vary from tens to hundreds of micrometres thickness and is continuously changing. Electrical current in the anode zone is flowing from metallic anode to the electrolytic cathode though the complex system: metal-plasma-gas-electrolyte. With the high intensity of the electrical field and high temperature ionization of vapours, ion and electron emission is taking place to sustain stable electrical discharge. According to the Duradji [257]–[259], high electrical intensity is occurring at the peaks and nearby on the surface of metallic anode where the pulsed spark discharges can take place. An analysis of the different gas discharges shows the improbability of the electric arc and corona discharge between the metallic electrode and electrolyte. Thus, glow discharge is a main discharge phenomenon under stable regime of processing, meanwhile more rarely some arcing as well (mostly on the micro-irregularities) can occur and can be seen as randomly "running" bright dots on the metal surface [260].

A further increase (EF) of the applied voltage leads to the more intensive glowing. The VGL no longer covers completely the anode and allows under high electric field intensity to permit arcing. Depending on the nature of the metal and solution, the current densities can increase or decrease. In such conditions no more polishing is taking place, remaining only the possibility of surface oxidation.

3.3 Available recipes

Currently, the most studied metal alloy for the PEP processing is steel of various compositions including mild, stainless, low-carbon and other modifications. As a matter of fact, due to the current applications, some Ti-alloys are studied as well, and solutions have been found. On the contrary, the colour metals, such as Cu, Al, Zn and their alloys are much less studied. Even though some of metals have a published solution for PEP processing, in most cases those solutions are not able to deliver compatible and repeatable results, for example Cu and Ti/Nb metals recipes. Below, a table with most of the available PEP solutions developed by different research groups is listed (see Table 3.1).

Table 3.1 - Available solution from the literature for PEP

Metal	Electrolyte	Temperature °C	Voltage, V	Reference
Stainless steel	2–5% $(NH_4)_2SO_4$	80–95	250–400	Wang [261], [262], Ding [263]
Stainless steel	2–6% $(NH_4)_2SO_4$	40–80	240–320	Stanishevsky [264]
Low-carbon steel	0.5–8% NH_4Cl	81–95	240–380	Stanishevsky [264]
Alloy steel	3–8% $(NH_4)_2SO_4$	70–85	260–310	Dyblenko [265]
Structural alloy steel	3% NH_4Cl, 1% $(NH_4)_2SO_4$, 0.5% Trilon B	90	270	Ablyaz [266]

Metal	Electrolyte	Temperature °C	Voltage, V	Reference
Carbon steel	3% NH_4Cl, added glycerol or oxalic acid	78–82	275–300	Belkin [248]
Brass/ Copper	0.5–8% aluminum potassium sulfate (or 0.5-6% by weight disubstituted ammonium citrate +0.5-3% Na_2CO_3; or 0.5-6% by weight sodium ethylenediamine tetraacetate)	40–90	220–400	Stanishevsky [264]
Copper alloy	NH_4Cl, NH_4F, $C_6H_5O_7 (NH_4)_3$	60–90	250–340	Dyblenko [259]
Aluminum alloy	2–3% KCl, 3–4% $FeCl_2$,0.1–0.2% HCl		270–290	Rakhcheev [267]
Aluminum	0.5–3% $FeCl_3$	70–90	260–400V	Stanishevsky [264]
Aluminum	10% NH_4Cl, 4% KCl, 3% $H_2C_2O_4$	60–80	280–360	Duradji [268]
Titanium or titanium alloy	1.5~3% NH_4Cl, 1.25~2.75% NH_4F	80-95	280–320	Lingath [269]
Titanium alloy	2–7% NH_4F and KF,0.3–0.8% TiF_4	70–90	320~340	Damir [270]
Titanium alloy	2% Na_2SiF_6	50–60	100~400	Smyslov [271]
CP-Ti, $Ti_6Al_3Mo_2Cr$, Ti_6Al, Ti_6Al_4V, $Ti_6Al_5Mo_5V_2Cr$	Ammonium tetrafluoroborate or Sodium fluosilicate Potassium fluoride	80°...85°C	210...350 B	Damir and Smyslov [270], [272]
Ti /Nb	4% NH_4F	75-95%	260-300	Aliakseyeu [273]
Ti-6Al-4V	4–6% hydroxylamine hydrochloride and 0.7–0.8% NaF or KF	85–95	260–280	Smyslova [274]
Ti/Zr and their alloys	Borhydrofluoric, fluorosilicic-, hexafluorotitanium, or hydrofluoric acids	80–85	200–400	Mirzoyev [275]
Iron chrome alloy	NH_4Cl	60–90	270–290	Mingazhev [276]
Cobalt-chrome alloy	$(NH_4)_2SO_4$ or NH_4HSO_4	>80	300–380	Stefan [277]
Gold	4% NH_4NO_3 and NH_4Cl (1:3)	50–60	100	Polak [278]
Platinum	4% NH_4NO_3 and NH_4Cl (1:3)	60	300	Polak [278]
Magnesium alloy	0,5% CH_3COONa, 0,15% $(HOCH_2CH_2)_3N$, 0,05% $C_6H_{11}NaO_7$, 0,01% $C_6H_8O_7$	65–95	340, 10kHz, duty cycle 90%	Zhang [279]

Metal	Electrolyte	Temperature °C	Voltage, V	Reference
Zr-based amorphous alloy	$(NH_4)_2SO_4$, NH_4HF_2	50–100	100–380	Wang [280]
Zr-based amorphous alloy	2% Na_2SO_4, 0.2% $H_8MoN_2O_4$, 0,2% NH_4HF_2	85	300, 15kHz, duty cycle 15%	Cao [281]

3.4   Theories on mechanism of PEP

A phenomenological physical description of the processes that could take place during electrolysis was studied in 19th century [282]. The first traces of electrolytic plasma treatments were described in 1950s [283], [284]. In this work Kellog suggested, that plasma-layer is a "primary water-vapour film". He explained the sparks inside this film by the ionisation of the gas inside the plasm-gas layer caused by the high intensity of electric field.

As mentioned before, the conditions for the PEP establishment include anode polarization. In the 1970s a decrease of stationary heating during the electrolysis at relatively high voltages of (140 – 290 V depending on the solution used) was found [257]. In such conditions, the sample temperature drops significantly, and the emitting colour of the plasma glow changes as well.

Nowadays, there is no recognised theory on the plasma electrolytic polishing mechanism. Instead, there are attempts to describe and explain the nature of the passing current through the vapour-gas layer film, mechanisms of metal removal, presence of a short-term contact of the solution with the metal surface, surface smoothening mechanism. Although, a range of similar process has been developed and models have been presented [285], such as PEO [286], Plasma Electrolytic Coating Stripping [287], Plasma Electrolytic Heat Treatment [288], Plasma Electrolytic Surface Cleaning [289].

A list of papers explains similar mechanisms of current conduction [258], [290]–[293]. The high field ionize the water-vapour film, which surrounds the anode surface, and the plasma ignites. The plasma layer consists of the anions and cations of electrolyte and metal cations from the anode surface. Some paper underlines the special role of the mentioned ions in the conduction of the plasma vapour layer. However, other opinions still confirm the key role of such charged species, but not as the main ones. According to these papers indeed, high current densities values cannot be explained only by those ions. Possibly, ions contribute to the electron release, which provide necessary conductivity [258], [292].

A similar point of view is described by Vana [294], is that plasma vapour layer is mainly based on the water steam. Under the high intensity of the electric field the steam layer is ionized. This leads to the formation of the electric current flowing in the form of the glow discharge. Those discharges melt the workpiece surface in the place where the peaks are higher (see **Figure 3.4**), and thus levelling effect takes place. According to Vana, each of the plasma discharges removes same quantity of the material (see **Figure 3.4**, $S_1=S_2$), however the thickness of the S_1 part h_1 is bigger than h_2, and this might

be an explanation why the removal rate with the time tends to decrease. On the other hand, the better results and high gloss results may be obtained only after optimisation of the electrolytic solution composition, and this might indicate the presence of the electrochemical part of the whole process.
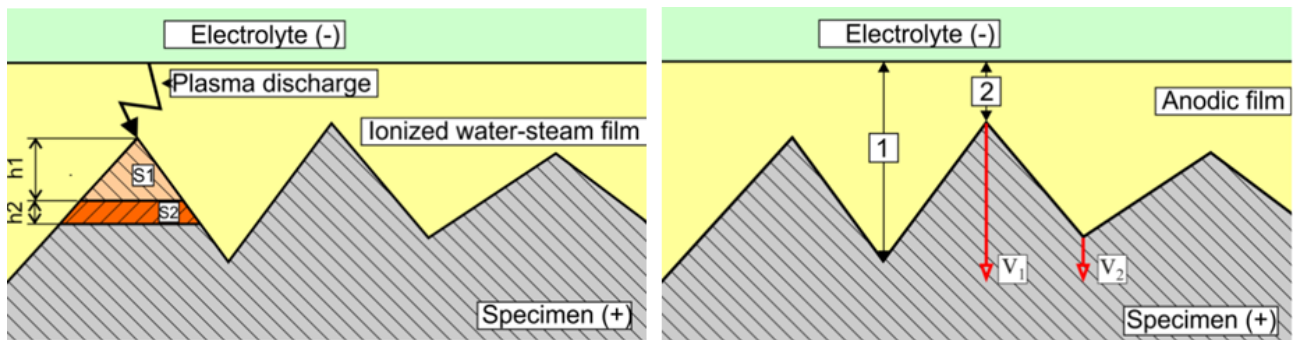
Figure 3.4: Scheme of the plasma electrolytic polishing and standard electropolishing

The main characteristic of the PEP processing is the volt-amper relationship curve together with the boiling characteristics [295], [296]. As described earlier, both have a nonlinear shape, (sometimes with negative slopes), and according to Parfenov [285] this may indicate that the process is rather complex and cannot be described only with electrochemical or plasma models. In the best scenario, some synergic approach will be found by adapting of the currently existing views.

Electrolyte bridges represent another attempt to describe electrical conductivity phenomena in the complex system of metal – plasma - vapour-gas – electrolyte system. As in other theories, the plasma-gas layer has not a stable thickness. In the presence of the high electric field and non-homogeneity of the plasma provide the zones with small thickness of the plasma-gas layer (see **Figure 3.5**). And with the ponderomotive force, the electrolyte can move closer to the workpiece surface, thus creating even smaller thickness zones. In such position, the electric field is higher, leading to the higher pondermotive force as well. According to the theory, once the distance between the workpiece surface and electrolyte are around a few micrometres, electrolyte bridges appear. The interaction between the bridges and the surface cause a current impulse and a quick boiling due to the Joule heating (see **Figure 3.5**d,e).Sinkevich compares this mechanism with explosive boiling. The theory explains the resulting current as a superposition of every small impulse of electrolyte bridges. The vibration of the VGL is also postulated due to the explosions. Sinkevich [297], [298] and Duradji [258], [299], [300] conclude, that the resulting current consist of the two components: constant and high frequency ones.

The PEP processing, being a special case of anodic polarisation, enables the formation of the oxide on the metal surface. Depending on the nature, conductivity, and semi-conductor properties, the formed Schottky type metal-oxide-electrolyte two junction system can be forward or reversed biased [301]–[303]. In the forward biased junction system allows the formation of the VGL around the anode. High electrical field intensity enables electrical discharges of various phenomena. In case of the reversed biased junction system most of the voltage drop will be maintained by the stationary

oxide formation process. After the achieving a breakdown of the energy value, micro discharges appear on its surface. These phenomena distinguish PEP from other electrolytic processes and support the "plasma" term usage. Valve metals (Nb, Ti, Al, Mg, Ta, Zr) form n-type semiconductor oxide due to the anionic vacancies at the metal – oxide layer and as well the space charge region within the film [304]. This makes polishing of such metals challenging, due to the preferability of oxide formation, instead of dissolution, as in most of the other metals (Cu, Fe, Ni, W and others), where the p-type oxide is either not stable or easily dissolvable.
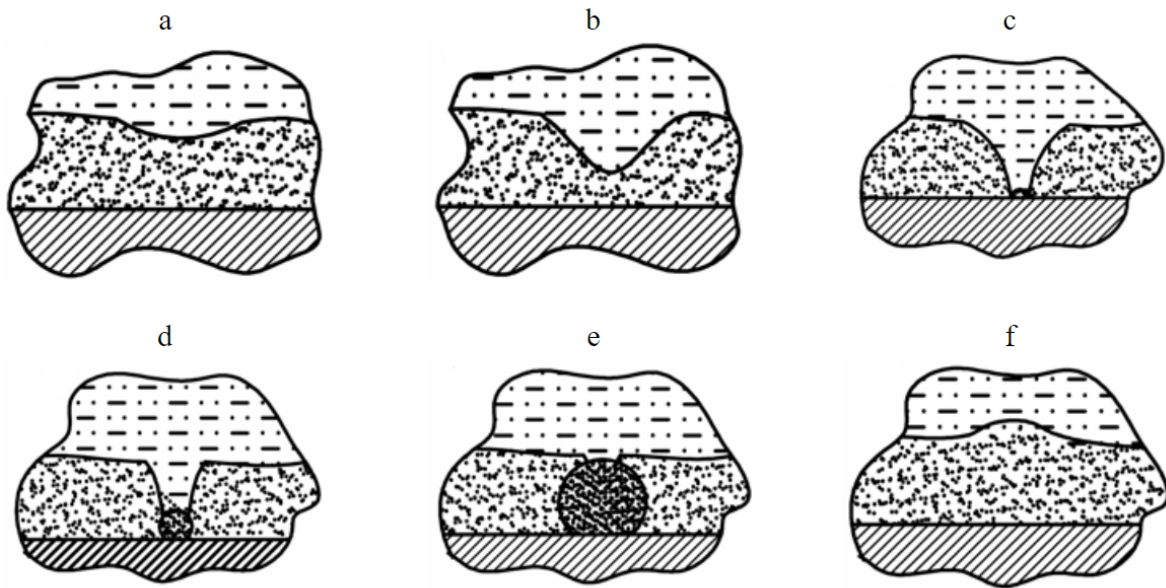
Figure 3.5: A scheme of vapour-gas envelope burst by electrolyte bridge [297]

Currently, it is believed that only three charge carriers are capable to explain the passage of the current through the VGE. The first option can be represented by ions and electrons, that take place inside the VGE (water vapour, gases, atomized metal of the anode), which are permitted to exist under certain conditions of the ionization under the electrical discharge. The second option are the classical electrolytic anions that are under the boiling conditions and high electric field can carry current. The last, as mentioned, is the electrolyte, that can stay in a short contact with the electrode. To overcome this issue, a fluoride composition can be used, along with steady treatments and even an AC regime to proceed [273], [305], [306].

The erosion of the metal is explained in case of ion and water vapour carriers by direct interaction between the anode surface with electrons and VGE ions. As a result, this interaction can be described as a bombardment of the surface accelerated by the electric field. In other cases (second and third options) the interactions can be described as a chemical or electrochemical nature with respective reactions that take place at the interface. Naturally the active force in such conditions is the activity (concentration) of anions, electrolytic solution, water in the system. These mechanisms are usually proved partially by correlations, such as (surface roughness trends, mass loss, anionic

composition of the electrolyte, fractional characteristics of the electronic or ion component in the measure currents [248].

The common view, at least on the partial contribution of the electrochemical process inside the PEP, results in several standard electrode reactions. The main two reactions are: oxygen production (1) and metal dissolution (2) on the anode. Depending on the nature of the metal and its oxide, the resulting reactions can be either the surface dissolution or formation of the anodic oxide film (3). Instead, on the cathode, commonly hydrogen reduction (4) and/or cation deposition (5) can take place on the electrode surface:

$$2H_2O \rightarrow O_2 \uparrow + 4H^+ + 4e^- \tag{3.3}$$

$$Me \rightarrow Me^{n+} + ne^- \tag{3.4}$$

$$xMe^{n+} + 1{,}5xyH_2O \rightarrow Me_xO_y + xyH_3O^+ \tag{3.5}$$

$$2H^+ + 2e^- \rightarrow H_2 \uparrow \tag{3.6}$$

$$Cat^{y+} + ye^- \rightarrow Cat^0 \tag{3.7}$$

$$2Me + nH_2O = 2MeO_{n/2} + 2ne^- + 2nH_{aq}^+ \tag{3.8}$$

$$2MeO_{n/2} + 2zA^- + 2nH_{aq}^+ + (2m-n)H_2O = 2(MeAz \cdot mH_2O)^{(n-z)+} \tag{3.9}$$
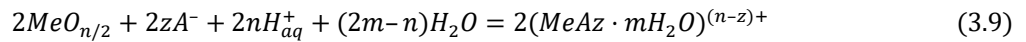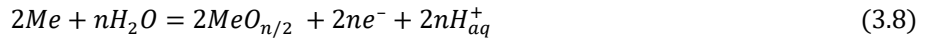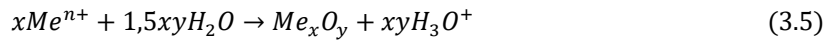
Streamer theory

The removal process is characterized by three stages [307], [308], see **Figure 3.6**. The *first one* is characterized by formation of the so-called avalanches. The electrolytic solution (1) is electrolyzed and accumulate electrons (4) and positive ions (3) between the solution and metal workpiece (5). Electrons are faster than ions, so that they are forming the "head" of the avalanche (7), instead the tail is formed by the positive ions. Secondary electrons (6) are formed because of photoionization (2) (**Figure 3.6**a).

The *second stage* describes the formation of the discharge channel. The first electron that are approaching the metal surface are forming the primary discharge channel, after which the secondary electrons are accelerated forming secondary avalanches (see **Figure 3.6**b). Those secondary avalanches are attracted to the primary discharge channel, due to the present field distortion. After a certain time, the process tends to stabilize which results in the forming of the stable discharge channel.

Finally, the *third stage* includes the gas explosion and resulting removal of the material (see **Figure 3.6**c-f). A high quantity of local collisions between electrons and positive ions leads to the heating. This causes the gas to expand in the raised temperature discharge channel. However, the inhibition of the expansion is present, due to the magnetic compression. Finally, those conditions force the gas to explode, and by that remove partially the peak on the surface. After the gas explosion, the channel is revoked, and the process can be initialized from the stage 1. This theory greatly explains the surface levelling. The explosion of the gas leads to the local melting of the metal surface, the

melting metal is carried away with the local gas explosion. Melting process can be described as a heat transfer process, that is induced by a local heat flux density. The energy gain of the surface of metal anode mainly from electron-bombardment [309].
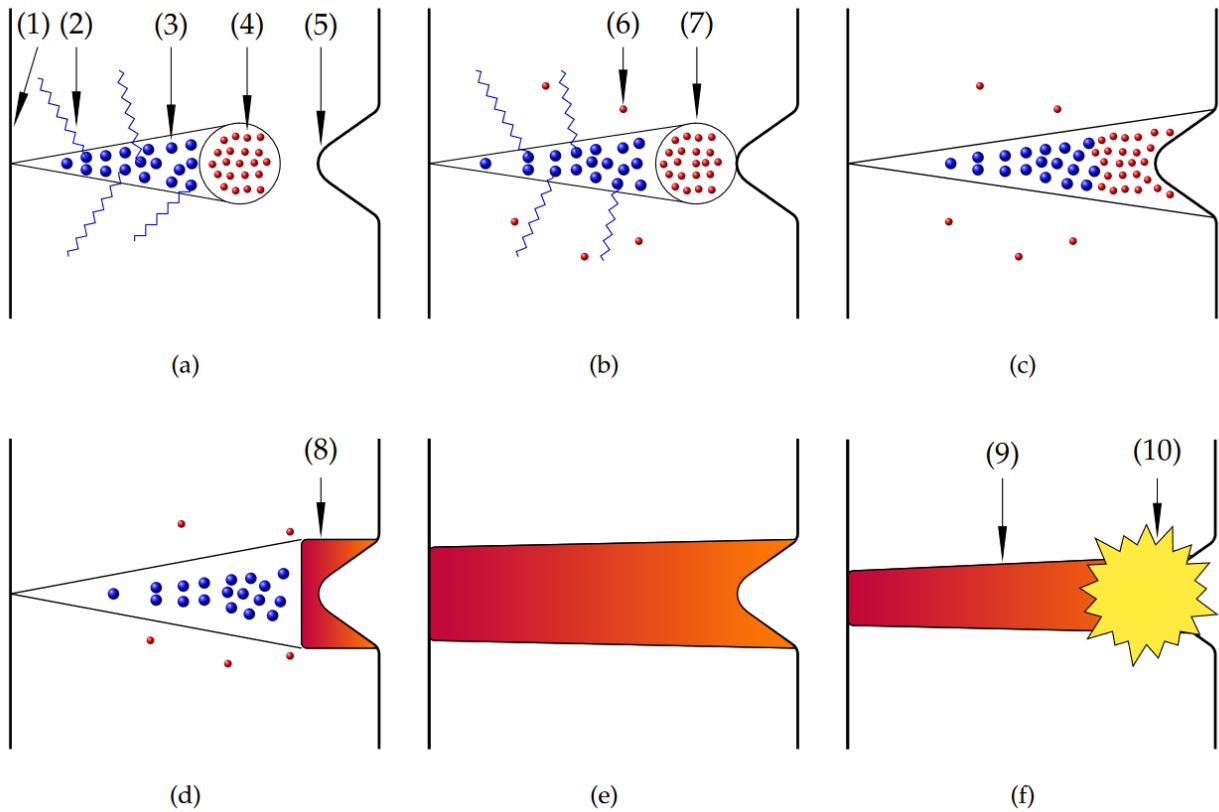
Figure 3.6: A Scheme of the formation of a plasma discharge according to streamer theory, where (1) is electrolyte, (2) a photoionization process, (3) ions, (4) electrons, (5) is a metal workpiece, (6) secondary electrons, (7) avalanche head, (8) the streamer, (9) the plasma channel, (10) gas explosion [308]

Moreover, it does not answer how exactly different chemical composition play a role in the specific metal removal, since the only proposed interactions are the physical ones.

The majority of theories in their attempt to describe the material removal process use the melting process as a main or as an important part [255], [261], [291], [293], [307], [308], [310], [311].

Plotnikov et al [293] proposed a combinational view of the removing process: melting and oxidation. The gas formation is mainly related to the high temperature. Due to the high intensity of the gas, ionization takes place inside the bubble, as a result high temperature plasma appear, that can melt the oxide layer on the surface locally. Due to the high temperature the gas bubble expands creating a shock wave. It is partially reflected from the vapour-gas layer and electrolyte, thus compressing the remaining gas bubbles. This causes the collapse of the bubble. It can be considered as a cavitation process, after which the ion gets trapped into the newly created void. Finally, the ion starts to oxidize the surface. An important restriction of this model relates to the relation between the

speeds of oxidation and material removal by the high-temperature plasma. The polishing is permitted only in case those rates are comparable. This may explain the role of the electrolyte, enabling some metals to be treated, and some metals to be oxidized. However, it is still not explaining the limited chemical compounds list that are able to treat metals like Ni, Fe and Cu.

And indeed, in case of on-site melting two possibilities can (co)happen: melting and removing of the metal (or metal oxide), remelting and spreading the metal over the surface, thus smoothing; and detaching and dissolution of the metal(oxide).

Electrochemical nature

Many researchers see the only or the important role of the electrochemical phenomena in the PEP processing [255], [290], [298], [305], [310], [312]–[315]. Kalenchukova et. al [290], states, that there is no melting during the PEP and the main polishing mechanism is electro dissolution (see **Figure 3.7**). The plasma-gas enriched layer is not uniform across the surface and it has a different thickness on the peaks. As it happens in electrolysis, the edges and peaks often have higher current densities, as well here leading to the higher removal rates preferentially on the peaks, finally conditioning a rapid decrease in roughness.
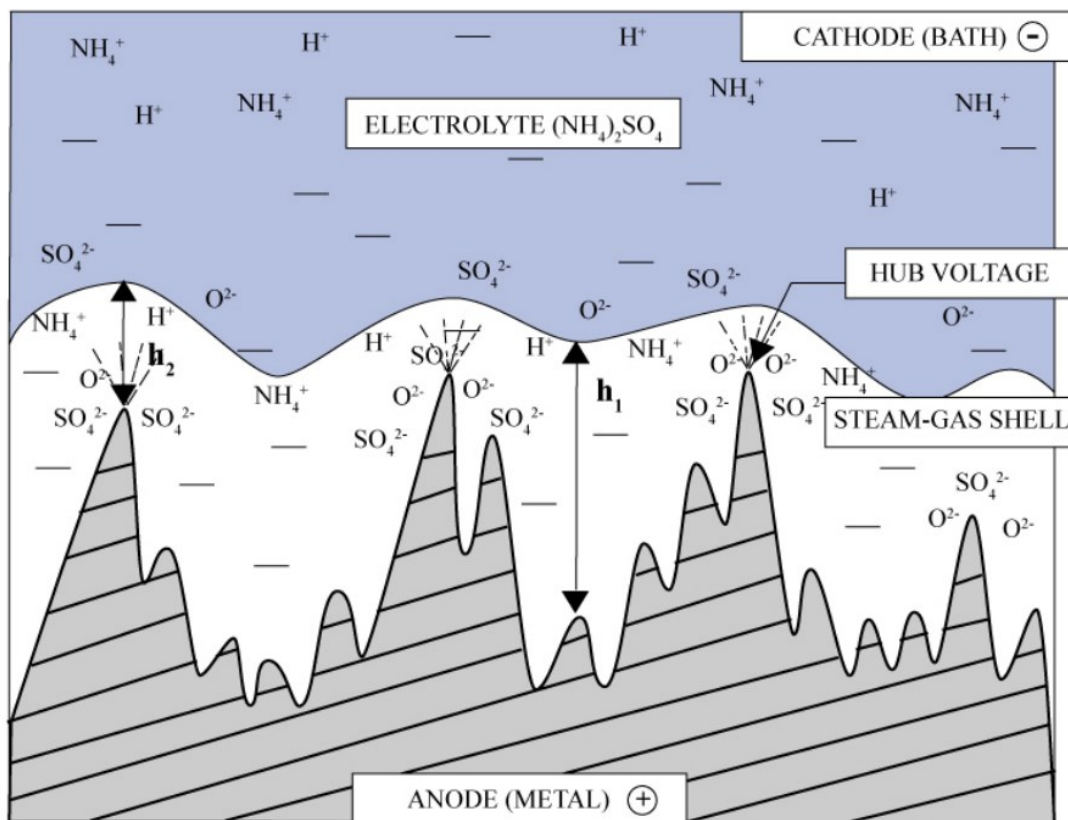
Figure 3.7: The schematic mechanism of PEP electrochemical dissolution [290]

Another variation of possible electrochemical mechanism is proposed by Smyslov et. al [305]. A superposition of simultaneous oxidation and oxide etching of the formed layer is proposed. The

levelling effect is explained by the preferential etching on the peaks position since the thickness of the oxide would be lower.

The current efficiency study made by Parfenov et.al [313], has led the scientist to the idea, that the PEP has only electrochemical character achieving about 30%. Despite the presence of sparks, there is not any melting phenomenon. Those conclusions lead to the fact, that the presence of the vapour-plasma layer somehow changes the electrochemical reactions. It is also mentioned the electrochemical machining (ECM), that has even lower current efficiency of 9%, and it is explained by the passivation of the surface with oxygen. In the case of PEP and the presence of stable VGL, it cannot be the oxygen formation on the anode. Even though the formation is still present between the plasma-gas layer and electrolyte [284]. This also enables the possibility of various simulation, as an electrochemical machining process [256].

Further steps were made by Sinkevich [298], [314], [315], who assumed that the PEP is a special case of anodic dissolution, whose steps can be presented as a complexation through the sequentially parallel or a series of sequential steps. The evidence of the anodic character of the material removal is proved by the surface analysis after the PEP, which indicates a formation of anodic films with the presence of anions from the electrolyte. The composition of such ultrathin film as well confirmed the presence of series of steps, semi-stable complex compound formation. That perfectly matches the electrochemical behaviour.

Volenko et.al. [310] used the electrolytic bridge model to describe the mechanism of removal of metal. It is also mentioned that the PEP process consists of two co-existed phenomena: electrochemical dissolution and electrical discharge machining.

Alekseev earlier, presented among the polishing mechanism: ion sputtering, various electrical discharges, and chemical sputtering [292].

Chemical and physical model of steam shell

For a successful polishing via PEP, one of the necessary conditions is to have film boiling (instead of bubble boiling phenomenon). Higher voltages increase the thickness of the vapour layer and thus promotes the increase of the resistivity of shell layer, causing heating to the anode (see **Figure 3.8**). The volume nearby the shell layer is saturated with steam ions, molecules of dissolved substances, water molecules. During the boiling, hydrated molecules contribute to the vapour phase exchange of ions. The conductivity is explained by the anion emission into the shell and further concentration of them near the bubbles. With high voltages, the surface of the bubble obtains significant negative charge, thus internally the gas is ionized, and the high temperature plasma ignites. It is assumed that the oxide layer of the surface is partially melted, thus there is no direct reaction with the metallic anode. Due to the high temperature, the bubble immediately increases, and additionally the electric field makes it to be elliptical shape. An enlargement of the bubble causes high shock wave and eventually the collision of the bubble. A somewhat cavitation process takes place. The anion is placed

in the void, with a further oxidation of the metallic surface. The lifetime of a one single bubble can be at the value of $10^{-6} – 10^{-7}$ s.
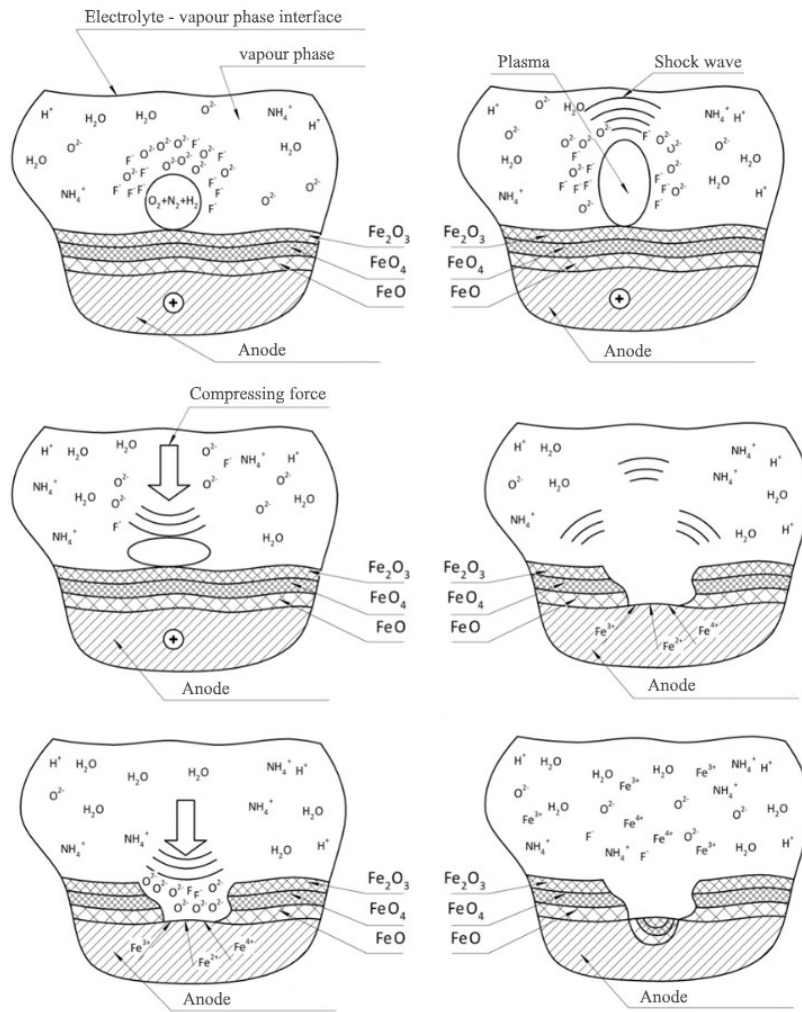
Figure 3.8: A scheme of steam-shell mechanism of PEP [293]

Together with the mechanism studies, equivalent circuit-schemes of the process both for the PEP and Jet-PEP process were proposed (see **Figure 3.9**).
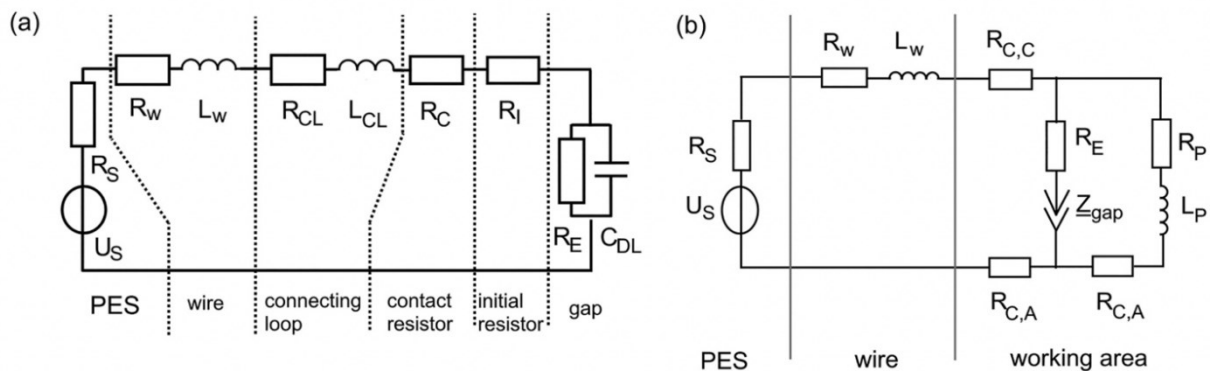
Figure 3.9: Equivalent circuit diagrams of (a) PeP [316] and (b) Jet-PeP [317]

4 Methods and Instrumentation

This chapter has united all the characterisation and related instrumentation description used in this dissertation and used by the author.

4.1   Characterization instrumentation

Most of the characterisation was carried out at the Surface Technologies and Superconductivity Service on-site at the Legnaro National Laboratories of INFN, using the following available equipment: XRD, SEM, EDS, linear profilometer, and optical microscopy.

4.1.1   Linear profilometer

A linear stylus profilometer is a powerful tool to study the surface with a soft direct contact. The tool is represented by the Veeco Dektak 8 model (see **Figure 4.1**).
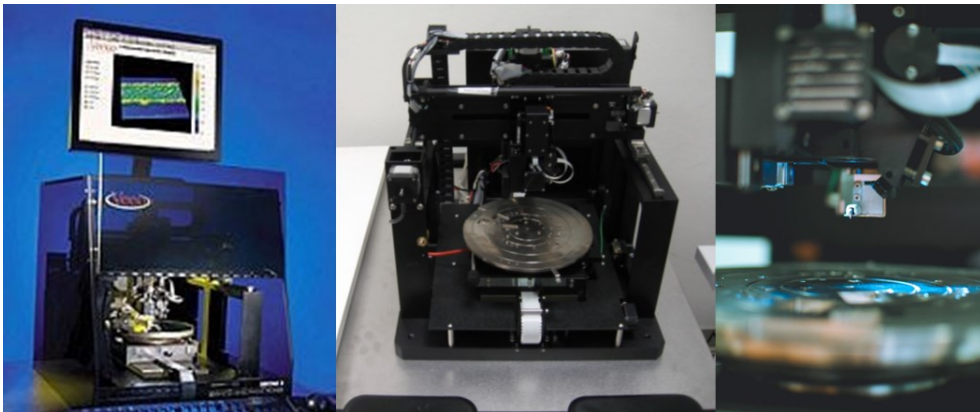
Figure 4.1: Veeco Dektak 8 linear profilometer with a stylus tip

The measurements are carried out electromechanically by moving the diamond stylus over the surface of the samples. The stylus and plate can be moved and programmed to scan a user-defined area or linear length. Additionally, the speed and stylus force can be adjusted for the chosen metal. The stylus is strongly fixed with the Linear Variable Differential Transformer (LVDR). During the scanning operation, the stage and sample can be moved to scan the surface. The surface scanning is performed by varying the vertical movement of the stylus. Electrical feedback signals are produced when the core positions of the LVDT change. The LVDT produces an analogue signal (related to the position change), which is conditioned and converted to digital form with the high-precision, integrated analogue-to-digital converter [318].

The Veeco Dektak 8 can analyse the surface and reveal the thickness between two positions, calculate Ra, Rq, Rz, and other functions to describe surface roughness. It is worth mentioning that due to physical limitations and the nature of the measurement, this kind of characterisation should be compared with other contact roughness meters, rather than with AFM, laser, or optical ones. Another factor that may affect the analysis is the scan length. Longer scans are well-suited for macro and medium roughness, while scans for micro-roughness are less reliable over longer distances. Conversely, micro-roughness structures are well-analysed with smaller areas/lengths but may not include statistically spread macro/medium defects of the studied surface. Thus, in this dissertation, primary attention was given to three length distances of 1000, 3000, and 6000 micrometres. An additional feature of interest is the mapping of the surface, where the area is set by the number of parallel lines (resolution), and multiple scans are performed to calculate a three-dimensional surface area with the Ra Roughness function.

arithmetic average height (*Ra*) – is the most common parameter used to describe surface roughness. It is defined as the average absolute deviation of the roughness (heights and pits) irregularities from the mean line over one sampling length. This parameter is easy to calculate and provides a good representation of the quality state of the surface. However, it does not provide any information regarding the wavelength, and it is not sensitive to minor changes in the analysis profile.

$$R_a = \frac{1}{l_r} \int_0^{l_r} [z(x)] \, dx \qquad (4.1)$$

quadratic average, or *root mean square* (*Rq*) – represents the standard deviation of the distribution of the surface height. It is more suitable for statistical applications and is more sensitive than the arithmetic average height (Ra) to large deviations from the mean line. The mathematical representation of this function is presented below:

$$R_q = \sqrt{\frac{1}{l} \int_0^l \{y(x)\}^2 dx} \qquad (4.2)$$

maximum peak to valley height of the profile, within a single sampling length (*Rz*) is the maximum height of the profile and indicates the absolute vertical distance between the maximum profile peak height and the maximum profile valley depth along the sampling length. This parameter is more sensitive to occasional high peaks or deep valleys than *Ra*.

$$R_{z(ISO)} = \frac{1}{n} \left(\sum_{i-1}^{n} [p_i] - \sum_{i-1}^{n} [v_i] \right) \qquad (4.3)$$

The measurements by the linear stylus profilometer are relative and not absolute, meaning that the values can be compared with each other at similar working linear distances. In addition, measurements with a linear profilometer cannot be compared with measurements done by Atomic Force Microscopy (AFM), optical, and laser instrumentation because the values cannot be directly compared due to the different linear or superficial dimensions of measurement length/area.

91

4.1.2   Scanning Electron Microscope

A Scanning Electron Microscopy (SEM) is a non-destructive analysing tool that allows detailed characterization of the surface morphology. It can reveal structures, patterns, or highlight surface defects, such as pitting, that may not be visible with the naked eye. As an inspection tool, it can also give an idea of the surface roughness, whether it is smooth or has a particular pattern that normally affects the roughness parameter.

SEM produces secondary electrons, back-scattered electrons (BSE), light (cathodoluminescence), characteristic X-rays (in case of the attachment of the EDS module, see chapter 4.1.3), specimen ground current and transmitted electrons by electron material interaction. The signals are produced by the interaction of the electron beam with the surface of the studied samples. The chamber, detectors and the electron column are kept in vacuum conditions to allow electron beam generation and free advancements [51]. In the standard mode, Secondary Electrons Imaging (SEI) can produce high quality and resolution images down to the 1...5 nm scale. Due to the narrow beam of electrons, images obtained with SEM have a large depth of focus allowing a characteristically three-dimensional analysis useful for the understanding of the surface topography.

In this dissertation two different SEM machines were used, both installed at Legnaro National Laboratories. The first *FEI-*formerly Philips, USA Scanning Electron Microscope *SEM XL-30* (see **Figure 4.2**a) and *COXEM* Company, model *CX-200plus* (see **Figure 4.2**b).

(a)   (b)
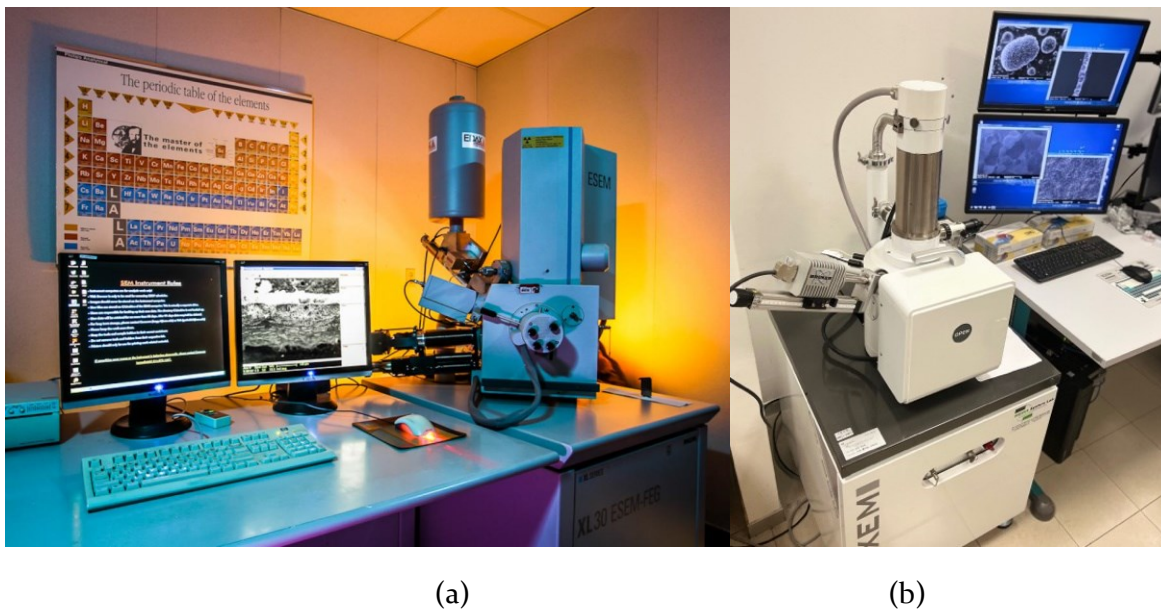
Figure 4.2: Photo of the two used SEM machines

Presented XL-30 and CX-200plus have a list of features and characteristics in the Table 4.1 below:

Table 4.1 - Characteristics of the FEI XL-30 SEM and CX-200plus

Parameter	XL-30	CX-200plus
Performance Resolution:	1.5nm at 10kV or higher. 2.5nm at 1kV.	<3nm at 30kV
Electron Source:	Schottky-based thermionic field emission electron gun. Fully automatic gun configuration control. Continuously variable beam acceleration voltage range 0.2~30KV. Beam current range 1 pA ~ 25 nA.	Pre-Centered Tungsten Filament. 1 - 30kV (adjustable in 1kV scale).
Specimen Stage:	Eucentric goniometer: 4-axis (X, Y, Z and R) . Tilt Range: 15 ~ 60 degree. Specimen chamber diameter 284 mm.	Stage: X: 40mm Y: 60mm Z: 0-60mm. Tilt range -20 to 90° R: 360°.
Vacuum:	One diffusion pump (lower chamber), two ion getter pumps (gun chamber).	High Vacuum, Rotary Pump, Turbo Molecular Pump
Vacuum regained:	Less than 5 min.	Less than 4 min.
Scanning System:	Survey mode, scan mode, and scan rotations. Magnification range: x20-x80.0000.	Magnification range: x15 ~ x300.000
Scanning modes	Secondary electron (SE) detector. Back-scattered electron (BSE) detector. Energy dispersive X-ray spectrometer (EDS).	Secondary electron (SE) detector. Back-scattered electron (BSE) detector. Energy dispersive X-ray spectrometer (EDS).
Automation	-	Focus, Filament, Brightness/Contrast.

Additionally, the SEMs were equipped with an EDX module for chemical composition analysis. All the samples studied were of small dimensions for convenience, and prior to mounting, they were always subjected to ultrasound cleaning using either GP 17.40 or Rodaclean soap. In some cases, such as for cross-sectional analysis, the samples were cut using electro-erosion techniques and gradually lapped, decreasing the abrasiveness of the lapping pad.

4.1.3 *Energy-dispersive X-ray spectroscopy (EDS, EDX, EDXS or XEDS)*

As mentioned before, this analytical technique allows elemental analysis or chemical composition of the characterized sample surface. The state of the art of this technique relies on a source of X-ray beam excitation of the studied sample. It relies on the basic principle that every element has its own atomic structure and consequently peak on the electromagnetic emission spectrum. Those peaks are well predicted with the Moseley's law. The analysis is done in a way that an X-ray source excites the electron in the inner shell, ejecting it from the shell it creates an electron hole and releases an exact value of energy (see **Figure 4.3**), that can be analysed with energy-dispersive spectroscope.

A powerful attachment to the modern SEM – EDS modules can provide both qualitative and quantitative analysis of the specimen chemical composition. A Bruker EDX (see **Figure 4.4**) unit was installed at a certain angle to provide the described analysis.
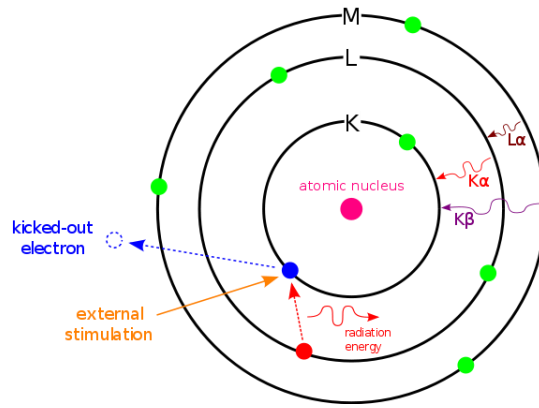
Figure 4.3: A scheme that represent the EDX basis of the technique [319]

Figure 4.4: Image of the Bruker EDX module and a supplied software for EDX spectroscopy analysis

4.1.4 *Optical microscopy*

ZEISS Axio Lab.A1 (see **Figure 4.5**) is an optical microscopy, which gives the possibility for the fast analysis of surfaces and materials with 5 different ZEISS EC EPIPLAN objectives (5x, 10x, 20x, 50x, 100x). With the magnification up to 100x it is possible to see texture of the material, macro and micro surface contaminations, morphology, and mechanical defects. It is also possible to analyse the powder material and make the comparison.

Undoubtedly, the main advantage of this microscopy over the SEM is the speed at which an operator can obtain preliminary results, such as the surface morphology overview. Operator has the possibility to save the photos acquired with the provided software and a webcam tool, connected with a parallel optical tube allowing the software acquisition mode. Naturally, from the physics of the analysis, some disadvantages are also present, such as a need in some case a manual calibration for the light intensity, application of the light filter and a manual search for the focus. In case of low magnifications (e.g., 5 – 20x, it is quite fast and precis), however in case of higher magnification values, it might become a challenge, especially if the studied surface has a significant difference on the height

(or simply high roughness). In that specific case, only a portion of the image will be in focus, unlike the SEM imaging, where most of the view normally is in focus, due to the large depth of focus.

Figure 4.5: An Axio Lab.Al microscopy and the typical output of the analog surface photo

4.1.5   6 GHz cavity inspection stand

The 6 GHz cavities were inspected with the dental camera and the pre-built stand in order to have a clear view of the hidden part of the elliptical cell. The camera inspection stand is presented on the photo below (see **Figure 4.6**):
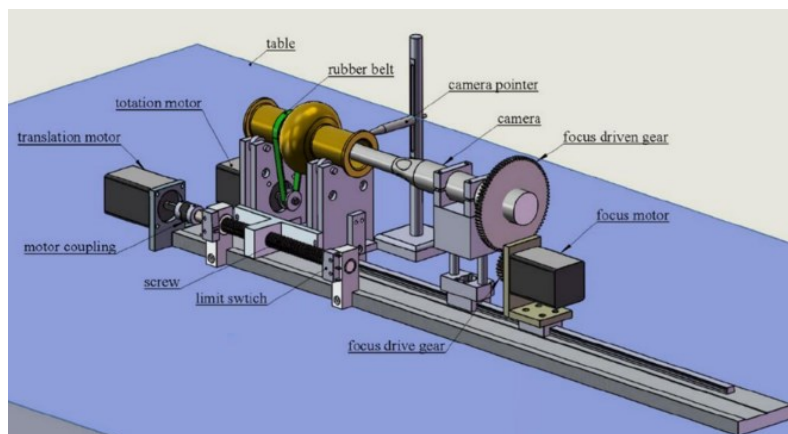
Figure 4.6: A scheme of optical inspection system for 6 GHz cavity [96]

The photo acquisition is normally done capturing the internal surface all along the length of the cavity, starting from the cut-off, passing to the iris, cell and again cut-off. During the inspection rotation of the cavity is done to ensure the surface is identical in every part of the elliptical shape. The inspections analysis is usually done for a complete history of a one cavity during the mechanical treatments path and sometimes during the chemical preparations. The camera offers a 60° view of the inner surface on a variable focal distance.

4.1.6 Spectrophotometry

Spectrophotometry is a standard and inexpensive technique used to measure light absorption or the concentration of chemicals in a solution. It uses a light beam that passes through or reflects off the sample and is then analysed with a photon analyser. Inside the machine, a monochromator (such as a prism or grating) refracts the light into a single spectrum and disperses polychromatic light into its essential wavelengths. A grating then divides the light into different sections. The analyser is a light-receiving element detector that absorbs the energy of the incident light. Such detectors can be photomultiplier tubes or photodiodes. Finally, they convert the light energy into an electrical signal, which is used to generate the absorption figure.

The portable spectrophotometer Konica Minolta CM-2600d is a great instrument for fast analysis of surface colour, measuring reflectance and transmittance. It is also capable of analysing the industrial gloss parameter in GU units at an 8° angle. The reflectance is measured at a specific wavelength, and a full evaluation is done at a range of wavelengths from 360nm to 740nm. A complete list of characteristics is shown in Table 4.2.

Table 4.2 – Characteristic of the spectrophotometer CM-2600d

Illumination / observation system	d/8° (diffuse illumination, 8-degree viewing), equipped with simultaneous measurement of SCI (specular component included)/SCE (specular component excluded)
Size of Integrating Sphere	Φ 52mm
Detector	Silicon photodiode array (dual 40 elements)
Spectral separation device	Diffraction grating
Wavelength range	360nm to 740nm
Wavelength pitch	10nm
Half bandwidth	Approx. 10nm
Reflectance range	0 to 175%, resolution: 0.01%
Light source	3 pulsed xenon lamps
Measurement time	Approx. 1.5 seconds (approx. 2 seconds for fluorescent measurement)
Measurement/Illumination area	MAV: Φ8mm / Φ 11 mm SAV: Φ 3mm/ Φ 6mm (Selectable between MAV and SAV)
Light source	3 pulsed xenon lamps
Observer	2/10° (CIE 1931/2°,CIE 1964/10°)
Color space / colorimetric data	L*a*b*, L*C*h, CMC (1:1), CMC (2:1), CIE94, Hunter Lab, Yxy, Munsell, XYZ, MI, WI (ASTM E313), YI (ASTM E313/ASTM D1925), ISO Brightness (ISO 2470), Density status A /T, WI/Tint (CIE/Ganz), CIE00

The reflectance data were measured at least three times for every tested sample, the values are averaged by the machine and its software (Spectra Magic NX 3.31.0000). The 8° gloss parameters are obtained as a distinct value of a measurement. The reflectance measurement consisted of a steadily acquisition of the reflectivity values across the above-mentioned range of wavelengths. For a practical reason, in some experiments thess values were averaged, resulting in a distinct % value for a single measurement.

4.1.7   pH measurement unit, temperature sonde, heating element

A pH value can be measured by means of chemical reaction with universal pH indicator paper or by instrument to increase the precision. Litmus papers are changing the colours of the indicator with the change of the pH value, considering the hydrogen ion content. In the case of the pH meter instrumentation, pH probe normally is a two-electrode system, which simply measures the potential (voltage) produced by the solution being tested. A solution that is acidic has more positive charged hydrogen ions that alkaline solution. Most of the pH probes contain two electrodes inside the body: one to measure potential (so-called glass electrode) and a reference electrode.

The measurements in this dissertation were obtained by both the universal pH indicator (in case of rough value acquisition) and with a pH/mV meter Delta OHM HD 2105.1 (with a pH electrode Delta OHM KP30; see **Figure 4.7**a). To confirm the value, another pH/mV meter was used: Hanna Instruments HI 9024C (with a pH probe HI 1230; see **Figure 4.7**b).

(a)   (b)

Figure 4.7: a) pH/mV meter Delta OHM HD 2105.1, b) Hanna Instruments HI 9024C

The precision and resolution of measurements are determined by the device specifications and pH probe used, more details are shown below in the Table 4.3, where some selected specifications of interest are shown.

Table 4.3 – Specifications of the pH meters

Instrument	HD 2105.1	HI 9024C
pH Range	-2.000...+19.999 pH	0.00 to 14.00 pH
pH Resolution	0.01 or 0.001 pH	0.01 pH
Accuracy	±0.001 pH ± 1 digit	±0.01 pH
Calibration error @25℃	Slope < 50mV/pH or Slope > 63mV/pH; Sensibility < 85% or Sensibility > 106.5%	Offset ±1 pH; Slope From 70 to 108%
Temperature compensation	Automatic or manual -50...+150 C°	Automatic or manual 0...100 C°

4.2 Experimental instrumentation

All the experiments were conducted at Legnaro National Laboratories as well, all the equipment and supplements were available at the Surface Technologies and Superconductivity Service chemistry laboratory. To comply with security risks and protocols, all the chemical and electrochemical processes were placed under the chemical hoods with a high aspiration force always turned on.

4.2.1 *DC power supplies*

Auto-adjustable Direct Current (DC) Power Supplies (PS) are essential tool in the electrochemical processes, which transfer AC energy source to form a specific voltage, current power load in the closed circuits (electrochemical cells). Those PS are characterized by the long list of characteristics, among which maximum power output value, maximum values of current and voltage output, polarization times. For the laboratory needs and relatively small-scale processes do not require more than 500-1000 W PS, and all the classical electrochemical processes described in this dissertation were conducted with the HP Agilent 6032A Variable DC Power Supply 0-60v/0-50A at peak power 1000w (see **Figure 4.8**a). Instead, as it was extensively discussed in the chapter 3, plasma processes need higher values both current and voltage PS (consequently even higher power values). In case of the PEP processing, two PS were used connected as a master and slave units in parallel connection: ITECH IT-6018C-500-90 (see **Figure 4.8**b). Some detailed characteristics of the powersupply are presented below in the Table 4.4.

(a)   (b)

Figure 4.8: Images of the used power supply a) HP Agilent 6032A; b) IT-6018C-500-90

Table 4.4 – Working characteristics of the DC power supplies

Power Supply	HP Agilent 6032A	IT-6018C-500-90
Output Rating	0 to 60 V; 0 to 50 A	0 to 500V; -90 to 90A
Output Power	1,200 W	-18000 to 18000W
Programming accuracy at 25℃ ±5℃	0.035% +40 mV	≤0.02% + 0.02%FS
Readback accuracy at 25℃ ±5℃	0.08% +20 mV 0.36% +35 mA	≤0.02% + 0.02%FS mV ≤0.1% + 0.1%FS
Command Response Time	2 mS	2mS
Ripple	8 mV	≤200mVpp(MAX:500mVpp)
(20Hz -20MHz)	25 mA	≤0.1%FS RMS

A manual control of the autoranging DC power supplies can be proceeded with available manipulators and controllers on the units itself. However, it is more convenient to use external PC controlling options with the controlling output and cables predisposed by the manufacturer: GPIB-USB (in case of HP Agilent 6032A) and LAN/RJ45 (or simply USB cable, in case of ITECH IT-6018C-500-90). A cross connection between the two power supplies: master and slave were done with the usage of fibre optic connection and three cables (see **Figure 4.9**).
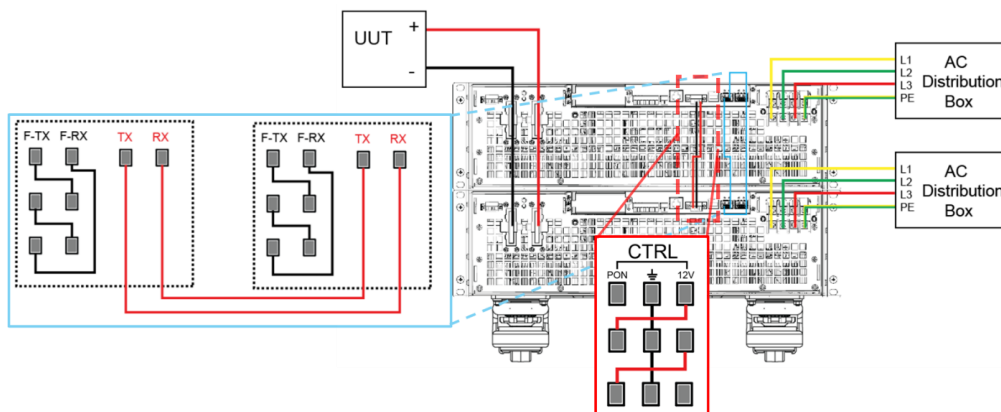
Figure 4.9: ITECH-IT-6018C-500-90 Master and Slave units wire connection (AC input, DC output, optic communication (in blue), control electrical connection (in red)

An HP Agilent PS was used mainly for conventional (low voltage treatments), that was operated with custom-written user interface controlling program in Visual Basic developed by Sergey Stark. The motivation and aspects of the usage, principles of the process control were also published and well-described [105], [320]–[322]. A typical window of the program is shown below **Figure 4.10**.
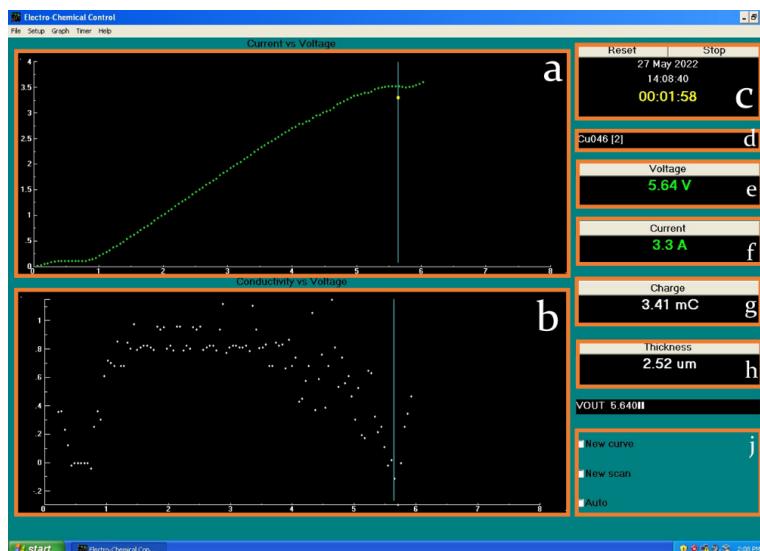
Figure 4.10: A typical window of the controlling program, where (a) is a curve I-V, (b) is a derivative dI/dV-V, (c) data and timing control section, (d) name of the treated object, (e) applied voltage, (f) current value, (g) total charge passed, (h) average thickness for the selected material and its surface area, (j) curve scan control section

In case of the PEP processing, more simple controlling is used – by simply application of the selected voltage value, that allow a passage of the current through the closed system. A minimal and maximal values of the current and voltage can be as well-adjusted, below or above, which the system will interrupt. Additionally, data logging feature allow power, current and voltage output values to save in the *.CSV data file with a selected frequency of time ≥0,5 s. A typical window of the manufacturer provided software is shown below (see **Figure 4.ll**).
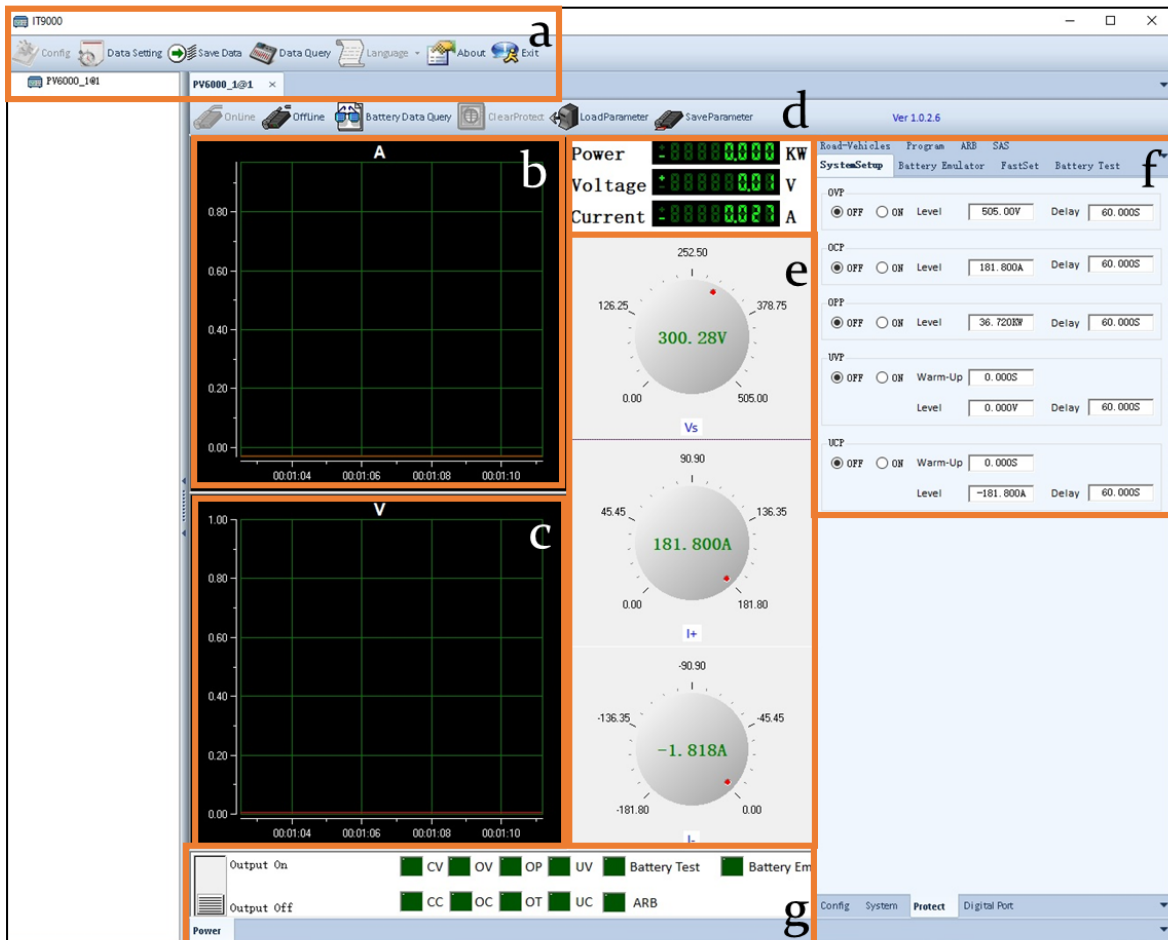
Figure 4.ll: A typical window of the ITECH PS controlling software, where (a) is a general controlling elements of the program, including datalogging, (b) current curve in time, (c) voltage curve in time, (d) numerical indicators in time for the power, voltage and current values, (e) control forms for the input voltage and current, (f) general system properties, in particular over and under power/current/voltage protections functions, (g) output control and indicators.

4.2.2 Ultrasound baths

As it was described the mechanism and utilization of the ultrasound generators in chapter 2.5.2.2, during the dissertation activity various equipment were used including industrial size baths with respective generators and a small-scale ultrasonic cleaning machine. Most of the cleaning

procedure was done in the Branson B5510-MTH (see **Figure 4.12**). Specifications include 9,5 L of water tank capacity, 40 kHz working frequency, heating element up to the 70 °C.

Figure 4.12: Branson B5510-MTH Ultrasonic cleaner at LNL-INFN

4.3   Example of calculations and computing

During the experimental phase many routine calculations were processed, most of which are related to the average thickness removed by process, current densities, and current efficiency. These calculations are not reported in the following experimental chapters, instead the results are presented. In this sub-chapter the way how the computing was done will be shown.

4.3.1   Average thickness removal

Two types of calculation were used: based on the weight removed (for vibro-tumbling, chemical and electrochemical polishing and PEP) and based on the current passed during the electrolysis (EP and PEP only).

Weight removed path

The average thickness removal δ calculation is done via the following formula:

$$\delta = \frac{\Delta m}{\rho \cdot A} \cdot 10^4 = \frac{g}{\frac{g}{cm^2} \cdot cm,} \cdot 10^4 = [\mu m], \tag{4.1}$$

where Δm is the difference in weight before and after the mass removal treatment, ρ – material density, A – treated surface area.

For automatization and rapid data logging, a small program in PowerApps was written, allowing calculation of the thickness removed values by inserting the weight difference in g, and the surface area. A pre-set of the density values for most common metals (copper, niobium, tantalum)

were done in addition to the custom value input (see **Figure 4.13**). Surface area values for most common objects were pre-set for e.g., 6 GHz cavity (cell only area, all internal area).
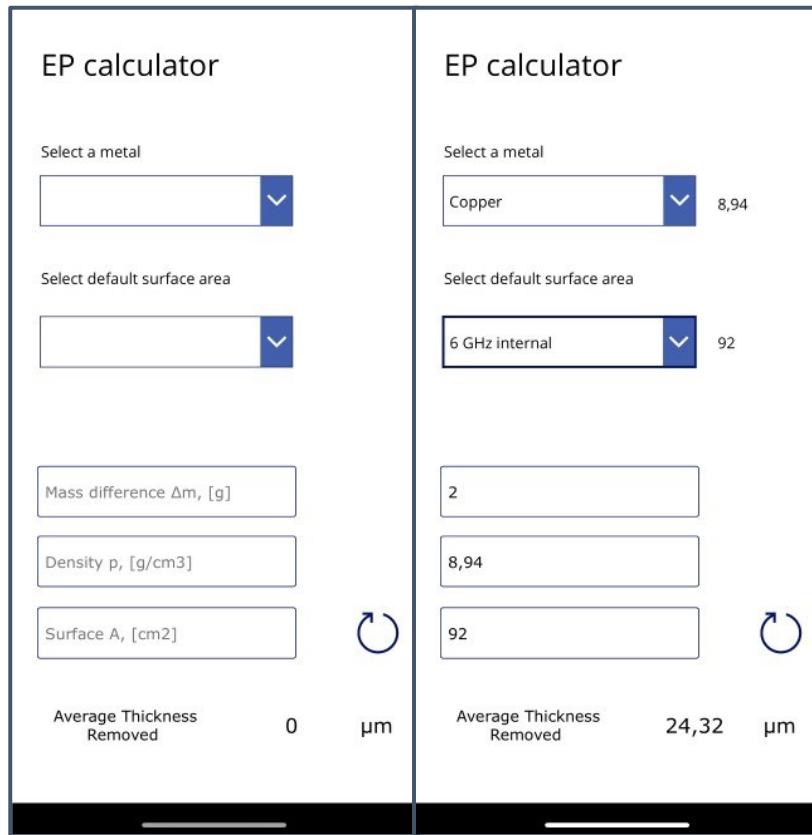
Figure 4.13: User-interface of the average thickness removed calculation program

Current passed during electrolysis path

The Faraday's law is a simple way to correlate the current with the average removed thickness for electrolysis-based process. The following formula describing the law is used as a reference:

$$\Delta m = KQ = \frac{M}{z \cdot F} \cdot I \cdot \tau = \frac{g/mole}{1 \cdot C/mole} C = \frac{g/mole}{1 \cdot (A \cdot s)/mole} A \cdot s = [g] \qquad (4.2)$$

where, K – electrochemical constant for a metal, M – molecular weight of the metal, F Faraday's constant (96,485 $A \cdot s$ or 26,8 $A \cdot h$), z – number of electrons in the dissolution reaction (e.g., for copper – 2, for niobium – 5), I – average or constant current of the process, τ – time of the process, $I \cdot \tau$ – charge of the process.

Since the process of electrolysis in many cases is held in constant mode, the values of current are not fixed. Therefore, a charge value may be used instead (obtained by integrating the current vs time curve or by summing the every-second logged current values).

Knowing the basic density formula for a material ($\rho = m/V$) and the volume of a geometrical object ($V = \delta \cdot A$) a final computing formula may be written as follows:

$$\delta = \frac{\frac{M}{z \cdot F} I \cdot \tau}{\rho \cdot A} \cdot 10^4 = [\mu m] \tag{4.2}$$

It is worth to mention, that such calculations are assuming the absence of any other concurring reaction that might take place on the anode, and thus "use" the current devoted to the main process.

4.3.2 Current efficiency

To evaluate the presence of parasitic process, current efficiency calculation may be used as follows:

$$CE = \frac{\Delta m}{KI\tau} \cdot 100\% \tag{4.3}$$

In practice this formula compares the difference of weigh that was measured before and after the process and correlate it with the theoretical weight difference, that must be equal in case all the current that passed through the electrochemical circuit was used for a metal dissolution.

Part II
Experimental part

5 Vibro-Tumbling. Upgrade, optimization, and implementation

In this chapter it is demonstrated the research activity conducted. Particularly in the sub-chapters it will be presented the upgrade of the old configuration, operated at LNL, optimisation of the parameters that may influence the process. Most of the attention was paid to the Cu 6 GHz cavities, however it was also studied the Nb vibro-tumbling to enhance the study.

5.1   Introduction

The production methods of elliptical cavities till now can present severe defects, that must be addressed, as was discussed in chapter 2.3. A grinding process was used in the standard protocol of 6 GHz cavity processing at National laboratories of Legnaro (see chapter 2.3.1.3), that on one hand can solve severe defects from the production stage, but on the other hand introduce other type of defects, that are non-uniform and difficult to process with the electropolishing (see **Figure 5.1**).
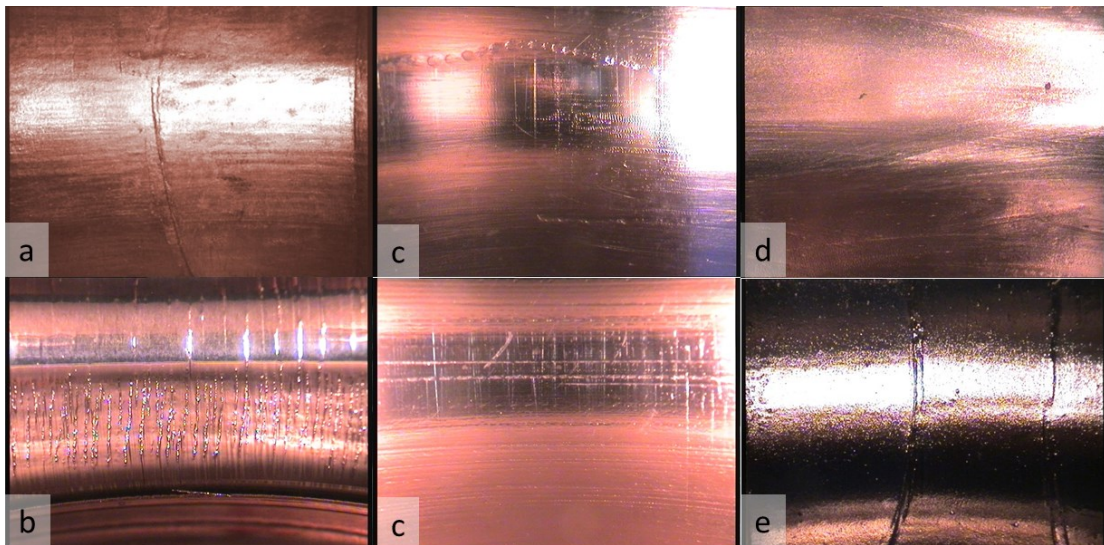
Figure 5.1: Internal photos of Cu 6 GHz cavities; a) cell defect after spinning, b) iris – cut-off vertical defects not removed by grinding, c) cut-off various defects not removed by grinding, d) cell scratched zone after grinding, e) after a complete cycle of surface preparation, macro defect from spinning die remain if not removed on the stage of mechanical preparation

The scope of the VT is always to smooth the surface uniformly, lowering the roughness good enough for further EP. However, different production methods may introduce various defects

depending on the location. However, the most important part is the *cell* part (see **Figure 5.2**), to verify how the polishing treatment works on real objects – 6 GHz cavity, similar inspection of the cavity is done. The critical part is *iris* that might be thinner, than expected due to the production or polishing. And lastly, *cut-off* is less important, and normally has more noticeable defects.
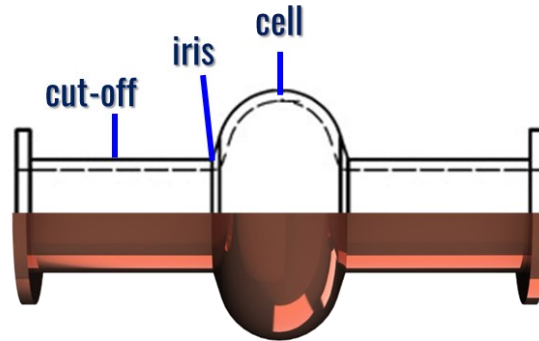
Figure 5.2: A scheme of the inspected regions of the cavities

5.2 Previous attempts of vibratory finishing

As was briefly described in the chapter 2.3.2.1 Vibro-Tumbling (VT), the system is composted from the eccentric motor, a physical stand, where the cavity is mounted with rotating holders, the motor is connected through the inverter, that allows modulation of the working frequency. The system was built at LNL site, and few iterations of it were described [96]. The initial design was inspired by the CBP machine (see chapter 2.3.1.2) and some industrial variations of mechanical tumbling and vibratory finishing, such as TURBULA® Shaker-Mixer (see **Figure 5.3**), which is produced by Glen Mills Inc.

Figure 5.3: TURBULA® Shaker-Mixer (model T2F) and a 6 GHz cavity polishing implementation.

A cavity was meant to be installed in the plastic holder (see **Figure 5.4**), where it is fixed with a unique clamping system, filled with plastic-media abrasive. Then accordingly placed in the mixing

turbula for a long treatment processing. The system can be described as a simple, relatively noiseless, however the main disadvantage is a low erosion rate (15 mg/h or 0,18 μm/h), which will not allow removal of the macro-defects. The reason for that, was the limitation of the variable maximum frequency, as higher values could lead to the instability of the system and eventual self-destruction.
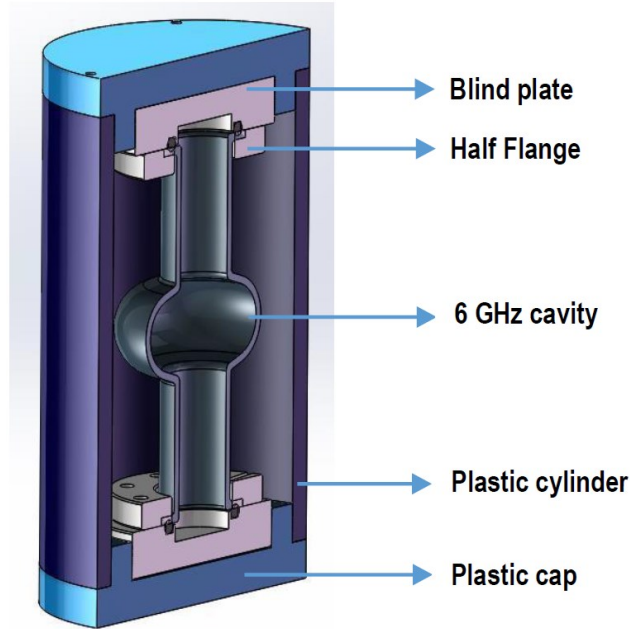
Figure 5.4: Section of the cavity plastic holder build for TURBULA® Shaker- Mixer

Another attempt was done by changing the holder structure, making it even easier to operate providing as well rotatranslator trajectory of movements (see **Figure 5.5**). The media inserted in the cavity rotate at lower speed than a cavity due to the gravity force, therefore a relative movement is exerted between the cavity and the media, to enhance the erosion rate. It was in two conditions: dry and wet polishing. Unfortunately, the expected erosion rates were not reached, which was explained by not sufficient high force applied on the internal surface of the elliptical resonator.
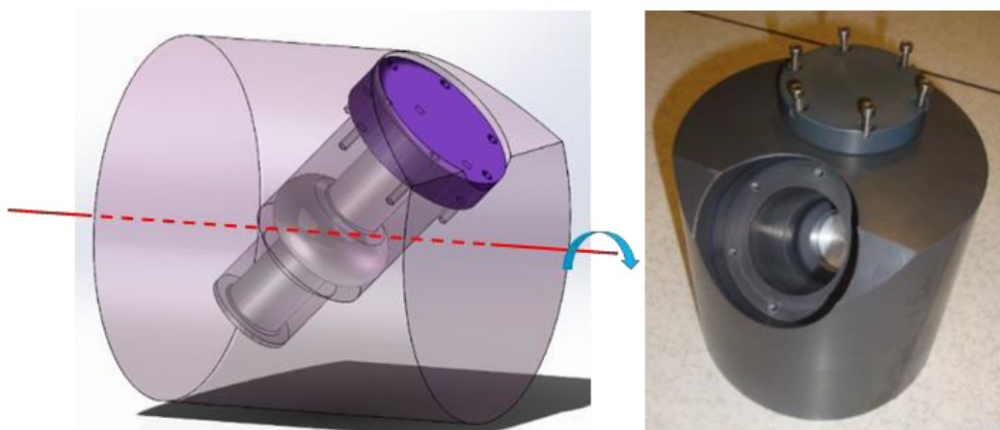
Figure 5.5: 3D drawing and picture of a rotatranslator tumbler

5.3 Vibro-tumbling first generation (2013)

A pre-final iteration introduced a vibratory finishing, inspired by the industrial fields and approaches. A first setup for holding the cavity is shown on the **Figure 5.6**.
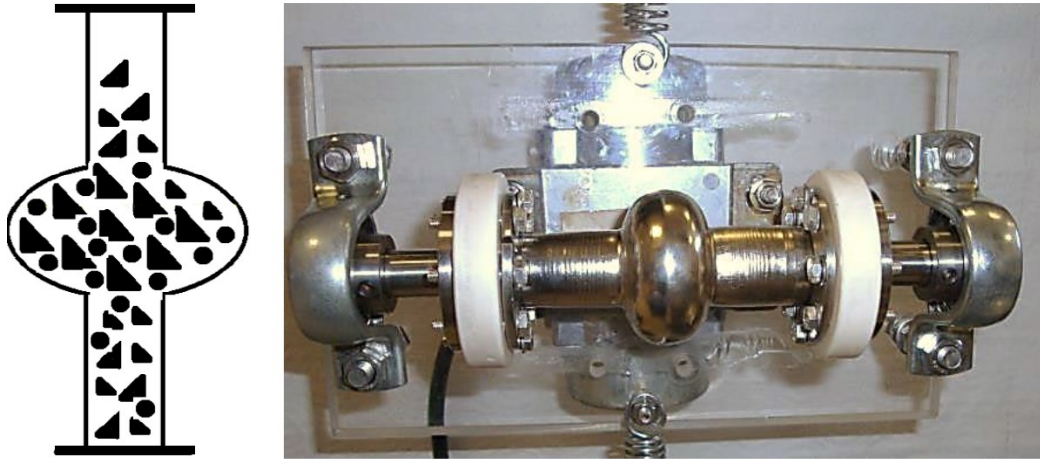
Figure 5.6: A scheme of the cavity filled with different abrasive and a first spring holder

A new configuration was characterised by better results in terms of surface finishing (in particular highest and most homogeneous erosion rate). It is mentioned a limit of 0,3 g/h erosion rate for Cu cavity. A small update was done as well, changing the bearings, which will allow some margins for inhomogeneity during rotation (see **Figure 5.7**).
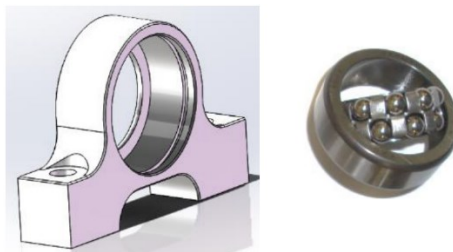
Figure 5.7: Drawing of bearing holder and image of self-aligning bearing

Vibratory and Control Box

A few commercial eccentric vibrating motors were bought for for this activity: MVSI 15/35 – S02, (see **Figure 5.8**) with centrifugal force of 30.2 kg, approximate weight of 5.6 kg and a maximal input of the power 85W at 50 Hz frequency. The power supply is characterised three-phased at working voltage load of 400V.
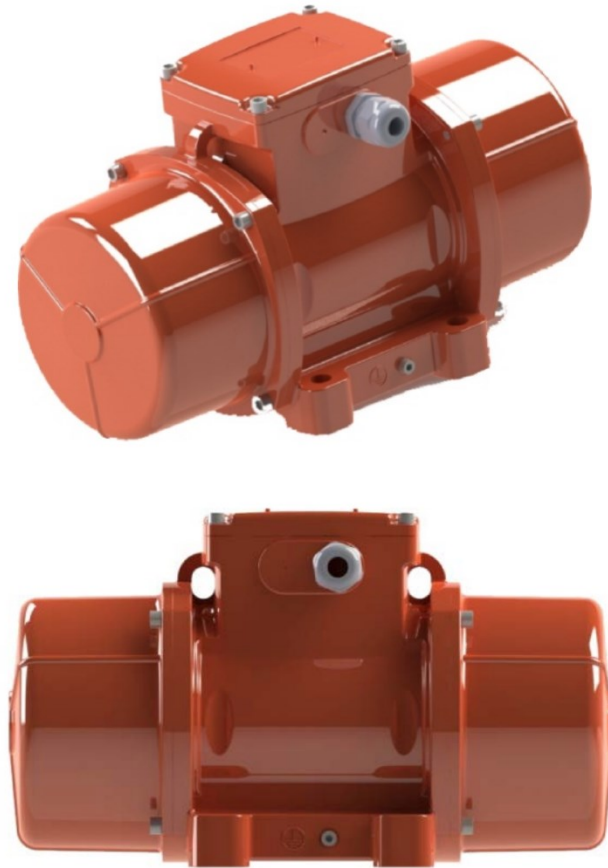
Figure 5.8: Photo renders of the MVSI 15/35-S02 [323]

The vibro-finishing has to operate at a custom frequency to ensure the maximum efficiency of erosion rate. To accomplish that, a control box unit (see **Figure 5.9**) was prebuilt to adjust three-phase power to the vibrator. Additional DC step motor was meant to provide constant rotation of the cavity. The so called, "system resonant frequency" depend on the many factors, among them: mass of the load, material, thickness of plate, construction and so on. «Fuji Electric Co. rectifier: type FRN4.0EIS-4E was used as an inverter, which is a standard type without EMC filter built-in. The operating rage of frequency is 0-400 Hz.

The first working stand was composted of few aluminium bars, where the stainless-steel plate was sustained in the air fixed by springles (see **Figure 5.10**). Such system had rubber shock absorbers and stable shape as well, to ensure zero-motion due to the vibration.
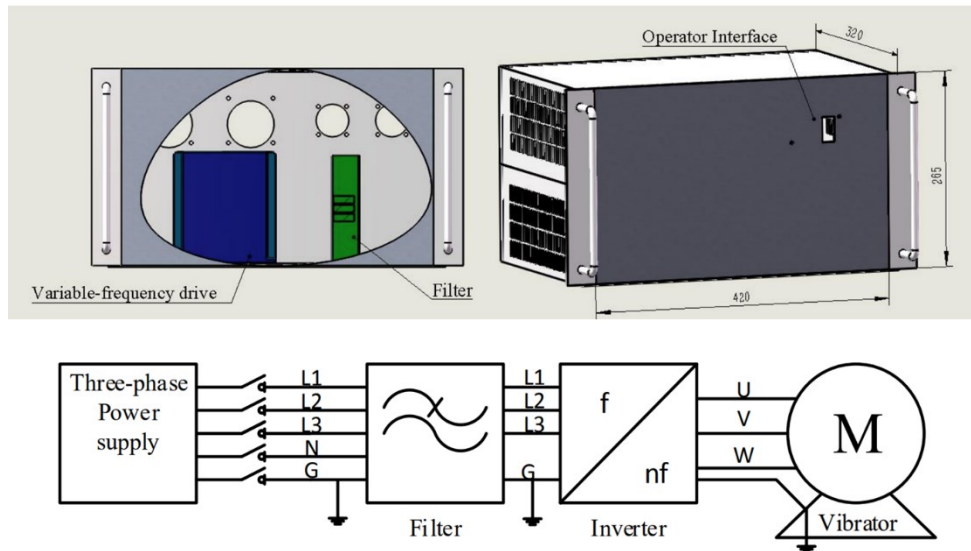
Figure 5.9: Control box drawings and diagram of the electrical connectivity
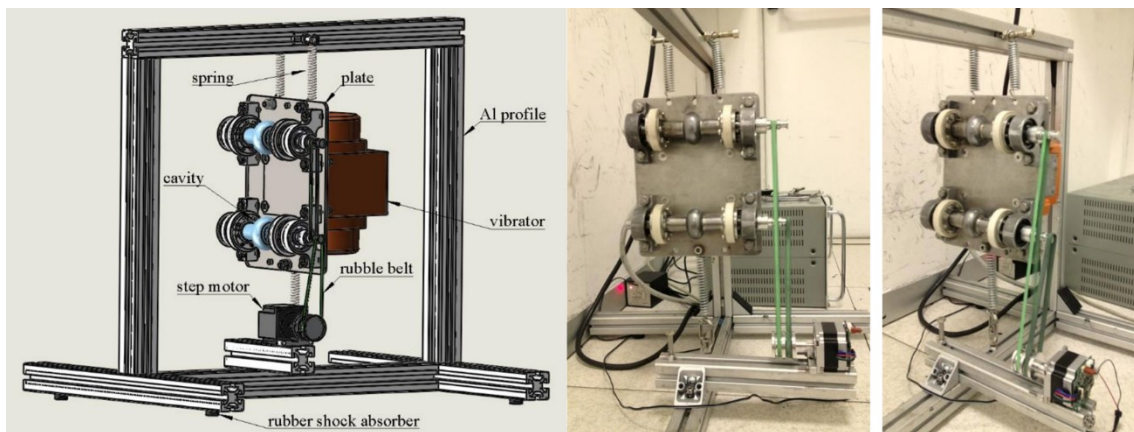
Figure 5.10: Stand design and photo view

The highest results obtained by Yu Goulong [96] for Cu cavity was around 0,7 g/h (8.8 μm/h) and for Nb 0,1 g/h (1,3 μm/h). In most cases, all previous experiments showed much lower rates. The development was in 2014 then interrupted due to the instability of the system, which eventually cause a severe damage to the system.

5.4   System upgrade (2019)

The system has been refurbished in this work. The components of the structure and system were collected as seen on the photo below (see **Figure 5.11**). Some parts of the construction were missing (such as a spring, bottom rubber shock absorbers). New rubber shock absorbers were installed to fix this issue. Instead, the source of the cavity rotation movement required different approach to fix. The operational frequency is transmitted over the whole structure, but it has to be limited only to

the plate (where the cavities are installed, and motor is assembled). Previously installed short springs were tried to be replaced with rubber shock adsorbers (see **Figure 5.12**).
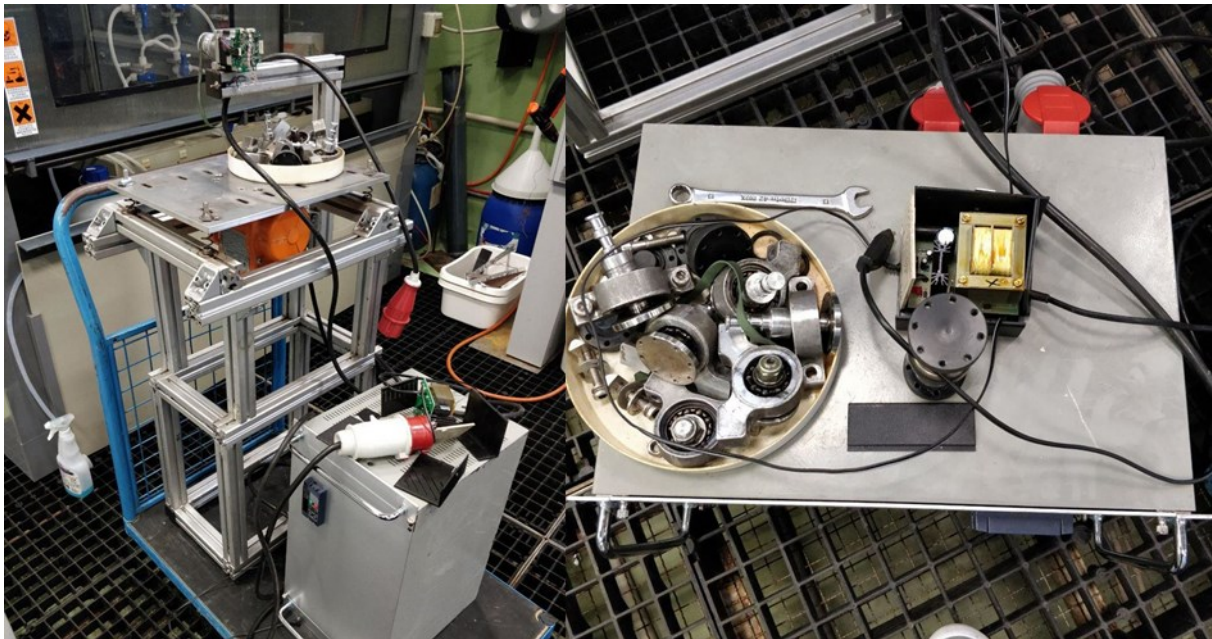
Figure 5.11: Recovered system after conservation: stand, inverter, motor and other components
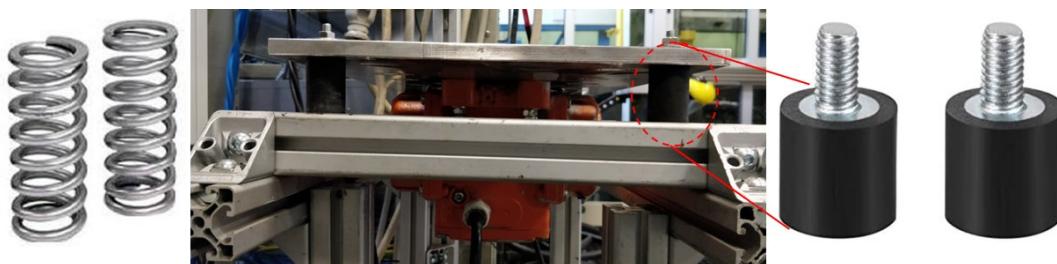
Figure 5.12: Substituted springs to test adsorbers between the plate and construction

Unfortunately, such modification did not lead to the complete vibration absorption due to the limitation of the material (rubber) that works well only with low frequencies of approximately 20 Hz. A working solution that was tested later was the idea to minimise the rigid contact between the vibrating plate and the construction by the usage of the plastic tubes inserted in the aluminium profiles, so that the that two profiles are not contacting each other (see **Figure 5.13**a). The following idea did not succeed as well, after few hours of operation, two aluminium profiles touched each other (see **Figure 5.13**b) and thus started to reproduce similar issues.

The further upgrade was meant to find a way to isolate 90-100% of vibration of a specific value or window of values. As a result of a research, it was found that wire rope anti-vibrants work quite well with low frequencies, in the meantime for ≤150 Hz frequencies it shows excellent isolation

of 90% and more depending on the variables (see **Figure 5.14**). Newly installed damping isolators showed excellent performance, thus allowing the further optimisation steps on material polishing.

(a)   (b)
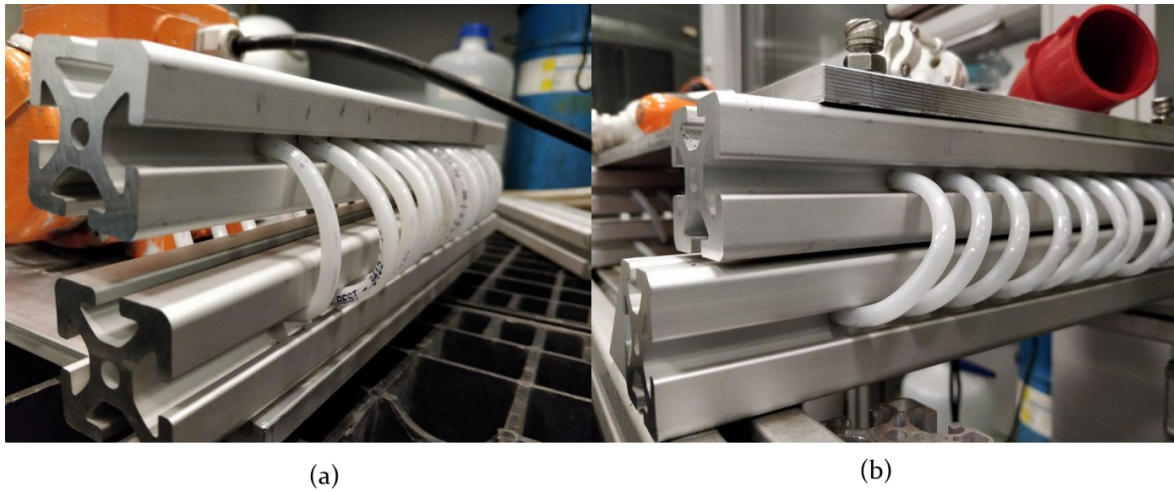
Figure 5.13: Anti-vibrant made of (a) plastic tubes and (b) double profile construction
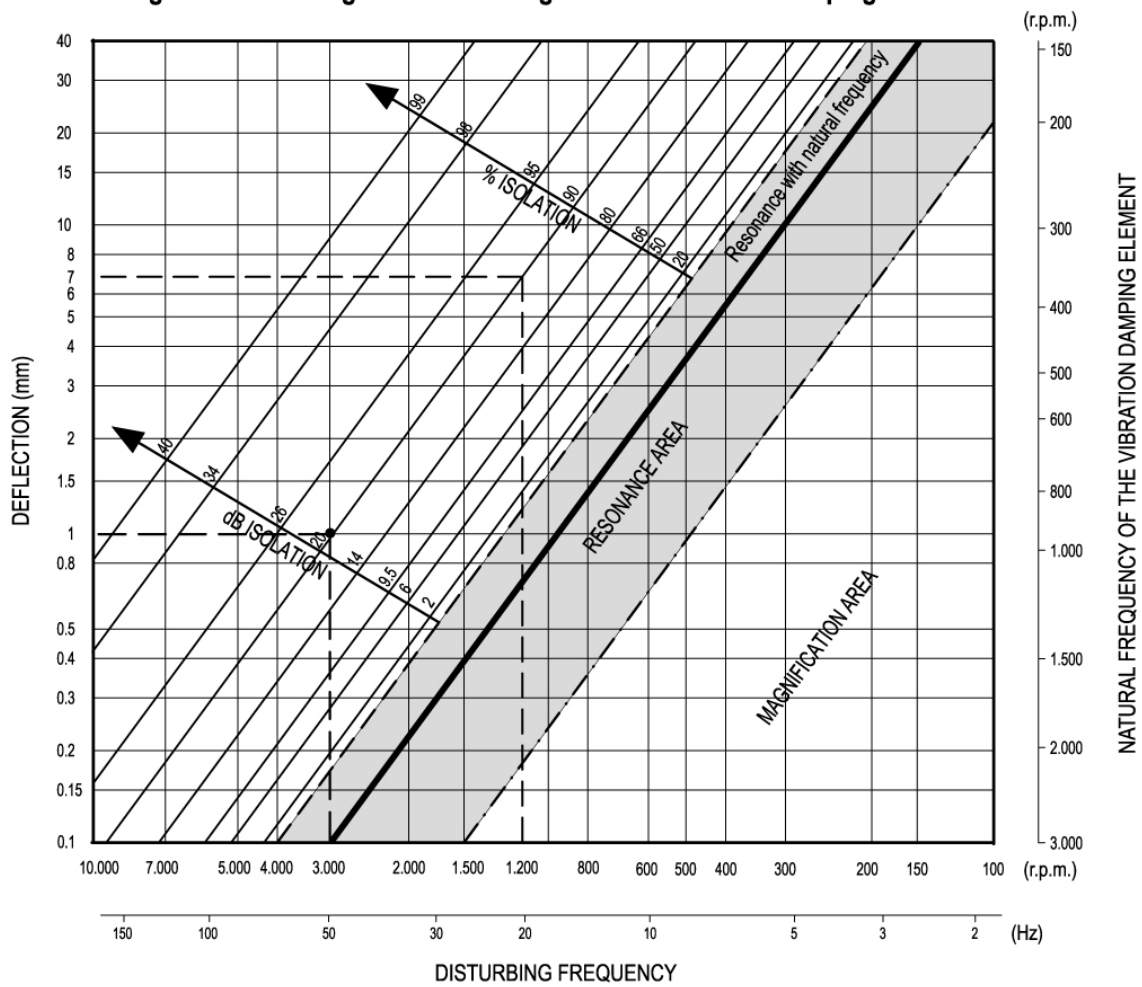
Figure 5.14: A diagram that represents the state of vibration (resonance, magnification or isolation) for the wire-rope damping mounts depending on the deflection [324]

Four anti-vibrant were installed to ensure homogeneous position of the plate with cavity (see **Figure 5.15**).
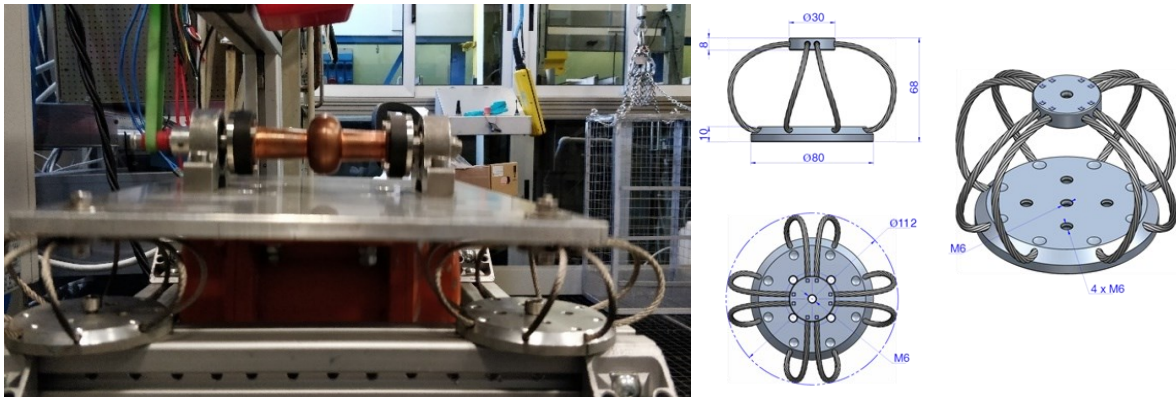
Figure 5.15: Newly installed anti-vibrant dumpers and their design sketch

Finally, the system was refurbished (as shown on the render scheme see **Figure 5.16**). It is composed of eccentric vibratory motor, a step-motor for rotary movement of the cavity, metal and plastic adapters (see **Figure 5.17**) for the mounting in the rotating bearings, a control box for a variable frequency.
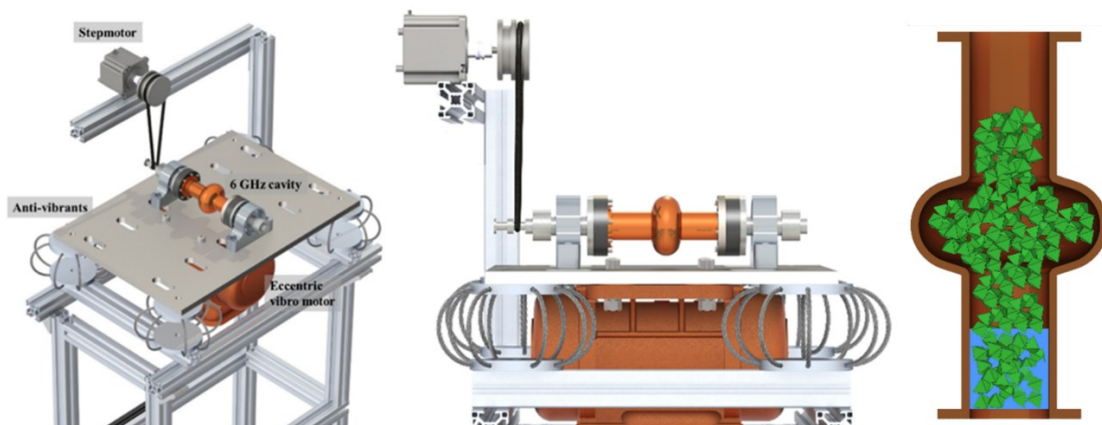
Figure 5.16: Rendered scheme of the refurbished VT system and the filling of the Cu 6 GHz cavity with the abrasive and wet media

1 - half flange; 2 - 6GHz cavity; 3 - O-ring; 4 - plastic blind flange; 5 - drive axis; 6 - bearing holder; 7 - self-aligning bearing; 8 - snap ring; 9 - belt axis.
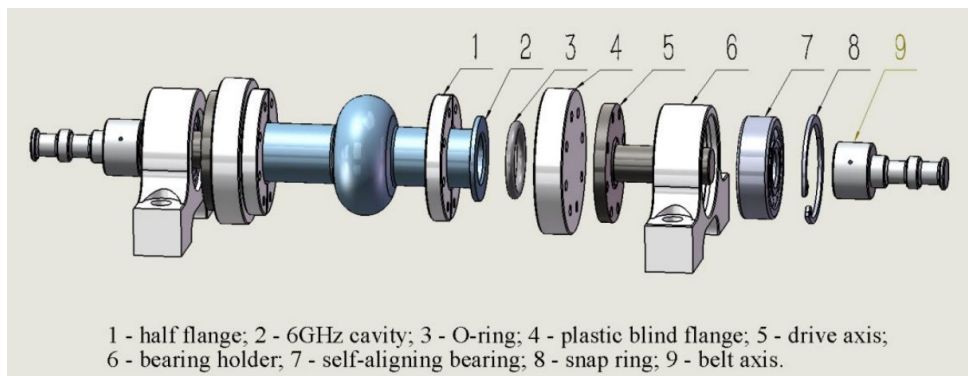
Figure 5.17: Drawing of the cavity assembling in the VT system

5.5   Process optimization

The experimental work on the VT processing was divided into two parts. The first was related to the elliptical 6 GHz cavities (both Cu and Nb), where the abrasive and media selection, working frequency, volume filling were studied. In practice, the internal inspection, erosion rates calculations (see chapter 4.3.1 for details) were analysed. The second part of the experimental work was done on the coupons, placed inside the dummy cavity (see **Figure 5.18**B), in the cell part of the elliptical shape. The dummy cavity is essentially a normal 6 GHz cavity, with two holes in the cell-part, where the cylinder (a coupon) with viton o-ring was placed. The coupons were then analysed with SEM, linear profilometer, AFM.
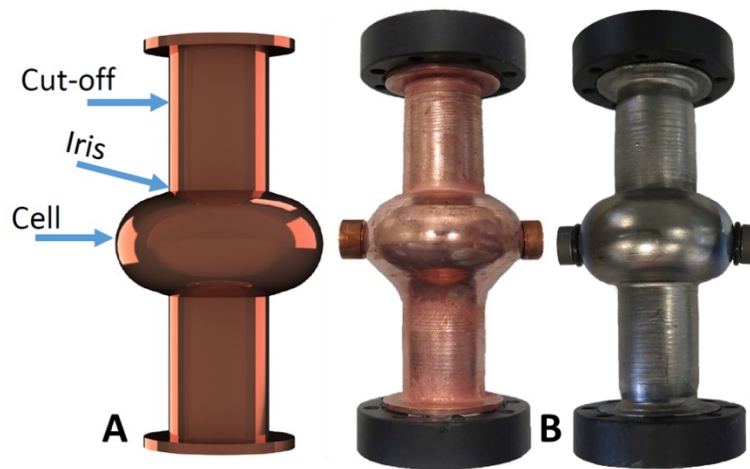
Figure 5.18: A) a scheme of the 6 GHz cavity and its main parts, B) photo of two dummy-cavities used for coupons study

The main scope of the optimization process was set to achieve a multi-step treatment protocol, to achieve relatively smooth surface, macro-defect free, ready to be polished with chemical (standard) treatments. This task was subdivided into some sub-tasks: 1) abrasive selection, 2) working frequency optimisation, 3) media filling optimisation, 4) adaption recipes for both the Nb and Cu metals. Around 40 preliminary tests (with some variations) were done before the first protocol was established for the polishing of the Cu cavities. Few changes, however, were introduced after once the statistics of treatments and behaviours were observed over a period of time. A total of 150 treatments were accomplished before the end of the 2022 calendar year.

5.5.1   Abrasive and media selection

A series of abrasives and media were tested, including solid abrasives and liquid solutions. A small portion of liquid in some cases might enhance the removing process, as it is noted in literature (for e.g., [325]) and discussed by Goulong [96]. In fact, the presence of liquid is beneficial, as it helps to delay the saturation of the process (e.g., formation salt layer, that prevent continuous erosion). That effect was found with both materials of interest: Nb and Cu. A typical erosion performance graph is

presented below (see **Figure 5.19**). In the case of wet (12 mL of distilled water) conditions, it is evident the superiority of the erosion rate, but also the longer saturation period (up to 400 minutes). Meanwhile the dry condition saturates at around 300 minutes. The conditions for the saturation were assumed as follows: the difference in the average weight loss is lower than 10% of first 60 minutes of the vibratory polishing.
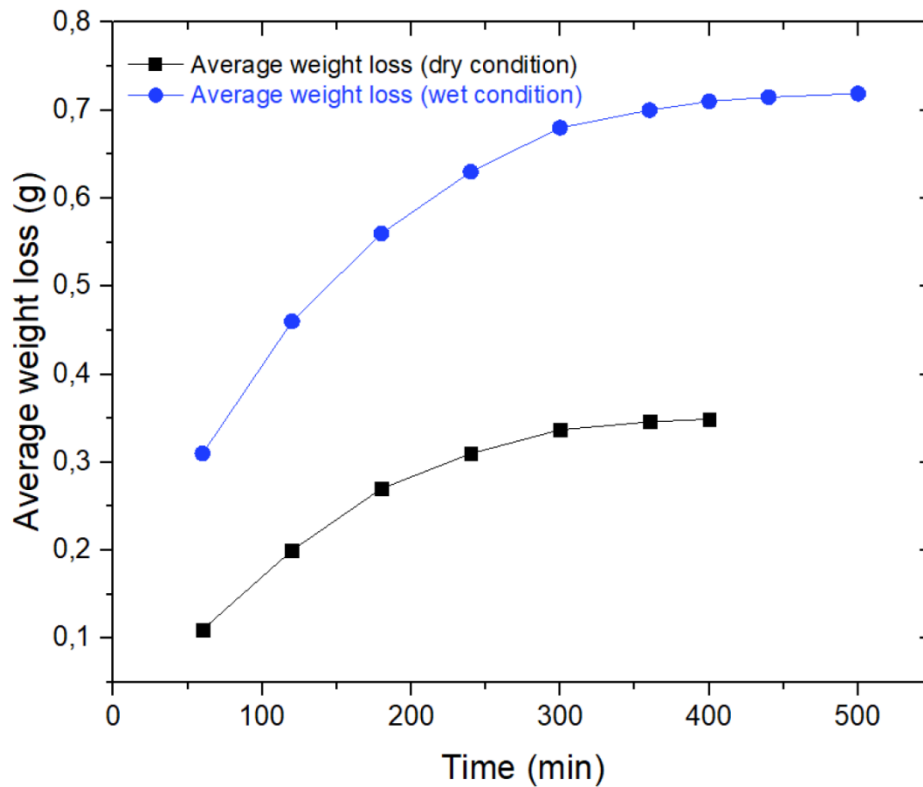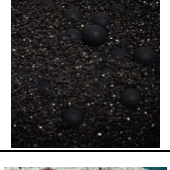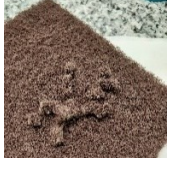
Figure 5.19: A typical erosion performance chart over time for 6 GHz Cu cavity

In the Table 5.1 all tested abrasives and chemical tested are listed with comments, technical data.

Table 5.1 – Tested abrasives with the VT

№	Naming	Formula or composition	Shape	Dimensions	Photo	Media	Metal	Comments
1	SiC	Silicon carbide abrasive	Triangular prism	10-15 mm		Dry	Nb, Cu	Too big for cavity dimensions, produced powder on the walls.
2	Metallic or s.s.	steel abrasive	Satellite shape	$\varnothing$ 6-8 mm		Dry, Wet	Nb, Cu	Extreme erosion rates. Inclusions, deep scratches.

№	Naming	Formula or composition	Shape	Dimensions	Photo	Media	Metal	Comments
3	Pl. Chips	Plastic/ceramic chips	Thin ellipsoids			Wet	Cu	Produce layers of dust, hard to clean.
4	Zr	Yttrium Stabilized Zirconium Oxide Grinding Balls	Ball	⌀ 6 mm		Dry, Wet	Cu	Can be used as a filler.
5	Al_2O_3	RKP: Polyester embed Al_2O_2 (Rösler italiana S.r.l.)	Cone			Dry, Wet	Cu	Dimensions limits the usage, to be used in pair.
6	Gr.Pyr.	RKG: Polyester embed SiO_2 (Rösler italiana S.r.l.)	Pyramid	6x5 mm		Dry, Wet	Cu	Meant for fine polishing but erode well.
7	RX	Plastic 5P (International Chips S.r.l.)	Pyramid	5,5x6,5 mm		Wet	Cu	Similar performance of RKG
8	RPMS	Plastic K (International Chips S.r.l.)	Cones	6x6 mm		Wet	Cu	Produce additional powder
9	SiC (tristar)	DZS* Ceramic (Rösler italiana S.r.l.)	Angle Cut Tristar	6x6 mm		Wet	Cu	n/d
10	SiC (small cyl)	ZS* Ceramic (Rösler italiana S.r.l.)	Angle Cut Cylinder	3x5 mm		Wet	Cu	n/d
11	Coconut shells	Nutshell Granulate	Powder and shells	1.70-2.40 approx. mm		Dry	Cu	Fine polishing, adsorbs dusts and powders, leave shining surface. No erosion
12	Corn shells	Maize-cellulose product	Powder and shells	2.0-5.0 approx. mm		Dry	Cu	Less shine / bright surface, similar mechanism as coconut.
13	Teflon balls	PTFE balls	Balls	⌀ 6-7 mm		Dry	Nb, Cu	Adsorb dusts, powders, might be used as a cleaner or volume filler

№	Naming	Formula or composition	Shape	Dimensions	Photo	Media	Metal	Comments
14	Cu powder	Copper powder	Powder	200 mesh		Dry	Cu	Low erosion rate, but smooth slightly the surface.
15	H.G. Diamond	Diamond powder	Powder	100-300 μm		Dry	Nb, Cu	Scratches, low erosion rate than expected.
16	Silicone	Si amorphous / crystalline,	Powder	30-60 μm		Dry	Cu	Surface contamination with powder.
17	B$_4$C	Boron Carbide powder	Powder	100 μm		Dry	Cu	Surface contamination with powder. Some erosion noted.
18	ScotchBrite	ScotchBrite ™ plastic sponge		n/a		Dry	Cu	Any effect observer. Meant to be used with heavy abrasive.

The chemical compounds were studied for VT wet conditions. Requirements for the etching compounds were as follows: 1) stable under normal conditions, 2) being nonexplosive, 3) do not produce gas, 4) relatively easy and safe to operate. A list of tested compounds was tested (see Table 5.2).

Table 5.2 – Chemicals that were tested with the abrasive during VT of Cu cavities

№	Name	Type	Comments	Average erosion rate, μm/h
1	Ammonium persulfate		The best enhancement effect	18-25
2	Sulfamic acid	Etchant	Bright and shine surface	0,6 - 1,7
3	Citric acid		Bright surface	0,3 – 2
4	GP 17.40 SUP	Industrial Soaps from NGL Group	Like a water	1 - 2
5	Rodastel 30		Enhance the erosion vs GP 17.40	1 - 4
6	Ethanol	Solvent	Evaporates often, leading to the saturation	0,2
7	Water		Cooler cavity, higher erosion rate vs dry conditions.	0,8 - 2,9

Among the tested abrasive, the maximal erosion performance and media conditions for Cu were summarised (see **Figure 5.20**). The usage of the wet conditions is favourable over the dry in terms of erosion rate. Moreover, the usage of the etchants, in some cases, can increase the erosion

rates significantly for copper (see for details chapter 5.5.2), as there is a variety of relatively safe compounds that can dissolve both copper and its oxide.
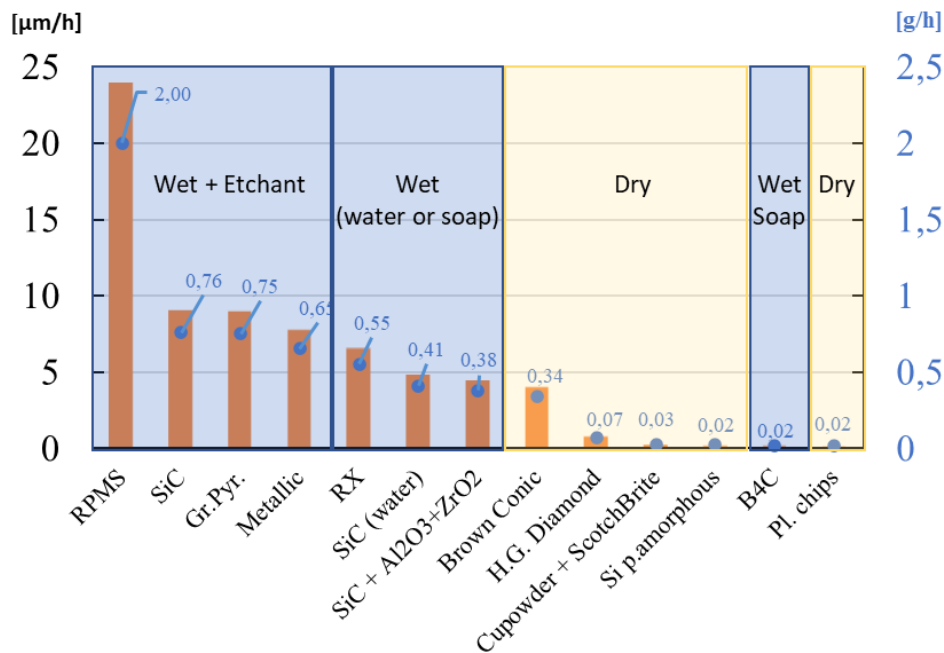
Figure 5.20: Peak erosion rates in both [g/h] and [µm/h] for tested abrasives with copper 6 GHz cavities

Nb VT is less efficient in terms of erosion rates due to the different mechanical properties of the metal in comparison with soft and malleable copper. It is notable (see **Figure 5.21**) the lower values of erosion rates for both wet and dry conditions. Nb erosion rate is almost 7 times lower in wet conditions and 4 times lower in dry conditions comparing respectively with the copper VT data. Unfortunately, any chemical etchant that can be used in such process and fit the security requirements, was not fond. As it was described in chapter 2.4.1, niobium chemistry normally requires hydrofluoric acid (or at least fluoride salt).

Summary: An optimisation of the abrasive and conditions has identified the most efficient abrasives in terms of erosion rates for both niobium (SiC & plastic media) and copper (plastic/ceramic media). The wet conditions (whether with etchant or with soap) has proven its superiority over the dry conditions. The peak erosion rates were recorded as 24 µm/h and 3,45 µm/h for copper and niobium respectively.
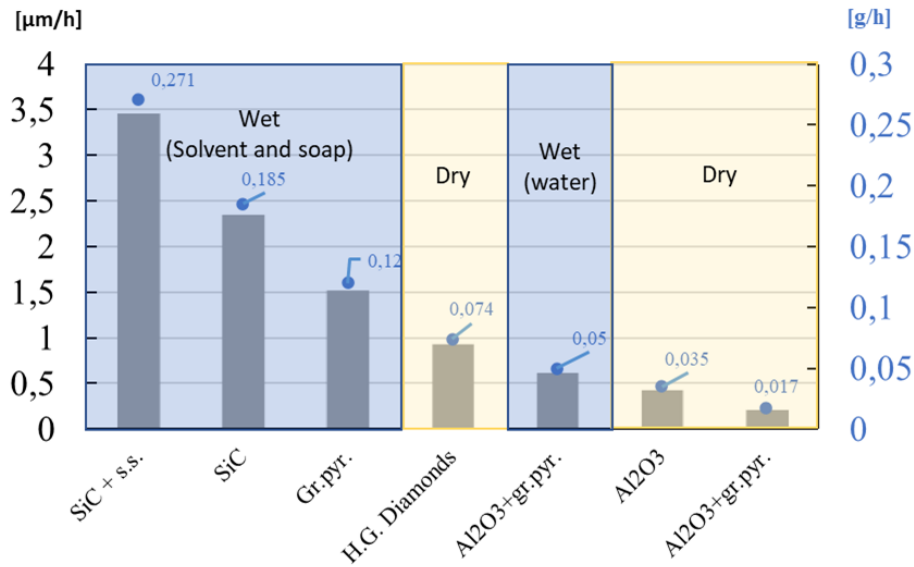
Figure 5.21: Peak erosion rates in both [g/h] and [μm/h] for tested abrasives with niobium 6 GHz cavities

5.5.2   *Synergetic effect of the etchant and abrasive during Cu VT*

As the erosion rates were still noticeably lower than an electropolishing and the wet-etchant approach has been seen as a potential route for the improvement of the erosion performance for Cu VT. That led to the continuous research of the application of chemical VT.

The presence of ammonium persulfate is not just contributing to the erosion rate but increase it by a factor of 4, was noticed. Comparting 4 treatments: a) RPMS abrasive, 70% volume and dry conditions, b) RPMS abrasive, 70% volume and wet conditions (15 ml H_2O), c) RPMS abrasive, 70% volume, 15 mL of oversaturated solution of $(NH_4)_2S_2O_8$ in addition added 0,5 g of $(NH_4)_2S_2O_8$ solid salt crystals, d) no abrasive, only 15 mL of saturated solution of $(NH_4)_2S_2O_8$ and 0,5 g of $(NH_4)_2S_2O_8$. The frequency of 190 Hz was maintained. The summary of the parameters is presented below (see Table 5.3).

Table 5.3 – Synergic effect of the etchant in Cu chemical VT experiment summary

Cavity	Time, min	Rotation	Abrasive	Frequency	Volume filling	Media
Cu	60; 120; 170; 240; 300; 360; 400	Fixed, 10 rpm	RPMS abrasive	190	70 %	Dry
	60; 120; 170; 240; 300; 360; 400; 440; 500		RPMS abrasive		70 %	Water
	60; 80; 100; 140; 200; 260; 360		RPMS abrasive		70 %	15 mL $(NH_4)_2S_2O_8$ (oversaturated)
	60; 80; 100; 120; 140		No abrasive. Only liquid etchant		n/a	15 mL $(NH_4)_2S_2O_8$ (oversaturated)

The results showed (see **Figure 5.22**) a 6 times higher erosion rate of saturated etchant solution and abrasive (green markers) compared to the water solution and same abrasive (blue

markers). Interestingly, erosion rate is as well ~10 times higher than just a 15 mL oversaturated solution can etch alone without an abrasive added during VT. This effect has a synergic behaviour between the abrasion and chemical etching process. Most likely, the mechanism consists of continuous formation of side-products such as CuO, $CuSO_4$, $CuHSO_4$, etc. The rough and porous structure of them, and bad adherence with the presence of abrasion lead to the superior removing rates. Summing the weight losses of only etchant process (pink markers) and dry process (black markers) with abrasive will result in approximately 5 times lower than oversaturated recipe. A synergetic condition and synergic effect calculation are shown below:

$$Synergy\ condition\ \Delta m_{chem} + \Delta m_{VT_{wet}} > \Delta m_{VT_{CVT}}; SE = \frac{\Delta m_{VT_{CVT}} - (\Delta m_{chem} + \Delta m_{VT_{wet}})}{\Delta m_{VT_{CVT}}} \cdot 100 = 73,1\%, (5.1)$$

Where Δm_{chem} – removed weight after 1h of VT process with no abrasive and 15 mL of oversaturated etchant, $\Delta m_{VT_{wet}}$ – removed weight after 1h of VT process with abrasive and 15 mL of water, $\Delta m_{VT_{CVT}}$ – removed weigh after 1h of chemical VT process with abrasive and 15 mL of oversaturated etchant.
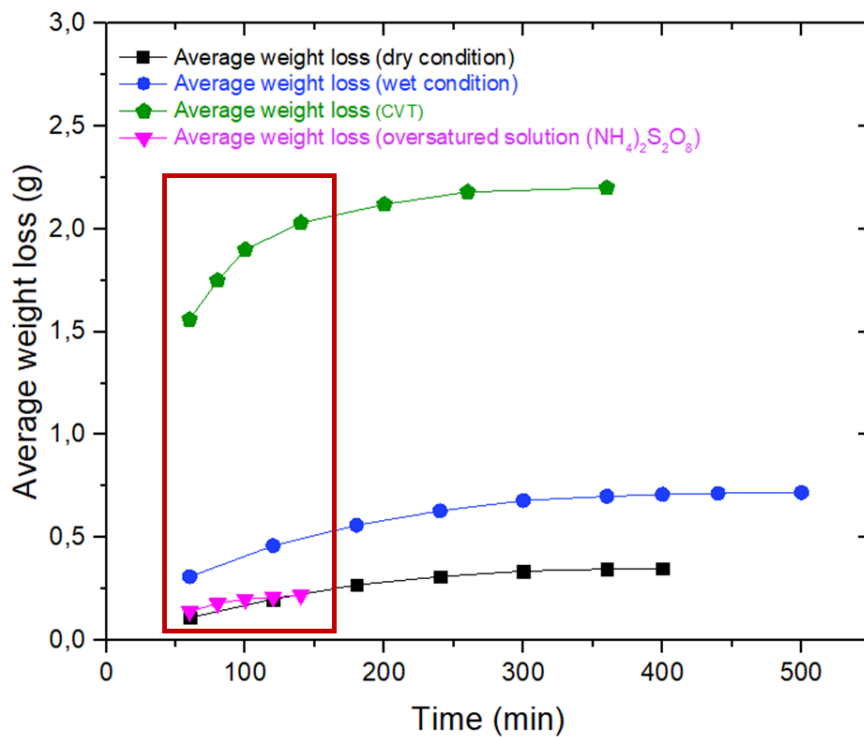
Figure 5.22: Average weight loss [g] for the four copper VT process and numerical synergic effect [98]

It was as well studied the role of the concentration of the etching components (see Table 5.4). The experiment consisted of 5 treatments, with RPMS abrasive, 75% abrasive filling volume, fixed 190 Hz frequency and 1 h time of processing. The synergic effect is observable above approximately 2 g/L concentration, when the erosion values are higher than in a wet condition water experiment.

121

Table 5.4 – Erosion rate of the chemically enhanced VT with different concentration of the etchant

№	Concentration of $(NH_4)_2S_2O_8$	Erosion rate [g/h]	Erosion rate [µm/h]
1	2 g/100 mL	0,30	3,65
2	20 g/100 mL	0,59	7,17
3	40 g/100 mL	1,07	13,01
4	80 g/100 mL	1,46	17,75
5	80 g/100 mL + 1 g of salt	2,01	24,32

It is worth to mention, that in this experiment, the effect of cavity heating during VT processing was not considered, and thus it might variate the solubility of the ammonium persulfate and side products, as the solubility normally is increased with temperature for persulphates.

Summary: the chemically enhanced VT of copper 6 GHz processing shows a clear superiority over other recipes and solution of vibratory treatments. A synergic effect was identified between the etchant and the abrasive action, which allowed to improve the erosion performance of the VT by 6 times comparing to the standard water wed conditions studied before. The possible mechanism is the simultaneous oxidation of the copper with the formation of a list of chemical products in porous and rough structure allowing the abrasion to erode easier.

5.5.3 *Working frequency*

A working frequency can be set from 0 to 400 Hz. According to the Goulong [96], a resonant frequency is characterised with the highest removing (erosion) rate. That is due to the difference between the inertia of the cavity and the abrasive. It is highly dependent on the weight of the cavity, abrasive media. An empiric way to calibrate the frequency is based on the noise produced by the system. The closer to the resonant frequency value is the more noise is produced.

A series of 9 experiments were done on the test Cu cavity in order to define the resonant frequency with the fixed conditions (see Table 5.5). As a result (see **Figure 5.23**), a relatively narrow window of the resonant frequency was identified: approximately 180-210 Hz, where it can be expected the highest removal rate.

Table 5.5 – Working frequency optimisation experiment for Cu VT

Cavity	Time	Rotation	Abrasive	Frequency	Volume filling	Media
Cu	1 h	Fixed, ~10 rpm	Gr. Pyr.	50 – 250 Hz	70%	Water, 12 ml

Summary: Frequency optimisation was done on the Cu cavity, varying the working values from 50 to 250 Hz, a parabolic behaviour with maximum was found for the wet VT process. A preferable value was identified as 190 ± 10 Hz.
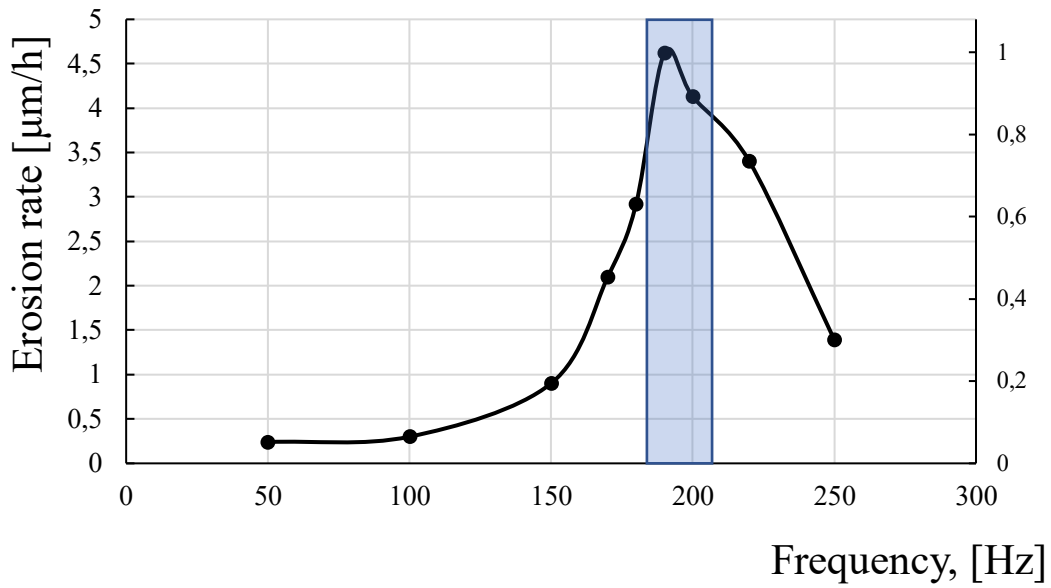
Figure 5.23: A dependency of the working frequency versus erosion rate

5.5.4   Volume filling

Consequently, it was studied the effect of the media volume (both solid and liquid). A window of optimised quantity of media that enhance the erosion rate was already known [96]. As mentioned earlier, in case of low liquid quantity – the saturation of the process (and low erosion rate) take place. It was found the average liquid volume that is recommended to add around 7- 15 ml. In the case of abrasives most of the case it is favourably to fill most of the volume with abrasive. However, in the case of exhaustive quantity, it is highly probable that erosion rate will also be severely reduced, most likely due to the damping effect between the abrasive and surface.

Cavity overheating was noticed in some cases after a standard 1 h of processing time. In case of ceramic or plastic abrasive media, it might indicate higher removal rates (compared to average values). The very same effect was also observed with copper powder abrasive. Thus, after noticing similar overheating issues, it was decided to confirm the correlation between the final temperature of the cavity in the end of the treatment and the total erosion rate. The experiment was done with the copper powder, same rotation speed, fixed 1 h processing time and 190 Hz frequency (see Table 5.6 and **Figure 5.24**).

Table 5.6 – VT Cu Volume filling optimisation experimental data for Cu powder abrasive

Cavity	Time	Rotation	Abrasive	Frequency	Volume filling	Media
Cu	1 h	Fixed, ~10 rpm	Cu powder	190 Hz	65 – 100 %	Dry
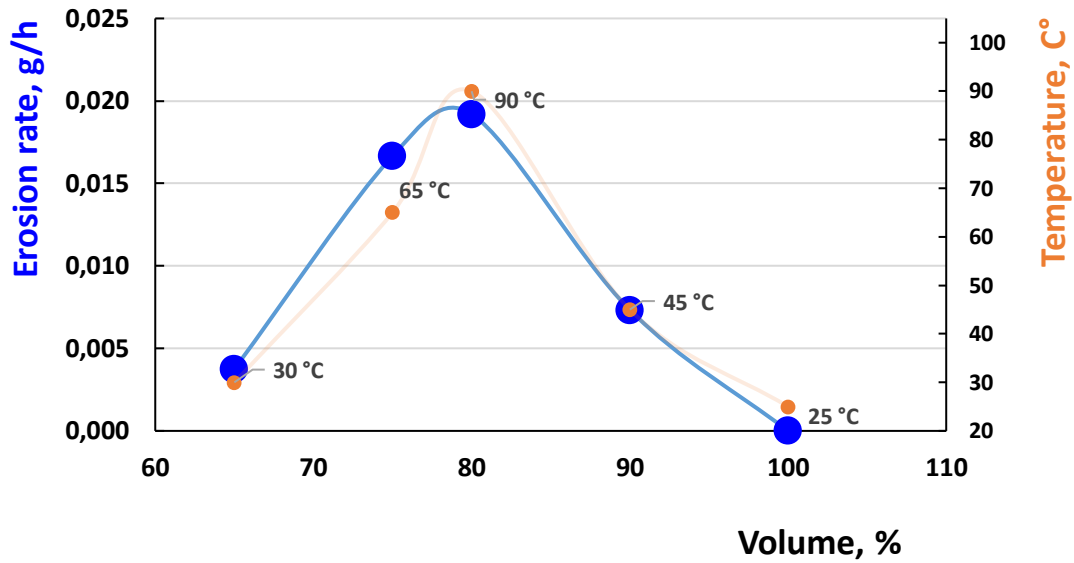
Figure 5.24: Erosion rate vs volume for copper powder abrasive filling and temperature chart for Cu VT

Summary: An optimal volume filling values were identified for cu powder VT in term of erosion rate. However, to avoid unnecessary oxidation, we suggest lowering the volume, and consequently the cavity will be only warm. Apparently, the temperature can be a parameter that, can influence the processing during VT.

5.5.5   Solution characterisation

To characterize the treated surface, an experiment was modulated, in which the planar cylindrical samples of 1 cm diameter were treated via vibro-tumbling of the newly proposed treatment protocol 1 (three-step polishing procedure). The samples were characterised before and after every single treatment with SEM and linear profilometer. Roughness data were acquired 6 times on random spot, to get a reliable statistic value. The initial samples were scratched with abrasive paper. For treatments, small cylindrical coupons were inserted inside the 6 GHz dummy cavity, where it was predisposed two holes (see **Figure 5.25**).

(a)   (b)   (c)   (d)   (c)
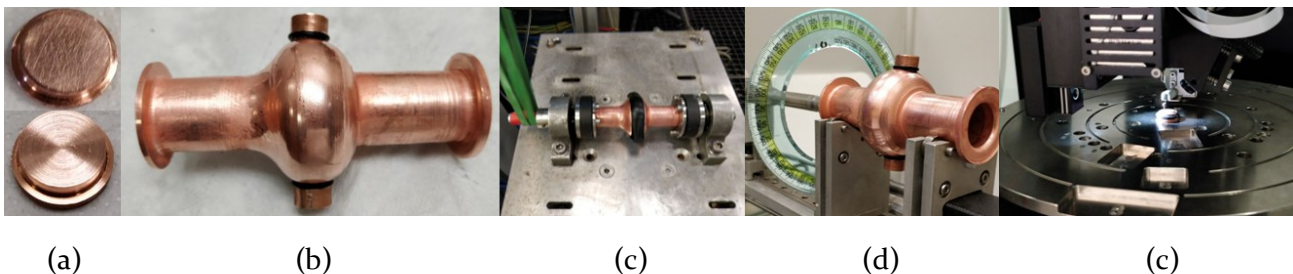
Figure 5.25: (a) Planar cylindrical samples, (b) dummy cavity with holes, (c) cavity VT processing, (d) cavity microscope inspection, (e) samples profilometer surface analysis

A scheme of the experiment is presented below (see **Figure 5.26**). Internally placed samples inspection after the protocolled treatments is presented (see **Figure 5.27**).

124
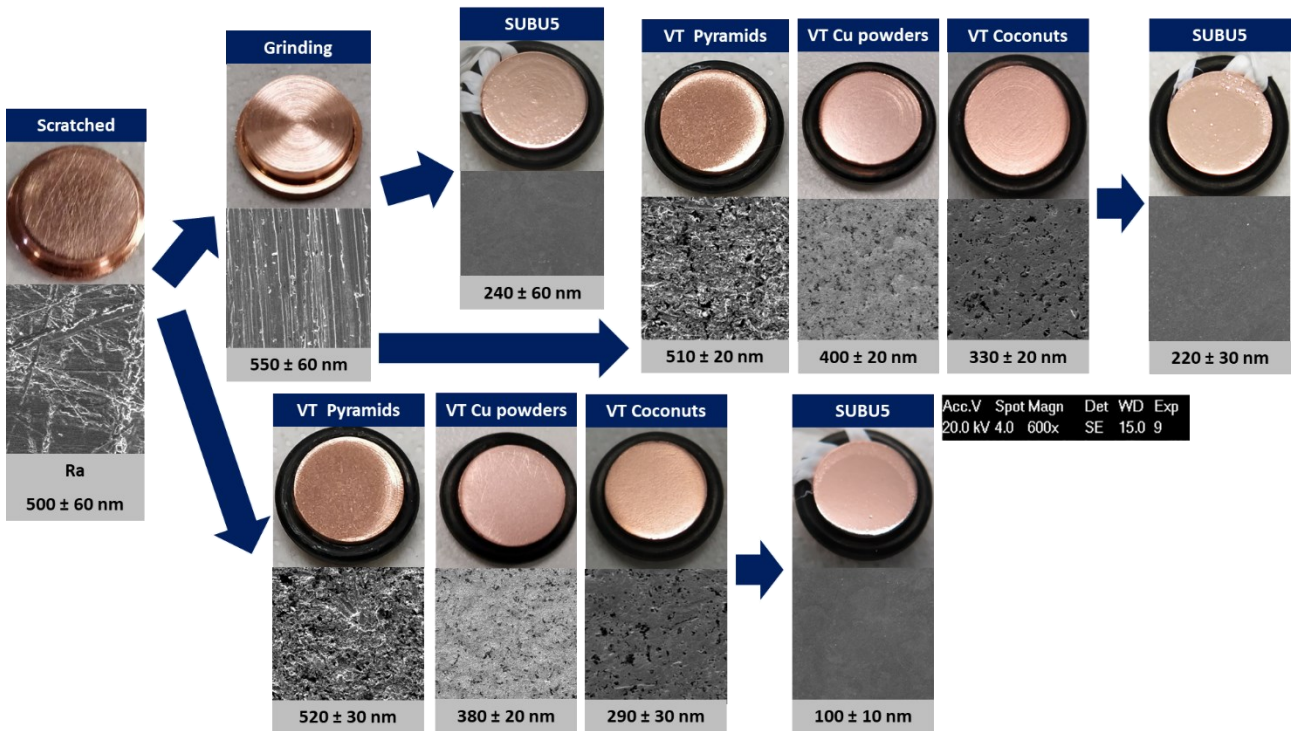
Figure 5.26: A scheme of experiment with corresponding every-step results (Initial scratched, grinded, vibrotumblings (gr.pyramides, Cu powder and coconut), chemical polishing SUBU5 [326]
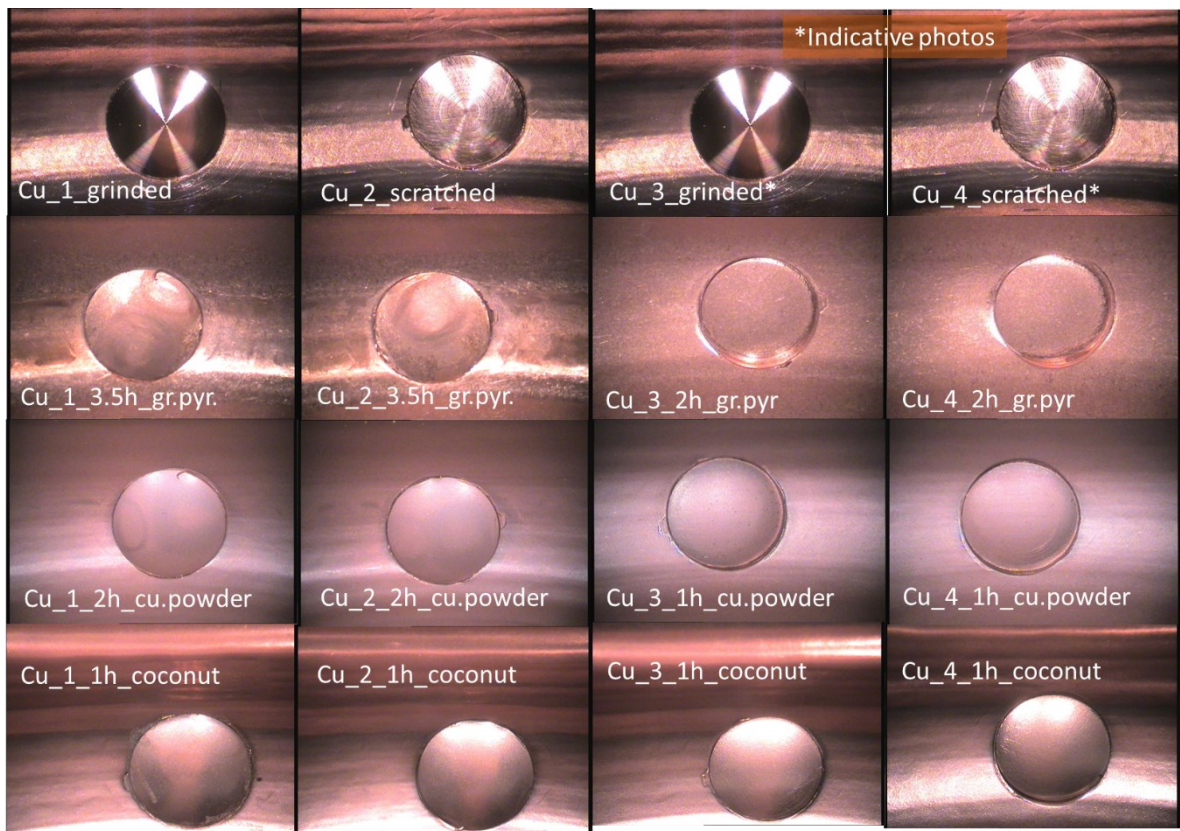
Figure 5.27: Internal inspections of the holed cavity after 3-step treatment

It was, developed a recipe to treat the Nb internal surface as well, the performance and experimental data is shown below (see **Figure 5.28**). The erosion rate is lower than VT of Cu, that is naturally. Moreover, the absence of suitable chemical etchant does not permit high erosion rate values. Despite that, relatively performant recipe is able to smooth deep defects (see the tests as well on the Nb 6 GHz cavities, for e.g., **Figure 5.29**).
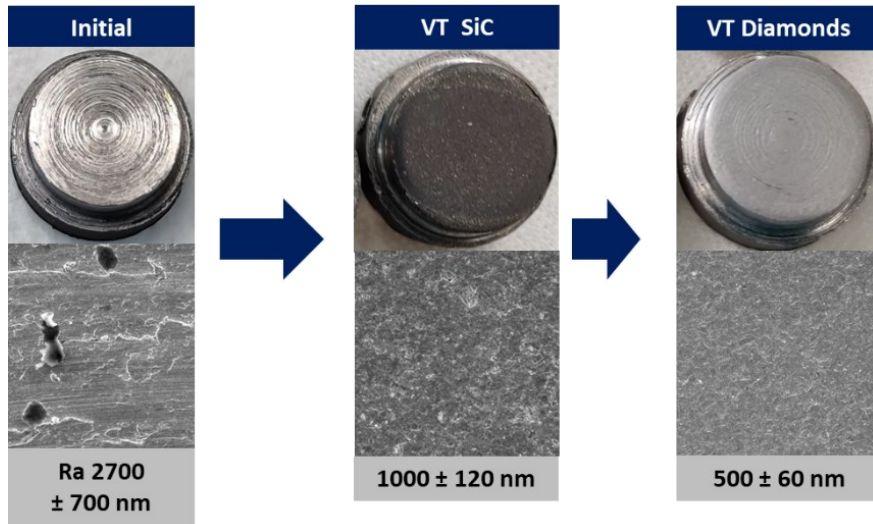
Figure 5.28: Experiment scheme of Nb VT and morphology analysis
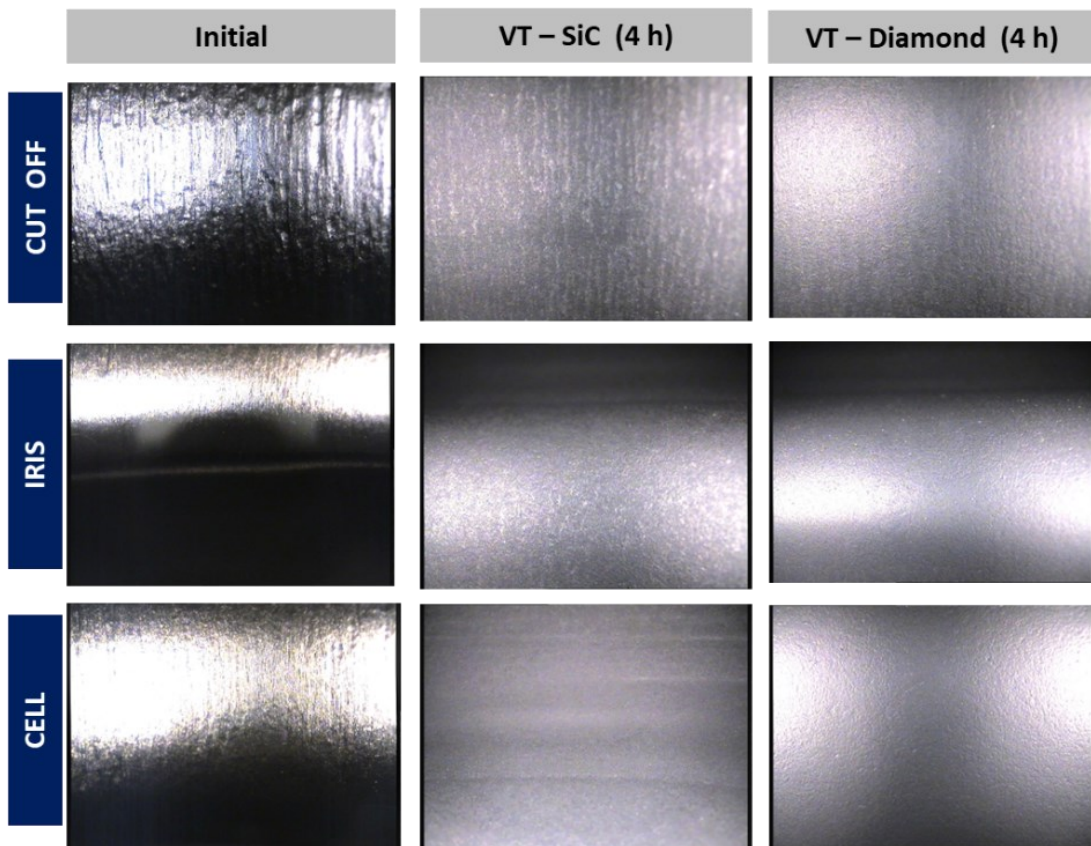
Figure 5.29: Internal inspection of a typical VT Nb 6 GHz treatment with SiC and Diamond

The three-step protocol is well reproducible and able to smooth the surface of the damaged Cu layer. The usage of the small samples confirmed with roughness and surface morphology analysis confirm the smoothening of each step. SEM micrography shows the presence of random damages that decreases among the steps. The first step of the three-step VT (see details below) protocol uses RKG polyester abrasive, which is meant to be for fine polishing in classic abrasive treatments. Instead, in such conditions is able relatively good smooth uniformly the surface. In other words, any present (not deep) surface defects are possible to eliminate. In the second step, copper powder continuously polishing of the surface, thus more "gently", resulting in smoother surface, but with copper micro-powder sticked to the surface, that most likely oxidised due to the heating conditions (see chapter 5.5.4). The final step uses an organic abrasive, able to de-adsorb the copper-copper oxide contaminants from the surface and provide fine polishing up to the bright conditions of the surface. The explanation of the shining effect is the presence of the organic oils, acid, fats in the coconut shells, that are released during heating and vibrational movements. After the last step, copper surface was never observed with a sign of oxidation.

The protocol has shown the possibility to eliminate most of the visible defects created by spinning production or grinding (see **Figure 5.30**). The overall protocol application time can be modulated depending on the surface, thus deep defects might require removal of 10-50 micrometres. For e.g., pitting is the most difficult defect, that can be removed by VT; however, it may require even higher values of the surface micrometres removed. Generally, such a kind of pitting issue appears only after chemical treatments, where the oxygen may evolute and in the case of a specific conditions may result in the deep pitting.
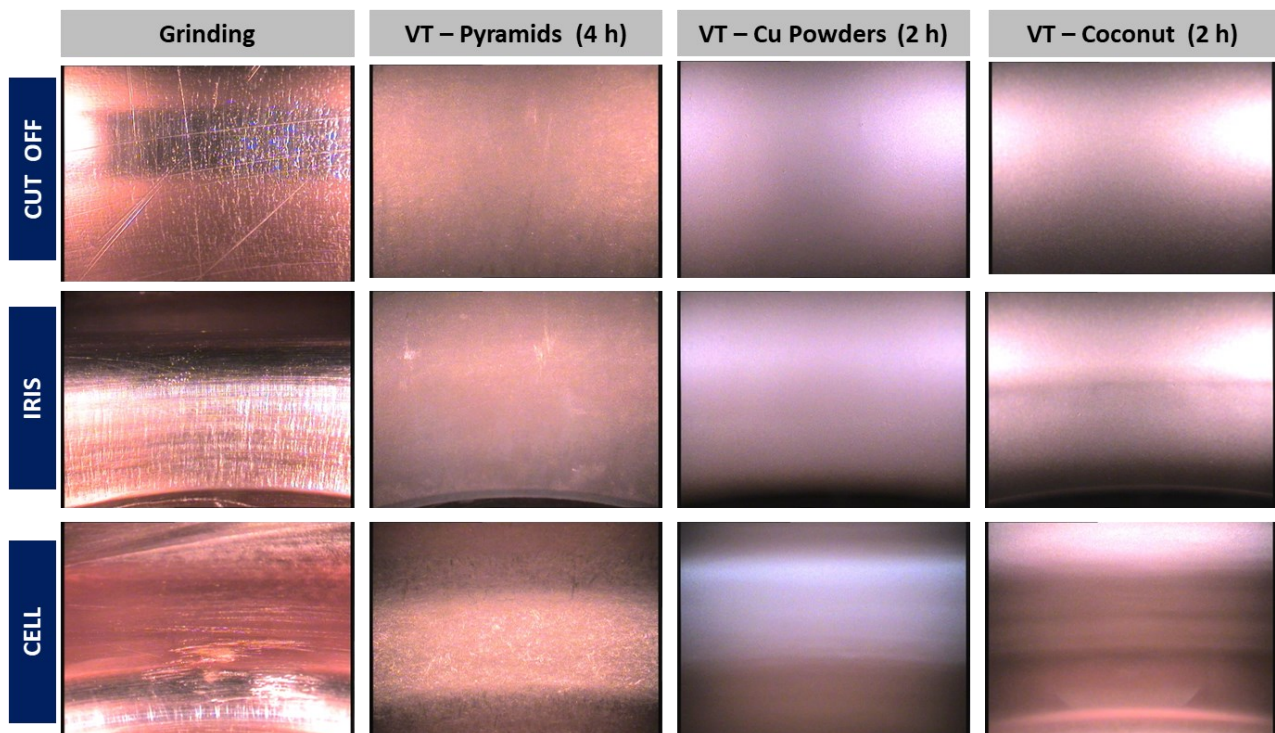
Figure 5.30: Internal inspection of the Cu cavity Cu031 after three-step protocol

To prevent Cu oxidation copper powder substitution with the corn chips was explored. It is similar to the coconut shells, but slightly bigger, and characterised as more abrasive, see **Figure 5.31**.
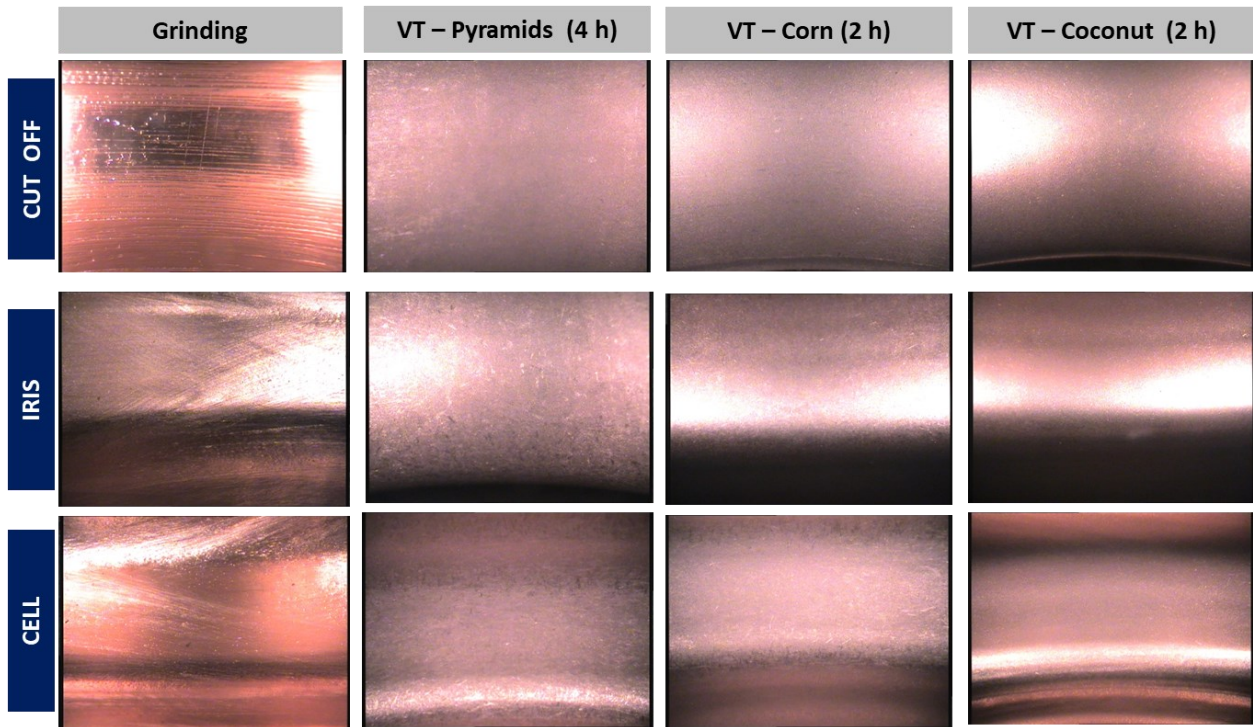
Figure 5.31: Internal inspection of the Cu cavity Cu028 after three-step VT protocol

5.6   Ultimate recipe for the Cu VT processing

After a successful study on the optimisation and enhancement of the first three-step protocol of VT, a last iteration of it has been made. As it was mentioned before, the copper powder was leaving traces of micro-powder inside the cavity and additionally provide oxidation, which might be not the best scenario for the substrate, it was decided to switch away from the Cu abrasive. An alternative approach of the corn shells abrasive was tested (see chapter 5.5.1), however a significant difference between the cu powder and corn abrasive after the third coconut treatment was not identified. Moreover, eliminating the second VT step has shown (see Fig. **Figure 5.32**) similar results. Application of the newer, so-called synergic approach – chemical vibro-tumbling, has led to a significant increase in erosion rates. Additionally, all the cavities are subjected to the at least 100 μm removal of the surface, so the importance of the Vibro-Tumbling is to ensure defects free and uniform surface, which is perfectly achieved with the two-step ultimate VT protocol.

Initial	VT – Pyramids (7,5 h)	VT – Coconut (1 h)
CUT OFF		
IRIS		
CELL		
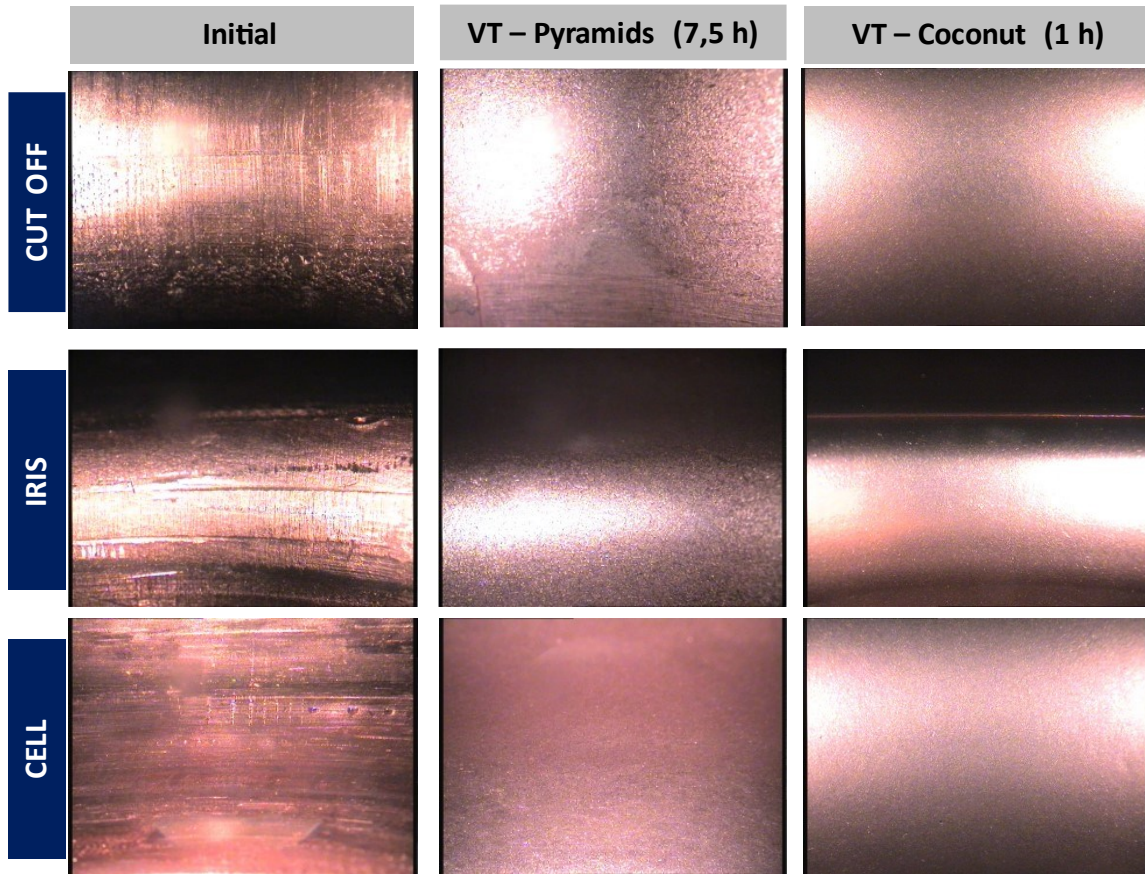
Figure 5.32: Two step protocol of VT applied on the Cu055 Cu 6 GHz cavity

The ultimate protocol has been studied as well on the small coupons to analyse the surface morphology. Surface roughness was identified with AFM XE-70 system. Cylindrical samples were studied after CVT, after coconut VT and after PEP (see **Figure 5.33**). Motor frequency 190 Hz, RPMS abrasive, 70% filling volume. Initially scratched and then grinded samples have shown a significant lowering of the roughness, additionally a planarization of the surface is observed after PEP.

Step I : CVT — Ra= 200 nm Step II : VT coconut — Ra= 100 nm Step III : PEP — Ra= 20 nm
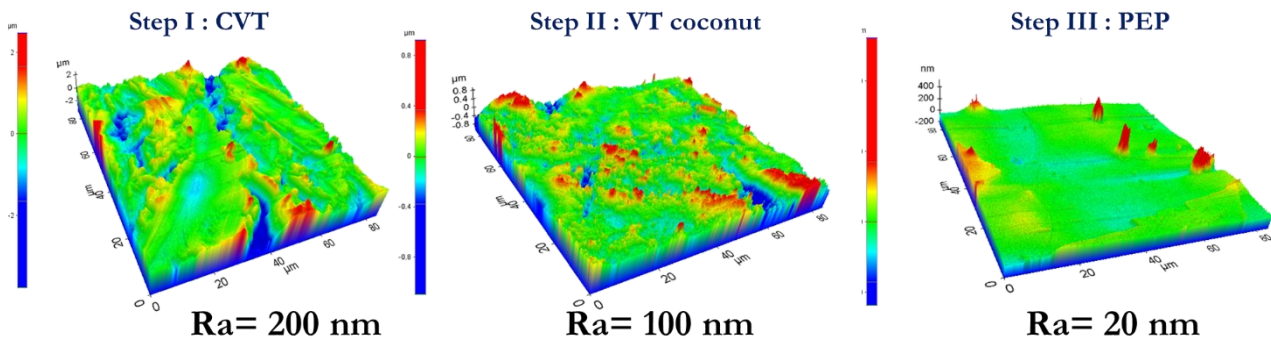
Figure 5.33: AFM analysis of the Cu coupons after chemical VT, coconut VT and after generic PEP treatment

Currently, the protocol (see below) has been implemented in the routine preparation of the 6 GHz Cu cavities at Legnaro laboratories.

Protocol for mechanical processing of Cu 6 GHz cavities at LNL

1. 1 h of ultrasonic cleaning with detergent GP 17.40. 10 min of ultrasound cleaning with distilled water. Rinsing with ethanol (C_2H_5OH) and drying with compressed nitrogen N_2. Weight the initial cavity mass. *Optional: cavity inspection.*

2. Filling the resonator with RPMS abrasive, add 10-20 mL of an oversaturated ammonium persulfate solution and then additionally add 1 g of $(NH_4)_2S_2O_8$ salt. Sealing plugs are inserted.

3. Assembly of the cavity in the VT setup machine. Check the working frequency.

4. Initialisation of the inverter and consequently the motor and step motor (for rotation).

5. After 60-120 minutes of treatment, it is recommended to stop the process. During processing every 20-30 minutes check for the sealing and status of the system.

6. Ultrasound cleaning (like the step 1). Rinsing with sulfamic acid (5 g/L), ethanol and drying with compressed N_2.

7. Weight the cavity. *Optional: inspection of the internal of the cavity.*

8. Repeat steps 2-7 till the surface looks smooth and do not have any visual defects.

9. Repeat steps 2-7 filling the cavity with 70% of coconut shells.

6 R&D on Plasma Electrolytic Polishing of Cu and Nb

In this chapter all the practical aspects of experiments done with PEP technology is presented for the processing of Cu and Nb substrates with the aim for further application to the SRF technology field. Solution study and optimisation, parameters analysis, polishing characterisation, system configuration study.

6.1   System configuration setup

As it was deeply described in chapter 3, the PEP requires powerful PS, that can deliver high voltage and high current values (at least 0,2-1 A/cm^2) to ensure the stable plasma discharge under static conditions. It was as well mentioned that the system is quite similar to the classic electropolishing solution, that normally consists of a bath, one counter electrode, connections and wires. Enhancing the mass-exchange process a stirring component may be added as well. A necessary part is naturally a heating element, that will provide initial heating of the solution temperature, necessary to decrease the working current, and ensure the ignition of the plasma, as one of the requirements of the process. Repeating this key characteristic, a significant number of the treatments were done in a relatively simply conditions (see **Figure 6.1**), where a glass beaker of 5 L volume was used as a bath. A metallic isolated stand was used for a stable positioning and current fixation to the electrodes.
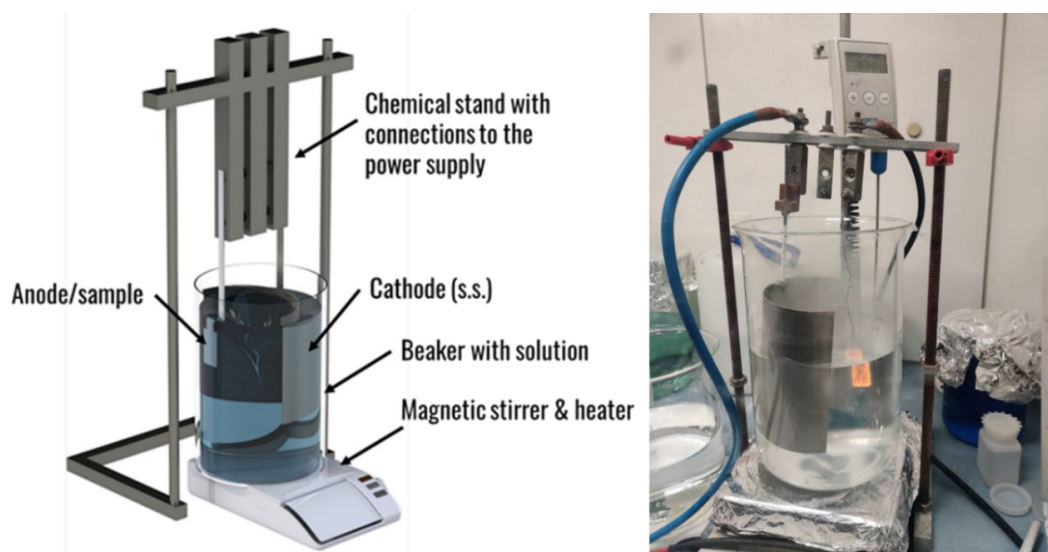
Figure 6.1: A schematic view of the PEP setup and a real photo during the Nb PEP

Bigger systems were as well considered to allow higher surface area (and thus better cooling, enhanced mass-transport of the system) as it is normally done in most of the PEP research studies or industrial implementations (see **Figure 6.2**).
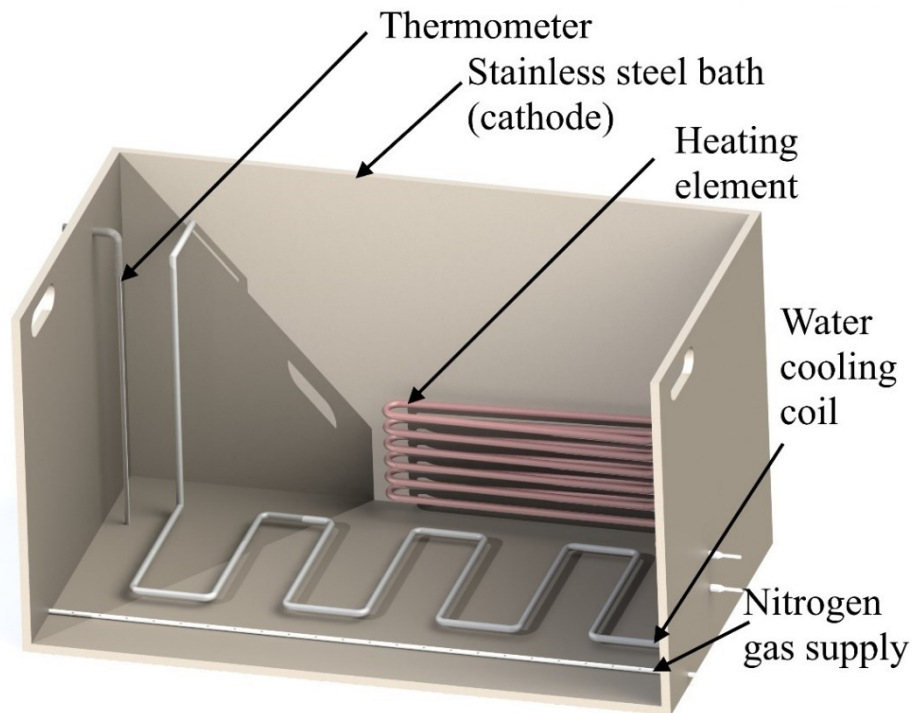
Figure 6.2: A render of a standard system setup, based on the bath as a cathode (stainless steel)

In the framework of the scaling study, at LNL an upgrade of the current system setup has started, and it will allow the future high surface area PEP treatments. A proposed system is shown below (see **Figure 6.3**).
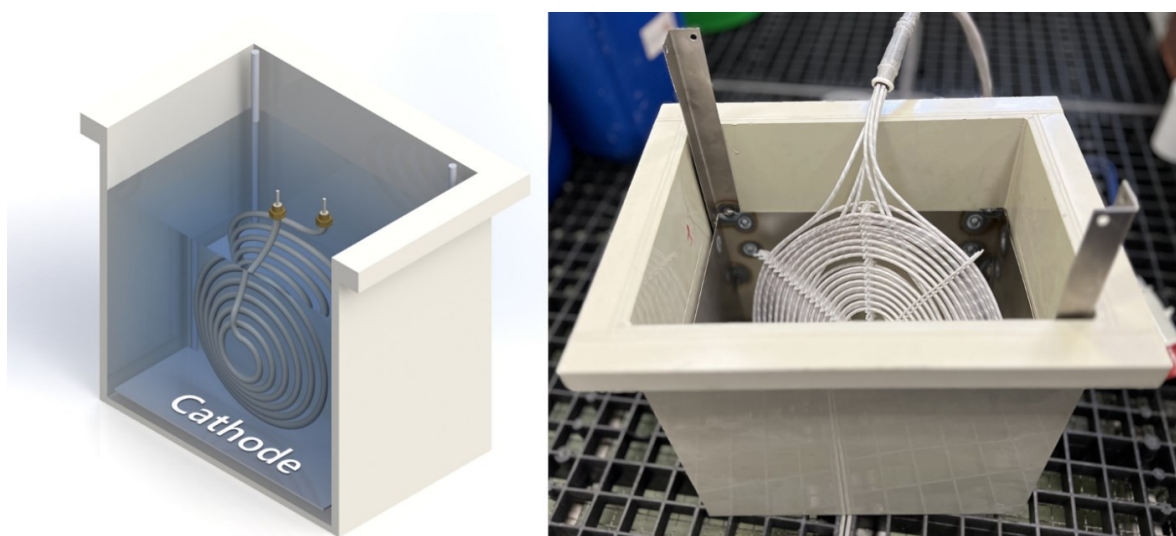
Figure 6.3: Upgraded plastic bath with a Niobium rectangular cathode and teflonated heating element

Lastly, some specific cases and experiments required more complex bath setup configurations, as for example in Jet-PEP, where some experiments were done to evaluate the feasibility of the technology. Basically Jet-PEP requires same conditions with the difference of continuous loop of solution fluxing over the treated surface, where the PEP similar process will take place, thus providing local PEP (see **Figure 6.4**).
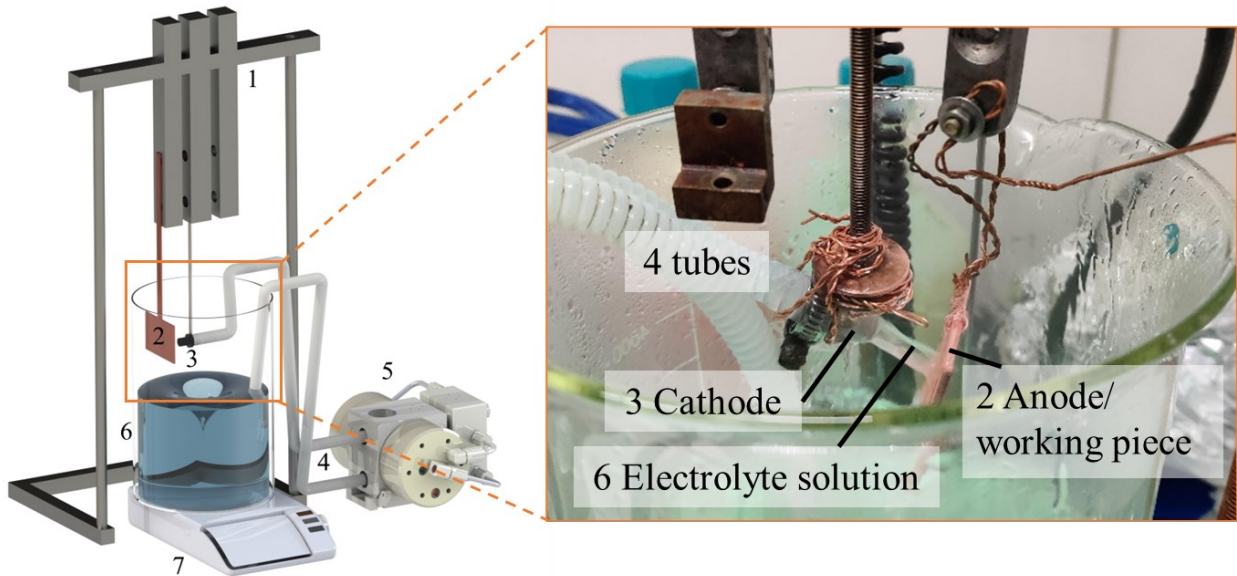
Figure 6.4: Jet-PEP setup build at LNL; 1 – chemical stand, 2 – anode / working piece, 3 – spraying head (cathode), 4 – input and output tubes, 5 – PTFE membrane pump, 6 – beaker with electrolytic solution, 7 – magnetic stirrer and heater

6.2   Solution selection and optimization

As it has been partially mentioned and described, available PEP recipes in the open sources solutions are mostly presented for the steel alloys and some other metals such as Ti, Al. In case of the Cu and especially Nb, there was a limited quantity of information available. Given the narrow experience at the time of PEP, it was done research on papers and first test were performed with the opened solutions. After a series of trial, most common problems were identified as salt production, oxidation, non-uniformity, irreproducibility, formation of transparent chemical films and others depending on the solution and metal used. Some of the tested solution worked for other materials as brass, Ti, Ta, V, Co, steels, aluminium, this kind of information is not showed in the dissertation.

6.2.1   Copper solutions

A few papers disclosed fully or partially solutions that may be used for Cu PEP [249], [299], [327] and some patents were found, a report on available solutions is presented below in Table 6.1. Our scope of the chemical selection based on the most common chemical products used in the Cu chemistry: citric acid, ammonium citrate, H_3PO_4, H_2SO_4, ammonium phosphate.

Table 6.1 – A summary on the available Cu PEP solution in the literature

№	Solution	Voltage range	Temperature	Reference	Comments
1	57% sodium phosphate (NaH_2PO_4) + 9% H_3PO_4 (phosphoric acid)	35 V	70 C°	Mayorov [328]	Time 2-10 s
2	$(NH_4)_2SO_4$ 0,7 – 1,3% Na_2-EDTA 2,5 – 3,5 %	180-230 V	70-90 C°	Bagaev [329]	
3	1) $(NH_4)_2HPO_4$ 3 – 5 % H_3PO_4 down to **pH 5-7** 2) $(NH_4)_2HPO_4$ 3 – 5 % K,Na-Tartrate – 1-3 %	300-360 V	60-90 C°	Amirkhanova [330]	1) 3 - 10 min 2) 10-30 s
4	Na_2SO_4 2-6 %	240-320 V	40-80 C°	Stanishevsky [331]	Mate, etching, nonuniform
5	NH_4F 1 – 3 % NH_4Cit 1 – 5%	240-400 V	70-90 °C	Ermakov [332]	5 min
6	NH_4Cl, NH_4F, $C_6H_5O_7 (NH_4)_3$	250–340 V	60–90 °C	Dyblenko [333]	

It is worth to underline that neither of the mentioned solutions could provide a mirror-like polishing performance, non-comparable to the standard EP. Some of them simply bright the surface, some produce non-uniform oxides or mate morphology. Finally, few solutions were found, that might be used for Cu PEP being capable to resolve the above-mentioned issues. A table with the selected solutions and experiments is showed below (see Table 6.2).

Table 6.2 – Original selected solutions and parameters tested for Cu PEP

№	Voltage	Solution	Time (min)	pH	T1 (°C)	T2 (°C)	RR, (µm/min)	Area, (cm²)	Comments	Photo
1	300	Citric acid 10%	5	1,71	75	93	6,2	12,5	No polishing, hard etching, salt production	
2	300	EDTA 4% + (NH4)2SO4 0,5%	2		75	86	1,97	9	Polishing, Oxidation.	
3	300	Old SUBU + EDTA 1% + (NH4)2SO4 0,5% + K.Na-Tartrate 0,5%	2		69	85	4	7,5	Smooth, mate	
4	300	NH4-Citrate 2% + NH4F 3% + n-Butanol 50mL/L							Mate, non-uniform	
5	340	(NH4)2HPO4 5%, + H_3PO_4 + K,Na-Tartrate 3%	0,15		74	85	0		Mate surface	

№	Voltage	Solution	Time (min)	pH	T1 (°C)	T2 (°C)	RR, (µm/min)	Area, (cm²)	Comments	Photo
6	300	$K_4P_2O_7$	1,5	11	72	83	6,1	11	Top mirror, Middle Bright, Bottom oxidation	
7	300	$K_4P_2O_7$ + H_3PO_4	1,5	4,25			10	11		
8	300	$K_4P_2O_7$ + H_3PO_4	1	3	75	85	12,2	11	Etching, sparks	
9	300	$K_4P_2O_7$ 3,2 % + NH_4Cl 1%	1		75	86			Shining, not reflective	
10	300	$K_4P_2O_7$ 4% + K,Na-Tartrate 7 g/L	2	11						
11	300	$K_4P_2O_7$ 4% + K,Na-Tartrate 7 g/L + H_3PO_4	2	5						
12	300	$K_4P_2O_7$ 4% + K,Na-Tartrate 7 g/L + H_3PO_4	2	3...4					Reflective, polishing, Uniform	
13	300	$K_4P_2O_7$ 4% + K,Na-Tartrate 7 g/L + H_3PO_4	2	2						
14	300	$(NH_4)_2HPO_4$ 3%		8,23					Etching	
15	300	$(NH_4)_2HPO_4$ 3% + H_3PO_4	1	5...6			8	12,5	polishing. reflective, uniform, stain, nor mirror	
16	300	$(NH_4)_2HPO_4$ 3% + H_3PO_4	1	2...3			11,5	12,5	Polishing, stain, less reflective	
17	300	$(NH_4)_2HPO_4$ 3% + H_3PO_4 + Ammonium Citrate 5%	1	3...4			11,9	7,5	Reflective, bright, uniform, polishing	
18	300	(NH4)-Cit 4%	2	6	70				Bright (not reflective)	

№	Voltage	Solution	Time (min)	pH	T1 (°C)	T2 (°C)	RR, (µm/min)	Area, (cm²)	Comments	Photo
19	300	(NH4)-Cit 4% + K,Na-Tartrate 4%	2		75				Mate	
2 0	300	(NH4)-Cit 4% + K,Na-Tartrate 4% + H_3PO_4	2	3	75				Mate	
21	300	(NH4)-Cit 4% + K,Na-Tartrate 4% + H_3PO_4 + Sulfamic Acid 5%	2		78				Reflective, thin oxide layer	
22	300	Na_2-EDTA 3%, $(NH_4)_2SO_4$ 0,5%;	5		84	87	9,3	12,5	etched but uniform, not reflective	
23	300	$(NH_4)_2SO_4$ 5% + H_3PO_4 0.5% + K,Na-tartrate 1%	5		72	87	6,44	12,5	etched but uniform, not reflective	
24	300	NH4-Cit 5%, Na2SO4 3%	2						Mate polishing, bright, oxides	
25	300	NH4-Cit 5%, Na_2SO_4 3% + Butanol 50 mL/L	2						Reflective, bright, polishing, oxide	
26	300	$(NH_4)_2SO_4$ 3% pH H_2SO_4	2	4			6,35	12,5	Polishing, but appears oxide-like layer	
27	300	SUBU5 without H_2O_2	2		85	90	6,71	l0	Etching, uniform	

After a series of trials with common and less common chemicals, a relative connection was found between the presence of polishing effect and a used compound. For instance, most of the recipes contain $(PO_4)^{3-}$ anion that as in classical EP, may be a key for the mechanism of Cu transformation and eventually transportation. Similarly $(SO_4)^{2-}$ can be characterised as an anion, that enhances the polishing process under certain conditions, however, in most cases solution with this ion yield to produce "oxidised" surface (but smooth and enough uniform). Such "oxidation" films (as the record n. 28 in table 6.2) are not removable under classical organic acid deoxidation (citric or sulfamic acid), that can be explained by the more complex nature of a such film, for e.g., formation of some intermediate compound between hydroxide, oxide and possibly bonded with an acid anion - $(SO_4)^{2-}$.

136

Another noticeable fact is that normally the solution has to be in the acidic pH interval, or at least close to pH 6-7 for a polishing effect, rather than salt, oxide formation in the base pH. So, generally, as most of the presented salts are alkaline based metals or $(NH_4)^+$ cation, their pH are ≥ 7. That is why an acid buffing is needed, however it remains unclear whether the acid is only pH changer, or somehow a donator of the $(PO_4)^{3-}$ anions. It is also noted that too low pH normally is not a good media for the polishing, as someone may expect similarly to the electropolishing. Another aspect that is vital to mention is the pyrophosphate anion, that, based on our experience with phosphate ion we were thinking might work as well, and thus it allows PEP of Cu. As for the cation for the pyrophosphate could work both the metal (e.g., potassium and sodium) and ammonium ions. However, from the solubility point of view, it was decided to work with the potassium cation salt.

As a moderator, surfactants, such as Sodium Lauryl Sulphate (LAS) or organic solvents (Butanol, ethylene glycol) did not show a significant impact on the quality of the treated surfaces or the process as well. To summarise all solutions and chemical compounds effect tested a Table 6.3.

Table 6.3 – Summary of chemicals used to test Cu PEP

Effect on the Cu PEP	Chemical compounds
Positive	$K_4P_2O_7$, $Na_2P_2O_7$, $(NH_4)_2HPO_4$, Na_3PO_4, Na_2HPO_4, H_3PO_4, Sulfamic acid, Ammonium citrate, K,Na-Tartrate
Somehow positive or perspective	Na_2-EDTA, Butanol, NH_4Cl, NH_4F, Ammonium Sulfamate, H_2O_2, $(NH_4)_2SO_4$, Na_2SO_4, H_2SO_4
Neutral	Ethylen glycole, Triton X-100
Negative	Oxalic acid, Citric acid, EDTA

As a consequent research and study three (see Table 6.4) solutions for the Cu PEP were found. These recipes were studied and selected for the patent evaluation in a combined application in Italy within the INFN Technological Transfer office.

Table 6.4 – Developed solution for Cu PEP (patented submitted [334], [335])

№	Solution	Voltage, V	Temperature, C°	Erosion rate, μm/min	Comments
1	SUBU5: Sulfamic Acid 5 g/L Ammonium citrate 1 g/L Hydrogen Peroxide 50 mL/L n-Butanol 50 mL/L	270-340	70-97	6 - 24	Maximum mirror reflecting effect. Passivation required.
	SUBU20: Sulfamic Acid 20 g/L Ammonium citrate 1 g/L Hydrogen Peroxide 50 mL/L n-Butanol 50 mL/L			12 - 30	
2	Potassium Pyrophosphate 2-6 % K,Na-Tartrate 0.2-1 % H_3PO_4 down to pH 2 - 5	280-320	40-85	6 – 12	Acidic pH correction requires
3	Diammonium phosphate 2-6 % H_3PO_4 down to pH 2 - 5	270-320	40-85	3 – 15	

6.2.2 *Niobium solutions*

As it was deeply discussed in chapter 3, PEP is a feasible approach to polish almost every metal, but in case of valve-metals (such as Al, Ti, Mg, Zr, Ta and Nb) the mechanism is different, that disables the possibility to use standard PEP solution of ammonium sulphate, as in case of most metals. Above mentioned metals have a n-type oxide film, that must be dissolved in some way; this complicates the PEP processing of Niobium. However, in literature there are some examples of successful valve metals PEP processing (Ti, Mg, Zr, Al and others, see Table 3.1). The only available solution is presented below Table 6.5. Similarly to the copper PEP chemistry, it was taken in consideration the available experience. Table 6.6 reports the selected experiments that had a significant value for the selection of the chemical compounds to develop a working electrolytic solution of Nb PEP.

Table 6.5 – Available literature solutions for Nb PEP

№	Solution	Voltage range	Temperature	Reference	Comments
1	4% Ammonium Fluoride NH_4F	260 - 300 V	75 - 95 C°	Aliakseyeu	Preferably oxide formation, with partial polishing.

Table 6.6 – Original selected solutions and parameters tested for Nb PEP

№	Voltage	Solution	Time (min)	pH	T_1 (°C)	T_2 (°C)	RR, (µm/min)	Area, (cm²)	Comments	Photo
1	290	1% NH_4F	2						Oxides, non-uniform	
2	290	2% NH_4F	2						Oxides, non-uniform	
3	300	3% NH_4F	2						Oxides, non-uniform	
4	290	3% NH_4F+ 2 mL/L H_2SO_4	2						Oxides, non-uniform, macro-oxidations	
5	290	3% NH_4F + 2 ml/L H_2SO_4 50 mL/L Butanol	2						Oxides, non-uniform, macro-oxidations	

№	Voltage	Solution	Time (min)	pH	T$_1$ (°C)	T$_2$ (°C)	RR, (µm/min)	Area, (cm²)	Comments	Photo
6	300	2% NH$_4$F, 0,5% NaF	2				5		Polishing, oxides	
7	310	2% NH$_4$F, 0,5% NaF + 1% NH$_4$HF$_2$	2				7,7		Polishing	
8	330	2% NH$_4$F, 0,5% NaF + 1% NH$_4$HF$_2$	2						Polishing	
9	310	3% NH$_4$F, 3% NaF 10 mL/L HF 5 mL/L H$_2$SO$_4$	2						Polishing	
10	300	3% NH$_4$F 3% NaF 4ml/L H$_2$SO$_4$	2						Polishing	
11	300	2% NH$_4$HF$_2$ 0,5% NaF	2	5	70	78,8	3,85	9	Grey, uniform, wire is shining	
12	300	2% NH$_4$HF$_2$ 0,5% NaF 1 mL/L H$_2$SO$_4$	2	5	75,4	79,8	9,1	4,55	Partially reflective, oxide. Wire shine	
13	300	2% NH$_4$HF$_2$ 0,5% NaF 1% NH$_4$F 1 mL/L H$_2$SO$_4$	2		77	81,6	5,15	9	Not uniform, oxide, reflective on the top part kind of mirror, the bottom part is grey	
14	300	2% NH$_4$F 2% NaCl	2	6.5	66	77	11,5	9	salty and rough	
15	300	2% NH$_4$F 2% NaCl 3mL/L HF 5%	2	6	74,2	80	4,5	9	oxide	

№	Voltage	Solution	Time (min)	pH	T$_1$ (°C)	T$_2$ (°C)	RR, (µm/min)	Area, (cm²)	Comments	Photo
16	300	2% NH$_4$F 2% NaCl 6mL/L HF 5%	2	5,8	83,6	87	2,5	9	oxide	
17	300	2% NH$_4$F 2% NaCl 6mL/L HF 5% 1% NH$_4$HF$_2$	2	5	79	85	4,5	9	POLISHED! Closer to cathode, reflective, uniform	
18	300	2% NH$_4$F 2% NaCl 6mL/L HF 5% 1% NH$_4$HF$_2$	2	5	83,4	88	3,25	9	Reflective, uniform, more far away from the cathode	
19	300	3% NH$_4$F 2% NaCl 16mL/LHF 5% 1% NH$_4$HF$_2$	3,75	5...6	77	86,8	3,45	9	oxides, not shining	
20	300	3% NH$_4$F 0.5% NaF	3	6...7	78	83,6	2,59	9	Polishing, reflective, oxides	
21	300	3% NH$_4$F	2	6...7	78	83	3,89	9	oxides, not uniform	
22	300	3% NH$_4$F 1% NaF	2	6...7	78	84	4,54	9	reflective, oxides, less uniform with non-reflective part on the edges	
23	300	3% NH$_4$F 1% NaF Et. Glycole 10mL/L	2	6...7	76,8	83,8	5,185	9	reflective, uniform oxides just a little bit on the top part	
24	300	4% NH$_4$F 0.5% NaF	5		67,8	86	3,888	9	reflective, almost all surface, mirror.	
25	300	4% NH$_4$F 0.5% NaF	2		79	86	3,25	9	reflective, mirror, near wire not shining	

№	Voltage	Solution	Time (min)	pH	T_1 (°C)	T_2 (°C)	RR, (µm/min)	Area, (cm²)	Comments	Photo
26	300	5% NH_4F 2% NaF	2		81,6	87	4,54	9	Reflective, mirror. Bottom edge oxide, 4/5	
27	300	6% NH_4F 2% NaF	2,5		72,4	85	5,188	9	40% polished, reflective, mirror, not uniform, thick oxide	
28	300	6% NH_4F 0.5% NaF	3		70	83	3,73	9	Not uniform, grey, bottom polished, middle oxides, cathode cage	
29	300	1% NH_4F 1.5% NaF	3		63	86	2,9	9	Top part shiny, not uniform not polished, oxides and grey parts	
30	300	4% NH_4F 2.5% NaF	2		77	87	4,35	9	almost uniform, small oxide, edges not reflective	
31	300	3% NH_4F 1% NaF	108,5				1,19	54	Excellent polishing	
32	300	3% NH_4BF_4	3.5	6	72	81			Etched in the center, yellow salt on the edges.	
33	300	3% NH_4BF_4 1% NaF	5,2		77	85			Grey oxide, rough	

After a series of experiments, at least those n° 1,2,3,21 (and others not showed in the table above) show significant problems with uniformity and oxide production, that does not provide claimed by Aliakseyue [273], [273], [336] recipe. However, during the processing, some kind of oscillation (see **Figure 6.5**), similar to the oscillation with EP Nb) can be observed, where the overall process is proceeding in two stages 1) oxidation 2) dissolution of oxide. It may suggest as well that there are two conquering processes of oxidation and dissolution, and in case of "unsuccessful" polishing, overall speed of oxidation is higher than a medium rate of oxidised compound dissolution resulting in thin oxide production or even hard oxide production (such as in n° 11, that is a pretty common result).

Figure 6.5: Photo of the sample during Nb PEP – oscillation of the VGL

It is also noticeable the wire connection effect on the surface of the treated anode samples. Such rainbow, oxidised part is often smoothed and reflective with a colourful oxide (meaning thin thickness). Most likely this effect is due to the fact of 2 conquering reactions and in the ending of the process remaining last anodic polarization impulses are locally "discharged" affecting only the local connection between wire and sample.

Noticeable negative effects of hard oxide production (e.g., n° 4,5,13,14) where, due to unknown reasons, a local production of oxide can be done even in the macro-scale. It is still unclear the reasons, low initial temperature and/or composition degradation are most possible explanations.

A key solution to statistically decrease the oxide production was found. Additional 0,5-2 % of sodium fluoride significantly improves the uniformity and permits longer treatments (also up to 1 h). A possible explanation of pH effect of such additive rather than a composition changed was considered. However, the usage of other more "alkaline" salt – sodium chloride, did not permit any successful polishing treatments (e.g., n° 14). More significant pH drop can be achieved by adding inorganic acids, such as sulfuric, fluoric, fluoroboric. Such additives, even in small quantities, are not desirable from the technological, ecological and security point of view for the further industrialisation (e.g., n° 4,9,10,12, 15, 16, 17,19 and others). However, the acid influence is rather unclear, and does not provide repeatable experimental data resulting in reflecting polishing or oxidised surface.

As a potential analogue to the NH_4F it can be used ammonium bifluoride, that is more acidic, and consequently more toxic, due to the hydrolysis in water into the hydrofluoric acid. Probably due to the more acidic reaction, the influence of bifluoride is more evident, and additional sodium fluoride is steel needed. Instead, a potassium and lithium fluoride can be used as equivalents of the sodium fluoride. any optimal polishing results were found with the usage of ammonium tetrafluoroborate, however it might be still a compound to consider for further developments similarly as ammonium fluorosilicate (that was not tested in this dissertation). Positive experiences of such salts were already mentioned in some open recipes of PEP of valve metals [248], [256], [308].

Still, a long list of different composition ratio was not able to clearly determine the working range of the chemical composition; that is why a planned experiment (see Table 6.7) was established for the critical missing data. An evaluation of the quality of every single experiment was done by four main parameters: polishing effect (smoothening and reflection) and quantity of the oxidation signs,

uniformity, presence of salt production. Quality of the above-mentioned characteristics were evaluated by colouring (where green colour stands for the perfect conditions, yellow for decent conditions, red for the unacceptable quality). More than 31 experiments with new solutions were conducted, with a working voltage at 300 V, and working temperature that did not exceed the range of 75-88 C° at the beginning and end of the treatment respectively. The sample was placed in the glass beaker previously preheated to the 75 C°. Anodic polarisation was maintained for the fixed time of 2 minutes.

Table 6.7 – Modulation of the solution composition for Nb PEP

Content NH$_4$F / NaF	0%	1%	2%	3%	4%	5%	6%
0%	n/a	n/a	n/a	S; O	O; S; P	n/a	O; S; P
0,5%	n/a	P; U, O	P; O;	P	P	P	U; P; O
1,0%	n/a	P, U	P	P	P	P; O	n/a
1,5%	n/a	P; U, O	P; U; O	P; U	P, U	P; U; O	n/a
2,0%	O; S	P; U	P; U	P; U	n/a	P; O	P; U; O
2,5%	n/a	P; U, O	n/a	P; U, O	P, O	n/a	O; U;
3,0%	S; O	n/a	n/a	n/a	n/a	n/a	O; U;

where, **P** stands for "Polishing", **O** – signs of oxides, **U** – uniformity, **S** – salts or hard oxides; Green – for ideal or best results, yellow – decent results with some drawbacks, red – worst results, to be considered not working.

Finally, a working solution based on ammonium fluoride and sodium fluoride water solution was identified and Nb PEP processing was as well optimised with that solution (see Table 6.8). As in case of copper solutions, developed solution was described in the application for the Italian Patent and Trademark Office with the number n° 102022000009899. Bicomponent solution of 2-6 % NH$_4$F and 0,5-2 % NaF is claimed to be a working solution for the PEP processing of the Nb, Ta, V and their alloys.

Table 6.8 – Summary of the developed Nb solution (patent submitted [337])

Solution	Voltage, V	Temperature, C°	Erosion rate, µm/min
Ammonium Fluoride NH$_4$F 2-6 % Sodium Fluoride NaF 0,5 – 2 %	300	78 - 85	2 – 8

6.3 Temperature factor

The temperature plays one of the key roles in the PEP processing due to the surface quality and removing rate (erosion rate) impact. Speaking of the quality influence of temperature it is widely noted that lower temperature might produce undesired oxide/salt formation, or simply etching instead of polishing. Higher temperatures are often beneficial for PEP processing in terms of uniformity and stability of the plasma. The only exception of high ($\geq 85\,°$) temperature PEP processing might be considered copper, that under certain conditions at high temperature tend to oxidise.

A characteristic curve of current density vs solution temperature has shown the inverse proportion behaviour (see **Figure 6.6**).
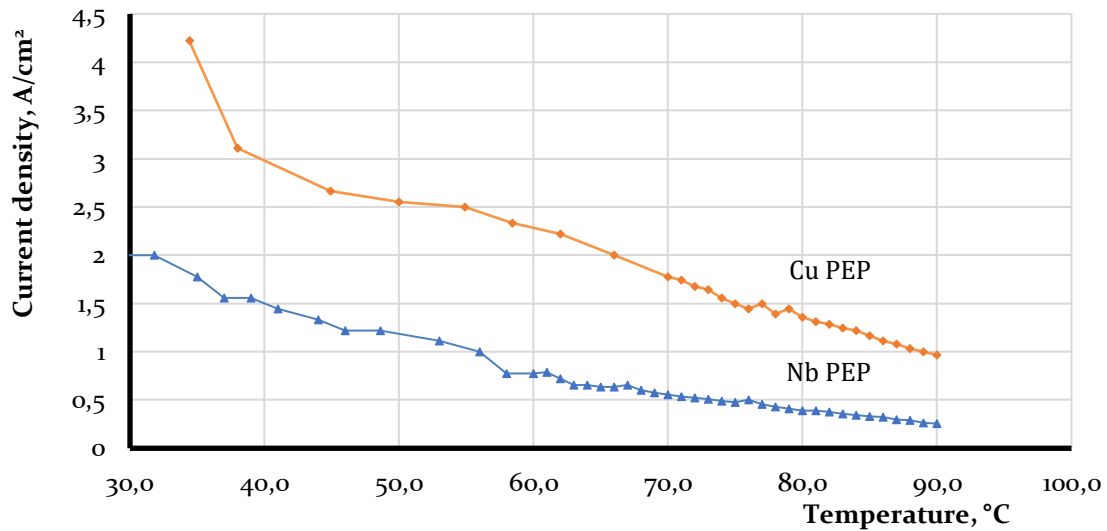
Figure 6.6: Current density vs bath temperature chart for Nb and Cu PEP (SUBU5 solution) at 300 V [338]

6.3.1 Copper PEP features

Some aspects of the copper PEP are related to both nature of the copper and its oxides and three different samples. From table 6.4 above, it is evident that developed solutions are behaving differently. Thus, a temperature range are different, in case of SUBU solution it is relatively high, >70 C° comparing to other phosphate/pyrophosphate-based compositions. This fact is correlated with the compositions of these electrolytic solutions together with different phenomena related to the boiling on the surface / solution interface – film boiling in case of phosphates, and bubble boiling in case of SUBU solution. This is evident during the process and can be distinguished with extensive bubbling and boiling in the last case, and vice-versa in case of film boiling, where the process is rather calm and quiet, with some crackling noise.

A significant difference in erosion rate might be observed starting from lower temperature, that might be explained by the relevant instability of the VGL between the solution and metal interface, resulting as well in undesired phenomena. From our experience it is recommended to apply higher voltage in the beginning of the process, and steadily it might be decreased by few tens of volts. Similarly with the temperature, initial low temperature in some cases may lead to the formation of the hard oxides/salts.

Temperature vs current density curves for three developed Cu PEP solutions are presented below (see **Figure 6.7**). Voltage was maintained at 300 V, and treatment time did not exceed 3 minutes. Pyrophosphate solution composted of 4% and K,Na-tartrate of 1 %, Diammonium phosphate

– 4%, SUBU – composition corresponds to SUBU5 (see table 6.4). Surface area of Cu samples were chosen to be 20 cm^2.
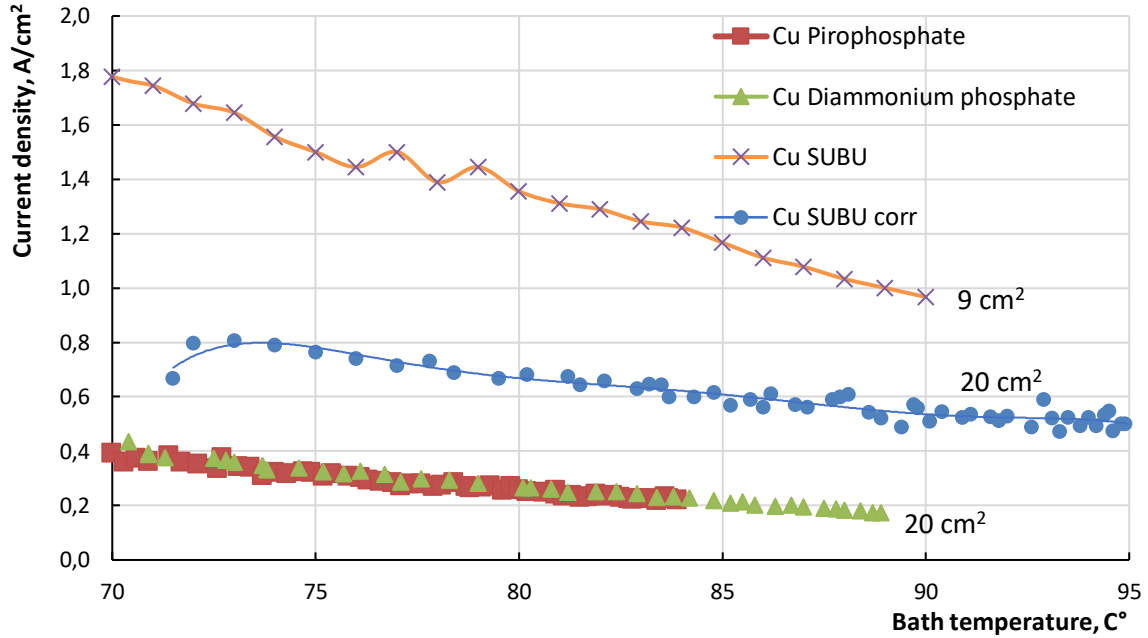
Figure 6.7: Current density vs Bath temperature for copper solutions and one solution of Nb PEP, at 300 V

A different coefficient of curves might relate to the mechanism of PEP erosion of a selected system (metal and solution) and/or the conductance of a specific system at a certain temperature. This as well may be related to the uniformity of the vapour-gas layer and resulting in the different current efficient values. A lower current efficiency may be related to the higher impact of the physical effects that take part between the vapour-gas – solution – metal interfaces, and vice-versa, once the classic electrolysis takes places (see chapter 6.5).

Summary: copper finishing is not dependent a lot from the temperature in the high temperature range (70-85 C°). Higher temperatures however might introduce oxidation to the final surface overview. Low temperature polishing is not feasible to establish, since at these conditions high current density regimes will significantly heat the solution and maintaining the low-temperature will not be a trivial task.

6.3.2 Niobium PEP features

In case of Niobium PEP, it was noted that in uncertain cases temperature might produce oxidations or nonuniform polishing (see **Figure 6.8**). A way to overcome those issues were found in the higher temperature working conditions, especially in the initial 0-60 sec of the process.

| Initial | 70 °C | 75 °C | 85 °C |
| Average | 80 °C | 85 °C | 88 °C |

Figure 6.8: Three different samples with different temperature profile during PEP of Nb

Higher temperatures are characterised with lower erosion rates (thus electrochemical oxidation in case of Nb), instead the dissolution rate of the oxide/salt/metal might remain equal or ever lower, resulting in overall polishing, instead of oxidation. The ratio between the oxidation and the dissolution rates during the processing might differ yielding to the surface local oxidation at relatively lower temperatures.

An understanding of the possible mechanisms of the niobium PEP might explain such observations. A possible mechanism of the niobium removal was suspected: formation of the niobium fluoride and its evaporation. Thus, to get a relevant information on the actual sample temperature it was required to measure the surface temperature without regard of the phenomena that happens on the interface of the metal. A long hollow sample of 1 cm diameter, 15 cm length, wall thickness of 5-10 mm (variable) was chosen as an object. A thermocouple was then inserted a sealed (see **Figure 6.9**)
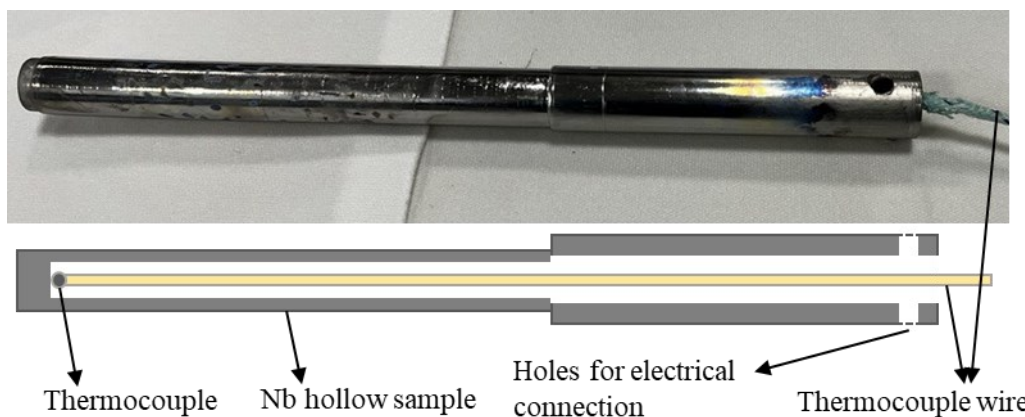
Figure 6.9: A photo and scheme of the used analytical Nb sample to measure the bulk temperature during the PEP processing

In case of correctly applied sealing of the thermocouple from humidity and vapours the deviation of the temperature was observed only in the beginning of the polishing, withing 1 minute, normally these values are converging. Additional investigation, on the effective dynamic change of both bath temperatures and current densities were done (see **Figure 6.10**).
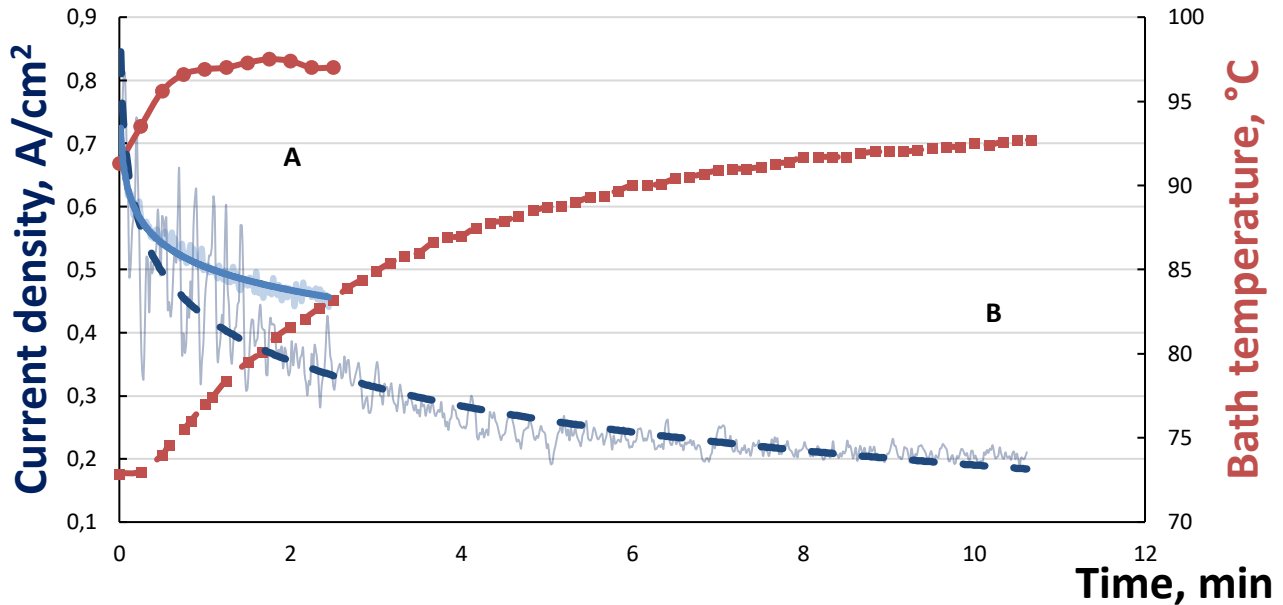
Figure 6.10: Current density vs bath temperature (70-99 C°) curves in time for two separate Nb PEP treatments of A) 2,5 and B) 10,5 minutes

Two experiments were conducted at different starting temperature for 2 different samples of 9 cm^2 area. The current density characteristics and bath temperature are clearly reverse proportional. A higher temperature allows faster stabilisation of the process, as seen from the current density curves.

Normally, the erosion rate, is lower at higher temperatures, however this is true for the similar processing time. We might assume that higher roughness may cause higher effective current densities and thus, within a polishing process, a lowering of the current density is observed, not only due to the heating of the solution, but to the levelling of the rough surface.

6.4   Voltage optimization

Applied voltage is a significant parameter to consider in the PEP treatments that determine the quality of the polishing. It is reported that every metal has a minimal value of the applied voltage under which it is possible to obtain decent quality of the polished area. For instance, some alloys of steel it is possible to decrease the working voltage down to 230 V without drawbacks, in case of Aluminium this threshold are relatively higher in the range of 270-290 V [255].

Not only energetical, but as well technological consideration of 350 V application has to be taken in mind, since the process may be interrupted within the electro-hydro-dynamic mode and thus the polishing is no longer possible [255].

6.4.1   Niobium PEP

A systematic analysis of various parameters including the applied voltage was done. A set of 5 Nb samples was chosen of 1x2,2x0,4 cm. To remove upper layer of oxidation and possible contaminations, samples were subjected to the ultrasound cleaning and BCP treatment of 1 minute all together (erosion rate does not exceed 1 μm). A selected range of voltage were applied: 260, 280, 300, 320, 340 V for a fixed time of 5 min. A reference sample was used to compare the effective difference after single treatments. A surface optical inspection with microscope is reported on the **Figure 6.11**.
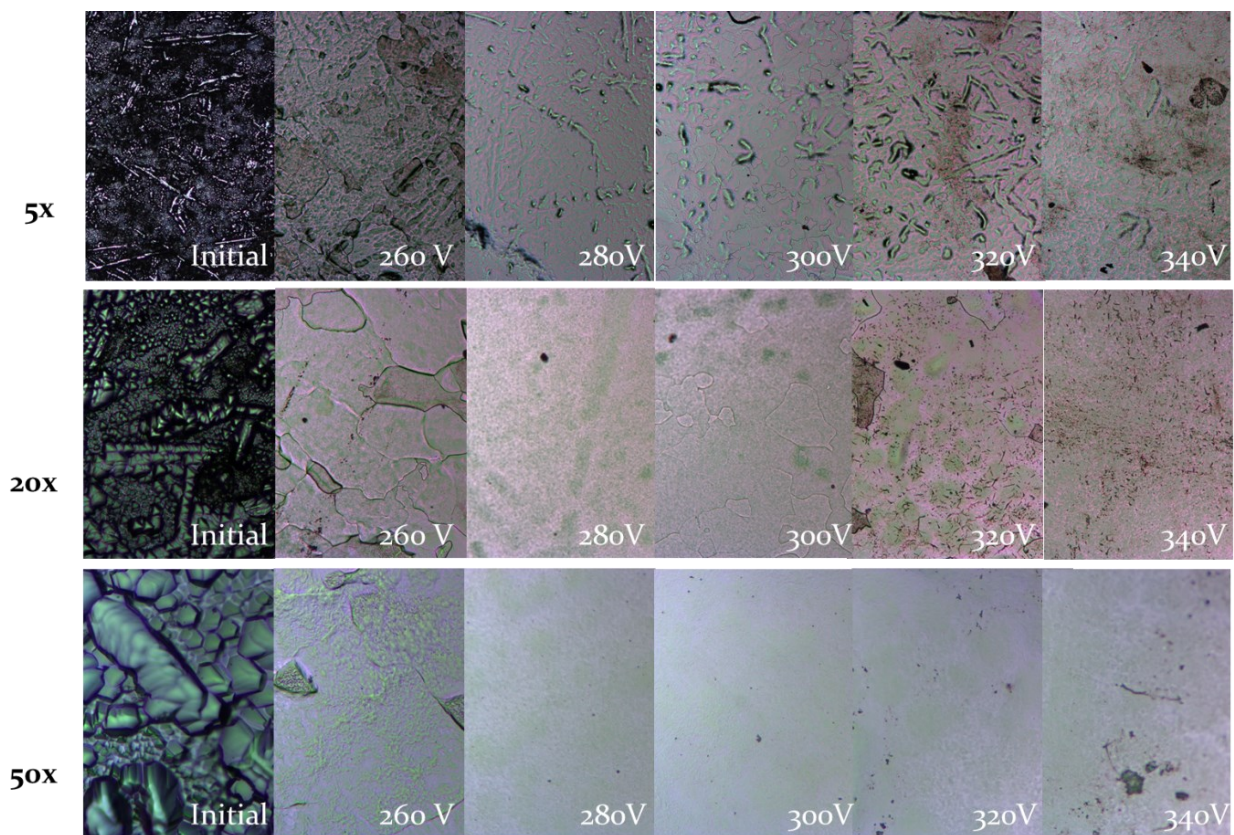
Figure 6.11: Optical microscopy inspections of the samples after the PEP in $NH_4F:NaF$ = 3:0.5 % at 86 ± 1 C° average temperature.

A quick observation of such morphologies and a simple overview of the samples indicates that lowest and highest tested applied voltages show the presence of some irregularities, like pitting, stains. In some cases, it is noticeable non-uniform grain etching (as in case of 260 V). Instead, middle values of voltages show relatively smooth surfaces resulting in lower roughness variation (see Table 6.9).

Table 6.9 – Unified data characterisation of Nb samples polished with various voltages

Sample	1	2	3	4	5
Voltage, V	260	280	300	320	340
Average erosion rate, μm/min	4	2,8	2,8	1,6	1,2
Current Efficiency, %	61	28	33,8	19	16
Δ reflectance Initial 47,83 %	4,80% ⇩	9,20% ⇧	10,10% ⇧	7,90% ⤴	4,40% ⇩
8º Gloss, GU Initial 200	985	1107	1222	1124	1000
Roughness Ra, nm Initial 1600 ± 290	4000 ± 500	950 ± 25	720 ± 40	990 ± 270	1000 ± 260

The above-mentioned data show a significant deviation of the process in the case of 260 both from visual and quantitative character; higher roughness indicates non optimal surface modification, most likely unbalanced reaction of dissolution of oxide and oxide production. However, in this case with the highest erosion rate and the highest current efficiency respectively. The other tested voltages resulted in an improvement on every other characterisation done: reflectance (see chapter 4.1.6), gloss comparing to the initial values. A 5-minute treatment normally cannot achieve low roughness values starting from the roughness of 1,6 μm.

During the PEP treatments time, current parameters were logged for the experiment of 260, 300, 320, 340 V (see **Figure 6.12**); the 280 V treatment has not been logged due to the operational problems. The summary of the obtained data is presented in the table 6.7.
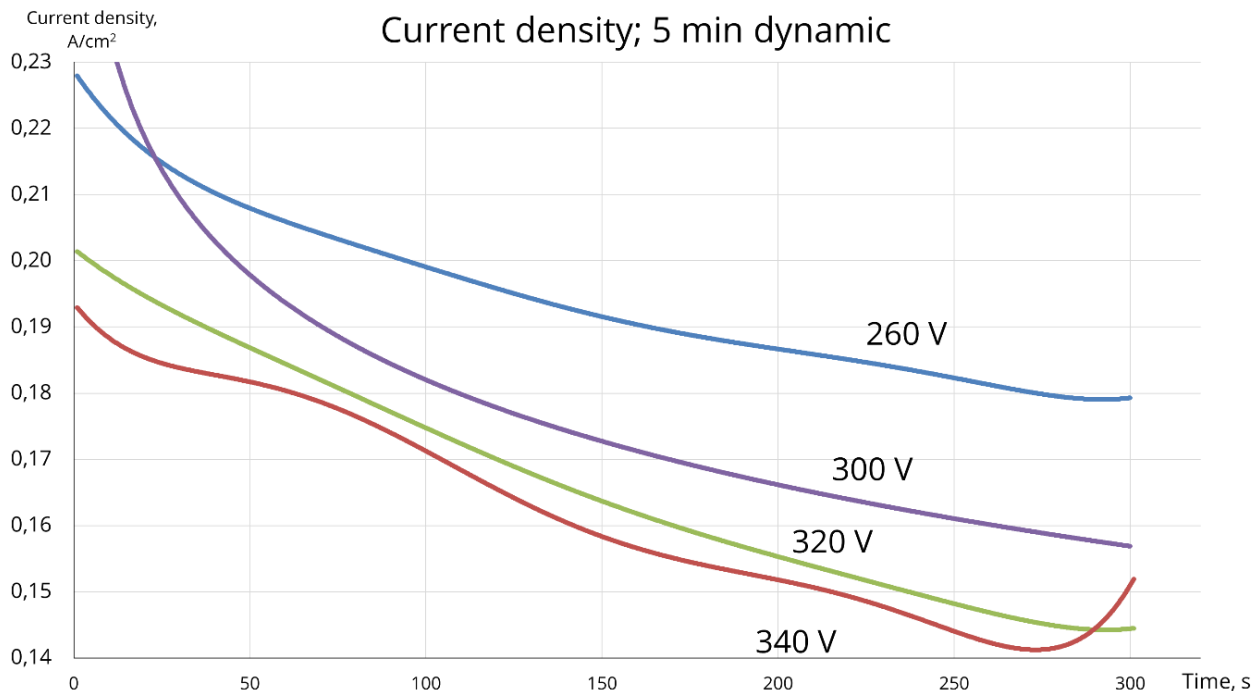
Figure 6.12: Current density vs Time at 260, 300, 320, 340 V for Nb PEP

The graph curves are well agreed with the variation of the erosion rate presented above. In practice, the first second of the treatment generally produces various peak currents of up to the 10x to the working current densities, that is why the initial part might be distorted slightly. The same principle is as well valid for the moment of switching off the power supply. The dynamic of the process is determined by the temperature, as discussed earlier in chapter 6.3. In the closed environment, where relatively high current was passing it was not a trivial task for fixing the working temperature, that is why in this case it was used the initial temperature (80 C°) as a starting value, and an average temperature (86 C° ± 1 C°) as a validation value for the experimental analysis.

Based on systematic analysis below and on the empiric data obtained, a 300 V was chosen as a primary working voltage. For a larger margin a wider range, from 280 to 320 relatively safe, can be used as well.

6.4.2 Copper PEP

Three copper solutions have shown quite similar range of voltages between each other, previously reported in table 6.4.

In case of *SUBU* solutions, the quality of surface normally does not depend much on the applied voltage, but rather on the quantity of material removed and the ratio between anode and cathode surface areas. The erosion rate similarly depends on the applied voltage (see Fig. 6.14).

In the case of other solutions, in particular pyrophosphate (4%, pH 4, + 10 g/L K,Na-Tartrate), diammonium phosphate (4%, pH 4) and disodium-EDTA (3%, + ammonium sulphate 0,5%) a similar trend is observed (see **Figure 6.13**). Unlike SUBU solutions, the visual quality of the samples may vary in terms of reflectivity and uniformity.
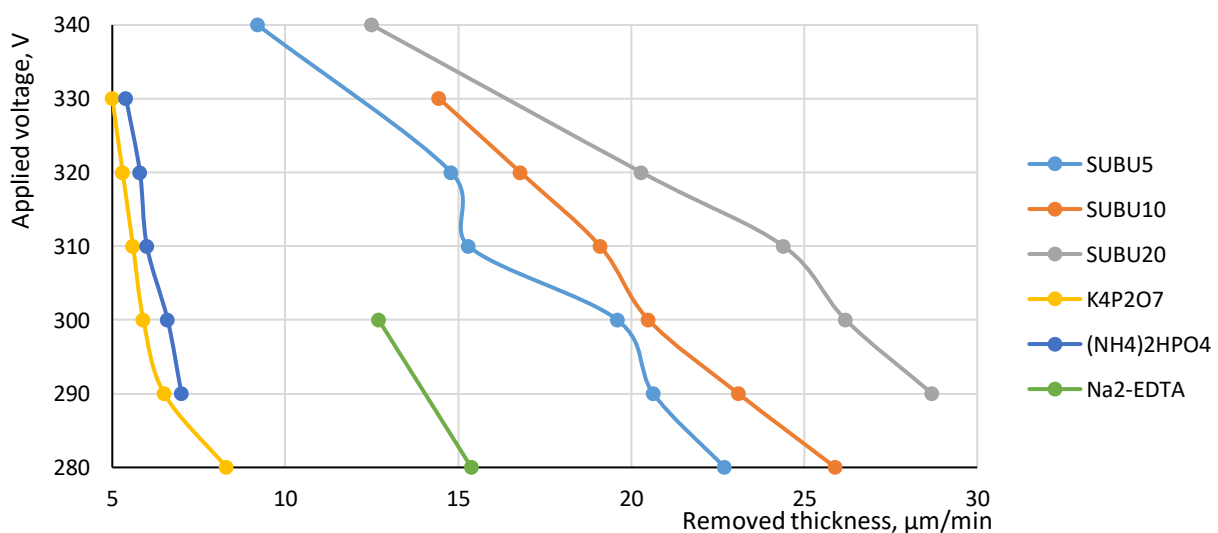
Figure 6.13: Applied voltage vs average removed thickness curves for Cu PEP solutions, with an average temperature of 85 C°

6.5 Current efficiency

The current efficiency is a qualitative value that normally determines the efficiency of the current that passed the electrolytic cell and effectively do the desired task. In many cases (both electrodeposition and electropolishing) are related to the undesired reactions (e.g., oxygen evolution, hydrogen reduction, secondary ions reduction/oxidation etc.). The calculation formula was presented earlier in the chapter 4.3.2.

It appeared that in case of Nb PEP the values are in the range of 15-35% [339]. However, in case of copper, the values of CE are significantly higher reaching 80-99%, that might indicate that electrolysis mechanism is taking place.

Interestingly, the CE for the SUBU solutions are beyond the 100%, that can be explained either by the influence of SUBU chemical polishing as a media (in fact, at 72 °C, it removes around 1-1,2 μm/min excluding the saturation effects) or as a different mechanism.

To exclude and analyse the chemical polishing effect of the bath, a simultaneous polishing of two copper identical samples was done. One connected as anode (in the PEP mode) and another simply placed at the same height and not connected to the power supply. This additionally eliminates the problem of heating, since during PEP the solution might reach 90 C°, and SUBU solution most likely etches more the surface, due to the chemical nature of the polishing. The starting temperature was 71,5 C°, and a final temperature reached 95,1 C°. Two samples were immersed at an equal quantity of time, that included 2 minutes of PEP polishing and few seconds for mounting and dismounting operations. Resulting removed thickness for the chemical polishing was 0,06 g (3,4 μm) and for the PEP 0,50 g (28,0 μm). From the formula (4.3) appeared Δm=KIτ = 0,462 g (25,84 μm) and CE = 108%. A summary of the experiment is presented below in Table 6.10:

Table 6.10 – Summary of the Cu PEP in "SUBU5" solution CE experiment

Sample	Temperature	Solution	Time	Erosion rate	Voltage	CE
"PEP in SUBU5"	71,5 – 95,1 C°	Same SUBU5 solution	2 minutes, in the same bath	1,7 μm/min	300 V	108 %
"SUBU5"				14,0 μm/min	n/a	-

According to the obtained results, it seems that the SUBU chemical etching is simply adding a value to the final removed thickness. However, other experiments, in particular with different surface area have shown CE even up to the 150%, where the SUBU solution was not contributing that much to cover the rest "50%" of the efficiency value.

Comparing a graph bath temperature vs current density for phosphor-based solutions and SUBU5 solution few conclusions might be extracted as well (see **Figure 6.14**). A summary of the confronting experiments is presented below in Table 6.11:

Table 6.11 – Summary of the PEP CE

Temperature	Solution	Time	Erosion rate	Voltage	CE	Surface area	Current density at 81 C°
71 – 95 C°	"SUBU5"		14 µm/min		108 %		0,67 A/cm²
69 – 84 C°	"Pirophosphate"	2 min	5 µm/min	300 V	92 %	20 cm²	0,25 A/cm²
70 – 89 C°	"Phosphate"		6 µm/min		80 %		0,27 A/cm²
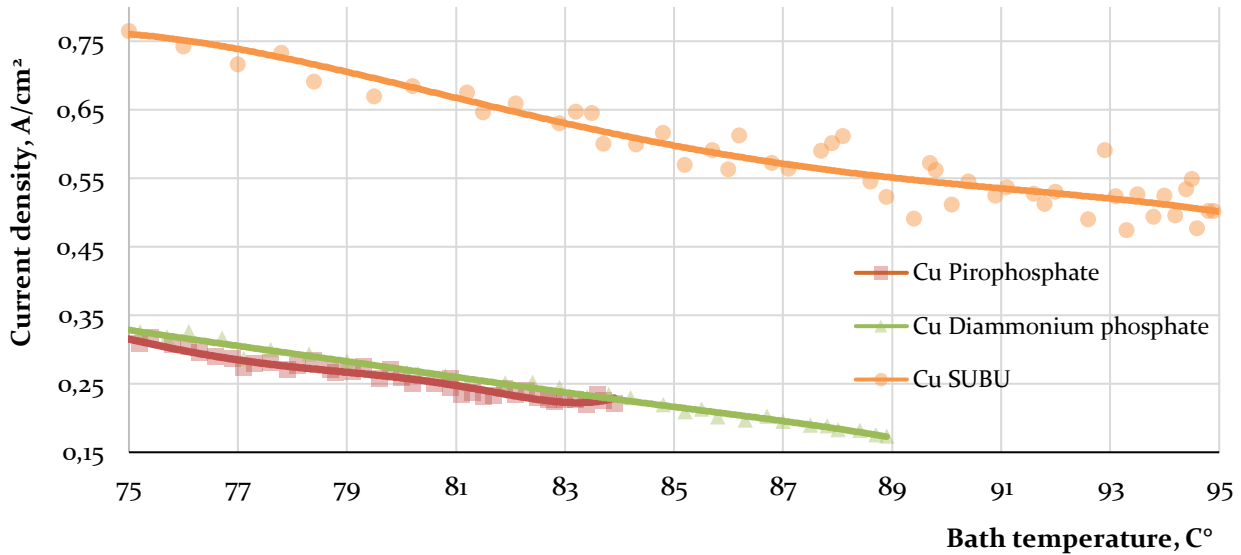
Figure 6.14: Current density vs Bath temperature curves for 3 developed solutions, recorded in one single experiment for each of the solution, samples area 20 cm², time – 2 min

Notably higher current densities for the SUBU solution might be explained by the higher conductivity of the solution or the overall lower resistance in the PEP circuit (at the interface between the vapour-gas-layer, solution and metal). The average difference in current density between phosphate based (that are almost identical from the graph), and SUBU solutions are roughly $\Delta i = 0{,}42$ A/cm². Assuming that the mechanism of PEP is completely electrolytical, we might expect the difference in weight loss (after 2 min) about: $\Delta m = KI\tau A = 0{,}33$ g ($\delta = 18{,}4$ µm). Adding the erosion rates of a phosphate solution (4,4 µm/min, considering CE), erosion rate of a sample immersed in the SUBU solution (1,7 µm/min) and the theoretical erosion rate of the current density difference between the "SUBU5" and "phosphate" solutions (9,2 µm/min) we obtain a 15,3 µm/min rate, that is comparable with the rates of PEP in "SUBU5" solution. Thus, the electrical conductance of the SUBU or different mechanism enhance the erosion rate comparing to the other solutions.

The removing rate is directly proportional to the current density, that is not a non-sense. However, we can assume that the SUBU solution is a beneficial media for the PEP, not only due to the exceptional surface quality, but to the higher erosion rate as well. And the superiority (in terms of erosion rate) can be calculated as follows:

$$SE = \frac{RR_{PEP(subu)} - (RR_P + RR_{subu})}{RR_{PEP(subu)}} = \frac{14 - (5,5 + 1,7)}{14} * 100 = 48,6\ \% \tag{6.1}$$

It was then noticed that different cathode/anode surface area ratio does not influence on the CE (see Table 6.12), for example two experiments (n° 2,5,9) show very similar values for current efficiencies. As it was described in chapter 6.3, higher temperatures lead to the lower erosion rates, in the series: n° 1,2,3 and n° 6,7,8,9 and noticeably, higher CE efficiencies. Another conclusion was made regarding the erosion rates, that with the increase of the cathode/anode ratio it rises as well. A n° 10 experiment on the planar part of the Cu/Nb QPR part, has shown around 14 µm/min removing rate, meanwhile a gradual decrease of surface area of the treated sample yields to the higher rates up to 29 µm/min, that is about a double value.

Table 6.12 – Current efficiency and cathode/anode surface area ratio data across experiments

N°	A_{anode}, cm^2	Cathode/anode ratio	CE, %	Erosion Rate, µm/min	Bath Temperature C°	Solution
1	8,0	87,5:1	117	28,7	84,4-94,5	
2	8,0	87,5:1	108	27,2	72,7-93,4	
3	8,5	82:1	100	22,4	74,5-92,6	
4	9,0	78:1	n/d	26	n/d	
5	14,5	48:1	109	19,67	72,5-94,6	"SUBU5"
6	19,5	36:1	133	17,5	75,3-95,6	
7	20,0	35:1	147	15,7	85,0-96,0	
8	20,0	35:1	135	15,1	77,0-94,0	
9	20,0	35:1	108	14,3	71,5-95,0	
10*	80,0	n/d	n/d	7	n/d	

Regarding the impact of the chemical solution "SUBU" on the erosion rates, it has shown that normally at 95 C° less than 2 µm/min are removed. In fact, the treatments when the two samples were simultaneously polished (one with the chemical solution bath and another by PEP) showed even lower values of erosion rate after 2 minutes of treatment: 1,3 – 1,9 µm/min, that is about 8% contribution to the CE % corresponding to the effective anode area. This results in the unknown source of contribution to the erosion rates of the PEP process in the SUBU for the experiments with the calculated CE > 110 %. In such treatments, the effect of the SUBU solution as a media for the PEP processing can be considered as synergetic, since not only the qualitatively and quantitatively is generally higher than any other developed solutions for Cu PEP, but also the resulting erosion rate is higher than simply partial erosion rates in "SUBU" solutions and separately "SUBU" etching. This effect became noticeable after a certain average temperature range.

6.6 Conventional treatments and PEP comparison

As it was intentionally discussed and observed in chapter 2.4, two different standard paths for the chemical and electrochemical polishing preparation of SRF substrate are in use. To highlight the performance of the PEP and compare it to its primal competitors this study was conducted and

showed below. The sub-chapter is divided by metal treatments to avoid confusion among the surface preparation techniques.

6.6.1   Nb treatments comparison study

For the experimental study, BCP and EP polishings were chosen to compare the newly developed solution for the PEP processing. An overview of compared treatments is showed below in the Table 6.13.

Table 6.13 – Process parameters comparison for Nb polishing techniques

Process / parameters	BCP (1:1:2)	EP (1:9)	PEP (3:0,5 %)
Solution composition	$HF:HNO_3:H_3PO_4$	$HF:H_2SO_4$	NH_4F NaF
Voltage	-	18 V	300 V
Current density	-	0.025 A/cm^2	0.3-0.5 A/cm^2
Power density	-	0.45 W/cm^2	~120 W/cm^2
Removing rate	1 μm/min (15°C)	0.3 μm/min (30°C)	~4 μm/min (78°C)

As demonstrated above, PEP processing can reach erosion rates up to 4x times faster than regular BCP and more than 10x times higher than a conventional electropolishing solution of Nb. It produces as well 270x times more heat. However, it is not a drawback, since higher temperatures normally produce smoother morphologies, and higher bath temperatures limit the current density, thus the heating auto balances the heat-exchange of the closed system. On the other hand, a huge quantity of vapor is produced, and it must be addressed correspondingly. A higher working current density practically is 10 times higher, yielding in a similar gain for the erosion rate. A simple calculation of the time necessary to remove a 150 μm (standard value in SRF protocols) demonstrates that a BCP needs at least 2,5 h, EP ~ 8h and PEP – 40 minutes.

Low thickness removing conditions

A general comparison of the treatment influence on the polishing of the same area (9cm^2) and pre-treatment conditions are shown below (see **Figure 6.15**). During the pre-analysis it was measured the roughness of sample by linear profilometer, at the distance of 1mm, in random spots, at least 6 measurements for a sample.

As demonstrated, there is a significant improvement in the surface area in case of PEP treated sample comparing to the initial state. At the parity of the removal material, a smoother surface in case of PEP processing is observed, also visible and confirmed by visual inspection (reflectivity of the object placed nearby the polished samples). Naturally, such low quantity of material removal is not yet enough to obtain a mirror-like surface. The surface morphology analysis confirms previous results (see

154

Figure 6.16), still showing the presence of macro-defected surface and preferential etching of the grains for BCP treated sample, smoothening with remaining texturing, and small surface defects for EP treated sample and almost perfectly smoothed surface in case of PEP treated sample.
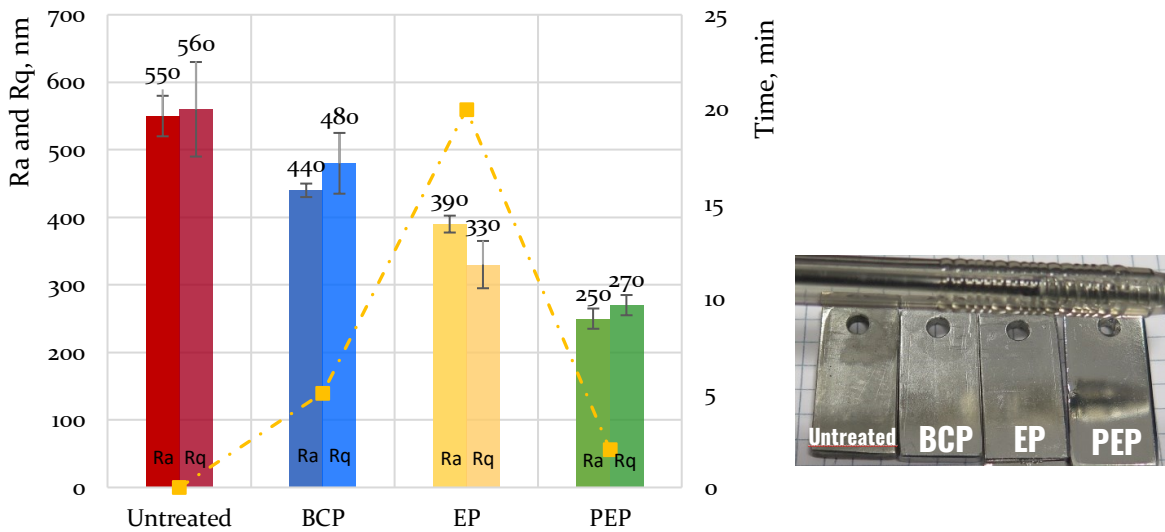
Figure 6.15: Roughness and treatment time (for a removal of 6,5 ± 0,5 μm) comparison for a Nb samples (9 cm^2) polishing
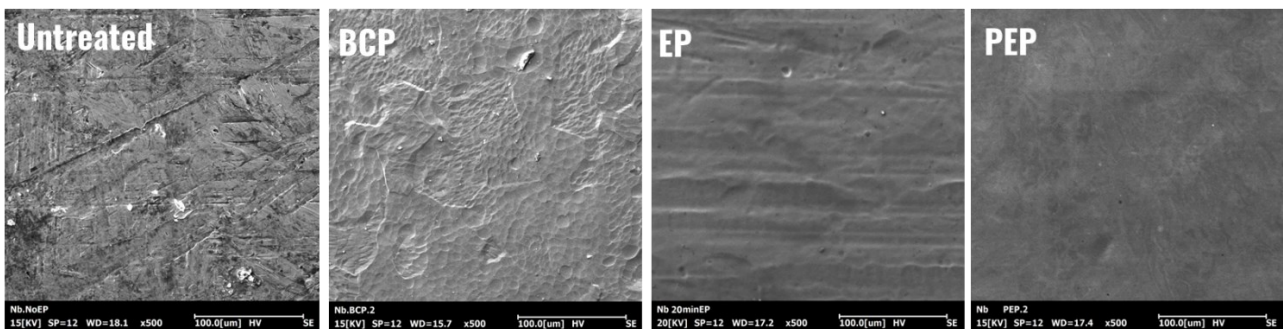
Figure 6.16: Surface morphology of non-treated and treated Nb samples with BCP, EP and PEP methods after a 6,5 ± 0,5 μm thickness removal

High thickness removing conditions

To demonstrate the performance of the longer treatments and its effect on the surface characteristics, it was conducted an experiment aimed to remove ~ 150 μm on the same Nb 9 cm^2 samples, see **Figure 6.17**.

Like the short thickness polishing test, PEP shows superior both roughness and reflectivity. Noticeably the EP presents some macro "waviness" near the wire connection, indicating the non-uniform removal due to the mass-exchange process happening during the EP. Relatively fast removing rate for EP was due to the temperature of the bath, that exceeded the 15 C°. In the case of PEP treatment, two rounds of treatment of 40 minutes in total were done, with the average of 80 C° bath

temperature and 300 Volts applied voltage. The surface morphology (see **Figure 6.18**) shows smoothening by both techniques, confirming the roughness measurements and visual observations. The EP treated sample can be characterized and relatively free of defects, with a visible grain (about 50-100 μm) indicating that etching took part during the process with slightly different rates depending on the orientation of the grain. The PEP treated sample shows some grainy structure as well (less visible due to the contrast/brightness difference), with a defect-free surface.
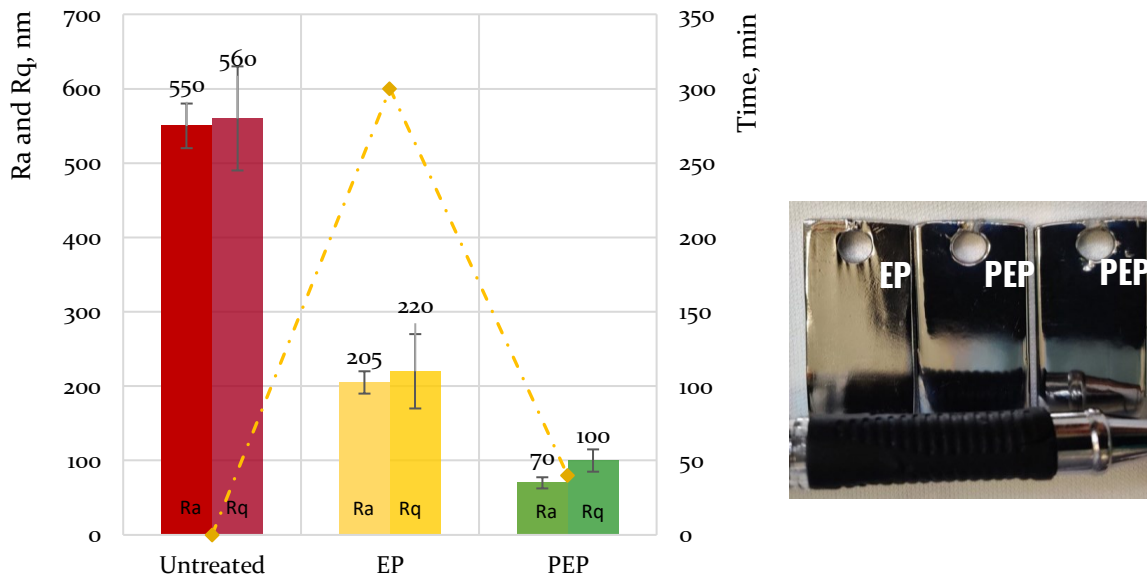
Figure 6.17: Roughness and treatment time (for a removal of 150 μm) comparison for a Nb samples (9 cm^2) polishing
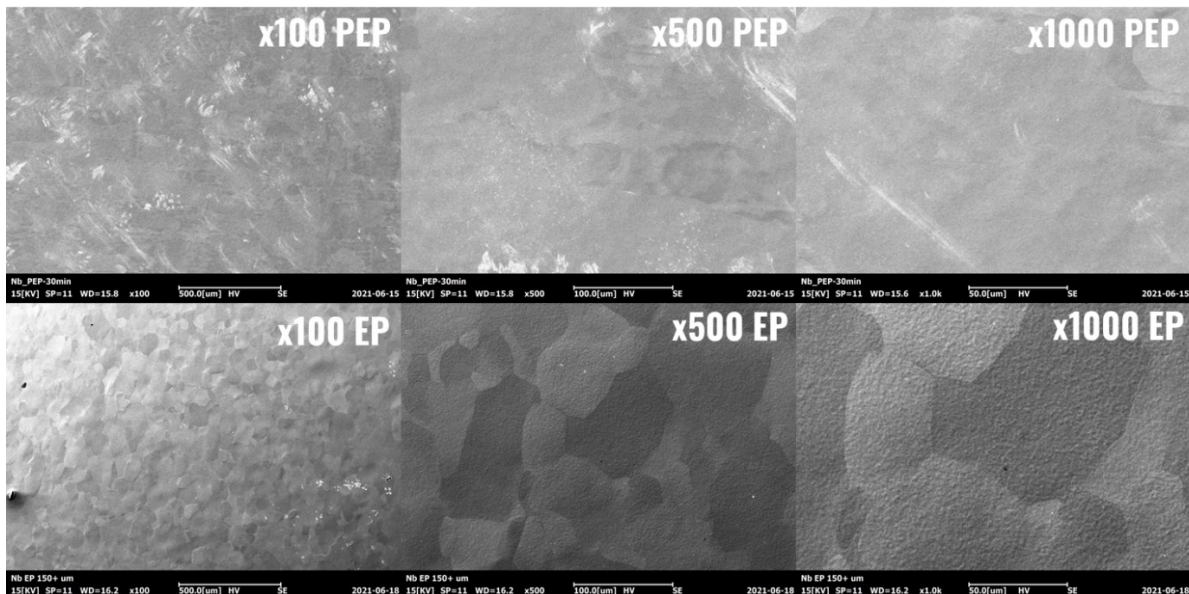
Figure 6.18: Surface morphology of Nb treated samples (9 cm^2) by EP and PEP at different magnifications after a 150 μm thickness removal

156

A similar comparison test was conducted later to analyse the surface with different techniques and with recently optimised treatment parameters. This time BCP solution was maintained at 25-30 C° temperature, 4 different bath of 250 mL were prepared, to ensure the proper working of the chemical polishing. The EP was maintained at lower temperatures of 10-20 C° (with a help of colling bath) as well, to decrease the heating, a 12 V polishing mode was used. A PEP has been applied with the one single run for 30 minutes in total, at the average temperature of 84 C°, that was cooled with nitrogen gas spraying. Newly prepared Nb samples from 300 RRR quality sheet, with the dimensions 1x2x0,3 cm was all initially etched for 5-10 seconds in the BCP solution, for a fast deoxidation and cleaning from superficial residuals.

The surface morphology has demonstrated similar conclusions already discussed below. On the macro-level (small magnification) the EP was not able to smooth the valleys and peaks, resulting in residual texturing from the initial state. Instead, the BCP treated sample presents some black pitting and non-uniform etching of the grains. Meanwhile the PEP treated surface shows excellent smooth surface with uniform etching of the different grain orientation. However, the PEP sample did present some point-like defects of unknown nature. For a better statistic data acquisition of the surface roughness, a mapping was conducted on the samples with a surface area 1 mm^2 (see **Figure 6.19**).
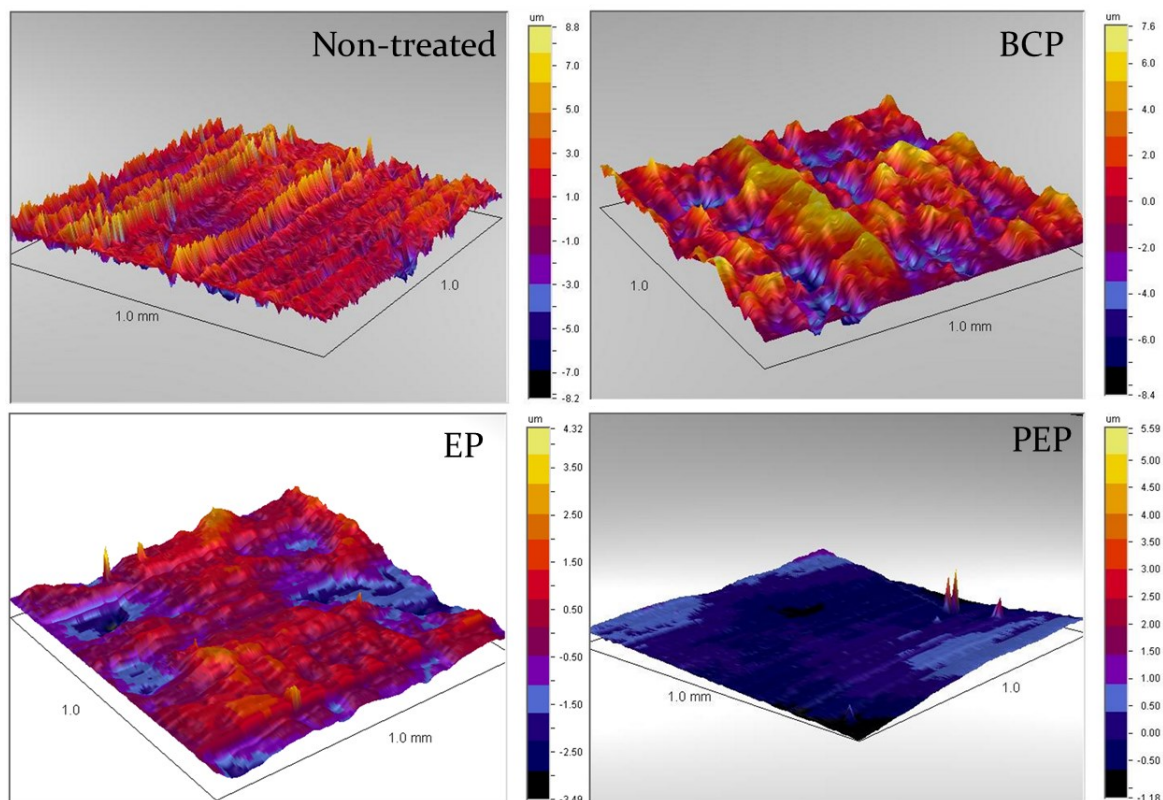
Figure 6.19: Mapping of the Nb samples non-treated and treated with BCP, EP and PEP after 100 µm removal, sampling 222 nm, array size: 4500x316

Naturally, the surface roughness measured by linear profilometer (even in the mapping mode) is relevant only for a comparison since it cannot be directly comparable with other techniques.

However, both visual inspection and roughness data (see **Figure 6.20**) are well-aligned and again prove the superior qualitative data of the surface polishing at the parity of removal thickness.
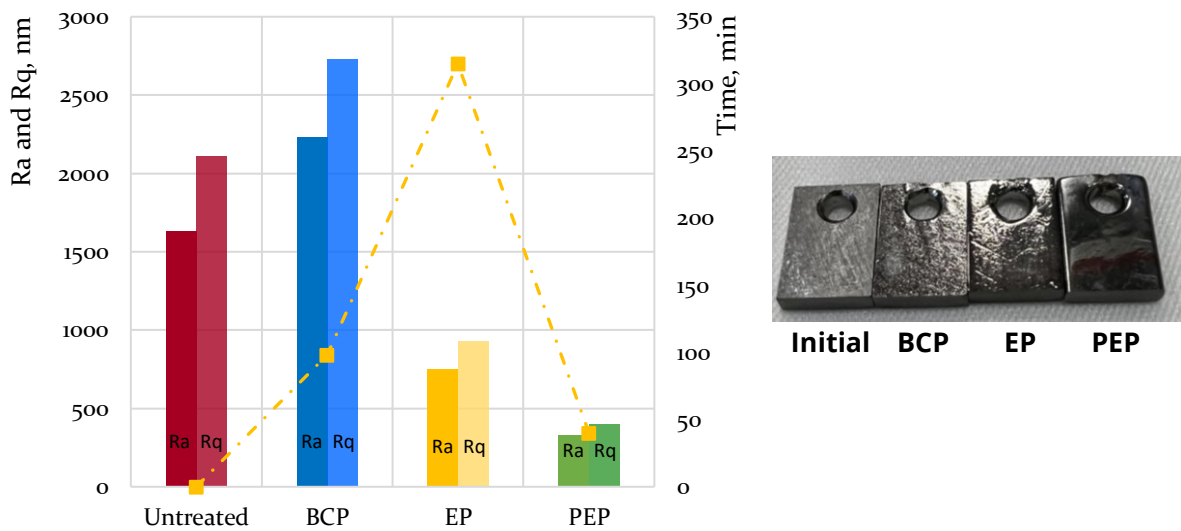
Figure 6.20: Roughness and treatment time data (for a removal of 100 μm) for the Nb treatments comparison

6.6.2 Cu treatment comparison study

For the Cu treatments comparison study, mainly SUBU and EP with the PEP techniques were selected. A brief comparison of the characteristics is shown in the Table 6.14 below.

Table 6.14 - Process parameters comparison for Cu polishing techniques

Process / parameters	"SUBU5"	EP (3:2)	PEP in "SUBU5"
Solution composition	Sulfamic acid 5 g/l; NH_4-citrate 1 g/l Butanol 50 ml/l; H_2O_2 50 ml/l	85 % H_3PO_4 60 p. 99% n-Butanol 40p.	Sulfamic acid 5 g/l; NH_4-citrate 1 g/l Butanol 50 ml/l; H_2O_2 50 ml/l
Voltage	-	2-6 V	300 V
Current density	-	0,01 – 0,03 A/cm²	0,35-1,2 A/cm²
Power draw	-	0,06 – 0,18 W/cm²	100 – 360 W/cm²
Removing rate	1,5 μm/min (70±2°C)	0,15-0,5 μm/min (25°C)	20 μm/min (80°C)

As presented above, the erosion rate is more than 10 times higher than a regular chemical polishing "SUBU" and from 20 to 100 times higher than a regular electropolishing. A significant difference between the electropolishing and PEP solutions are the conductivity, taking into account the applied voltage results in much higher power draw and higher current densities.

Low thickness removing conditions

For the experiment a series of Cu samples with surface area of 9 cm^2 was chosen. The experimental plan consisted in the removal of $8 \pm 0,5$ µm. The resulting roughness was measured and compared after different time of treatment. For the chemical polishing SUBU5 solution was chosen , for EP phosphoric acid and butanol mixture was chosen. In case of PEP processing only "SUBU5" was tested. Roughness measurements and process time for treatment is presented below on the **Figure 6.21**.
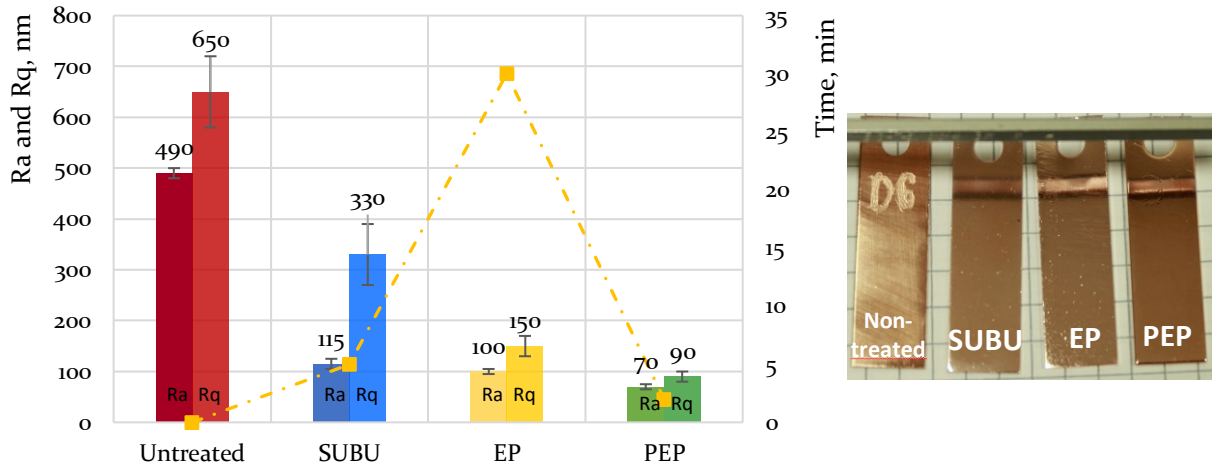
Figure 6.21: Roughness and treatment time charts (for a removal of $8 \pm 0,5$ µm) comparison for Cu samples (9 cm^2) polishing with different techniques

All the treatments in the comparison experiment were able to significantly polish the surface, resulting in ~ 100 nm roughness. However, with naked eyes it is visible the difference, where the EP and SUBU treated surfaces result with pitting defect. The reflectivity as well shows the superior values on the whole range of measurement (see **Figure 6.22**) and noticeable with visual inspection analysis.
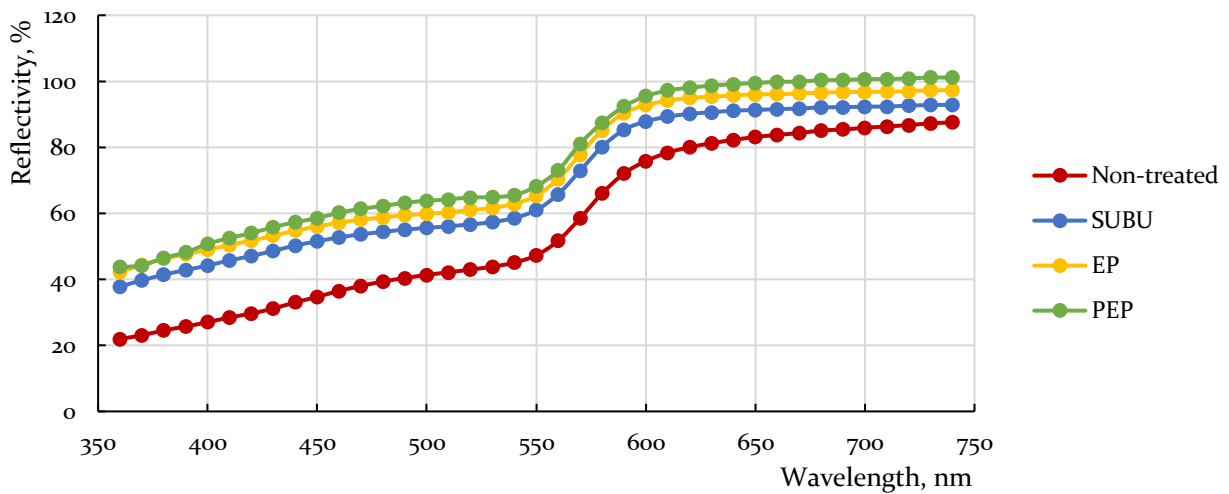
Figure 6.22: Reflectivity chart at the range of 360 – 740 nm wavelength for non-treated and 3 samples treated with "SUBU", EP and PEP techniques.

The surface morphology study confirms quite similar roughness values for treated samples (see **Figure 6.23**). Surface is smooth all cases, with a significant difference, that "SUBU" treated sample present some point defects. The grains with the boundaries are highlighted as well, meaning different speed of etching for the various grain orientation. The EP treated sample instead presents very smooth slightly highlighted grains, with some point-shape defects. A similar or better surface smoothing is demonstrated as well by PEP.
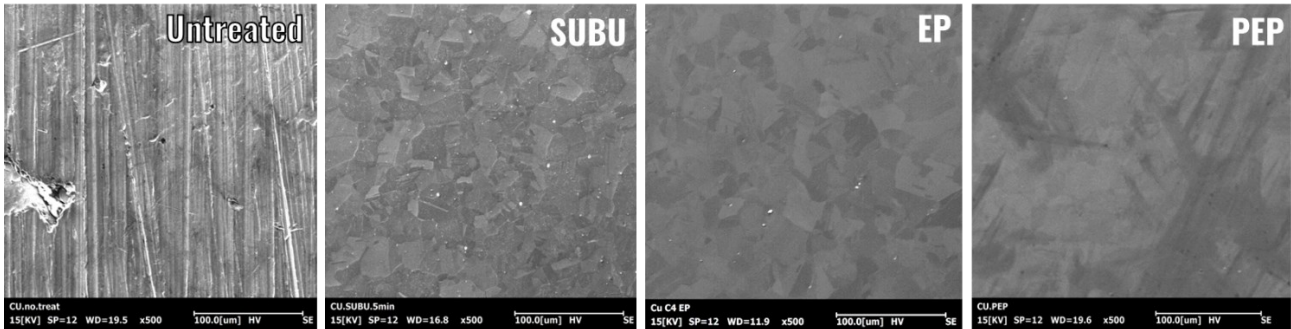
Figure 6.23: Surface morphology acquisition by SEM at 500x magnification for non-treated and treated by "SUBU", EP and PEP Cu samples

High thickness removing conditions

To verify how the longer treatments influenced the roughness and morphology (see **Figure 6.24**), a similar test was carried out. The "SUBU" treatment was not studied since it is normally used for a short period of time due to its limitation. Unfortunately, the removing rates for the EP and PEP treatments did not match (150 vs 200 μm respectively), however such values can still be considered comparable.
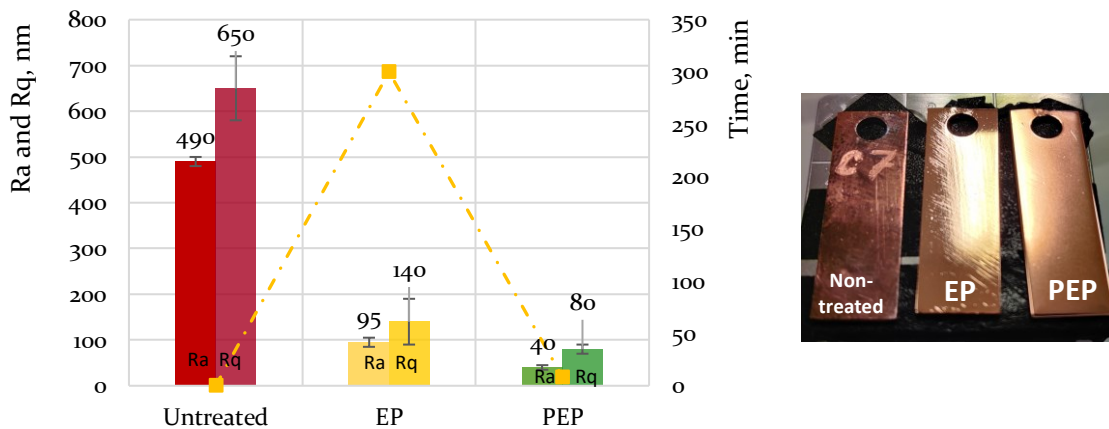
Figure 6.24: Roughness and treatment time charts after EP and PEP (for a removal of 150 and 200 μm respectively) comparison for Cu samples (9 cm^2)

Surface morphology (see **Figure 6.25**) revealed a smooth and very similar surface for both samples with a distinct grain. the different grain etching is evident as well. This time the Cu surface presents a small portion of pitting in some spots, most likely due to the saturation of the solution or

due to the presence of oxygen bubbles, that are usually responsible for such defects. The origin of such bubbles can be both the electrolytic production on the anode, or they are simply present in the solution (SUBU5).
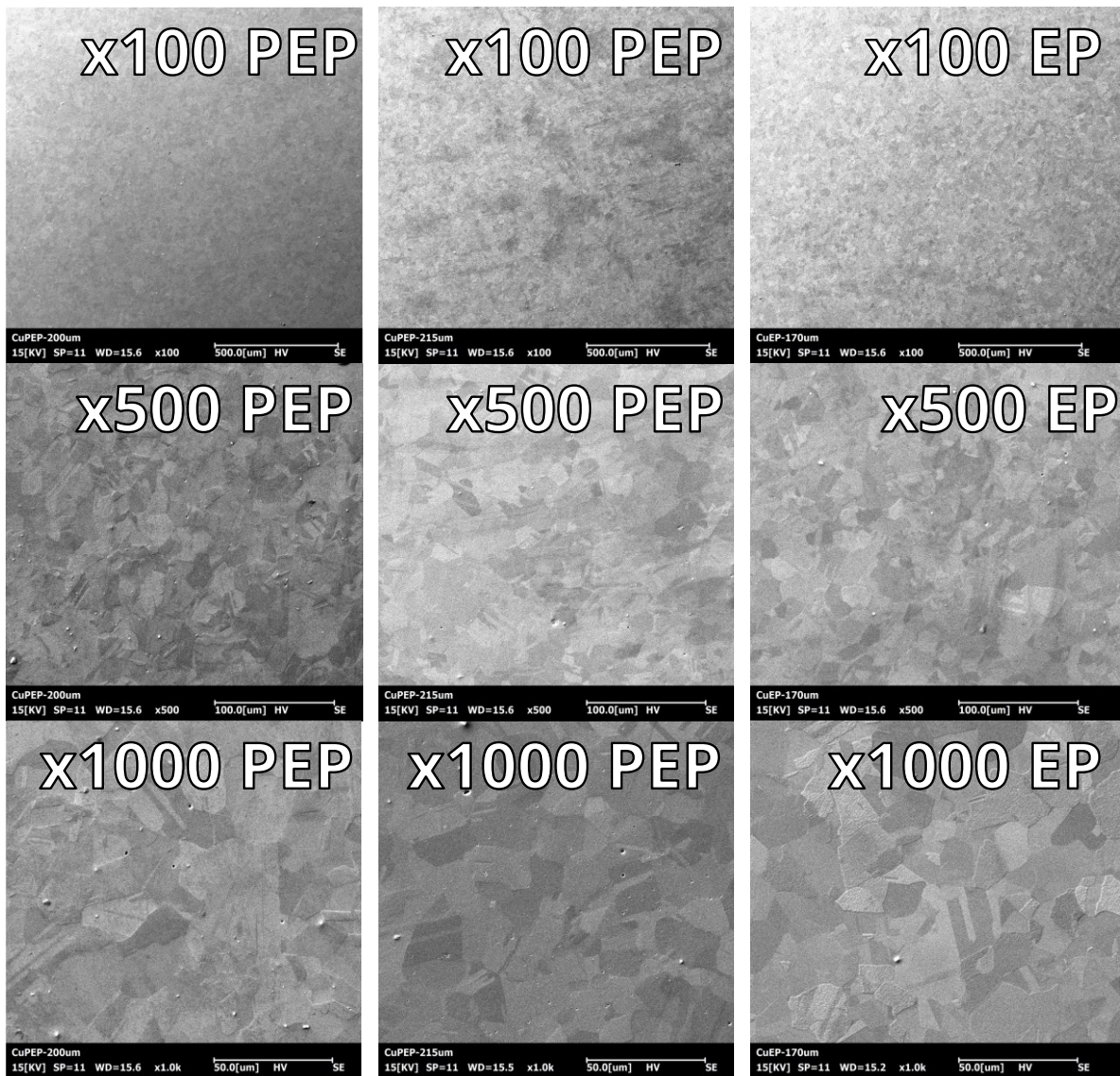
Figure 6.25: Surface morphology of PEP (200 and 215 μm) and EP treated samples (170 μm) obtained with 100, 500 and 1000x magnification

6.7 Scalability to large areas and complex 3D structures

The scalability of the PEP process from the small samples to the large areas of elliptical cavities is definitely a challenge. The discussed list of advantages of PEP has its price – the enormous power demand if we speak about elliptical cavities and production of vapor-gas mixtures.

Assuming the internal surface area of a single-cell 1.3 GHz cavity to be around 1000 cm^2, and parameters of the Nb and Cu processing (see chapter 6.6) a summary of the potential power values can be shown as follows in Table 6.15:

161

Table 6.15 – Estimation of the power supply usage during PEP of 1.3 GHz

Process	Current density, A/cm^2	Voltage, V	Vertical system Current$_{needed}$, A Power$_{needed}$, kW	Horizontal system Current$_{needed}$, A; Power$_{needed}$, kW
Nb PEP	0,2	300	200 A, 60kW	100 A, 30kW
Cu PEP	0,4		400 A, 120 kW	200 A, 60 kW

From the rough estimation, a conclusion may be extracted: the horizontal system looks as a promising setup, similarly as in the standard EP technology. However, the quantity of gas produced requires it to be removed from the internal of the cavity. A produced heat, due to the Joule effect is used for the heating of the bath solution, and thus lowering the working current density (see chapter 6.3). More possible solutions on how to address the extreme power consumption during the PEP will be given in the conclusion section.
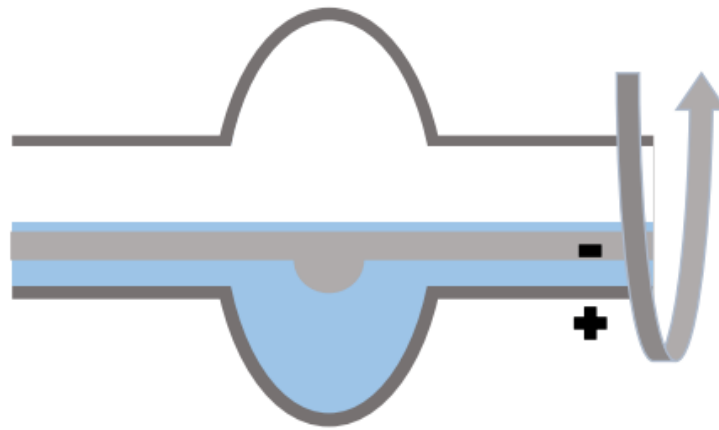
Figure 6.26: Single cell 1.3 GHz in horizontal polishing configuration

In this sub-chapter more experiments conducted are described, those with limited success, or with a certain geometry substrate. The final scope of such experiments is the polishing of the elliptical cavities.

6.7.1   Complex / closed geometry Cu substrates

6.7.1.1   Attempt 1

PEP (similarly as EP) cannot polish long tubes (hollow cylinders) internally with the external cathodes. Additionally, high area objects may require extensive values of current provided by the DC power supply. An isolation test was done, to see whether it is possible to cover and partially isolate the metallic surface from the electrical fields. Among the possible isolations, a relatively simple solution was found in the usage of thick isolating tape, that does not degrade for 5-10 minutes in the PEP conditions. By usage of such isolation technique, a controlled surface can be polished (see **Figure 6.27**).

A summary of the two sample PEP treatment experiment is presented below Table 6.16:

Table 6.16 – Attempt 1 experiment summary

Temperature	Solution	Time	Erosion rate µm/min	Voltage	Effective area, cm²
72 - 94	"SUBU5"	2 min	18,3	300	6,7
82 - 95			16,5		9,5
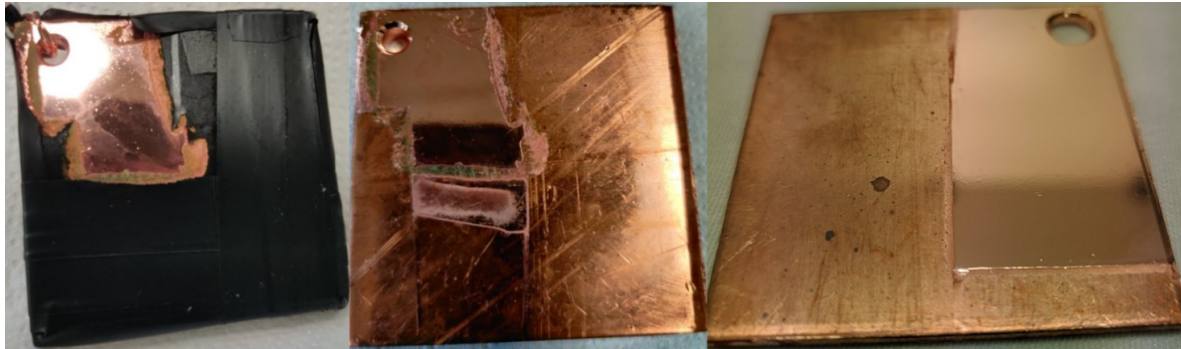
Figure 6.27: Photo example of isolating tape protection of the surface and resulting surface after PEP treatment

6.7.1.2   Attempt 2

The process scaling to the elliptical cavities is not a trivial task, that is why mainly on the similar but simpler geometry – cylinder samples with the diameter equal to the cut-off diameter was checked. A cathode was then placed using the screw and perpendicularly installed isolated planar plate. To eliminate undesired discharges the connection wires were isolated with Teflon tape. To allow formed gasses escape the closed geometry, the cathode is installed on the bottom of the cylinder (see **Figure 6.28**). A summary of the process parameter conducted is presented below Table 6.17:

Table 6.17 – Summary of the attempt 2 experiment process parameters

Temperature, C°	Solution	Time, min	Erosion rate, µm/min	Voltage, V
71 - 95	"SUBU5"	2	n/a	300
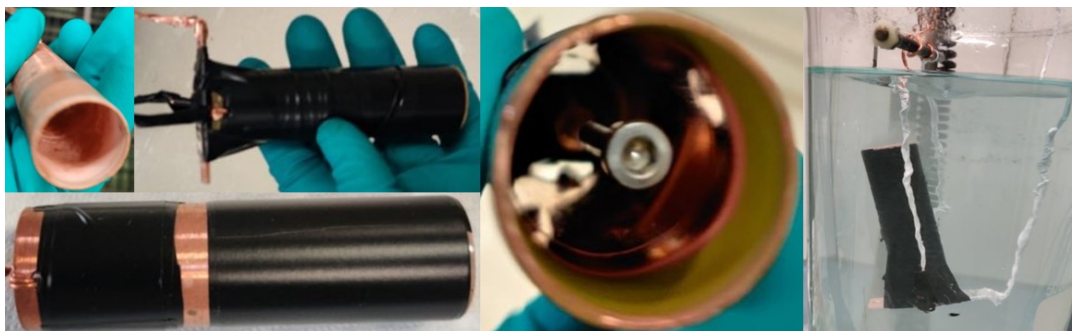
Figure 6.28: Photo of the copper cylinder for a test PEP isolated with tape and Teflon, and installed cathode

The huge drawback of such configuration was the inability to adjust the distance between the cathode and anode, moreover this distance might change according to the inclination. The experiment resulted in the partial polishing (see **Figure 6.29**), in practice where the cathode was installed. However, the process did not last more than 1 minute, due to the huge oscillation of the current and eventually the configuration started to shake a lot, allowing undesired discharges.
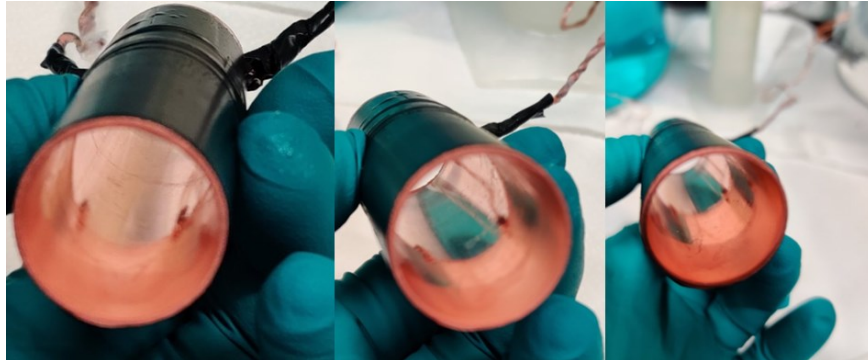
Figure 6.29: Internal surface photo after the PEP treatment

6.7.1.3   Attempt 3

A flange-less 6 GHz cavity was chosen for a test, where the cathode of elliptical shape was placed inside the cavity, with additional thick Teflon isolation to prevent discharges on the close situated cut-off areas (see **Figure 6.30**). An isolated tape was placed in order to reduce the anode area and prevent solution action outside of the cavity. A summary of the experiment is presented below:

Table 6.18 – Attempt 3 experiment summary

Temperature, C°	Solution	Time, min	Erosion rate, µm/min	Voltage, V	Effective area, cm²
72 - 94	"SUBU5"	3	11,2	300	90
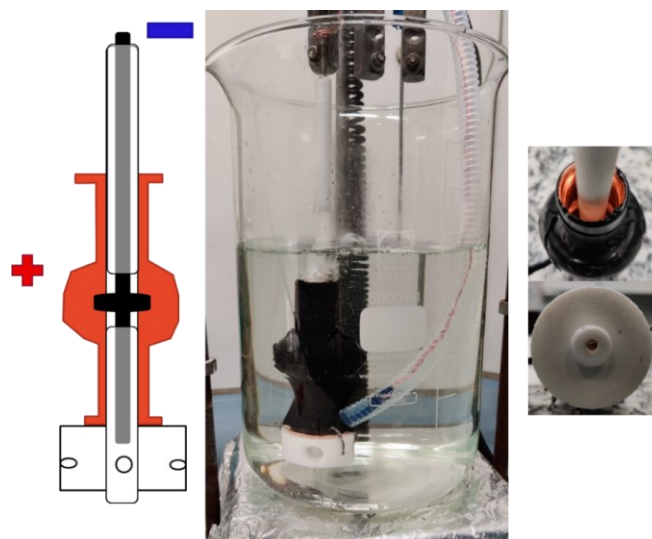
Figure 6.30: Scheme and photo of the installed cavity treatment

It was not possible to apply the intended 300 V voltage in one go, as the current reached its limit at much lower voltages. Therefore, the cavity was gradually immersed in the solution while the voltage was applied. With such a "trick", the plasma regime, or at least the applied 300 V mode was achieved. The quantity of produced gasses and vapours were noticeable, so that the cavity was slightly moving. After a relatively short time the voltage was turned off, and the internal surface was observed (see **Figure 6.31**).
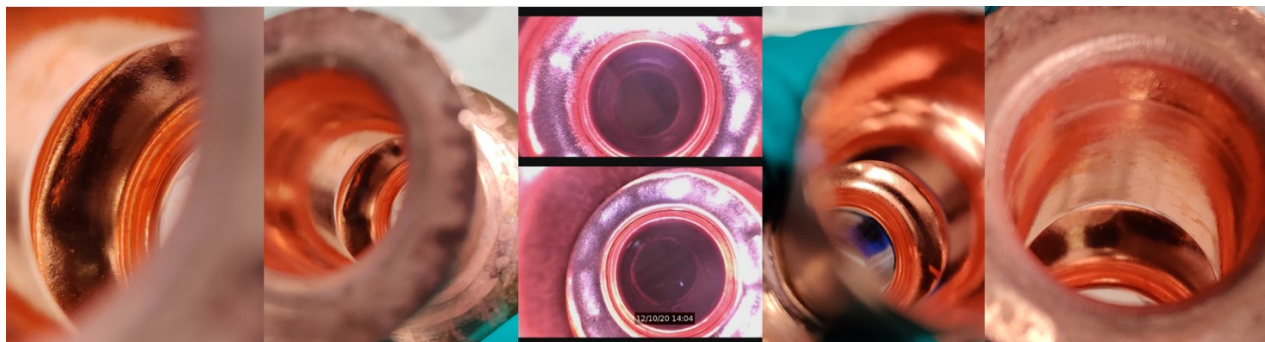
Figure 6.31: Internal surface inspection of the 6 GHz cavity treatment

Summary: Overall, the result may be characterised as successful, however the instability of the process and complexity of the used connection and details must be underlined. Unfortunately, it is difficult to say if the formation of the VGL was present. Another drawback of such experiment is the very limited space for the isolation, cathode and formed bubbles.

6.7.1.4   Attempt 4

A very similar experiment was conducted with some optimization in the distances between the cathode and anode and mounting of the structure. Interestingly the cavity internal surface resulted more matte (quite uniform, but not reflective) (see **Figure 6.32**). A summary of the experiment is collected below Table 6.19:
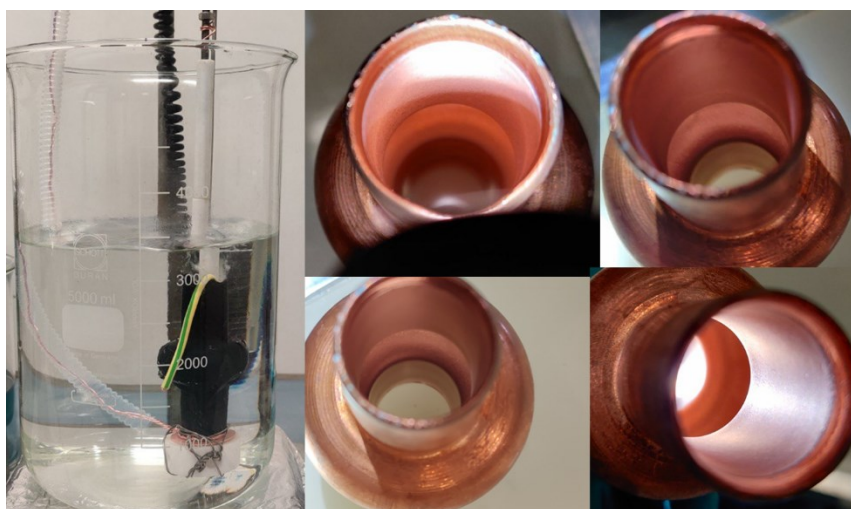
Figure 6.32: Photo of the PEP configuration and the resulting 6 GHz cavity surface

Table 6.19 – Summary of the fourth attempt experiment

Temperature, C°	Solution	Time, min	Erosion rate μm/min	Voltage, V	Effective area, cm²
68 - 86	"SUBU5"	1	4	300	90

Summary: as the formation of the vapour-gas mixture proceeded, the volume of the cavity was filled with gases, resulting in the decrease of the current values, but eventually not polishing. Most likely the solution was not able to refill from the bottom excluding the possibility of the metal – solution interface contact.

6.7.1.5   Attempt 5

In order to verify whether the successful PEP of the elliptical cavity shape is dependent on the cavity diameter, a dummy cell was taken (after the 6 GHz spinning production) with the average external diameter of ~ 7 cm. A double cathode system was done with the external bended stainless-steel sheet and the copper bar inserted inside the cavity (see **Figure 6.33**). The purpose of the double cathode was introduced as the requirement of cathode/anode ratio was reconsidered. The internal cathode enables the process to take place in the cave part of the cavity, and the external cathode is meant for the increasement of the area ratio. A "SUBU5" solution was used at 300 V anodic polarisation. A short process of the 1,5 min was conducted at the temperatures of 71 – 95 C° range. The external part of the cavity was additionally isolated with the thermos-shrinking isolator. A summary of the experiment is presented below Table 6.20:

Table 6.20 – Summary of the fifth experiment

Temperature, C°	Solution	Time, min	Erosion rate, μm/min	Voltage, V	CE, %
70 - 97	"SUBU5"	5	n/a	300	166,7

Figure 6.33: Photo of the double-cathode system, isolation and dummy substrate

The resulting surface (see **Figure 6.34**) presented a very shine, and in some zones mirror-like, polished quality. One of such zones was in the bottom of the sample, where the part of the Cu was not isolated, resulting in the local discharging – polishing. Inside the cavity, the polishing circumferences are visible, even if not-uniform, in some spots.
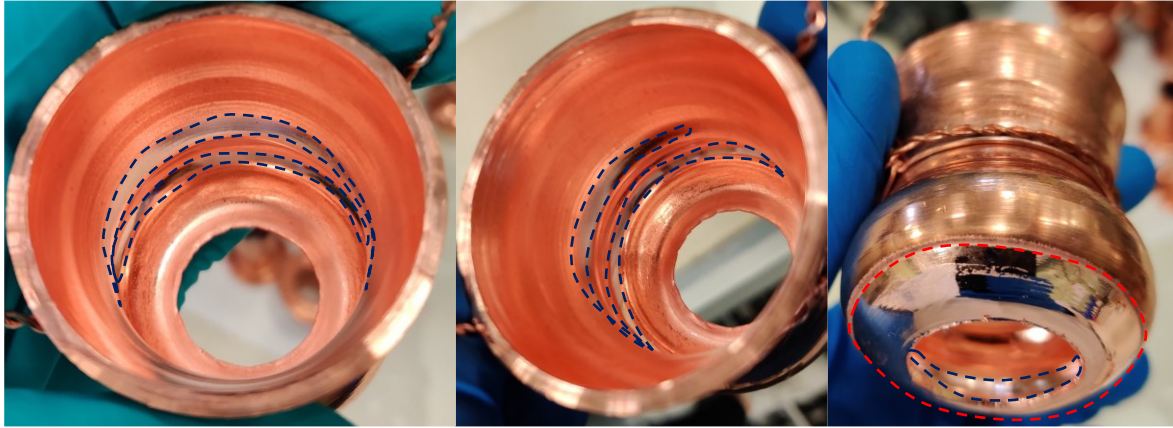
Figure 6.34: Photo inspection of the treated dummy elliptical Cu cavity

The current of the process dropped from the 20 A to the average of 10 A (excluding the first peak of current of up to the 30 A). Interestingly, according to the current values and the assumption of the presence of electrolysis process, the theoretical weigh removal is 0,42 g, meanwhile in practice it resulted in the 0,70 g. The overall current efficiency is 166,7 %, which is higher than normally expected (see chapter 6.5).

Summary: the double cathode system has shown the mild promise as a workaround of compact complex geometries substrates. Remains however the necessity to isolate most of the external surface, that is not a trivial task. Unless any non-covered surface part will take part of the discharge and might limit the performance of the desired process.

6.7.2 QPR sample treatments

In the framework of ARIES and IFAST projects [340], [341], a protocol for a chemical treatment for Cu/Nb QPR samples was established, as described in details [342], [343]. Within the project collaboration the polishing of both Cu/Nb and bulk Nb QPR samples was expected. A standard path, derived from the LNL protocol of surface preparation of the 6 GHz cavities [51], [321] included both the electropolishing and "SUBU" as a main treatment for polishing of the copper substrate. Being a relatively simple planar geometry, the Cu/Nb QPR sample was tested with PEP for a future surface preparation in the above-mentioned collaborations.

6.7.2.1 Nb QPR sample polishing

After a delivery of a QPR A1 sample in the framework of ARIES project, a PEP treatment study on the QPR sample geometry was scheduled. The initial state of the QPR A1 sample presents severe texturing after the production at Research Instruments (RI), see **Figure 6.35**. The successfully

developed solution for Nb PEP allows the polishing of planar surface and should not present any problem. The first attempts were done in the quite closed environment of a glass beaker of 5 L volume. That is why cooling was implemented by the nitrogen compress gas line blowing inside the beaker. The cavity was isolated with a plastic film to decrease the effective anode area to the planar disk and around 1 cm of heigh of the cylinder structure. The electrical connection was provided by the screw connection inside the QPR sample.
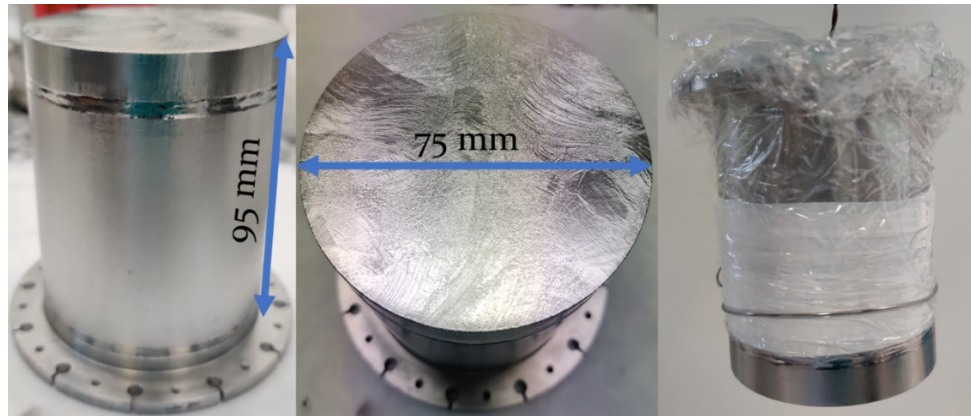
Figure 6.35: A QPR A1 sample view after the production state, dimensions, and isolation for a PEP treatment

A series of treatments (see Table 6.21) were applied in the developed solution for Nb PEP (3:1 % NH_4F:NaF) processing. In all cases the initial temperature was 75 C°, during the process it raised up to 90 C°. Higher values of temperature were limited by the applied compressed nitrogen gas cooling. The scope of such experiments was to evaluate the possibility of scaling the process to the higher surface areas substrate.

The error of the experiment was not considered, as the active surface area might variate between the rounds, due to the different isolation (subjected to the human error), and consequently measurements of the weight with further calculations. The surface area in thickness and erosion rate calculations was assumed to be 56 cm². Two solutions (of 3 L) were used to ensure the effectiveness of the treatment and avoid Nb saturation: one for 1 – 8, and second for 9 – 16 rounds.

Table 6.21 – Characteristics and data of the conducted PEP treatments for the QPR A1 sample

Round	Time, min	Δm, g	Removed thickness, µm	Erosion rate, µm/min	Current efficiency, %
1 - 2	3 (1,5+1,5)	0,50	10,00	3,33	98
3 - 5	10 (3+2,5+4,5)	1,00	20,84	2,08	35
6	10	1,08	22,50	2,25	45
7	10	1,18	24,59	2,46	47
8	10	1,00	20,84	2,08	
9 - 10	4 (3+1)	1,01	20,84	5,21	
11 - 13	8 (2+3+3)	0,70	14,59	1,82	
14 - 15	6 (3+3)	0,46	9,58	1,59	
16	10	0,83	17,29	1,73	
Total	**71**	**6,83**	**141,32**	**2,00**	

Notably, the overall erosion rate summing the 71 min process reaches 2 μm/min, that can explain the conclusions from the chapter 6.5, where it was noticed lower erosion rates for higher anode surface areas (or smaller ratio between cathode and anode area). It might be related as well to the limited volume of PEP bath. Interestingly for a short treatment (round 1-2), the current efficiency raises to the 100% that is as well aligned with higher erosion rates. Higher rates can be related to the newly prepared solution as well, as it was in the case of round 1-2 and round 9-10. In case of round 3 – 5, 6 and 7 are well aligned with the current efficiencies previously studied. A visual inspection after single treatments of the QPR A1 samples are presented below (see **Figure 6.36**).

A noticeable smoothing of the Nb surface is taking place, after a very rough initial surface. Possible light oxidation normally takes place and are fixed with the proper ultrasound cleaning and optional diluted hydrofluoric acid deoxidation. The nature of such oxidation might be related to the ending of the anodic polarisation, when the lower voltage moment can take place (with higher currents comparing to typical values of the process) via electrolysis produce colour oxide.

The QPR A1 surface after the round 8 presented dark blue defects, that are the thick oxide by nature. With ultrasound and additional steps of newly prepared solution for PEP processing defects have disappeared, however leaving the crater-like defects. These grooves have a quite deep depth. Such defects were not observed earlier in any of the previous experiments conducted.
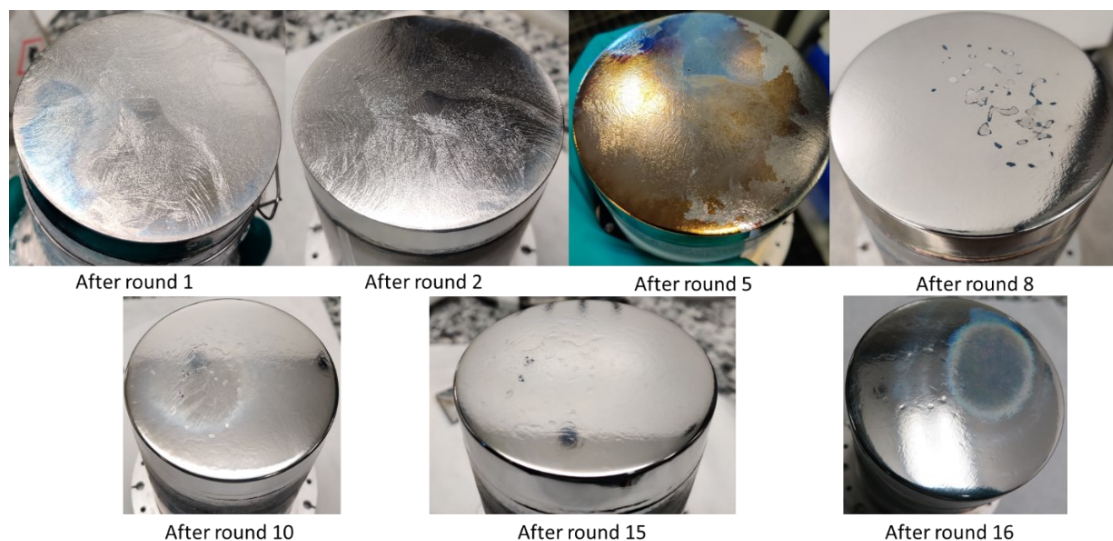
Figure 6.36: Photo-visual inspection of the QPR A1 surface after a series of PEP treatments

During long treatments, such as in round 7, due to the boiling of the solution, the level of the bath solution had been dropping. That is why a portion of distilled water were added manually. This process influences the dynamic of the PEP (see **Figure 6.37**), because the current density was instantly increased (due to the cooling of the solution). Such behaviour agrees with the previously described temperature studies of the process in chapter 6.3. A solution to overcome this issue is a bigger bath with a bigger quantity of solution, and a better thermal exchange process as a result.
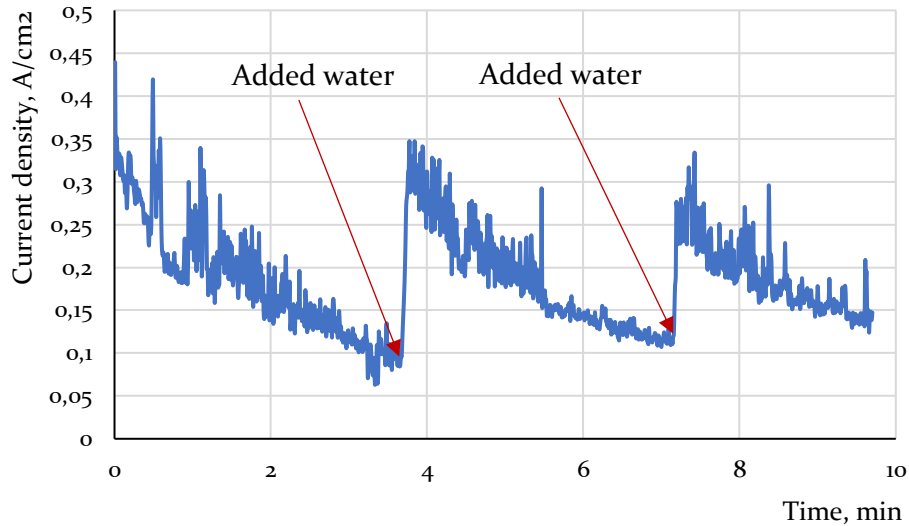
Figure 6.37: Current density dynamic during the PEP of QPR A1 (round 7)

Summary: the possibility of PEP treatment of object with a higher area surface than regular samples, used for the R&D stage was shown. The possibility of undesired oxidation, that might result in crater-like defects was identified. The reasons relate to the oxide formation and system configuration (volume, solution saturation, cathode/anode area ratio). A further improvement of the system configuration is needed for a final evaluation of QPR PEP possibility.

6.7.2.2   Cu QPR sample polishing

Dummy sample

To establish the feasibility of the application of Cu PEP solution to treat a Cu/Nb QPR sample a test on the dummy sample was done: QPR sample without a flange, cylinder structure in Nb and a Cu disk to be polished welded Nb structure. As a solution SUBU5 was chosen, with a working voltage of 300 V, time of treatment 2 min. As a cathode a stainless-steel cage perforated was chosen. The motivation of such geometry of the cathode was done to have a ratio between the cathode - anode surface area >10. The dummy sample was inserted partially, to avoid unnecessary oxidation of the Nb structure. The wire connection of the cathode was isolated with plastic supports, and anode wire connection was screwed directly to the Cu disk from the internal part (see **Figure 6.38**). A summary of the treatment is shown below Table 6.22:

The treatment of 2 min resulted in the 14 μm of removed material (7 μm/min). The initial surface was machined with turning machine and presented quite good starting point. The resulting surface was uniform, shining, and reflective. Some small imperfections may be observed by eyes. Overall, the test was labelled as successful. The niobium structure, as expected, presents thick oxidation, even in the parts where the solution was not immersed, due to the boiling and consequential splashing of the solution. The strategy of the removal of niobium oxide products was planned to use

the diluted solutions of the hydrofluoric acid or "strip" solution of industrial composition, for a selective etching of the Nb.

Table 6.22 - Dummy QPR sample PEP summary

Temperature, C°	Solution	Time, min	Erosion rate, μm/min	Voltage, V	Effective area, cm²
71 - 92	"SUBU5"	2 min	7,0	300	45
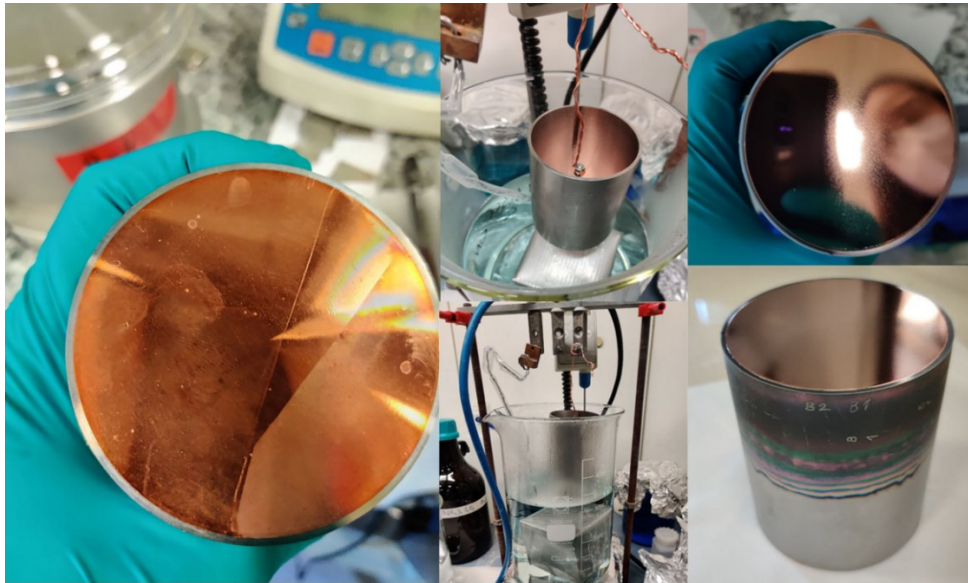
Figure 6.38: Photos of the dummy Cu/Nb QPR sample, connection, and the surface before and after the treatment

QPR B4 sample

The following research was conducted on the QPR B4 sample, that at the time was already mechanically treated, chemical polished, sputtered (coated), stripped 3 times. So that the surface of the copper (but also the Nb) did not present the ideal case. After the ultimate check, a copper thin part of circle was noticed; that might indicate not a complete sputtering or some mechanical defects of the welding filler between the Cu and Nb (see **Figure 6.39**). After a series of stripping procedures, a deposited Nb coating was removed resulting in a slightly etched Cu structure, as well. A protocol foresees the usage of the ammonium persulfate etching to highlight the Cu grains, and eventually evidence the possible presence of the Nb non-stripped coating.

The copper grains are visibly different in terms of sizes (in the middle, close to the welding circumference and the rest of the Cu disk). This effect might be related to the different history of heating (annealing) of the sample and might affect the resulting quality of the treatments.
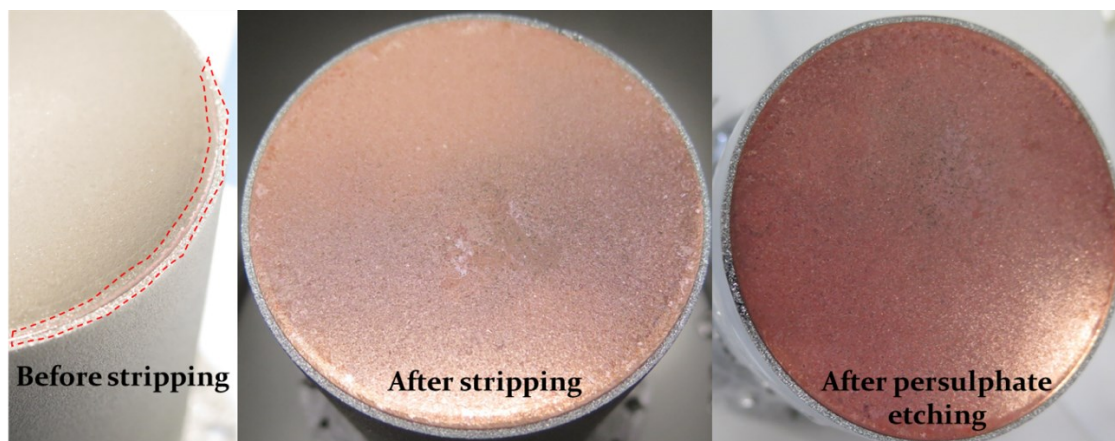
Figure 6.39: Photo of the QPR B4 sample before stripping, after stripping and after the persulphate etching

To eliminate or minimise the oxidation of the Nb structure, it was decided to wrap the cavity with a plastic film and a Teflon tape (see **Figure 6.40**). For a better stability of such protection, additionally niobium wire was used to hold tight. The same stainless-steel cage was used as a cathode. The resulting surface (see **Figure 6.41**) after 2 minutes of treatment presented very reflective and enough uniform surface, however some stains of oxidation (etching) was present, due to the residuals of the SUBU solution that under the high temperature conditions and presence of air quickly oxidises the copper surface. To prevent this a fast rinsing with water/ethanol is needed after the ejecting the cavity from the solution. The second issue was observed: the spike like defects, that had a higher height than the resulting copper surface. From the photo, it is observed as pitting, white dot across the surface. It is worth to mention that similar defects also appeared in the standard protocol of preparation of the QPR samples from the same series of production and might be related to the substrate quality or annealing treatments the sample undergoes. A summary of the treatments on the QPR B4 samples are listed below Table 6.23:
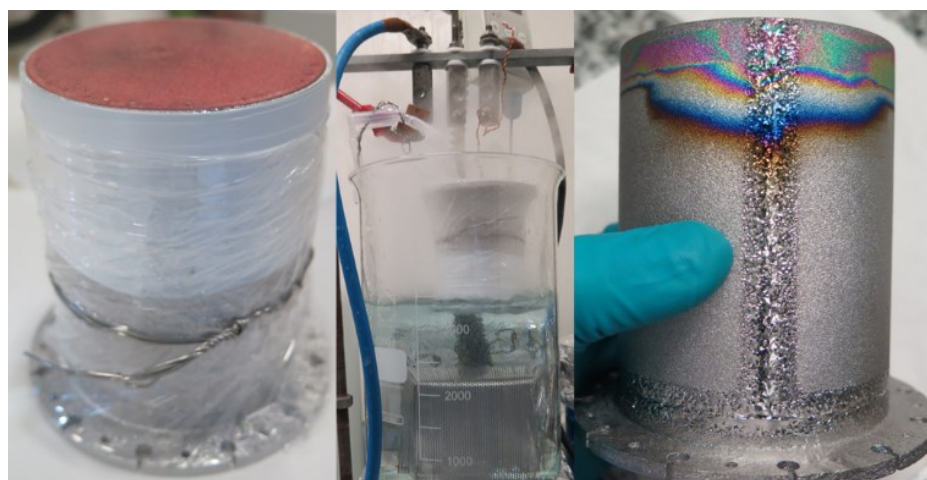
Figure 6.40: Photo of the QPR B4 sample prepared for the PEP, during PEP and after polishing

Table 6.23 – Summary of the QPR B4 sample treatments

#	Treatment	Temperature	Solution	Time	Removed	Erosion rate	Voltage	Effective area
1	Stripping	71 – 92 C°	n/a	5 h				
2	Persulphate etching	ambient	20 g/L $(NH_4)_2S_2O_8$	20 min				
3	PEP	70-92 C°	"SUBU5"	2 min	14 µm	7,0 µm/min	300 V	45 cm²
4	Stripping	ambient	n/a	6 h				
5	PEP	78-85 C°	"SUBU5"	1 min	6,5 µm	6,5 µm/min	300 V	45 cm²
6	PEP	84-96 C°	"SUBU5"	2 min	9,0 µm	4,5 µm/min		
			Total	**5 min**	**29,5 µm**	**5,9 µm/min**		

Figure 6.41: Photo of the QPR B4 sample after PEP treatment at different angles

It was supposed that the cause of the spikes might be related to the residual of the Niobium as well or to other superconducting structure coating. A stripping process was done, where the whole surface was immersed in the solution. The resulting surface still surprisingly presented reflective copper. After the angular photo the spike defects were captured (see **Figure 6.42**).

Figure 6.42: Photo of the QPR B4 sample after stripping

To proceed with the cavity and possibly eliminate the spikes, additional rounds of PEP were applied, always with the same conditions. The time of treatment was limited to avoid abnormal etching and possible cracks between the copper disk and the niobium structure. Two rounds of treatment were applied, resulting in much smoother surface observed by visual inspection, in particular the spikes rounded or partially disappeared. Unfortunately, after the ultimate treatment, during the drying process, it was noticed how the liquid was leaking in one spot (see **Figure 6.43**) where the brazing probably corroded the most. Due to the nature of the defect, this QPR sample will not be utilized any more. The final total removing rate (excluding the stripping effect) for a series of treatment 5 minutes in total was calculated to be 6,9 µm/min. The erosion rate is smaller than normal with planar samples, but it is explained by the different ratio of the electrodes and compact electrolysis cell.

Figure 6.43: Ultimate photos of the QPR B4 sample and the defective spot

Summary: the copper surface with the niobium interface can be polished with a relatively simple PEP "SUBU" solution. A strategy must be adopted for a better isolation of the niobium avoiding the oxidation. Therefore, thin films of niobium oxide are still possible to be eliminated without damaging the copper surface visual aspects. A further coating of the SC layer with cryogenic measurements are necessary to validate the results and compare them with the conventional paths.

6.7.3   Jet-PEP

Jet spraying plasma electrolytic polishing (Jet-PEP) is a variation of the standard PEP treatment that does not require a complete immersion of an anode inside the electrolyte solution. Instead, the solution is sprayed of the anode from the cathode nozzle. The plasma processes are taking place on the interface metal – solution – air. A jet-PEP mode of polishing requires a separate study varying new parameters in addition to the existing ones. Moreover, previously optimised parameters and solutions might not be suitable for the jet-spraying process. Positioning of the spraying nozzle/head and the desired sample play as well a significant role in the success of the process. In this experiment a very preliminary study was conducted to verify the possibility of the Jet-PEP of developed solutions. As it was described in chapter 6.1, the system composed of the 5 L beaker, membrane PVDF

pump those fluxes through the PVDF tubes and custom-made cathode head onto the anode sample surface (see as well **Figure 6.4**).

6.7.3.1   Copper Jet-PEP

First attempt

The initial try was consisted of a simple system, described below, with the distance of 3-4 cm between the electrodes. The used SUBU5 solution was selected, at the process temperature of 64-67 C°. The process characterised with relatively low current –0,5 A. A sample of 6 x 6 cm was treated for 10 minutes. The photos of the sample after treatments are presented below (see **Figure 6.44**) and a summary of the experiment is in the Table 6.24.
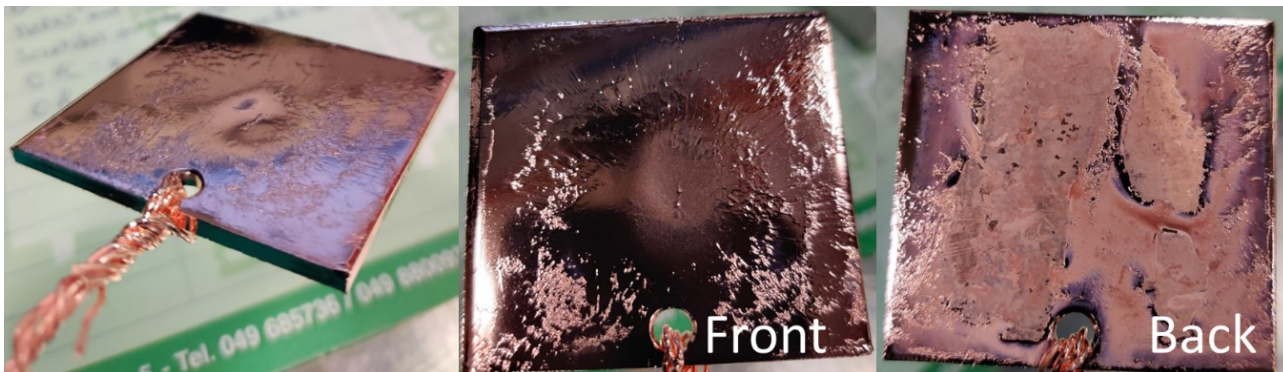
Figure 6.44: The photos of the Cu sample treated with the Jet-PEP

Table 6.24 – Cu planar samples Jet-PEP experiment summary

Electrode Distance, cm	Temperature, C°	Solution	Time, min	Removed, μm	Erosion rate, μm/min	Voltage, V	Effective area, cm^2	Current density, A/cm^2
4	64-67	"SUBU5"	10	90	9,0	300	36	~0,013

The front part of the sample resulted reflective and shining with a noticeable waviness in the central part, where the flux of the solution was directed. Assuming that 3 g of weigh was removed (90 μm) and assuming all the current used for electrolysis, 0,2 g (6 μm) are expected to be removed. Considering this calculation, most likely the process was mainly chemical rather than Jet-PEP.

Second attempt

For the second attempt, a half-cell of the Cu 6 GHz cavity was used, and the electrode distance was reduced to 2-3 cm. A process characterised (see details in Table 6.25) as relatively stable (see **Figure 6.45**) and has led to the heating of the solution from the 67 to the 72 C°. A half cavity noticeably polished without defects, as in the previous attempts (including backward oxidation or selective wave-like central etching).

Table 6.25 – Half-cell 6 GHz Cu Jet-PEP experiment summary

Electrode Distance, cm	Temperature, C°	Solution	Time, min	Removed, μm	Erosion rate, μm/min	Voltage, V	Effective area, cm²	Current density, A/cm²
3	67-72	"SUBU5"	19,6	14,4	0,74	300	46	0,027
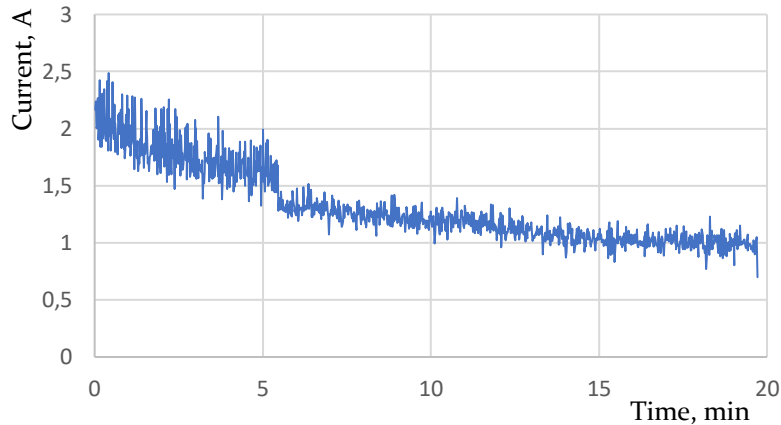
Figure 6.45: Current curve in time for the Jet-PEP at 67 – 72 C°, 300 V

The resulting surface of the cavity presented a significant improvement, together with the theoretical calculation of the removed material (0,50 g) and practical data (0,59 g) resulted in the 118 % current efficiency of the process. The CE values are comparable with the standard PEP process, with probably lower currents due to the higher resistance in the Jet-PEP approach. It is still unclear what is the impact of the SUBU solution on the surface polishing via jet spraying. Such experiments are scheduled for the nearest future to study better the effect of the PEP discharge and chemical solution itself.

The third attempt

To prevent the chemical polishing (or erosion) by the SUBU solution, an experiment using the pyrophosphate solution was scheduled (4% $K_2P_2O_7$, 7 g/L K,Na-Tartrate pH 4) at 300 V and temperatures 80-87 C° for both PEP and Jet-PEP part of the experiment. Two samples 2,5x2,5x0,2 cm were chosen (14,5 cm² area). A summary of the obtained results and data are presented in the Table 6.26 below.

The results indicate the presence of the electrolysis with the Jet-PEP process, since an erosion rate of 3,9 μm/min was obtained (a pyrophosphate solution does not etch chemically copper for such short periods of time). On the other hand, the results cannot be characterised as uniform and successful in terms of polishing. An optimisation of the parameters is vital. The erosion rates are comparable to the standard PEP process from the list of conducted experiments and the one listed below in the same solution.

Table 6.26 – Summary of the PEP and Jet-PEP process in the pyrophosphate solution at 300 V

Process	Temperatures	Time	Effective area	Thickness removed	Erosion rate	Photo
PEP	82-86 C°	1,5 min	14,5 cm²	11,6 µm	7,7 µm/min	
Jet-PEP	85-87 C°	10 min	6,25 cm²	39,4 µm	3,9 µm/min	Front Back

Summary: The Jet-PEP is a promising upgrade of the existing technology with developed solutions of Cu PEP. Systematic optimization of the electrode distance, working voltage, and solution composition is required to proceed with the application of this approach. Therefore, successful Jet-PEP of the Cu substrate at this stage was not achieved, as the polishing did not resulted in reflective surface.

6.7.3.2   Niobium Jet-PEP

After a preliminary success of the Cu PEP, a similar experiment was conducted with the Nb PEP solution of 3:1 composition (NH_4F:NaF). A sample of 6 cm diameter was chosen as an anode. The solution was maintained at the 82 C° in the bath. The distance between the cathode and anode was maintained at the 2,5 cm. The distance was chosen so that there is a continuous bridge of the solution between electrodes. The summary of the process is presented below in the Table 6.27.

Unfortunately, the process failed in polishing of the Nb, instead the oxidation took place (see **Figure 6.46**). After the ultrasound cleaning, a significant quantity of oxide detached. As a result of calculation, around 6 µm were removed.
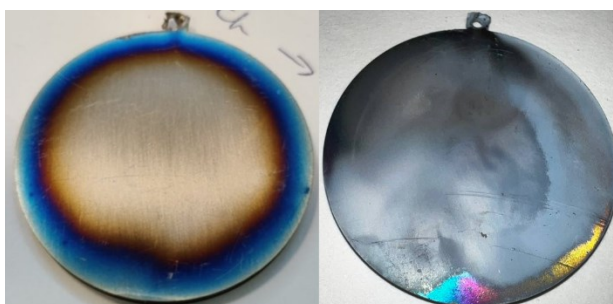
Figure 6.46: Photo of the non-treated and after 10 min jet-PEP

After a closer look to the dynamic of the current during the processing, a significant current oscillation and a decrease of the effective values are evident (see **Figure 6.47**), as normally happens either during the heating or with the polishing of the process (roughness decreasing). A calculation of an estimate weigh removal showed, that assuming the process to be 100% electrolytic, after 10 minutes

of treatment 0,5 g should be removed. In contrast only 0,16 g was removed. Considering the possible low values of current efficiency, the process might take place, however with a preferential oxidation.

Table 6.27 – Planar sample Nb Jet-PEP experiment summary

Electrode Distance, cm	Temperature, C°	Solution	Time, min	Removed, μm	Erosion rate, μm/min	Voltage, V	Effective area, cm²	Current density, A/cm²
2,5	84-82	NH4F:NaF (3:1)	10	9,53	0,96	300	19,6	0,23
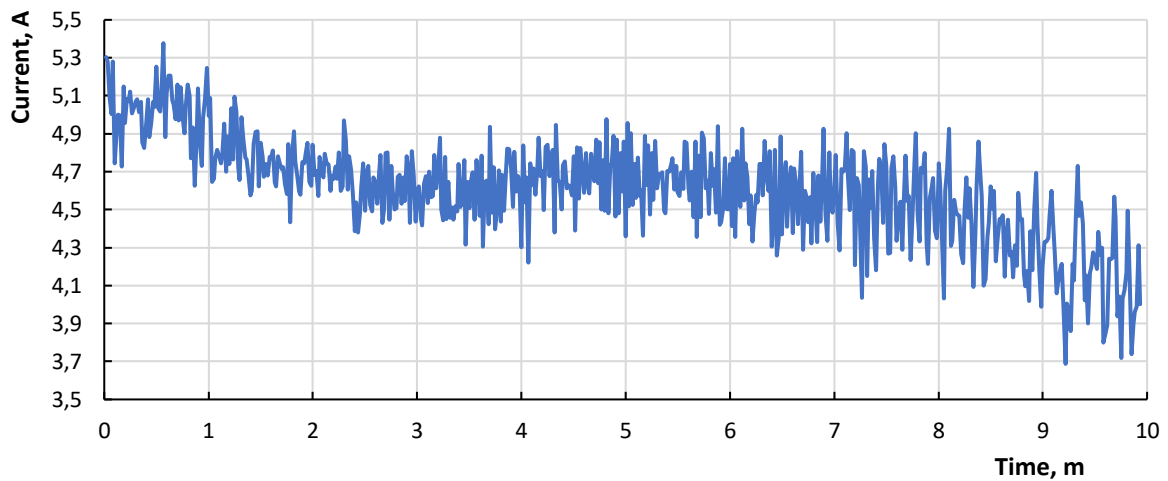
Figure 6.47: Current vs time curve for the Nb Jet-PEP at 300 V

Summary: An additional study and optimisation of the jet-processing is required. the effect of the temperature was not studied, in particular no temperature measurement was done at the output of the fluxing solution. A different shape of the nozzle must be implemented in addition to the different geometries of the anode positioning. Higher voltages were not tested. as well.

6.7.4   *PEP for Additive Manufacturing*

6.7.4.1   PEP of the 3d printed Cu

Attempt 1

A series of Cu 3d printed samples were obtained printed with an unknown technique. The planar samples with dimensions 3,1x3,1x0,5 cm with around 25 cm² surface area characterised and polished. Samples were characterised with the linear profilometer at two different lengths of scan – 6mm and 1mm. Each scan length was measured at least 4 times. The presented results are averaged (see summary in the Table 6.28 and see **Figure 6.48**)

Table 6.28 – Cu 3d printed samples PEP in pyrophosphate solution

#	Solution	Temperature	Voltage	Time	Surface Area	Δm	Erosion rate	Ra (6mm)	Ra (1mm)
Initial	-	-	-	-		-	-	11 μm	11 μm
1	$K_4P_2O_7$ - 4% K,Na-tartate - 7g/l H_3PO_4 till pH 2..3	55 – 85 C°	325 V	11,7 min	25 cm²	1,98 g	7,44 μm/min	1,6 μm	0,6 μm
2	$K_4P_2O_7$ - 4% K,Na-tartate - 7g/l H_3PO_4 till pH 2..3	60 – 85 C°	300 V	8,5 min		1,31 g	6,82 μm/min	1,3 μm	0,6 μm
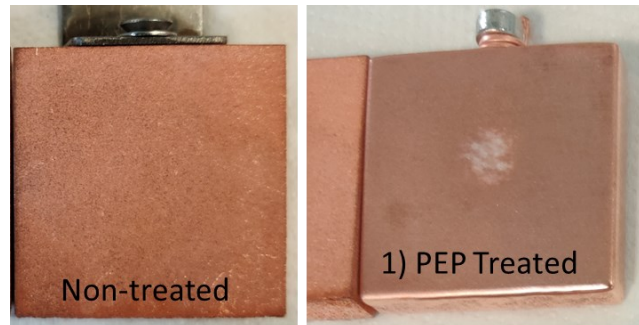
Figure 6.48: Photo of the non-treated and PEP treated 3d printed Cu samples in pyrophosphate solution

Attempt 2

A different bath of non-planar samples was studied in terms of PEP performance. The surface of the samples presented macro-defects in the form of peaks (spikes), especially on the curvature parts, that is related to the printing behaviour of angular structures (see **Figure 6.49**). The reflectivity was not observed. Unfortunately, any roughness measurements was taken from these samples, due to their complex form and equipment limitations. The initial roughness was around 10-16 μm according to the producer. A summary of the experiments is presented below in the

Table 6.29.

A summary of the experiments and photos of the samples are shown below:
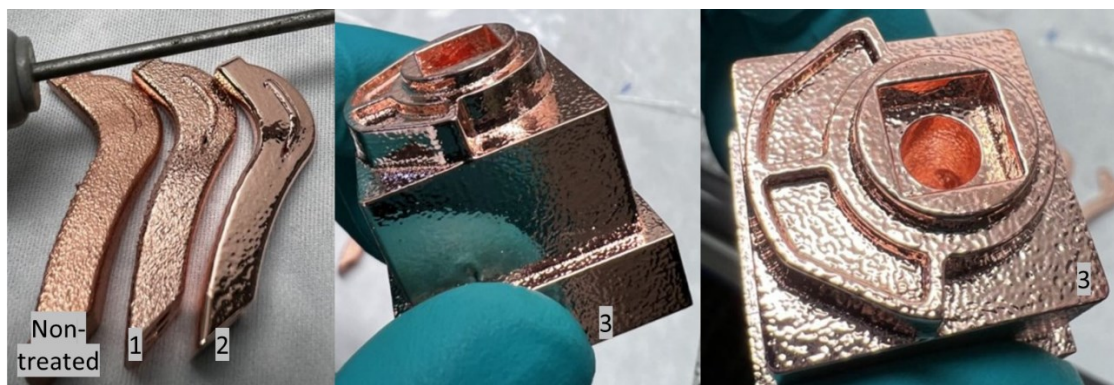
Figure 6.49: "SUBU" PEP treatments on the printed samples

Table 6.29 – "SUBU" PEP experiment on the 3d printed samples

# Sample	Solution	Temperature	Voltage	Time	Surface Area	Δm	Erosion rate
Initial	-	-	-	-		-	-
1	"SUBU5"	70 – 85 C°	300	2 min	~35	0,9 g	14,4 μm/min
2		72 – 88 C°		10 min		4,8 g	16,4 μm/min
3		70-93 C°		6 min	~ 90	6,1 g	unknown

The "SUBU5" solution was able to improve the surface roughness of the presented samples in less than 10 minutes, resulting in reflective and shining surface. Partially the macro-defects (like spikes) were completely removed, however a still visible waviness of the sample can be related to the structure of the printed sample or to the mechanism of the PEP, that might not be able to planarize the treated surfaces. More systematic studies must be done to finalise the conclusions. The micro roughness is improved, the remaining macro-defects, that influence the macro-roughness values, are still needed to address. The results are promising, indicating that possibly just one chemical treatment is enough to smooth the additively printed surface, without any mechanical polishing technique involved.

Summary: two solutions tested ("pyrophosphate" and "SUBU5") have shown the significative performance in terms of surface polishing in case of 3d printed rough structures. The "SUBU5" has an advantage in terms of reflectivity and higher erosion rates. Unlike the chemical and electrochemical methods, PEP seems to be a proper tool to smooth the surface, that will require more than 10 minutes or more, depending on the solution and the initial roughness of the samples.

6.7.4.2   PEP of the 3d printed Nb

PEP polishing on 3d printed samples of pure Niobium by Laser Powder Bed Fusion (EOS M100 DMLS machine) obtained from the DIAM group of INFN Padova section research group in the framework of the IFAST project has been explored. The samples were printed together with the elliptical shapes (6 GHz resonant structure) and present almost planar surface with a small curvature. The width is 0,8 cm, thickness of 0,25 cm and different length that determine the surface area.

The scope of such experiment is to verify the efficiency of the developed PEP method to achieve smooth surface for additive manufacturing of SRF cavities. Two samples were treated with the 3:1 Nb PEP solution (NH_4F:NaF) at an average temperature of 91...92 C°, at 300 V applied anodic polarisation in the 5 L beaker. Surface morphology is presented below (see **Figure 6.50**). A summary of the process is presented in the Table 6.30 below.

Table 6.30 – Summary of the Nb printed PEP parameters used

#	Solution	Voltage, V	Time, min	Length, cm	Surface Area, cm²	Q, A·s	Δm$_{theor}$, g
1		300	20	2,8	6,64	2064	0,40

2	3% NH$_4$F 1% NaF		30	3,4	8,4	2729	0,53

A noticeable smoothening of the initially rough surface structure is taking place both on the micro and macro levels. A quite significant improvement of the surface is obtained after 20 min (44 µm) of treatment. From the small magnification it is noted that some of the defects are still present and can be characterised as a post-printing structures. These grooves represent the hidden parts of the 3d structure, that was shadowed during polishing, and thus remain. Overall layered structure after laser printing is characterised as rough and clearly determined by the powder dimensions and distribution of its sizes.
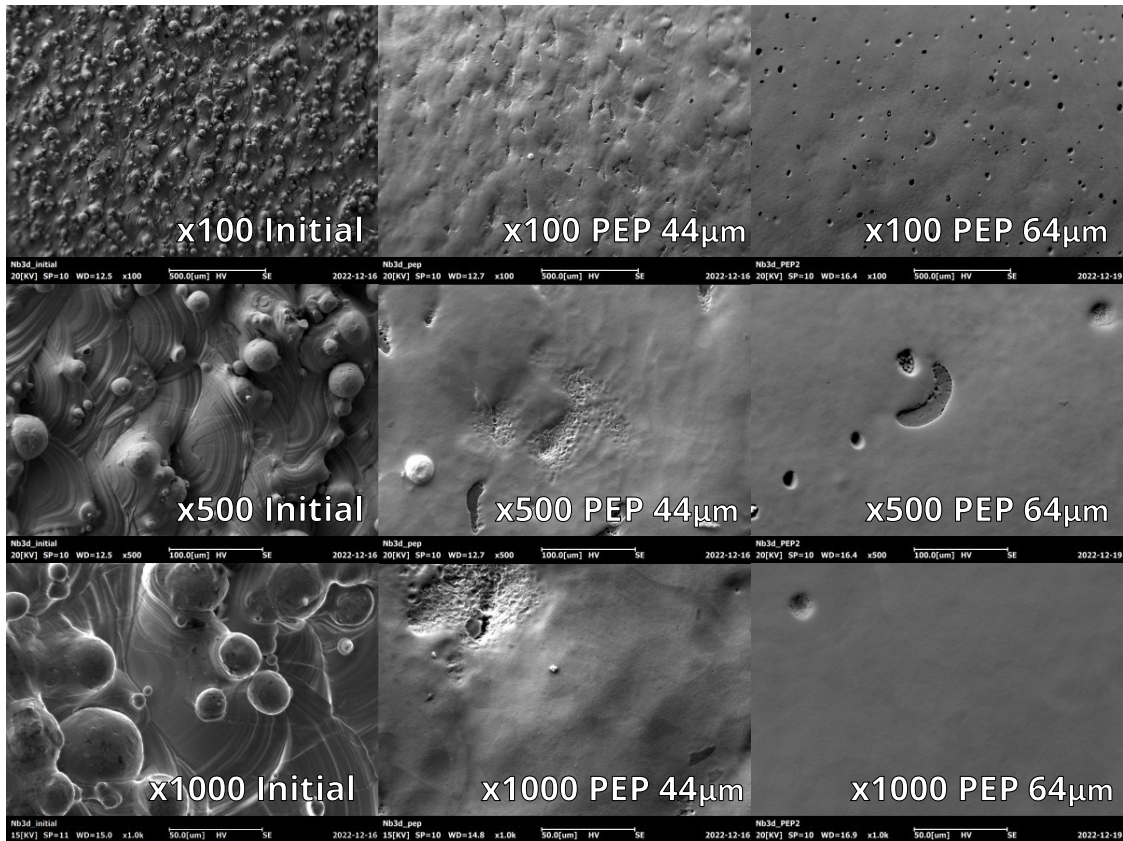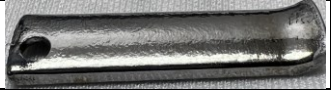
Figure 6.50: Surface micrographs for non-treated, PEP treated samples at 100, 500, 1000x magnifications

A summary of the conducted treatments is presented in the Table 6.31 below:

Table 6.31 – PEP processing data of the 3d printed Nb samples

Parameter /Sample	Time, min	Removed thickness, µm	Erosion rate, µm/min	Roughness, nm	CE, %	Photo
Initial	-	-	-	Ra 13.000±1600 Rq 16.000±1900	-	
1	20	44	2,2	Ra 2900 ± 590 Rq 3550 ± 650	62,5	

				Ra 1500 ± 540 Rq 1950 ± 600		
2	30	64	2,1	Ra 1500 ± 540 Rq 1950 ± 600	87,0	

Summary: An evident improvement of the resulting surface is observed both visually and by the linear profilometer and roughness values. Apparently, the values for the erosion rates are smaller respect to the average ones, and simultaneously relatively high current efficiency values. The analysis of the dynamic of the current density during the process may be a key for understanding the difference of the CE (see **Figure 6.51**). The stabilisation of the process in the initial time might contribute to the Joule heating, VGL establishment and uniformity of the VGL. In case of longer process, it seems this effect is lower, thus resulting in higher CE. We expect that higher thickness removal processing may decrease the roughness even more by eliminating the macro defects cave (pit-like) defects.
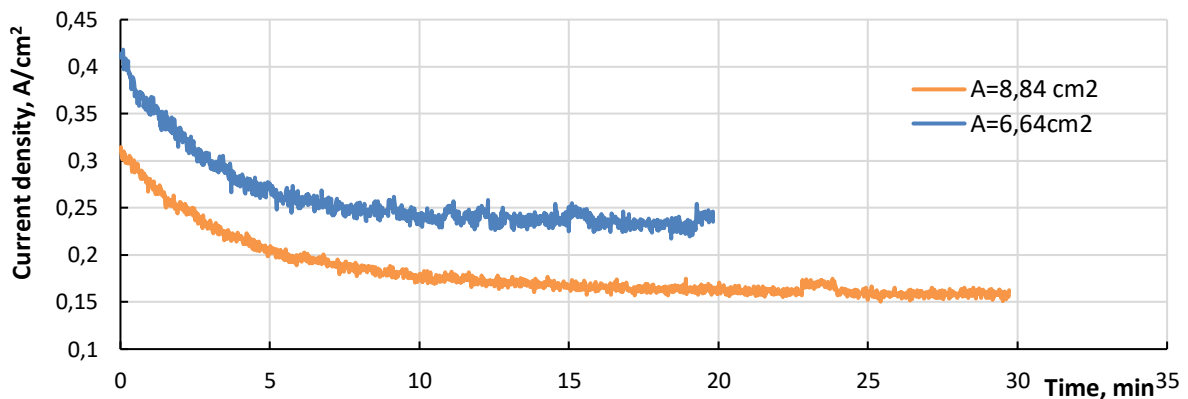
Figure 6.51: Current density vs time of treatments for Nb PEP 3d printed samples

6.7.4.3   PEP of the 3d printed Ta

Additive manufactured Ta samples have been additionally studied for an evaluation of the possibility of PEP of this metal for accelerators general purposes. The initial state of samples is presented below (see **Figure 6.52**), very rough surface of Sa 10...13 μm, Sq 13...16 μm. Printed by Laser Powder Bed Fusion (EOS M100 DMLS machine) with Yb fiber laser (λ = 1064 nm), spot diameter: 40 μm and maximum power: 200 W. The working atmosphere was substituted with Ar (oxygen level <0.11%), used power 110 W, at speeds 350, 400, 450 mm/s for BCP, PEP, EP treated samples respectively.
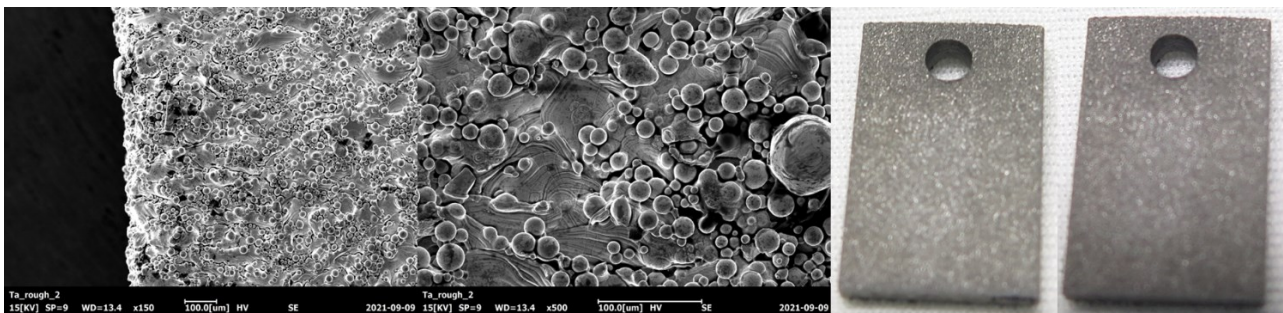
Figure 6.52: SEM micrographs of the 3d printed Ta samples of 4 cm² area

For a purpose of comparison, three treatments were applied, assuming similar chemical properties of Ta to the Nb one: BCP, EP and PEP (Nb solution). The BCP solution temperature was ambient and not regulated, with a total time of 170 min, resulting in the 110 µm in average thickness removal. The EP process was applied for 210 minutes (3,5 h) at 12 V voltage. The resulting thickness removal was 101 µm. (In case of PEP three rounds of treatments were conducted in the 3:1 NH₄F:NaF. A total time of treatments is 65 min with a ~200 µm removal thickness (see in detail in Table 6.32).

Table 6.32 – Process characteristics of the Ta 3d printed samples

#	Time, min	Δm, g	Removed layer, µm	Erosion rate, µm/min	Comments
1	30	0.79	119	2,98	Smoother, not reflective, mate-like.
2	10				
3	25	0.52	78	3,12	Smoother, not reflective, mate-like.

The BCP treated sample morphology presented below see **Figure 6.53**, characterised as rough, with visible defects that came from the printing (balls-like structure), pitting and possibly BCP. The EP sample shows a clear polishing effect on the micro-scale; however, the sample remains to be rough on the macro-scale (**Figure 6.54**). A slight reflectivity and brightness are noted. Finally, the PEP treated sample presents defective surface, but visible smoothed on the macro-scale. No reflectivity is observed, that is due to the micro-roughness, that is visible on SEM micrographs (see **Figure 6.55**). Different parts of the sample show a different surface morphology.
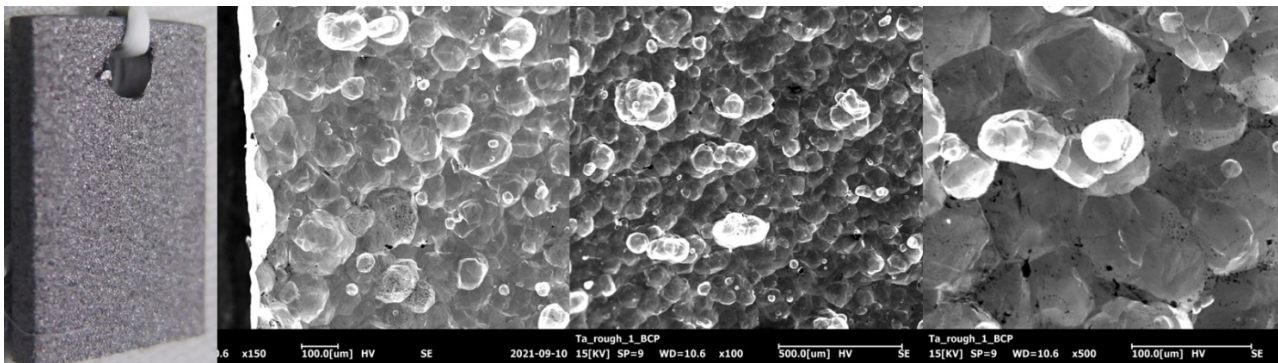
Figure 6.53: SEM micrography of the BCP treated Ta 3d printed sample (110 µm removed)
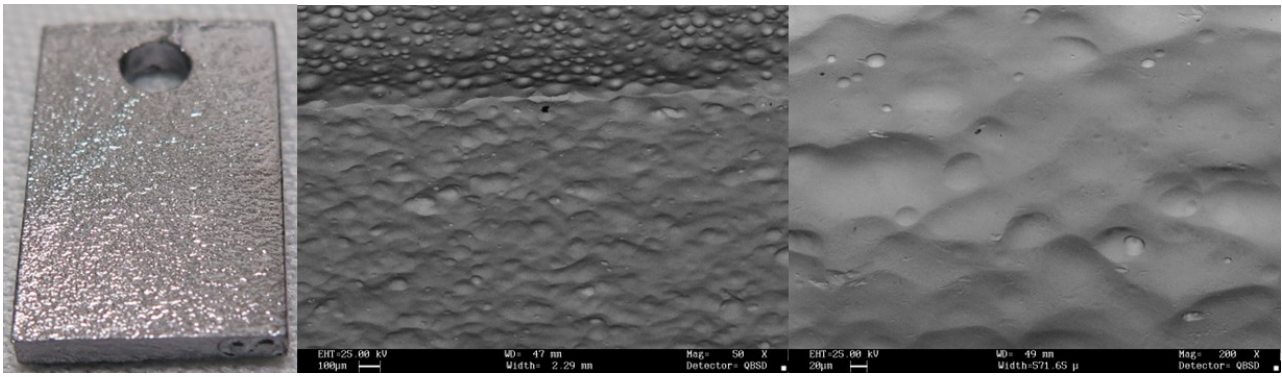
Figure 6.54: SEM micrography of the EP treated Ta 3d printed sample (101 μm removed)
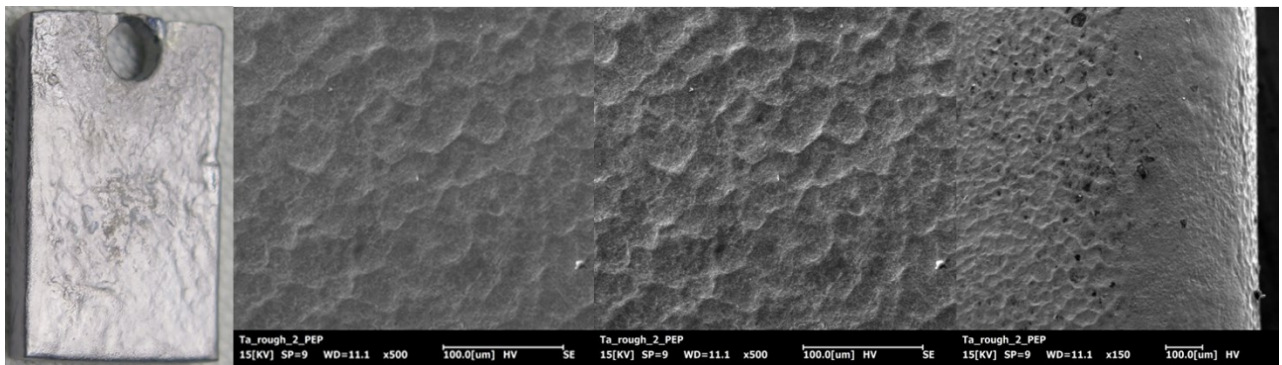
Figure 6.55: SEM micrography of the PEP treated Ta 3e printed sample (200 μm removed)

Roughness measurements were obtained with optical microscopy Sensofar S neox and objective EPI 20x v35 (area 3x3 cm², resolution 0,64 μm/pixel), roughness data, surface analysis are presented below on the **Figure 6.56**.

For a verification, a Ta ring, was treated with the identical PEP solution and condition. Resulting quality was more like the Nb behaviour (light oxide production, smoothing) (see **Figure 6.57**).

Sa 11,5 µm
Sq 14,7 µm

Sa 10,9 µm
Sq 13,9 µm

Sa 12,7 µm
Sq 16,1 µm

Sa 8,7 µm
Sq 13,0 µm

Sa 4,5 µm
Sq 5,8 µm

Sa 8,9 µm
Sq 11,5 µm

BCP

EP

PEP
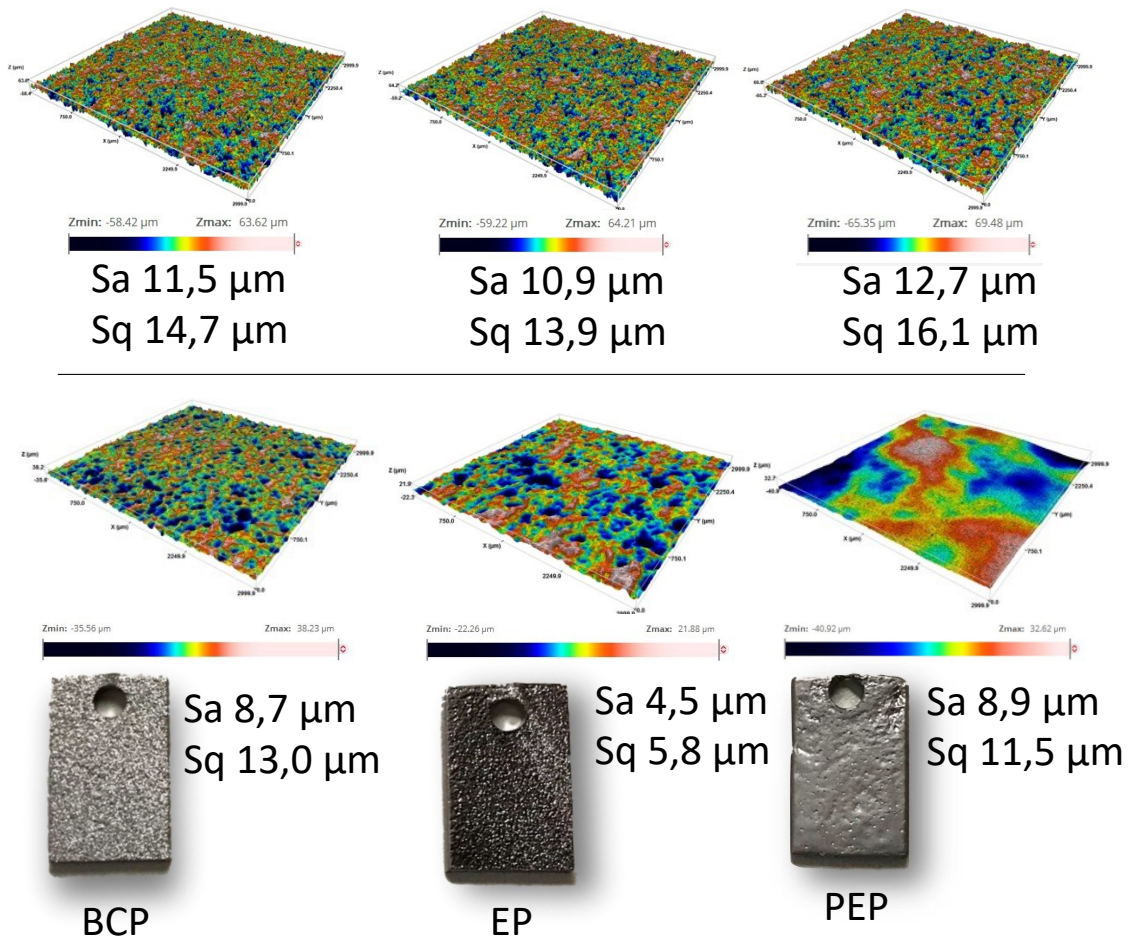
Figure 6.56: Surface roughness and morphology analysis of the 3d printed Ta samples
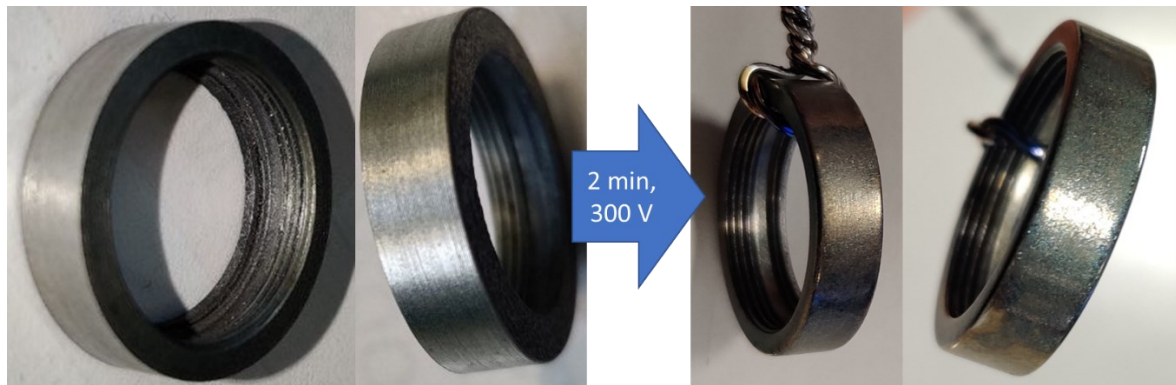
Figure 6.57: Visual photo of the non-treated and PEP treated Ta ring after 2 minutes

Summary: being chemically similar metal Ta is sharing the PEP recipe solution as well. Even without an optimisation to the solution and conditions, a decent quality of the polishing was achieved, considering very rough initial state after the 3d printing production. Unfortunately, a mirror-like reflective effect was not achieved after 200 µm thickness removal. Longer times of treatment might improve the situation, however on the micro-level the structure still present post powder-like structure, after the additive manufacturing. Depending on the requirements just PEP may be enough

to pass the quality control, in other case a mechanical polishing might be consider prior to the PEP processing. Interestingly the roughness measurements indicated the lower roughness for the EP treated sample, that might be connected with the more uniform EP etching, instead some macro-waviness plus pitting like defect were presented on the PEP treated sample sufficiently increased the roughness. Most likely the optical tools are not the ideal methods to evaluate the surface roughness in such situation.

6.7.5   Damaged layer

The damaged layer plays a significant role in the surface preparation of the substrates for the accelerators needs as it was already discussed. Conventionally, most of the protocols are removing a fixed value of thickness, thus avoiding the upper defects. With the scope of evaluation of the exact thickness of the damaged layer, it was found with the selected Nb substrates, that this layer exceeded a standard thickness of 200 µm. This data was obtained and confirmed on a series of samples (prepared from the same bath) and are relative specifically to this experiment and materials.

In our test we normally remove close to the E-XFEL protocol values of average thickness (150-200 µm). The E-XFEL uses sheets of Nb after lamination, meanwhile for our experiments the samples were produced from the deep-drawing production wastes. That is why, a test was done to identify the possible values of a damaged layer for our materials.

All the samples were cleaned and analyzed with the SEM (back-scattered electrons, COMPO mode) micrography prior to the electroerosion cutting the cross-section part of the sample. After a series of lapping with steadily finer pads (P80, P160, P400, P800, P2000) cross section planes were prepared. The defective structure can be divided in 3 regions: the upper rough region (90 µm), mild defective region (210 µm), bulk region, where the quantity of defect is lowest (see **Figure 6.58**).
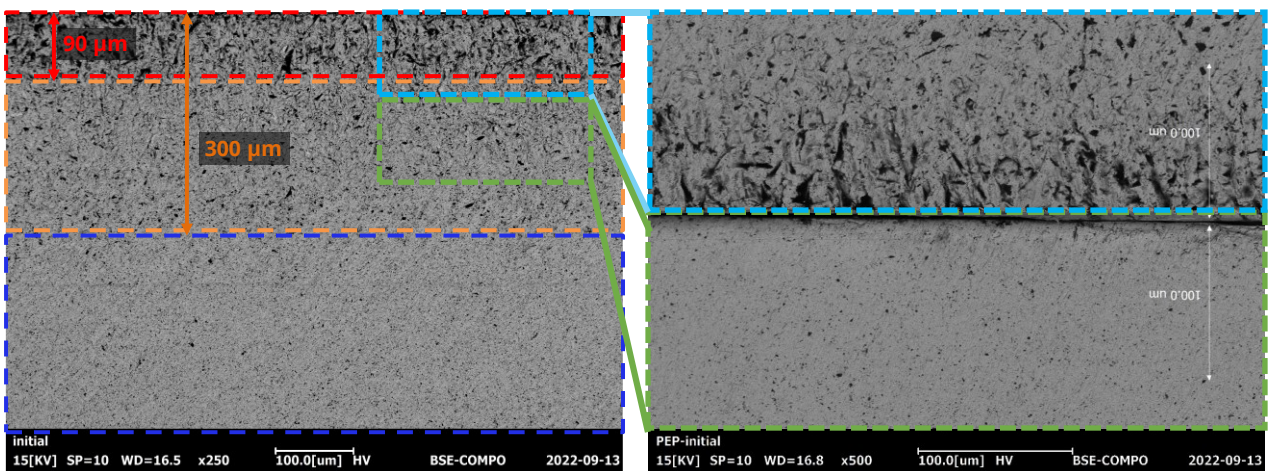
Figure 6.58: SEM micrography of non-treated Nb samples, and after 100 µm thickness removal

In practice, removing of only 50-150 μm are by chemical means will not be sufficient to achieve the bulk region (see **Figure 6.59**). We expect to further improve the surface quality after removing 300 μm via PEP.
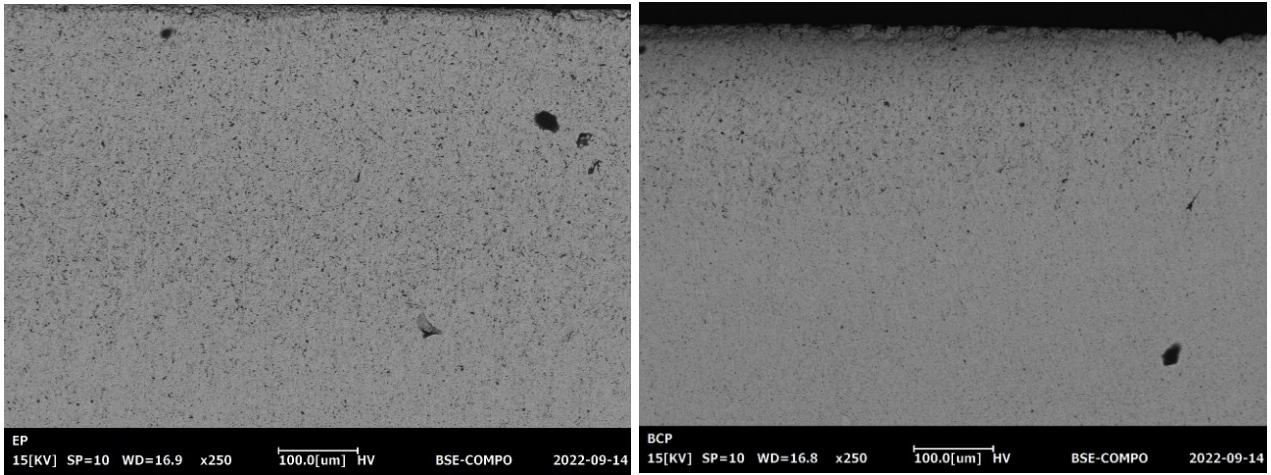
Figure 6.59: SEM microhraphy of the cross-section surfaces after EP (190 μm) and BCP (100 μm) treatments

Summary: The Nb material that was used in all our experiments has shown worser structure, compared to E-XFEL Nb sheets, in terms of defects thickness remained after production. A 300 μm layer (instead of 150 of XFEL protocol) has to be removed according to our observation and will become the standard in future tests with this type of samples.

Conclusions

The scope of the dissertation was devoted to the discovery, study, and application of innovative treatments for the superconducting radio frequency (SRF) cavities. Two techniques were studied: vibro-tumbling (VT) and plasma electrolytic polishing (PEP).

Vibrotumbling
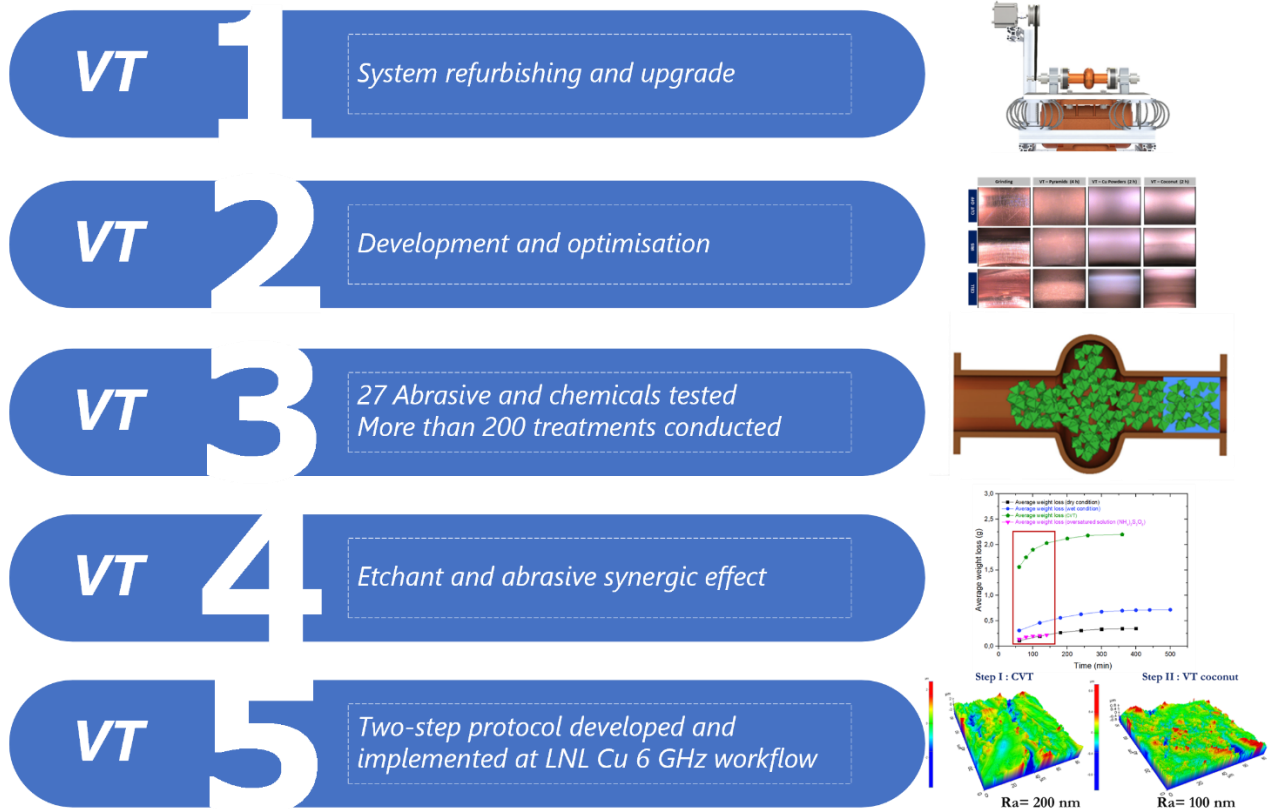
Figure I: Vibrotumbling dissertation activity summary scheme

- The VT system was refurbished and updated in 2019. It consisted of an eccentric motor, step motor for rotation, frequency changer and mounting accessories for the cavity.
- Working parameters were optimized: working frequency (190 ± 10 Hz), abrasive and media volume feeling (75% of internal volume, wet conditions - 12 ± 3 mL of liquids) as well as time. A saturation of the erosion process is observed after 300 minutes; thus, the processing time is suggested to be around 1 h for a maximal erosion efficiency for the first step, and around 1h for the coconut finishing.
- A list of 20 different abrasives and 7 chemicals were tested in dry and wet conditions. More than 150 test vibro-finishing treatments were done onto the elliptical 6 GHz cavities (both Nb and Cu)

and around 20 treatments on the coupons inserted in the 6 GHz dummy cavities. A total of 22 Cu 6 GHz cavities were prepared with a complete protocol, that included VT.

- A chemical etchant solution was found, that enabled 4 times increase of the erosion rate. A synergic effect between the oversaturated solution of ammonium persulphate and RPMS abrasive was identified and calculated to be around 70 %.
- A final protocol of mechanical treatment was developed and since 2020 the VT has been placed in the routine preparation schedule of every LNL 6 GHz cavity. The new protocol of Cu VT processing involves two stages of treatments:

  I. chemical VT, RPMS abrasive and 15 mL of oversaturated solution of $(NH_4)_2S_2O_8$, high erosion rate up to 24 µm/min;

  II. fine VT, coconut shell abrasive, erosion rate close to 0 µm/min.

- The final processing can reach ~100 nm internal surface cavity cell roughness, eliminating any defects from the production stage. Thus, allowing the complete elimination of the grinding process that produces scratched surface and could not remove deep defects, resulting in higher roughness of ~ 500 nm at least. Another advantage of VT is that it is a fully automatic process, contrary to grinding where a mechanical technician is involved for several hours.

Plasma electrolytic polishing
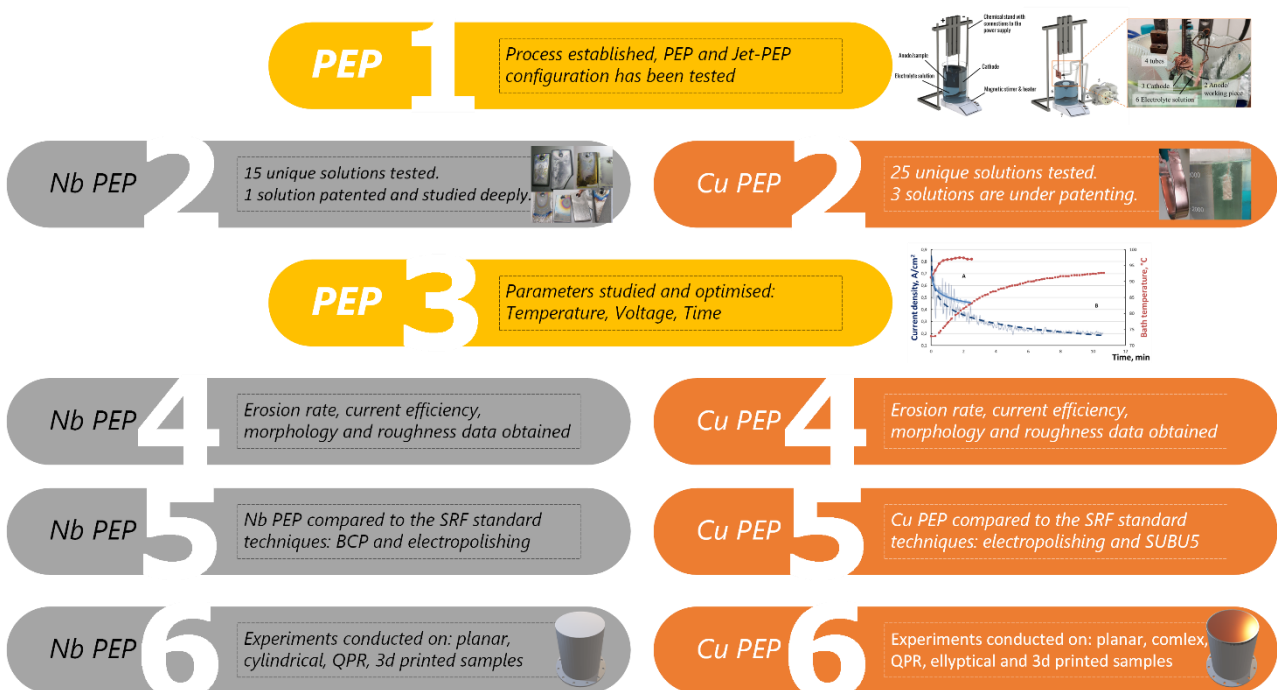
Figure II: Plasma electrolytic polishing dissertation activity summary scheme

The PEP technique was studied and developed to polish Nb and Cu substrates. A total of 40 different solutions were tested. Different systems, cathodes were tested, including a Jet-PEP

190

configuration. Parameters dependences were studied, such as: bath temperature, applied voltage, current density, process time. Characterization was done by linear profilometer, scanning electron and optical microscopies. During the PhD period, more than 100 experiments were done on various samples. Most of the treatments were done on the planar samples. However, PEP scaling on more complex geometry substrates was also a part of this work. In particular, PEP was tested on 6 GHz dummy-cavities, cylindrical samples, QPR samples, 3d printed materials.

Point by point the role of the different process parameters were explored and the results achieved with miscellaneous considerations are explained below.

- *Original PEP solutions.* Three solutions for Cu PEP were developed ("SUBU5", "Pyrophosphate", "Phosphate") and one solution was developed for Nb processing ($NH_4F:NaF = 3:1$). Nb solution has been already patented [337]. The three Cu PEP solutions are currently under patent evaluation.

- *Cathode.* According to the sources [249] the cathode to anode ratio is recommended to be 10:1. We confirm this suggestion. The PEP process is less sensible to the geometry of electrodes, thus the cathode has not necessarily to copy the anode shape. In case of Nb PEP, a contamination was found from the stainless-steel cathode, to avoid such issues, a Nb cathode was produced, for future treatments.

- *Jet-PEP* configuration requires a fluxing of the electrolytic solution onto the anode surface from the cathode nozzle. A discharge process during the jet-processing has been proved, however the stable polishing effect has not been achieved yet.

- *Voltage.* A working voltage range 300 ± 20 V was identified for all solutions. Higher voltage shows lower erosion rate for Nb PEP. Instead, Cu PEP in "SUBU5" solution has an inverse behaviour.

- *Temperature* may influence the quality of the processing, for Nb PEP low starting and average temperatures (less than 80 C°) cause undesired oxidation (still with polishing effect). Deviation of the protocolled temperature range might severely decrease the reflectivity and raise roughness. On the other hand, temperature seams less critical for Cu PEP in "SUBU5" solution. Uniform low roughness surface can be achieved in a wide range of temperatures: 70 – 95 C°. Generally, temperature of PEP solutions closed to water boiling point are beneficial in terms of final surface quality. In case of "phosphate" and "pyrophosphate" based solutions high temperature might cause oxidation instantly after the processing bath, thus a deoxidising solution (dilute solution of sulfamic or citric acid solution) is necessary to apply. It is as well important to have a stable temperature working range, as the high area samples in small volume bath will instantly heat up the solution. A correct planning of the sample and bath dimension ratio should be done. Water correction of the solution must be considered, as during the process a huge quantity of water vapours may be formed, consequently the waterline of the solution may decrease.

- *Current Density.* The polishing rate is directly connected with the current density of the process. It was noted that different higher cathode/anode ratio leads to higher erosion rates. The current

density value depends on the solution (and its conductivity) as well. Interestingly, a direct correlation between the electrode distance and current density was not found.

- *Erosion Rate.* The erosion (polishing) rates were studied: for Nb it is in the range of 2-8 μm/min, for Cu the range is wider 3 – 30 μm/min. The study has shown that Cu current efficiencies (CE) values for the "phosphate" and "pyrophosphate" solutions are similar to the standard electrolysis ones 80-100 %. PEP solution "SUBU5" is characterised with atypical CE, exceeding a 100% theoretical barrier, achieving up to the 150 % (not explainable by the joint electrochemical and chemical polishing effect of SUBU). Meanwhile the Nb PEP CE shows a lower value at 30 - 50 %. This leads us to think of different mechanisms for PEP depending on the material and solution used.

- *Comparison with SRF standard polishing processes*. The developed solution has been compared to its competitors from SRF standard protocol lists. Cu PEP has shown a superior polishing rate higher by 10-100x times than SUBU chemical or electrochemical polishing methods. Nb PEP, instead 4-10x times faster compared to the BCP and EP. Notably, PEP shows a higher smoothing efficiency. Smoother surface can be achieved via PEP rather than EP (up to 3 times) and chemical polishing solutions at the parity of the removed layer. All the solutions are based on diluted salt/acid solutions, much safer and sustainable than the standard ones.

- *Scaling to large surface areas / QPR.* The polishing of both Nb and Cu QPR was completed. Unfortunately, a list of issues was obtained (Cu QPR PEP: rapid heating and destruction of brazing material between the Nb and Cu metals; Nb QPR PEP: formation of deep and solid oxides, resulted in crater-like defects, occasional oxide formation). The encountered problems have shown the critical relationship between the treated area and bath dimensions (cathode area, solution volume). In case of QPR samples in compact systems (5 L beaker bath) these issues can emerge, it is, as well, explainable by complexity of maintaining stable temperature conditions following the protocol requirements, which we know is a critical parameter. An estimation of power need for PEP of 1.3 GHz cavity processing has shown at least a 30 kW in a horizontal setup for Nb PEP. The heat produced due to the Joule effect is used for heating the solution, and thus lowering the current density, which is beneficial both for the process and the resulting surface. Strategies to address the high power need may include the usage of local Jet-PEP, pulsing (or even pulse-reverse) mode of PEP, and lowering the voltage after triggering the plasma, as suggested in literature [255].

- *6 GHz Elliptical cavities.* During the PEP of elliptical cavities, a series of difficulties was encountered as well. The process required a high current regime; hence the isolation approaches were tested: isolating tape, plastic foils, PVDF tapes. The ignition of the process in bath with external cathode configuration did not start internally, therefore a series of test were conducted with internal cathodes and different approaches of isolation. In order to compile with high cathode/anode ratio a double cathode (one internal and one external) configuration was used. A limited success of internal polishing was obtained. A compact 6 GHz cavity substrate has been a

difficult configuration to polish with PEP, due to the short distances between the electrodes and the amount of vapour-gas mixture that is produced and consequently limit the polishing.

- *Additive Manufacturing substrates.* Samples with 3d printed structure were successfully polished with the PEP technique. The PEP processing has shown extreme performance in lowering the roughness (from tens of μm to < 1 μm) and levelling the surface being a chemical non-destructive method of polishing. Standard approaches (chemical and electrochemical polishings) in most of the cases showed significantly higher roughness and were not able to level both the macro and micro defects. However, few hundred micrometres removed might be needed to achieve 100-300 nm roughness. The PEP is a promising candidate for polishing of AM materials, of which high roughness is one of the principal defects, that limits its usage in the fields, where the surface quality is fundamental.

In conclusion, two different PEP processes for Nb and Cu, respectively, were designed and developed in this work with original patented (or patent pending) solutions. The obtained results are remarkable because prior to this work, no PEP solutions for these materials existed in the literature capable of producing mirror-like surfaces. The processes developed are superior to traditional processes (EP and chemical polishing) both in erosion speed and in final quality achieved, visible to the naked eye and confirmed by roughness, reflectivity, and SEM microscopy measurements.

The main advantage, however, lies in the composition of the chemical bath, which consists of very dilute aqueous solutions of salts. In contrast, all chemical and electrochemical copper and niobium polishing technologies require very aggressive chemical baths composed of concentrated acids, in the case of Nb also with hydrofluoric acid, with clear environmental and safety problems.

Being able to scale up to resonant cavities the processes developed in this PhD work would represent a unique technological breakthrough for SRF, both in terms of production efficiency (the polishing process would be reduced from the current 1-2 days to a few hours), and especially in terms of safety for operators and environmental sustainability, as indicated by the European Strategy for Particle Physics - Accelerator R&D Roadmap [247].

Future developments

Scaling of the working bath has been already initiated to the 50 L volume. Thus, the ultimate engineering work is remaining, for the system heating implementation. Such upgrade will allow more stable processing of the Nb QPR samples and other details bigger than usual planar samples.

The development of 1.3 GHz polishing separate system is scheduled for the 2023 and 2024. The bigger dimensions of elliptical cavity will simplify issues of PEP polishing that we experienced with 6 GHz compact cavities.

Jet-PEP processing is an alternative route. More attention will be paid to the micromachining technologies and already available studies of Jet-PEP treatments.

Bibliography

[1]   'ELSA - Particle Accelerators Around the World'. http://www-elsa.physik.uni-bonn.de/accelerator_list.html (accessed Nov. 14, 2022).

[2]   T. Feder, 'Accelerator school travels university circuit', *Phys. Today*, vol. 63, no. 2, pp. 20–22, Feb. 2010, doi: 10.1063/1.3326981.

[3]   S. Möller, *Accelerator technology: applications in science, medicine and industry*. Cham: Springer, 2020.

[4]   A. Gurevich, 'Superconducting Radio-Frequency Fundamentals for Particle Accelerators', *Rev. Accel. Sci. Technol.*, vol. 05, pp. 119–146, Jan. 2012, doi: 10.1142/S1793626812300058.

[5]   A. P. Banford and G. H. Stafford, 'The feasibility of a superconducting proton linear accelerator', *J. Nucl. Energy Part C Plasma Phys. Accel. Thermonucl. Res.*, vol. 3, no. 4, p. 287, 1961.

[6]   E. Cenni, 'SRF accelerator cavities', presented at the EASISchool 2 on Cryogenics, Paris, CEA, France, Sep. 30, 2019. Accessed: Nov. 23, 2022. [Online]. Available: https://indico.cern.ch/event/792215/contributions/3408423/

[7]   J. D. Jackson, *Classical electrodynamics*. American Association of Physics Teachers, 1999.

[8]   C. Antoine, 'Materials and surface aspects in the development of SRF Niobium cavities', EuCARDBOO-2012-001, 2012.

[9]   A. A. Abrikosov, L. P. Gorkov, and I. E. Dzyaloshinskii, 'On the application of quantum-field-theory methods to problems of quantum statistics at finite temperatures', *Sov Phys JETP*, vol. 9, no. 3, pp. 636–641, 1959.

[10]   J. P. Turneaure, J. Halbritter, and H. A. Schwettman, 'The surface impedance of superconductors and normal conductors: The Mattis-Bardeen theory', *J. Supercond.*, vol. 4, no. 5, pp. 341–355, 1991.

[11]   M. A. Hein, 'Microwave properties of superconductors', in *Microwave Superconductivity*, Springer, 2001, pp. 21–53.

[12]   PJRay, *English: Overview of superconducting critical temperatures for a variety of superconducting materials since the first discovery in 1911*. 2015. Accessed: Nov. 14, 2022. [Online]. Available: https://commons.wikimedia.org/w/index.php?curid=46193149

[13]   D. Proch, 'Superconducting cavities for accelerators', *Rep. Prog. Phys.*, vol. 61, no. 5, p. 431, 1998.

[14]   G. Ciovati, P. Kneisel, and A. Gurevich, 'Measurement of the high-field Q drop in a high-purity large-grain niobium cavity for different oxidation processes', *Phys. Rev. Spec. Top.-Accel. Beams*, vol. 10, no. 6, p. 062002, 2007.

[15]   G. Ciovati, G. Myneni, F. Stevie, P. Maheshwari, and D. Griffis, 'High field Q slope and the baking effect: Review of recent experimental results and new data on Nb heat treatments', *Phys. Rev. Spec. Top. - Accel. Beams*, vol. 13, no. 2, p. 022002, Feb. 2010, doi: 10.1103/PhysRevSTAB.13.022002.

[16]   B. Visentin, M. F. Barthe, V. Moineau, and P. Desgardin, 'Involvement of hydrogen-vacancy complexes in the baking effect of niobium cavities', *Phys. Rev. Spec. Top.-Accel. Beams*, vol. 13, no. 5, p. 052002, 2010.

[17]   H. Lengeler, 'RF superconductivity for high energy accelerators', CERN, CM-P00061169, 1986. [Online]. Available: https://cds.cern.ch/record/171756/files/CM-P00061169.pdf

[18]   J. P. Turneaure and N. T. Viet, 'SUPERCONDUCTING Nb TM $_{010}$ MODE ELECTRON-BEAM WELDED CAVITIES', *Appl. Phys. Lett.*, vol. 16, no. 9, pp. 333–335, May 1970, doi: 10.1063/1.1653215.

[19]   C. Benvenuti, N. Circelli, and M. Hauer, 'Niobium films for superconducting accelerating cavities', *Appl. Phys. Lett.*, vol. 45, no. 5, pp. 583–584, Sep. 1984, doi: 10.1063/1.95289.

[20]   A. W. Chao and K. H. Mess, *Handbook of Accelerator Physics and Engineering*. World Scientific, 2013.

[21]   C. W. Leemann, D. R. Douglas, and G. A. Krafft, 'THE CONTINUOUS ELECTRON BEAM ACCELERATOR FACILITY: CEBAF at the Jefferson Laboratory', *Annu. Rev. Nucl. Part. Sci.*, vol. 51, no. 1, pp. 413–450, Dec. 2001, doi: 10.1146/annurev.nucl.51.101701.132327.

[22]   T. Aaltonen *et al.*, 'Evidence for a Particle Produced in Association with Weak Bosons and Decaying to a Bottom-Antibottom Quark Pair in Higgs Boson Searches at the Tevatron', *Phys. Rev. Lett.*, vol. 109, no. 7, p. 071804, Aug. 2012, doi: 10.1103/PhysRevLett.109.071804.

[23]   S. Myers and E. Picasso, 'The design, construction and commissioning of the CERN large Electron–Positron collider', *Contemp. Phys.*, vol. 31, no. 6, pp. 387–403, Nov. 1990, doi: 10.1080/00107519008213789.

[24]   the FCC Collaboration *et al.*, 'HE-LHC: The High-Energy Large Hadron Collider: Future Circular Collider Conceptual Design Report Volume 4', *Eur. Phys. J. Spec. Top.*, vol. 228, no. 5, pp. 1109–1382, Jul. 2019, doi: 10.1140/epjst/e2019-900088-6.

[25]   D. Gonnella *et al.*, 'The LCLS-II HE high q and gradient r&d program', Fermi National Accelerator Lab.(FNAL), Batavia, IL (United States); Thomas ..., 2019.

[26]   B. Horst *et al.*, 'Experiences on improved cavity preparation cycles with a vision on industrialization of the XFEL cavity preparation', in *SRF'09*, Berlin, Germany, 2009. [Online]. Available: https://accelconf.web.cern.ch/SRF2009/papers/thppo072.pdf

[27]   M. Vogel, *Accelerator Physics, 3rd edn., by SY Lee: Scope: textbook. Level: graduate students*. Taylor & Francis, 2012.

[28]   H. Padamsee, *RF Superconductivity: Science, Technology, and Applications*, 1st ed. Wiley, 2009. doi: 10.1002/9783527627172.

[29]   C. Pira, 'Nb thick films in 6 GHz superconducting resonant cavities', PhD Thesis, Università degli Studi di Padova, 2018.

[30]   M. Weiss, 'Introduction to rf linear accelerators', p. 42, 1994.

[31]   J.-L. Biarrotte, 'High power proton/deuteron accelerators', in *Proc. SRF*, 2013. [Online]. Available: https://accelconf.web.cern.ch/srf2013/papers/moiob01.pdf

[32]   J. K. Sekutowicz, 'Superconducting elliptical cavities', 2012, doi: 10.48550/ARXIV.1201.2598.

[33]   D. Rice and D. Rubin, '1.1 Colliding Beams at the Cornell Electron Storage Ring CESR'.

[34]   J. Auerhammer *et al.*, 'The S-DALINAC facility—Operational experience from the accelerator and the experimental installations', *Nucl. Phys. A*, vol. 553, pp. 841–844, 1993.

[35]   G. Bisoffi *et al.*, 'ALPI QWR and S-RFQ operating experience', in *Proceedings of the 13th Workshop on RF Superconductivity, Peking University, Beijin, China*, 2007.

[36]   G. Fortuna *et al.*, 'The ALPI project at the Laboratori Nazionali di Legnaro', *Nucl. Instrum. Methods Phys. Res. Sect. Accel. Spectrometers Detect. Assoc. Equip.*, vol. 287, no. 1–2, pp. 253–256, Feb. 1990, doi: 10.1016/0168-9002(90)91803-J.

[37]   E. Kugler, 'The ISOLDE facility', *Hyperfine Interact.*, vol. 129, no. 1, pp. 23–42, 2000.

[38]   J. A. Nolen, 'Accelerator complex for a radioactive ion beam facility at ATLAS', in *Proceedings Particle Accelerator Conference*, 1995, vol. 1, pp. 354–356.

[39]   N. Holtkamp, 'Status of the SNS linac: an overview', in *LINAC*, 2004, vol. 4, p. 5.

[40]   C. Leemann, 'The CEBAF superconducting accelerator-an overview', 1986.

[41]   J. N. Galayda, 'The LCLS-II: A high power upgrade to the LCLS', SLAC National Accelerator Lab., Menlo Park, CA (United States), 2018.

[42]   S. Kurokawa, K. Satoh, and E. Kikutani, 'Accelerator design of the KEK B-factory', National Lab. for High Energy Physics, 1991.

[43]   M. Ball *et al.*, 'The PIP-II conceptual design report', Argonne National Lab.(ANL), Argonne, IL (United States); Fermi National ..., 2017.

[44]   A. Jansson *et al.*, 'Overview of ESS Beam Diagnostics', in *Proceedings of the First International Beam Instrumentation Conference (IBIC'12). Tsukuba, Japan*, 2012, pp. 543–549.

[45]   S. U. De Silva, 'Superconducting Cavities of Interesting Shapes (Non-Elliptical Cavities)', 2020.

[46]   K. Saito, 'Surface smoothness for high gradient niobium SC RF cavities', in *Proceeding of the XI workshop on RF Superconductivity, Lubeck*, 2003, vol. 516, no. 213.

[47]   G. Wu *et al.*, 'Investigations of surface quality and SRF cavity performance', 2012, doi: 10.48550/ARXIV.1206.6331.

[48]   C. Xu, C. E. Reece, and M. J. Kelley, 'Simulation of nonlinear superconducting rf losses derived from characteristic topography of etched and electropolished niobium surfaces', *Phys. Rev. Accel. Beams*, vol. 19, no. 3, p. 033501, 2016.

[49] V. Palmieri and R. Vaglio, 'Thermal contact resistance at the Nb/Cu interface as a limiting factor for sputtered thin film RF superconducting cavities', *Supercond. Sci. Technol.*, vol. 29, no. 1, p. 015004, Jan. 2016, doi: 10.1088/0953-2048/29/1/015004.

[50] H. Padamsee, 'SRF Accelerators Flourish In a Golden Age', 2015.

[51] V. A. Garcia Diaz, 'Nb thick films for superconducting radiofrequency cavities', Università degli Studi di Ferrara, 2021.

[52] A. Grassellino, 'Field-dependent losses in superconducting niobium cavities', University of Pennsylvania, 2011.

[53] J. Knobloch, 'The "Q disease" in superconducting niobium RF cavities', in *AIP Conference Proceedings*, 2003, vol. 671, no. 1, pp. 133–150.

[54] H. Padamsee, 'Calculations for breakdown induced by "Large defects" in superconducting niobium cavities', *IEEE Trans. Magn.*, vol. 19, no. 3, pp. 1322–1325, May 1983, doi: 10.1109/TMAG.1983.1062561.

[55] P. Kneisel *et al.*, 'Review of ingot niobium as a material for superconducting radiofrequency accelerating cavities', *Nucl. Instrum. Methods Phys. Res. Sect. Accel. Spectrometers Detect. Assoc. Equip.*, vol. 774, pp. 133–150, Feb. 2015, doi: 10.1016/j.nima.2014.11.083.

[56] H. Tian and C. E. Reece, 'Evaluation of the diffusion coefficient of fluorine during the electropolishing of niobium', *Phys. Rev. Spec. Top. - Accel. Beams*, vol. 13, no. 8, p. 083502, Aug. 2010, doi: 10.1103/PhysRevSTAB.13.083502.

[57] H. Tian, S. G. Corcoran, C. E. Reece, and M. J. Kelley, 'The Mechanism of Electropolishing of Niobium in Hydrofluoric–Sulfuric Acid Electrolyte', *J. Electrochem. Soc.*, vol. 155, no. 9, p. D563, 2008, doi: 10.1149/1.2945913.

[58] L. Zhao, 'Sulfur residues in niobium electropolishing', 2011.

[59] H. Tian and C. E. Reece, 'Quantitative EP Studies and Results for SRF Production', in *contributed to this conference*.

[60] L. Lilje *et al.*, 'Achievement of in the superconducting nine-cell cavities for TESLA', *Nucl. Instrum. Methods Phys. Res. Sect. Accel. Spectrometers Detect. Assoc. Equip.*, vol. 524, no. 1–3, pp. 1–12, May 2004, doi: 10.1016/j.nima.2004.01.045.

[61] C. Z. Antoine, 'How to Achieve the Best SRF Performance: (Practical) Limitations and Possible Solutions', 2014, doi: 10.5170/CERN-2014-005.209.

[62] L. Lilje *et al.*, 'Improved surface treatment of the superconducting TESLA cavities', *Nucl. Instrum. Methods Phys. Res. Sect. Accel. Spectrometers Detect. Assoc. Equip.*, vol. 516, no. 2–3, pp. 213–227, Jan. 2004, doi: 10.1016/j.nima.2003.08.116.

[63] I. Kulik, V. Palmieri, R. Preciso, V. Ruzinov, and S. Stark, 'Chemical and electrochemical finishing of OFHC copper surface for Niobium sputtering', INFN-LNL, Annual report, 1994. [Online]. Available: https://www1.lnl.infn.it/~annrep/read_ar/1993/annual_report_1993.pdf

[64] A. Tsymbaliuk, 'Nb/Cu QWR superconductive cavities production for the ALPI upgrade in the framework of the SPES facility', Ph.D. Thesis, Università degli Studi di Ferrara, 2021.

[65] D. Gonnella *et al.*, 'Industrialization of the nitrogen-doping preparation for SRF cavities for LCLS-II', *Nucl. Instrum. Methods Phys. Res. Sect. Accel. Spectrometers Detect. Assoc. Equip.*, vol. 883, pp. 143–150, Mar. 2018, doi: 10.1016/j.nima.2017.11.047.

[66] D. Gonnella *et al.*, 'Industrial cavity production: Lessons learned to push the boundaries of nitrogen-doping', SLAC National Accelerator Lab., Menlo Park, CA (United States); Thomas ..., 2019.

[67] W. Singer, 'SRF Cavity Fabrication and Materials', 2014, doi: 10.5170/CERN-2014-005.171.

[68] K. K. Schulze, 'Preparation and Characterization of Ultra-High-Purity Niobium', *JOM*, vol. 33, no. 5, pp. 33–41, May 1981, doi: 10.1007/BF03354422.

[69] K. Schulze, O. Bach, D. Lupton, and F. Schreiber, 'Purification of niobium', in *Niobium-Proceedings of the international symposium*, 1984.

[70] V. Palmieri, 'Seamless cavities: the most creative topic in RF Superconductivity', *Part Accel*, vol. 61, pp. 215–239, 1998.

[71]   V. Palmieri, R. Preciso, V. L. Ruzinov, S. Y. Stark, and S. Gambalonga, 'Forming of seamless high beta accelerating cavities by the spinning technique', *Nucl. Instrum. Methods Phys. Res. Sect. Accel. Spectrometers Detect. Assoc. Equip.*, vol. 342, no. 2–3, pp. 353–356, 1994.

[72]   V. Palmieri, R. Preciso, R. VL, and S. Y. Stark, 'SEAMLESS 1.5 GHz CAVITIES OBTAINED BY SPINNING A CIRCULAR BLANK OF COPPER OR NIOBIUM'.

[73]   L. Cerasti, 'Chemical and Electrochemical treatments of Copper components for special applications', Master in surface treatments for industrial applications, Università degli studi di Padova, 2016.

[74]   V. Palmieri, 'Metal forming technology for the fabrication of seamless Superconducting radiofrequency cavities for particle accelerators', *MATEC Web Conf.*, vol. 21, p. 04015, 2015, doi: 10.1051/matecconf/20152104015.

[75]   P. Frigola *et al.*, 'Advance Additive Manufacturing Method for SRF Cavities of Various Geometries', *Proc. 17th Int. Conf. RF Supercond.*, vol. SRF2015, p. 4 pages, 1.135 MB, 2015, doi: 10.18429/JACOW-SRF2015-THPB042.

[76]   F. Motschmann, R. Gerard, and F. Gilles, 'Purification of Selective Laser Melting Additive Manufactured Niobium for Superconducting RF-Applications Transactions on Applied Superconductivity', *IEEE Trans. Appl. Supercond.*, vol. 29, no. 5, pp. 1–5, Aug. 2019, doi: 10.1109/TASC.2019.2900521.

[77]   R. Gerard, 'Additive manufacturing for RF and superconducting RF applications', in *Proceedings of the Colloque Fabrication Additive Physique des Deux Infinis, Bures-sur-Yvette, France*, 2018, vol. 14.

[78]   'DIAM workgroup', *INFN Sezione di Padova*. https://www.pd.infn.it/eng/diam/ (accessed Nov. 14, 2022).

[79]   T. Grundey, J. Labedzki, P. Schütz, and U. Trinks, 'The superconducting accelerating cavities for the Tritron', *Nucl. Instrum. Methods Phys. Res. Sect. Accel. Spectrometers Detect. Assoc. Equip.*, vol. 306, no. 1–2, pp. 21–26, 1991.

[80]   G. W. Mellors and S. Senderoff, 'Electrodeposition of Coherent Deposits of Refractory Metals: I. Niobium', *J. Electrochem. Soc.*, vol. 112, no. 3, p. 266, 1965.

[81]   C. Graeme-Barber, B. J. Maddock, R. A. Popley, and P. N. Smedley, 'Tubular niobium/copper conductors for ac superconductive power transmission', *Cryogenics*, vol. 12, no. 4, pp. 317–318, 1972.

[82]   S. Parussatti, 'Mechanical Technologies Division, MT : Mise au point d'un appareillage de laboratoire pour l'étude des courants pulsés. Aspect théorique et application à un bain d'argent cyanuré', Note Technique-MT-SM-94-10, Nov. 1994. [Online]. Available: https://cds.cern.ch/record/65951

[83]   L. L. Amador *et al.*, 'Electrodeposition of copper applied to the manufacture of seamless superconducting rf cavities', *Phys. Rev. Accel. Beams*, vol. 24, no. 8, p. 082002, 2021.

[84]   G. Rosaz, 'Cu electrodeposition for the manufacturing of seamless SRF cavities'.

[85]   C. Hauviller, 'Fully hydroformed RF cavities', in *Proceedings of the 1989 IEEE Particle Accelerator Conference,.'Accelerator Science and Technology*, 1989, pp. 485–487.

[86]   H. Padamsee *et al.*, 'Superconducting rf activities at Cornell University', in *Proceedings of the 4th Workshop on RF Superconductivity [Kojima 1990], KEK Report*, 1987, pp. 89–21.

[87]   M. Yamanaka, H. Inoue, H. Shimizu, K. Umemori, J. A. Hocker, and T. Tajima, 'Hydroforming SRF cavities from seamless niobium tubes', *THPB041these Proc. SRF2015 Whistler Can.*, 2015.

[88]   M. Yamanaka *et al.*, 'Hydroforming SRF Three-cell Cavity from Seamless Niobium Tube', in *7th Int. Particle Accelerator Conf.(IPAC'16), Busan, Korea, May 8-13, 2016*, 2016, pp. 2170–2173.

[89]   C. Compton *et al.*, 'Studies of alternative techniques for niobium cavity fabrication', *Proc. SRF2007 Peking Univ. Beijing China WEP01*, 2007.

[90]   K. Umemori *et al.*, 'Comparison of cavity fabrication and performances between fine grains, large grains and seamless cavities', in *Proc. Int. Conf. on RF Superconductivity SRF2015 (Whistler, BC, Canada, 16 December)*, 2015, pp. 1006–11.

[91]   T. Sokolowski, K. Gerke, M. Ahmetoglu, and T. Altan, 'Evaluation of tube formability and material characteristics: hydraulic bulge testing of tubes', *J. Mater. Process. Technol.*, vol. 98, no. 1, pp. 34–40, 2000.

[92]   Y. Aue-U-Lan, G. Ngaile, and T. Altan, 'Optimizing tube hydroforming using process simulation and experimental verification', *J. Mater. Process. Technol.*, vol. 146, no. 1, pp. 137–143, Feb. 2004, doi: 10.1016/S0924-0136(03)00854-9.

[93]   K. Watanabe, H. Hayano, and Y. Iwashita, 'Cavity inspection and repair techniques', *SRF Chic. USA*, 2011.

[94]   C. Mayer-Laigle, C. Gatumel, and H. Berthiaux, 'Mixing dynamics for easy flowing powders in a lab scale Turbula ® mixer', *Chem. Eng. Res. Des.*, vol. 95, pp. 248–261, Mar. 2015, doi: 10.1016/j.cherd.2014.11.003.

[95]   C. Cooper, K. Saito, B. Bullock, S. Joshi, and A. Palczewski, 'CENTRIFUGAL BARREL POLISHING OF CAVITIES WORLDWIDE', p. 5, 2011.

[96]   Y. Goulong, 'Development of a new mechanical surface treatment for the internal finishing of 6 GHz superconducting cavities', Master in surface treatments for industrial applications, Università degli Studi di Padova, 2013. [Online]. Available: https://surfacetreatments.infn.it/development-of-a-new-mechanical-surface-treatment-for-the-internal-finishing-of-6-ghz-superconducting-cavities-master-thesis-guolong-yu/

[97]   A. Palczewski, 'R&D progress in SRF surface preparation with centrifugal barrel polishing (cbp) for both Nb and Cu', Thomas Jefferson National Accelerator Facility (TJNAF), Newport News, VA (United States), JLAB-ACC-13-1699; DOE/OR/23177-2820, Sep. 2013. Accessed: Nov. 15, 2022. [Online]. Available: https://www.osti.gov/biblio/1164417

[98]   L. Lazzaroni, 'Chemical Vibro-Tumbling (CVT) technique: a new approach to Cu surfaces finishing', Master in surface treatments for industrial applications, Università degli Studi di Padova, 2019.

[99]   O. Hryhorenko, 'Development and optimization of mechanical polishing process for superconducting accelerating cavities', PhD Thesis, 2019. [Online]. Available: http://www.theses.fr/2019SACLS566/document

[100]   O. Hryhorenko, C. Antoine, M. Chabot, and D. Longuevergne, 'Metallographic Polishing Pathway to the Future of Large Scale SRF Facilities', *Proc. 19th Int. Conf. RF Supercond.*, vol. SRF2019, p. 5 pages, 9.407 MB, 2019, doi: 10.18429/JACOW-SRF2019-THP002.

[101]   J. Seo, 'A review on chemical and mechanical phenomena at the wafer interface during chemical mechanical planarization', *J. Mater. Res.*, vol. 36, no. 1, pp. 235–257, 2021.

[102]   O. Hryhorenko, 'A private conversation', Dec. 28, 2022.

[103]   G. Petzow, *Metallographic Etching, 2nd Edition: Techniques for Metallography, Ceramography, Plastography*. ASM International, 1999.

[104]   M. L. Kinter, I. Weissman, and W. W. Stein, 'Chemical polish for niobium microwave structures', *J. Appl. Phys.*, vol. 41, no. 2, pp. 828–829, 1970.

[105]   V. Palmieri, F. Stivanello, S. Y. Stark, C. Roncolato, and M. Valentino, 'Besides the standard niobium bath chemical polishing', in *Proceedings of the 10th Workshop on RF Superconductivity*, 2001, p. 408.

[106]   P. Kneisel, 'Surface preparation of niobium', 1980.

[107]   C. Z. Antoine, A. Aspart, M. Berthelot, J. P. Poupeau, F. Valin, and Y. Gasser, 'Morphological and chemical studies of Nb samples after various surface treatments', SIS-2002-103, 1999.

[108]   C. Xu, H. Tian, C. E. Reece, and M. J. Kelley, 'Topographic power spectral density study of the effect of surface treatment processes on niobium for superconducting radio frequency accelerator cavities', *Phys. Rev. Spec. Top. - Accel. Beams*, vol. 15, no. 4, p. 043502, Apr. 2012, doi: 10.1103/PhysRevSTAB.15.043502.

[109]   L. Zhao, C. E. Reece, and M. J. Kelley, 'Genesis of Topography in Buffered Chemical Polishing of Niobium for Application to Superconducting Radiofrequency Accelerator Cavities', in *18th International Conference on RF Superconductivity, JACoW, Lanzhou, China*, 2017.

[110]   L. Lilje, 'High Gradients in Superconducting Multi-Cell Cavities', in *11th Workshop on RF-Superconductivity*, 2003.

[111]   L. Popielarsk, 'Cavity Processing and Clean Assembly', presented at the SRF'21, Online, Jun. 24, 2021. [Online]. Available: https://indico.frib.msu.edu/event/38/attachments/159/1144/SRF2021_Cavity_Processing_and_Clean_Assembly_L_Popielarski.pdf

[112]   W. C. Elmore, 'Electrolytic polishing', *J. Appl. Phys.*, vol. 10, no. 10, pp. 724–727, 1939.

[113]   W. C. Elmore, 'Electrolytic polishing. II', *J. Appl. Phys.*, vol. 11, no. 12, pp. 797–799, 1940.

[114]   J. Edwards, 'The mechanism of electropolishing of copper in phosphoric acid solutions: II. The mechanism of smoothing', *J. Electrochem. Soc.*, vol. 100, no. 8, p. 223C, 1953.

[115]   C. Wagner, 'Contribution to the theory of electropolishing', *J. Electrochem. Soc.*, vol. 101, no. 5, p. 225, 1954.

[116]   *Circular of the Bureau of Standards no. 524: electrochemical constants*. National Bureau of Standards, 1953. Accessed: Nov. 15, 2022. [Online]. Available: http://archive.org/details/circularofbureau524unse

[117]   D. C. Grahame, M. A. Poth, and J. I. Cummings, 'The Differential Capacity of the Electrical Double Layer. The Role of the Anion', *J. Am. Chem. Soc.*, vol. 74, no. 17, pp. 4422–4425, 1952.

[118]   J. O. Bockris, B. E. Conway, and R. E. White, *Modern aspects of electrochemistry*, vol. 22. Springer Science & Business Media, 1992.

[119]   S. Glasstone, K. J. Laidler, and H. Eyring, 'The theory of rate processes; the kinetics of chemical reactions, viscosity, diffusion and electrochemical phenomena', McGraw-Hill Book Company, 1941.

[120]   H. Diepers, O. Schmidt, H. Martens, and F. S. Sun, 'A new method of electropolishing niobium', *Phys. Lett. A*, vol. 37, no. 2, pp. 139–140, 1971.

[121]   K. Saito, 'Superiority of Electropolishing over Chemical Polishing on High Gradients, 8th Workshop on RF Superconductivity', *Abano Terme Padova Italy*, 1997.

[122]   K. Saito, Y. Kojima, and T. Furuya, 'R and D of superconducting cavities at KEK', 1990.

[123]   T. Reid, Z. Conway, B. Guilfoyle, M. Kedzie, M. Kelly, and M.-K. Ng, 'New SRF Structures Processed at the ANL Cavity Processing Facility', *Proc. 19th Int. Conf. RF Supercond.*, vol. SRF2019, p. 4 pages, 1.614 MB, 2019, doi: 10.18429/JACOW-SRF2019-TUP018.

[124]   C. Cooper *et al.*, 'Cavity processing research laboratory at Fermilab: SRF cavity processing R&D', in *Proceedings of SRF*, 2011.

[125]   D. Sertore, 'SRF Cavity Fabrication', presented at the EASISchool 3, 2018. [Online]. Available: https://indico.cern.ch/event/883251/contributions/3846217/attachments/2111528/3551951/CavityFabrication-DSertore.pdf

[126]   C. Reece, S. Castagnola, P. Denny, and A. L. Mitchell, 'New Improved Horizontal Electropolishing System for SRF Cavities', *Proc. 20th Int. Conf. RF Supercond.*, vol. SRF2021, p. 4 pages, 0.539 MB, 2022, doi: 10.18429/JACOW-SRF2021-MOPTEV014.

[127]   F. Furuta, D. Bice, A. Crawford, and T. Ring, 'Fermilab EP Facility Improvement', *Proc. 19th Int. Conf. RF Supercond.*, vol. SRF2019, p. 3 pages, 1.294 MB, 2019, doi: 10.18429/JACOW-SRF2019-TUP022.

[128]   C. Reece, 'An Experimental Analysis of Effective EP Parameters for Low-Frequency Cylindrical Nb Cavities', *Proc. 19th Int. Conf. RF Supercond.*, vol. SRF2019, p. 5 pages, 1.953 MB, 2019, doi: 10.18429/JACOW-SRF2019-TUP029.

[129]   E. Viklund, L. Grassellino, S. Posen, T. Ring, and D. Seidman, 'Studies on the Fundamental Mechanisms of Niobium Electropolishing', *Proc. 20th Int. Conf. RF Supercond.*, vol. SRF2021, p. 3 pages, 0.417 MB, 2022, doi: 10.18429/JACOW-SRF2021-SUPCAV016.

[130]   F. Furuta, D. Bice, M. Martinello, and T. Ring, 'Extra-Cold EP Process at Fermilab', *Proc. 20th Int. Conf. RF Supercond.*, vol. SRF2021, p. 3 pages, 0.577 MB, 2022, doi: 10.18429/JACOW-SRF2021-MOPTEV012.

[131]   V. Chouhan *et al.*, 'Vertical electropolishing for 1.3 GHz single- and nine-cell superconducting niobium cavities: A parametric optimization and rf performance', *Phys. Rev. Accel. Beams*, vol. 22, no. 10, p. 103101, Oct. 2019, doi: 10.1103/PhysRevAccelBeams.22.103101.

[132]   V. Chouhan *et al.*, 'Vertical Electropolishing of 1.3 GHz Niobium Nine-cell SRF Cavity: Bulk Removal and RF Performance', *Proc. 29textsuperscriptth Linear Accel. Conf*, vol. LINAC2018, p. 3 pages, 1.065 MB, 2018, doi: 10.18429/JACOW-LINAC2018-TUPO068.

[133]   F. Eozenou *et al.*, 'Development of an advanced electropolishing setup for multicell high gradient niobium cavities', *Phys. Rev. Spec. Top.-Accel. Beams*, vol. 15, no. 8, p. 083501, 2012.

[134]   S. Calatroni *et al.*, 'Status of the EP Simulations and Facilities for the SPL', 2010.

[135] S. Jin, X. Lu, L. Lin, A. T. Wu, and K. Zhao, 'Buffered electropolishing parameters on niobium sheet', *Phys. Rev. Spec. Top. - Accel. Beams*, vol. 13, no. 6, p. 061001, Jun. 2010, doi: 10.1103/PhysRevSTAB.13.061001.

[136] G. Ciovati, H. Tian, and S. G. Corcoran, 'Buffered electrochemical polishing of niobium', *J. Appl. Electrochem.*, vol. 41, no. 6, pp. 721–730, Jun. 2011, doi: 10.1007/s10800-011-0286-z.

[137] K. Nii *et al.*, 'Vertical electropolishing of niobium nine-cell cavity with a cavity flipping system for uniform removal', in *19th International Conference on RF Superconductivity (SRF'19), Dresden, Germany, 30 June-05 July 2019*, 2019, pp. 467–469.

[138] A. F. Brown, 'Surface effects in plastic deformation of metals', *Adv. Phys.*, vol. 1, no. 4, pp. 427–479, 1952.

[139] 'Perfectionnements aux traitements électrolytiques des métaux', FR707526A, Jul. 09, 1931 Accessed: Nov. 15, 2022. [Online]. Available: https://patents.google.com/patent/FR707526A/

[140] P. Jacquet, 'Sur une nouvelle methode d'obtention de surfaces metalliques parfaitement polies', *CR Acad Sci Paris*, vol. 201, no. 27, pp. 1473–1475, 1935.

[141] P. A. Jacquet, 'Electrolytic method for obtaining bright copper surfaces', *Nature*, vol. 135, no. 3426, pp. 1076–1076, 1935.

[142] P. Jacquet, 'CR, 201 (1935), 1473; P. Jacquet', *Bull Soc Chim*, vol. 3, p. 705, 1936.

[143] P. A. Jacquet, 'The mechanism of electrolytic polishing of Copper', *CR Acad Sci*, vol. 202, p. 402, 1936.

[144] P. A. Jacquet, 'On the anodic behavior of copper in aqueous solutions of orthophosphoric acid', *Trans. Electrochem. Soc.*, vol. 69, no. 1, p. 629, 1936.

[145] J. A. Allen, 'Oxide films on electrolytically polished copper surfaces', *Trans. Faraday Soc.*, vol. 48, pp. 273–279, 1952.

[146] H. F. Walton, 'The anode layer in the electrolytic polishing of copper', *J. Electrochem. Soc.*, vol. 97, no. 7, p. 219, 1950.

[147] S. H. Glarum and J. H. Marshall, 'The anodic dissolution of copper into phosphoric acid: i. voltammetric and oscillatory behavior', *J. Electrochem. Soc.*, vol. 132, no. 12, p. 2872, 1985.

[148] E. C. W. Perryman, 'A New Solution for the Electrolytic Polishing of Copper and Copper-Base Alloys, Particularly Tin Bronze', *Metallurgia*, vol. 46, pp. 55–57, Jul. 1952.

[149] A. A. Taha, 'Study of the effect of ethylene glycol and glycerol on the rate of electropolishing of copper by the rotating disk technique', *Anti-Corros. Methods Mater.*, vol. 47, no. 2, pp. 94–104, Apr. 2000, doi: 10.1108/00035590010316458.

[150] G. M. El-Subruiti and A. M. Ahmed, 'Kinetic Study of Corrosion of Copper in Phosphoric Acid Tert-Butanol Electropolishing Mixtures':, *Port. Electrochimica Acta*, vol. 20, no. 4, pp. 151–166, 2002, doi: 10.4152/pea.200204151.

[151] A. M. Awad, N. A. A. Ghany, and T. M. Dahy, 'Removal of tarnishing and roughness of copper surface by electropolishing treatment', *Appl. Surf. Sci.*, vol. 256, no. 13, pp. 4370–4375, Apr. 2010, doi: 10.1016/j.apsusc.2010.02.033.

[152] N. M. Elmalah, S. M. Abd Elhaliem, A. M. Ahmed, and S. M. Ghozy, 'Effect of some organic aldehydes on the electropolishing of copper in phosphoric acid', *Int J Electrochem Sci*, vol. 7, no. 8, pp. 7720–7739, 2012.

[153] H. A. Rahman, A. H. E. Moustafa, and M. K. Awad, 'Potentiodynamic and quantum studies of some amino acids as corrosion inhibitors for copper', *Int. J. Electrochem. Sci.*, vol. 7, no. 2, pp. 1266–1287, 2012.

[154] A. A. Taha, A. M. Ahmed, H. A. Rahman, and F. M. Abouzeid, 'The effect of surfactants on the electropolishing behavior of copper in orthophosphoric acid', *Appl. Surf. Sci.*, vol. 277, pp. 155–166, 2013.

[155] V. Palmieri, V. L. Ruzinov, S. Y. Stark, and F. Stivanello, 'Electropolishing of seamless 1.5 GHZ OFHC copper cavities', in *Proc. of the 7th workshop on RF Superconductivity, Gif Sur Yvette, France*, 1995.

[156] J. D. Adams, J. P. Birabeau, J. Guerin, and S. Pousse, 'Procédés de préparation de surface de cuivre compatibles avec un dépôt de Niobium réalisé par pulvérisation cathodique: Présentation d'un bain de polissage chimique répondant à ce critère', CERN-Technical-Note-85, 1985. [Online]. Available: https://cds.cern.ch/record/2646136/files/85-SB-AC-B-3199-gp.pdf

[157]   Michbich, *A binary phase diagram showing the eutectic composition, eutectic temperature, and the eutectic point*. 2009. Accessed: Nov. 16, 2022. [Online]. Available: https://commons.wikimedia.org/wiki/File:Eutectic_system_phase_diagram.svg

[158]   P. Walden, 'Molecular weights and electrical conductivity of several fused salts', *Bull Acad Imper SciSt Petersburg*, vol. 1800, 1914.

[159]   J. T. P. Wier and F. H. Hurley, 'Electrodeposition of aluminum', US2446349A, Aug. 03, 1948 Accessed: Nov. 16, 2022. [Online]. Available: https://patents.google.com/patent/US2446349A/

[160]   F. H. Hurley and T. P. WIer, 'The electrodeposition of aluminum from nonaqueous solutions at room temperature', *J. Electrochem. Soc.*, vol. 98, no. 5, p. 207, 1951.

[161]   F. H. Hurley, 'Electrodeposition of aluminum', US2446331A, Aug. 03, 1948 Accessed: Nov. 16, 2022. [Online]. Available: https://patents.google.com/patent/US2446331A/en

[162]   H. Ohno, *Electrochemical aspects of ionic liquids*. Wiley Online Library, 2005.

[163]   R. D. Rogers and K. R. Seddon, *Ionic liquids IIIB: fundamentals, progress, challenges, and opportunities: transformations and processes*. ACS Publications, 2005.

[164]   A. P. Abbott and K. J. McKenzie, 'Application of ionic liquids to the electrodeposition of metals', *Phys. Chem. Chem. Phys.*, vol. 8, no. 37, pp. 4265–4279, 2006.

[165]   F. Endres and S. Z. El Abedin, 'Air and water stable ionic liquids in physical chemistry', *Phys. Chem. Chem. Phys.*, vol. 8, no. 18, pp. 2101–2116, 2006.

[166]   A. P. Abbott, J. C. Barron, K. S. Ryder, and D. Wilson, 'Eutectic-based ionic liquids with metal-containing anions and cations', *Chem. Eur. J.*, vol. 13, no. 22, pp. 6495–6501, 2007.

[167]   A. P. Abbott, G. Capper, K. J. McKenzie, A. Glidle, and K. S. Ryder, 'Electropolishing of stainless steels in a choline chloride based ionic liquid: an electrochemical study with surface characterisation using SEM and atomic force microscopy', *Phys. Chem. Chem. Phys.*, vol. 8, no. 36, pp. 4214–4221, 2006.

[168]   S. Zein El Abedin and F. Endres, 'Ionic liquids: the link to high-temperature molten salts?', *Acc. Chem. Res.*, vol. 40, no. 11, pp. 1106–1113, 2007.

[169]   A. P. Abbott, G. Capper, D. L. Davies, R. K. Rasheed, and V. Tambyrajah, 'Novel ambient temperature ionic liquids for zinc and zinc alloy electrodeposition', *Trans. IMF*, vol. 79, no. 6, pp. 204–206, 2001.

[170]   S. Z. El Abedin, M. Pölleth, S. A. Meiss, J. Janek, and F. Endres, 'Ionic liquids as green electrolytes for the electrodeposition of nanomaterials', *Green Chem.*, vol. 9, no. 6, pp. 549–553, 2007.

[171]   R. D. Rogers, K. R. Seddon, D. of I. and E. C. S. A. C. Society, and M. S. A. C. Society, *Ionic liquids as green solvents*. ACS Publications, 2003.

[172]   A. I. Wixtrom, J. E. Buhler, C. E. Reece, and T. M. Abdel-Fattah, 'Electrochemical Polishing Applications and EIS of a Novel Choline Chloride-Based Ionic Liquid', *ECS Trans.*, vol. 50, no. 11, pp. 199–202, Mar. 2013, doi: 10.1149/05011.0199ecst.

[173]   V. Rupp, 'Electropolishing of Niobium 6 GHz rf cavities in fluorine-free electrolyte', Master in surface treatments for industrial applications, Università degli Studi di Padova, 2009.

[174]   D. Rizzetto, 'Applicabilità dei Liquidi Ionici all'Elettropulitura del Niobio', Master degree, Università degli Studi di Padova, 2009.

[175]   V. Palmieri, V. Rampazzo, V. V. Rupp, and F. Stivanello, 'Niobium Electropolishing by Ionic Liquids'.

[176]   M. Ceccato, 'Elettropulitura del Niobio con Elettroliti a base di Liquidi Ionici', Master in surface treatments for industrial applications, Università degli studi di Padova, 2007.

[177]   G. Mondin, 'Utilizzo di Liquidi Ionici per l'Elettropulitura di cavità superconduttive in Niobio', Master degree, Università degli Studi di Padova, 2008.

[178]   V. Pastushenko, 'Industrial R&D on Innovative Surface Treatments for an Ecological Descaling of "Acciaierie Valbruna" Stainless Steel Wire Rods in Replacement of the Traditional Acid Etching', PhD Thesis, Università degli Studi di Ferrara, 2014. [Online]. Available: https://surfacetreatments.infn.it/industrial-rd-on-innovative-surface-

treatments-for-an-ecological-descaling-of-acciaierie-valbruna-stainless-steel-wire-rods-in-replacement-of-the-traditional-acid-etching-vlada/

[179] O. Malkova, 'Study of the Electropolishing of 6GHz Niobium cavity in ionic liquids', Master in surface treatments for industrial applications, Università degli Studi di Padova, 2013.

[180] A. Valente-Feliciano, 'Alternative processes for bulk Nb technology', presented at the USPAS - Rutgers, Jun. 2015. [Online]. Available: https://uspas.fnal.gov/materials/15Rutgers/AMVF_Alternative_Surface_Preparation.pdf

[181] N. Eliaz and O. Nissan, 'Innovative processes for electropolishing of medical devices made of stainless steels', *J. Biomed. Mater. Res. A*, vol. 83A, no. 2, pp. 546–557, Nov. 2007, doi: 10.1002/jbm.a.31429.

[182] E. J. Taylor, M. E. Inman, T. D. Hall, S. Snyder, A. Rowe, and D. Holmes, 'Economics of electropolishing niobium SRF cavities in eco-friendly aqueous electrolytes without hydrofluoric acid', *SRF2015 Whistler BC Can.*, p. 359, 2015.

[183] F. Furuta and G. Hoffstaetter, 'Electropolishing of Niobium SRF Cavities in Eco-Friendly Aqueous Electrolytes Without Hydrofluoric Acid', 2015.

[184] H. Tian *et al.*, 'New Progress with HF-free Chemical Finishing for Nb SRF Cavities', *Proc. 29textsuperscriptth Linear Accel. Conf*, vol. LINAC2018, p. 4 pages, 0.735 MB, 2018, doi: 10.18429/JACOW-LINAC2018-TUPO043.

[185] 'A Pulse/Pulse Reverse Electrolytic Approach to Electropolishing and Through-Mask Electroetching'. https://www.pfonline.com/articles/a-pulsepulse-reverse-electrolytic-approach-to-electropolishing-and-through-mask-electroetching (accessed Nov. 16, 2022).

[186] H. Tian, M. Lester, J. Musson, L. Phillips, C. Reece, and C. Seaton, 'Commissioning of JLab Vertical Cavity Processing System for SRF Nb Single Cell and Multicell Cavity With HF-Free Pulse-Reverse Electopolishing', *Proc. 9th Int Part. Accel. Conf*, vol. IPAC2018, p. 4 pages, 1.449 MB, 2018, doi: 10.18429/JACOW-IPAC2018-THPAL143.

[187] G. Hinds, F. E. Spada, J. M. D. Coey, T. R. Ní Mhíocháin, and M. E. G. Lyons, 'Magnetic field effects on copper electrolysis', *J. Phys. Chem. B*, vol. 105, no. 39, pp. 9487–9502, 2001.

[188] R. Rokicki, 'Apparatus and method for enhancing electropolishing utilizing magnetic fields', US7632390B2, Dec. 15, 2009 Accessed: Nov. 16, 2022. [Online]. Available: https://patents.google.com/patent/US7632390B2/

[189] T. Hryniewicz, 'On discrepancies between theory and practice of electropolishing', *Mater. Chem. Phys.*, vol. 15, no. 2, pp. 139–154, Aug. 1986, doi: 10.1016/0254-0584(86)90119-7.

[190] T. Hryniewicz, 'Concept of microsmoothing in the electropolishing process', *Surf. Coat. Technol.*, vol. 64, no. 2, pp. 75–80, May 1994, doi: 10.1016/S0257-8972(09)90006-8.

[191] R. Rokicki and T. Hryniewicz, 'Enhanced oxidation–dissolution theory of electropolishing', *Trans. IMF*, vol. 90, no. 4, pp. 188–196, 2012.

[192] T. Hryniewicz, 'Electropolishing processes for better implants' performance', *Biomed. J. Sci. Tech. Res.*, vol. 11, no. 1, pp. 8262–8266, 2018, doi: 10.26717/BJSTR.2018.11.002046.

[193] T. Hryniewicz, K. Rokosz, and R. Rokick, 'Magnetoelectropolishing process improves characteristics of finished metal surfaces: Intensity of externally applied magnetic field, plus oxygen control, manipulates rate of dissolution in electropolishing.', *Met. Finish.*, vol. 104, no. 12, pp. 26–33, 2006.

[194] T. Hryniewicz, R. Rokicki, and K. Rokosz, 'Metal surface modification by magnetoelectropolishing', in *Proceeding of 16th International Metallurgical & Materials Conference METAL*, 2007, pp. 22–24.

[195] T. Hryniewicz, K. Rokosz, and M. Filippi, 'Biomaterial studies on AISI 316L stainless steel after magnetoelectropolishing', *Materials*, vol. 2, no. 1, pp. 129–145, 2009.

[196] T. Hryniewicz, K. Rokosz, and R. Rokicki, 'Electrochemical and XPS studies of AISI 316L stainless steel after electropolishing in a magnetic field', *Corros. Sci.*, vol. 50, no. 9, pp. 2676–2681, 2008.

[197] T. Hryniewicz and K. Rokosz, 'Analysis of XPS results of AISI 316L SS electropolished and magnetoelectropolished at varying conditions', *Surf. Coat. Technol.*, vol. 204, no. 16–17, pp. 2583–2592, 2010.

[198] T. Hryniewicz, K. Rokosz, J. Valíček, and R. Rokicki, 'Effect of magnetoelectropolishing on nanohardness and Young's modulus of titanium biomaterial', *Mater. Lett.*, vol. 83, pp. 69–72, 2012.

[199] T. Hryniewicz, R. Rokicki, and K. Rokosz, 'Corrosion and surface characterization of titanium biomaterial after magnetoelectropolishing', *Surf. Coat. Technol.*, vol. 203, no. 10–11, pp. 1508–1515, 2009.

[200] R. Rokicki, T. Hryniewicz, P. Konarski, and K. Rokosz, 'The alternative, novel technology for improvement of surface finish of SRF niobium cavities', *World Sci. News*, vol. 74, pp. 152–163, 2017.

[201] T. Hryniewicz, P. Konarski, and R. Rokicki, 'Hydrogen Reduction in MEP Niobium Studied by Secondary Ion Mass Spectrometry (SIMS)', *Metals*, vol. 7, no. 10, p. 442, Oct. 2017, doi: 10.3390/met7100442.

[202] H. Padamsee and J. Knobloch, 'The nature of field emission from microparticles and the ensuing voltage breakdown', in *AIP Conference Proceedings*, 1999, vol. 474, no. 1, pp. 212–248.

[203] P. Kneisel, 'Clean Work And Its Consequences - Contamination Control Considerations', in *SRF'85*, Geneva, Switzerland, 1985, p. 509. [Online]. Available: https://accelconf.web.cern.ch/srf84/papers/srf84-28.pdf

[204] D. Reschke, 'Cleanliness techniques', in *12th International Workshop on RF Superconductivity, Cornell, USA*, 2005.

[205] J. Kudlacek and P. Chabera, 'Advanced Technologies for Determination of Surface Cleanliness', *Technol. Eng.*, vol. 11, no. 1, pp. 16–19, Dec. 2014, doi: 10.2478/teen-2014-0003.

[206] B. Liu *et al.*, 'Nitrogen doping with dual-vacuum furnace at IHEP', *Nucl. Instrum. Methods Phys. Res. Sect. Accel. Spectrometers Detect. Assoc. Equip.*, vol. 993, p. 165080, 2021.

[207] E. M. Lechner, J. W. Angle, F. A. Stevie, M. J. Kelley, C. E. Reece, and A. D. Palczewski, 'RF surface resistance tuning of superconducting niobium via thermal diffusion of native oxide', *Appl. Phys. Lett.*, vol. 119, no. 8, p. 082601, Aug. 2021, doi: 10.1063/5.0059464.

[208] P. Dhakal, G. Ciovati, P. Kneisel, and G. R. Myneni, 'Enhancement in Quality Factor of SRF Niobium Cavities by Material Diffusion', *IEEE Trans. Appl. Supercond.*, vol. 25, no. 3, pp. 1–4, Jun. 2015, doi: 10.1109/TASC.2014.2359640.

[209] 'Meeting Medical Manufacturing's Tough Demands'. http://www.processcleaning.com/articles/meeting-medical-manufacturings-tough-demands (accessed Nov. 15, 2022).

[210] D. M. Turley and L. E. Samuels, 'The nature of mechanically polished surfaces of copper', *Metallography*, vol. 14, no. 4, pp. 275–294, 1981.

[211] D. Williams, *Guide to cleaner technologies: cleaning and degreasing process changes*. DIANE Publishing, 1994.

[212] P. Kneisel and B. Lewis, 'Advanced surface cleaning methods-three years of experience with high pressure ultrapure water rinsing of superconducting cavities', *Part Accel*, vol. 53, pp. 97–121, 1996.

[213] D. Sertore *et al.*, 'High pressure rinsing system studies', *Proc. SRF2007 Peking Univ. Beijing China*, 2007.

[214] Y. Jung, M. Joung, J. Lee, M. K. Lee, and J. Seo, 'High Pressure Rinsing for Niobium Superconducting Cavity', *Proc IPAC'16*, 2016.

[215] J. Mammosser, T. Rothgeb, T. Wang, and A. T. Wu, 'Investigation into the effectiveness of the JLab High Pressure Rinse system', in *Proceedings of the 2003 Particle Accelerator Conference*, 2003, vol. 2, pp. 1386–1388.

[216] I. Malloch, E. Metzgar, L. Popielarski, and S. Stanley, 'Design and Implementation of an Automated High-Pressure Water Rinse System for FRIB SRF Cavity Processing', *Proc. 28th Linear Accel. Conf*, vol. LINAC2016, p. 4 pages, 1.951 MB, 2017, doi: 10.18429/JACOW-LINAC2016-TUPRC024.

[217] S. Takano, S. Mitsunobu, Y. Morita, M. Nishiwaki, and A. Kabe, 'HORIZONTAL HIGH PRESSURE WATER RINSING FOR KEKB SUPERCONDUCTING CAVITY'.

[218] K. Nakanishi, K. Hirosawa, T. Kobayashi, and M. Nishiwaki, 'SRF System for KEKB and SuperKEKB', *Proc. 62th ICFA ABDW High Luminosity Circ. Ee- Collid.*, vol. eeFACT2018, p. 8 pages, 4.228 MB, 2019, doi: 10.18429/JACOW-EEFACT2018-WEYAA03.

[219] R. G. Poulsen, 'Plasma etching in integrated circuit manufacture—A review', *J. Vac. Sci. Technol.*, vol. 14, no. 1, pp. 266–274, 1977.

[220] J. H. Greiner, 'Josephson tunneling barriers by rf sputter etching in an oxygen plasma', *J. Appl. Phys.*, vol. 42, no. 12, pp. 5151–5155, 1971.

[221] M. Gurvitch, M. Washington, H. Huggins, and J. Rowell, 'Preparation and properties of Nb Josephson junctions with thin Al layers', *IEEE Trans. Magn.*, vol. 19, no. 3, pp. 791–794, 1983.

[222] A. Shoji, F. Shinoki, S. Kosaka, M. Aoyagi, and H. Hayakawa, 'New fabrication process for Josephson tunnel junctions with (niobium nitride, niobium) double-layered electrodes', *Appl. Phys. Lett.*, vol. 41, no. 11, pp. 1097–1099, 1982.

[223] M. Rašković, 'High Etching Rates of Niobium in Ar/Cl2 Microwave Discharge', presented at the 3rd International Workshop on Thin films and New Ideas for pushing the limits of RF Superconductivity, Jul. 24, 2008. [Online]. Available: https://www.jlab.org/conferences/tfsrf/Thursday/Th2_6-TFSRF%20presentation_M-Raskovic.pdf

[224] T. Zhu *et al.*, 'Applying the plasma physical sputtering process to SRF cavity treatment: Simulation and Experiment Study', *Appl. Surf. Sci.*, vol. 574, p. 151575, Feb. 2022, doi: 10.1016/j.apsusc.2021.151575.

[225] M. Rašković, S. Popović, J. Upadhyay, L. Vušković, L. Phillips, and A.-M. Valente-Feliciano, 'High etching rates of bulk Nb in Ar/Cl 2 microwave discharge', *J. Vac. Sci. Technol. Vac. Surf. Films*, vol. 27, no. 2, pp. 301–305, 2009.

[226] M. Rašković, J. Upadhyay, L. Vušković, S. Popović, A. M. Valente-Feliciano, and L. Phillips, 'Plasma treatment of bulk niobium surface for superconducting rf cavities: Optimization of the experimental conditions on flat samples', *Phys. Rev. Spec. Top.-Accel. Beams*, vol. 13, no. 11, p. 112001, 2010.

[227] J. Upadhyay *et al.*, 'Cryogenic rf test of the first SRF cavity etched in an rf Ar/Cl2 plasma', *AIP Adv.*, vol. 7, no. 12, p. 125016, 2017.

[228] J. Upadhyay, D. Im, S. Popović, A.-M. Valente-Feliciano, L. Phillips, and L. Vušković, 'Plasma processing of large curved surfaces for superconducting rf cavity modification', *Phys. Rev. Spec. Top.-Accel. Beams*, vol. 17, no. 12, p. 122001, 2014.

[229] J. Upadhyay, D. Im, S. Popović, A.-M. Valente-Feliciano, L. Phillips, and L. Vušković, 'Etching mechanism of niobium in coaxial Ar/Cl2 radio frequency plasma', *J. Appl. Phys.*, vol. 117, no. 11, p. 113301, 2015.

[230] J. Upadhyay *et al.*, 'Apparatus and method for plasma processing of SRF cavities', *Nucl. Instrum. Methods Phys. Res. Sect. Accel. Spectrometers Detect. Assoc. Equip.*, vol. 818, pp. 76–81, 2016.

[231] S. Belomestnykh, B. Giaccone, and P. Berrutti, 'Plasma processing at FNAL', presented at the TTC2022, 2022. [Online]. Available: https://www.ttc2022aomori.org/event/2/contributions/60/attachments/10/147/TTC2022_Plasma%20Processing%20at%20FNAL.pdf

[232] R. Ruber, T. Powers, T. Ganey, and N. Brock, 'Plasma Processing SRF Cavities at Jefferson Lab', presented at the TTC2022, Oct. 13, 2022.

[233] R. Poprawe, Ed., *Tailored Light 2*. Berlin, Heidelberg: Springer Berlin Heidelberg, 2011. doi: 10.1007/978-3-642-01237-2.

[234] E. Ukar, A. Lamikiz, L. L. de Lacalle, D. Del Pozo, and J. L. Arana, 'Laser polishing of tool steel with CO2 laser and high-power diode laser', *Int. J. Mach. Tools Manuf.*, vol. 50, no. 1, pp. 115–125, 2010.

[235] T. L. Perry, D. Werschmoeller, N. A. Duffie, X. Li, and F. E. Pfefferkorn, 'Examination of selective pulsed laser micropolishing on microfabricated nickel samples using spatial frequency analysis', *J. Manuf. Sci. Eng.*, vol. 131, no. 2, 2009.

[236] T. A. Mai and G. C. Lim, 'Micromelting and its effects on surface topography and properties in laser polishing of stainless steel', *J. Laser Appl.*, vol. 16, no. 4, pp. 221–228, 2004.

[237] M. Bereznai *et al.*, 'Surface modifications induced by ns and sub-ps excimer laser pulses on titanium implant material', *Biomaterials*, vol. 24, no. 23, pp. 4197–4203, 2003.

[238] L. Zhao, J. M. Klopf, C. E. Reece, and M. J. Kelley, 'Laser polishing for topography management of accelerator cavity surfaces: Laserpolieren als Topographiemanagement zur schnellen Herstellung von Oberflächen mit Mulden', *Mater. Werkst.*, vol. 46, no. 7, pp. 675–685, 2015.

[239] B. Rosa, P. Mognol, and J. Hascoët, 'Laser polishing of additive laser manufacturing surfaces', *J. Laser Appl.*, vol. 27, no. S2, p. S29102, Feb. 2015, doi: 10.2351/1.4906385.

[240] L. Zhao, J. M. Klopf, C. E. Reece, and M. J. Kelley, 'Parameter optimization for laser polishing of niobium for SRF applications', Thomas Jefferson National Accelerator Facility (TJNAF), Newport News, VA ..., 2013.

[241] V. Porshyn, P. Serbun, H. Bürger, S. Soykarci, and D. Lützenkirchen-Hecht, 'Laser treatment of niobium surfaces for SRF applications', in *Journal of Physics: Conference Series*, 2018, vol. 1067, no. 8, p. 082011.

[242] L. Zhao, 'Surface polishing of niobium for superconducting radio frequency (SRF) cavity application', 2015.

[243] R. Ries *et al.*, 'Improvement of the first flux entry field by laser post-treatment of the thin Nb film on Cu', *Supercond. Sci. Technol.*, vol. 34, no. 6, p. 065001, Jun. 2021, doi: 10.1088/1361-6668/abf54d.

[244] R. Ries, E. Seiler, F. Gömöry, A. Medvids, C. Pira, and O. B. Malyshev, 'Superconducting properties and surface roughness of thin Nb samples fabricated for SRF applications', in *Journal of Physics: Conference Series*, 2020, vol. 1559, no. 1, p. 012040.

[245] R. Ries *et al.*, 'Surface quality characterization of thin Nb films for superconducting radiofrequency cavities', *Supercond. Sci. Technol.*, vol. 35, no. 7, p. 075010, Jul. 2022, doi: 10.1088/1361-6668/ac7261.

[246] A. Medvids *et al.*, 'Improvement of Nb/Cu adhesion and increase of Nb crystal size by laser radiation', *Appl. Surf. Sci.*, vol. 525, p. 146528, Sep. 2020, doi: 10.1016/j.apsusc.2020.146528.

[247] C. Adolphsen *et al.*, 'European Strategy for Particle Physics -- Accelerator R&D Roadmap', p. 30MB, Mar. 2022, doi: 10.23731/CYRM-2022-001.

[248] P. N. Belkin, S. A. Kusmanov, and E. V. Parfenov, 'Mechanism and technological opportunity of plasma electrolytic polishing of metals and alloys surfaces', *Appl. Surf. Sci. Adv.*, vol. 1, p. 100016, Nov. 2020, doi: 10.1016/j.apsadv.2020.100016.

[249] K. Nestler, F. Böttger-Hiller, W. Adamitzki, G. Glowa, H. Zeidler, and A. Schubert, 'Plasma Electrolytic Polishing – An Overview of Applied Technologies and Current Challenges to Extend the Polishable Material Range', *Procedia CIRP*, vol. 42, pp. 503–507, 2016, doi: 10.1016/j.procir.2016.02.240.

[250] H. Tavakoli, S. M. Khoie, S. P. H. Marashi, and S. H. Mogadam, 'Characterization of submicron-size layer produced by pulsed bipolar plasma electrolytic carbonitriding', *J. Alloys Compd.*, vol. 583, pp. 382–389, 2014.

[251] D. L. Boguta, V. S. Rudnev, O. P. Terleeva, V. I. Belevantsev, and A. I. Slonova, 'Effect of ac Polarization on Characteristics of Coatings formed from Polyphosphate Electrolytes of Ni (II) and Zn (II)', *Russ. J. Appl. Chem.*, vol. 78, no. 2, pp. 247–253, 2005.

[252] Y. G. Ko, E. S. Lee, and D. H. Shin, 'Influence of voltage waveform on anodic film of AZ91 Mg alloy via plasma electrolytic oxidation: Microstructural characteristics and electrochemical responses', *J. Alloys Compd.*, vol. 586, pp. S357–S361, 2014.

[253] A. L. Yerokhin *et al.*, 'Oxide ceramic coatings on aluminium alloys produced by a pulsed bipolar plasma electrolytic oxidation process', *Surf. Coat. Technol.*, vol. 199, no. 2–3, pp. 150–157, 2005.

[254] V. Dehnavi, B. L. Luan, D. W. Shoesmith, X. Y. Liu, and S. Rohani, 'Effect of duty cycle and applied current frequency on plasma electrolytic oxidation (PEO) coating growth behavior', *Surf. Coat. Technol.*, vol. 226, pp. 100–107, 2013.

[255] I. Kulikov, S. Vaschenko, and A. Kamenev, *Электролитно-плазменная обработка материалов (Electrolyte-plasma treatment of materials)*. Litres, 2010.

[256] I. Danilov, M. Hackert-Oschätzchen, M. Zinecker, G. Meichsner, J. Edelmann, and A. Schubert, 'Process Understanding of Plasma Electrolytic Polishing through Multiphysics Simulation and Inline Metrology', *Micromachines*, vol. 10, no. 3, p. 214, Mar. 2019, doi: 10.3390/mi10030214.

[257] V. N. Duradji and I. V. Briantsev, 'Некоторые особенности нагрева металлов в электролитной плазме при анодном процессе (Some features of heating metals in an electrolyte plasma during the anodic process)', *Electron Obrab Mater*, no. 1, pp. 45–48, 1977.

[258] V. Duradji, 'Особенности установления электрогидродинамического режима, используемого для полирования металлов в электролитной плазме (Features of the establishment of the electrohydrodynamic regime used for polishing metals in electrolytic plasma)', *Metaloobrabotka*, no. 3 (75), pp. 35–39, 2013.

[259] V. N. Duradji and M. Dyblenko, 'Method of electrolite-plasma processing of metal surface.', RU2013129493A, Jan. 10, 2015 Accessed: Nov. 16, 2022. [Online]. Available: https://patents.google.com/patent/RU2013129493A/

[260] B. R. Lazarenko, V. N. Duradzhi, and I. V. Brjancev, 'O strukture i soprotivlenii pri jelektrodnoj zony pri nagreve metallov v jelektrolitnoj plazme', *Jelektronnaja Obrab. Mater.*, no. 2, pp. 50–55, 1980.

[261] J. Wang, X. Zong, J. Liu, and S. Feng, 'Influence of Voltage on Electrolysis and Plasma Polishing', in *Proceedings of the 2017 International Conference on Manufacturing Engineering and Intelligent Materials (ICMEIM 2017)*, Guangzhou, China, 2017. doi: 10.2991/icmeim-17.2017.3.

[262] J. Wang, L. C. Suo, L. L. Guan, and Y. L. Fu, 'Optimization of processing parameters for electrolysis and plasma polishing', in *Applied Mechanics and Materials*, 2012, vol. 217, pp. 1368–1371.

[263] Ding Z., 'Plasma electrolyte polishing process for precision structural parts of stainless steel', CN105220218A, Jan. 06, 2016 Accessed: Nov. 16, 2022. [Online]. Available: https://patents.google.com/patent/CN105220218A/

[264] V. K. Stanishevsky *et al.*, 'Method of electrochemical machining of articles made of conducting materials', US5028304A, Jul. 02, 1991 Accessed: Nov. 16, 2022. [Online]. Available: https://patents.google.com/patent/US5028304A/

[265] M. Dyblenko, 'Fabrication of reinforced layer on treaded surface of part from alloyed steels', RU2013138998A, Feb. 27, 2015 Accessed: Nov. 16, 2022. [Online]. Available: https://patents.google.com/patent/RU2013138998A/

[266] T. Ablyaz, K. Muratov, L. Ushomirskaya, D. Zarubin, and S. Sidhu, 'Electrolytic plasma polishing technique for improved surface finish of ED machined components', *Eng. Solid Mech.*, vol. 7, no. 2, pp. 131–136, 2019.

[267] V. Rakhcheev, A. Pashentsev, K. Lukjanov, and E. Rakhcheeva, 'Method of combined treatment of parts made from aluminum and its alloys.', RU2003134218A, May 10, 2005 Accessed: Nov. 16, 2022. [Online]. Available: https://patents.google.com/patent/RU2003134218A/

[268] V. N. Duradji, D. E. Kaputkin, and A. Y. Duradji, 'Aluminum Treatment in the Electrolytic Plasma During the Anodic Process.', *J. Eng. Sci. Technol. Rev.*, vol. 10, no. 3, 2017.

[269] K. Lingath, H. Zeidler, and A. Parshuta, 'Plasma polishing of objects made of titanium or titanium alloys comprises applying a voltage to the object positioned in a warm aqueous electrolyte solution, followed by processing using plasma polishing.', DE10207632A1, Sep. 11, 2003 Accessed: Nov. 16, 2022. [Online]. Available: https://patents.google.com/patent/DE10207632A1/

[270] P. Damir, 'Method of electrolytic-plasma grinding of parts from titanium and its alloys', RU2461667C1, Sep. 20, 2012 Accessed: Nov. 16, 2022. [Online]. Available: https://patents.google.com/patent/RU2461667C1/

[271] A. Smyslov, M. Smyslova, and A. Mingazhev, 'Method of electrolytic-plasma polishing of metals works.', RU2355829C2, May 20, 2009 Accessed: Nov. 16, 2022. [Online]. Available: https://patents.google.com/patent/RU2355829C2/

[272] A. Smyslov, V. Gordeev, and A. Ostatina, 'Method of multistage electrolyte-plasma polishing of products made of titanium and titanium alloys', RU2373306C2, Nov. 20, 2009 Accessed: Nov. 16, 2022. [Online]. Available: https://patents.google.com/patent/RU2373306C2/

[273] Y. Aliakseyeu, A. Bubulis, V. Minchenya, A. Korolyov, V. Niss, and R. Kandrotaitė Janutienė, 'Plasma Electrolyte Polishing of Titanium and Niobium Alloys in Low Concentrated Salt Solution Based Electrolyte', *Mechanics*, vol. 27, no. 1, pp. 88–93, Feb. 2021, doi: 10.5755/j02.mech.25044.

[274] M. K. Smyslova, D. R. Tamindarov, N. V. Plotnikov, I. M. Modina, and I. P. Semenova, 'Surface electrolytic-plasma polishing of Ti-6Al-4V alloy with ultrafine-grained structure produced by severe plastic deformation', *IOP Conf. Ser. Mater. Sci. Eng.*, vol. 461, p. 012079, Dec. 2018, doi: 10.1088/1757-899X/461/1/012079.

[275] R. A. Mirzoyev and M. I. Styrov, 'Process of electrochemical smoothing of metal articles.', RU2168565C1, Jun. 10, 2001 Accessed: Nov. 16, 2022. [Online]. Available: https://patents.google.com/patent/RU2168565C1/

[276] A. Mingazhev, 'Method of processing of turbomachine blades made of iron-chromium-nickel alloys', RU2649128C1, Mar. 29, 2018 Accessed: Nov. 16, 2022. [Online]. Available: https://patents.google.com/patent/RU2649128C1/

[277] S. Fecher, M. Haizmann, L. Volkl, and L. Weisensel, 'Process for the polishing of metallic dental prostheses', US8444914B2, May 21, 2013 Accessed: Nov. 16, 2022. [Online]. Available: https://patents.google.com/patent/US8444914B2/

[278] M. Polak, K.-D. Weltmann, R. IHRKE, M. Fröhlich, and A. Quade, 'Method for polishing conductive metal surfaces', WO2018019532A1, Feb. 01, 2018 Accessed: Nov. 16, 2022. [Online]. Available: https://patents.google.com/patent/WO2018019532A1/

[279] Zhang G., 'A surface polishing method for magnesium alloys.', CN101845662A, Sep. 29, 2010 Accessed: Nov. 16, 2022. [Online]. Available: https://patents.google.com/patent/CN101845662A/

[280] Wang C. and He X., 'An electrolyte and polishing method of amorphous alloy', CN108660504A, Oct. 16, 2018 Accessed: Nov. 16, 2022. [Online]. Available: https://patents.google.com/patent/CN108660504A/

[281] Cao C., 'Polishing solution used for amorphous alloy and polishing method of amorphous alloy', CN102453444A, May 16, 2012 Accessed: Nov. 16, 2022. [Online]. Available: https://patents.google.com/patent/CN102453444A

[282] N. Sluginov, 'On luminous phenomen, observed in liquids during electrolysis', *Russ Phys Chem Soc*, vol. 12, pp. 193–203, 1880.

[283] I. Z. Yasnogorodskiy, 'Heating of metals and alloys in electrolytes', FOREIGN TECHNOLOGY DIV WRIGHT-PATTERSON AFB OH, 1962.

[284] H. H. Kellogg, 'Anode effect in aqueous electrolysis', *J. Electrochem. Soc.*, vol. 97, no. 4, p. 133, 1950.

[285] E. V. Parfenov, A. Yerokhin, R. R. Nevyantseva, M. V. Gorbatkov, C.-J. Liang, and A. Matthews, 'Towards smart electrolytic plasma technologies: An overview of methodological approaches to process modelling', *Surf. Coat. Technol.*, vol. 269, pp. 2–22, May 2015, doi: 10.1016/j.surfcoat.2015.02.019.

[286] S. V. Gnedenkov *et al.*, 'PEO coatings obtained on an Mg–Mn type alloy under unipolar and bipolar modes in silicate-containing electrolytes', *Surf. Coat. Technol.*, vol. 204, no. 14, pp. 2316–2322, 2010.

[287] R. R. Nevyantseva, S. A. Gorbatkov, E. V. Parfenov, and A. A. Bybin, 'The influence of vapor–gaseous envelope behavior on plasma electrolytic coating removal', *Surf. Coat. Technol.*, vol. 148, no. 1, pp. 30–37, 2001.

[288] Y. N. Tyurin and A. D. Pogrebnjak, 'Electric heating using a liquid electrode', *Surf. Coat. Technol.*, vol. 142, pp. 293–299, 2001.

[289] P. Gupta, G. Tenhundfeld, E. O. Daigle, and D. Ryabkov, 'Electrolytic plasma technology: Science and engineering—An overview', *Surf. Coat. Technol.*, vol. 201, no. 21, pp. 8746–8760, Aug. 2007, doi: 10.1016/j.surfcoat.2006.11.023.

[290] O. V. Kalenchukova, P. K. Nagula, and D. L. Tretinnikov, 'About changes in the chemical composition of the electrolyte in the process of electrolytic-plasma treatment of materials', *Mater Methods Technol*, vol. 9, pp. 404–413, 2015.

[291] V. R. Mukaeva, 'Управление Технологическим Процессом Электролитно-плазменного Полирования на Основе Контроля Шероховатости пов. по Импедансным Спектрам (Management of Processing Procedure of Electrolytic-Plasma Polishing on the Base of Control of Surface Roughness by Impedance Spectra)', Ph.D. Thesis, Ufa State Aviation Technical University, 2014.

[292] J. G. Alexeev, A. A. Kosobutskij, A. J. Korolev, V. S. Niss, V. D. Kucheijavyj, and A. A. Povzhik, 'PECULIARITIES OF THE PROCESSES OF THE METAL ARTICLES DIMENSIONAL PROCESSING BY ELECTROLIT-PLASMA WAY', *Litiyo i Metallurgiya*, no. 4, pp. 188–195, 2005.

[293] N. V. Plotnikov, 'On the question of the model for electrolytic-plasma polishing surface', *Ufa USATU*, vol. 17, no. 4 (57), pp. 90–95, 2013.

[294] D. Vana, S. Podhorsky, M. Hurajt, and V. Hanzen, 'Surface properties of the stainless steel X10 CrNi 18/10 after aplication of plasma polishing in electrolyte', *Int J Mod Eng Res*, vol. 3, pp. 788–792, 2013.

[295] A. L. Yerokhin, X. Nie, A. Leyland, A. Matthews, and S. J. Dowey, 'Plasma electrolysis for surface engineering', *Surf. Coat. Technol.*, vol. 122, no. 2–3, pp. 73–93, Dec. 1999, doi: 10.1016/S0257-8972(99)00441-7.

[296] D. I. Slovetskii, S. D. Terent'ev, and V. G. Plekhanov, 'The Mechanism of Plasma--Electrolytic Heating of Metals', *Teplofiz Vys Temp*, vol. 24, no. 2, pp. 353–363, 1986.

[297] Yu. V. Sinkevitch, 'Conceptual model of commutation mechanism for electric conductivity of vapor-gas envelope in electro-impulse polishing mode', *Sci. Tech.*, vol. 15, no. 5, pp. 407–414, Jan. 2016, doi: 10.21122/2227-1031-2016-15-5-407-414.

[298] Yu. V. Sinkevich, *Электроимпульсное полирование сплавов на основе железа, хрома и никеля (Electropulse Polishing of Alloys Based on Iron, Chromium and Nickel)*. BNTU, 2014. [Online]. Available: https://rep.bntu.by/handle/data/10963

[299] V. N. Duradji and D. E. Kaputkin, 'Metal Surface Treatment in Electrolyte Plasma during Anodic Process', *J. Electrochem. Soc.*, vol. 163, no. 3, pp. E43–E48, 2016, doi: 10.1149/2.0011603jes.

[300] V. N. Duradji, D. E. Kaputkin, and A. Y. Duradji, 'Electrolyte-Plasma Modification of Surface of Ti-Based Alloy during Electrohydrodynamic Mode of Anodic Process', *J. Electrochem. Soc.*, vol. 164, no. 9, pp. E226–E232, 2017, doi: 10.1149/2.0451709jes.

[301] P. S. Gordienko, E. S. Panin, A. V. Dostovalov, and V. K. Usol'Tsev, 'Voltammetric characteristics of the metal-oxide-electrolyte system at electrode polarization with pulse voltage', *Prot. Met. Phys. Chem. Surf.*, vol. 45, no. 4, pp. 487–493, 2009.

[302] J. W. Schultze and M. M. Lohrengel, 'Stability, reactivity and breakdown of passive films. Problems of recent and future research', *Electrochimica Acta*, vol. 45, no. 15–16, pp. 2499–2513, 2000.

[303] S. A. Kusmanov, I. G. Dyakov, P. N. Belkin, L. A. Gracheva, and V. S. Belkin, 'Plasma electrolytic modification of the VT1-0 titanium alloy surface', *J. Surf. Investig. X-Ray Synchrotron Neutron Tech.*, vol. 9, no. 1, pp. 98–104, Jan. 2015, doi: 10.1134/S1027451015010139.

[304] M. M. Lohrengel, 'Thin anodic oxide layers on aluminium and other valve metals: high field regime', *Mater. Sci. Eng. R Rep.*, vol. 11, no. 6, pp. 243–294, 1993.

[305] A. Smyslov and M. Smyslova, 'Многоэтапная электролитно-плазменная обработка изделий из титана и титановых сплавов', *J. Ufa State Aviat. Tech. Univ.*, vol. 13, no. 1, pp. 141–145, 2009.

[306] D. A. Dobrynin, 'Electrolytic-plasma polishing of titanium alloys VT6 and VT8M-1', *Proc. VIAM*, no. 7, pp. 2–2, Jul. 2017, doi: 10.18577/2307-6046-2017-0-7-2-2.

[307] J. Wang, L. C. Suo, L. L. Guan, and Y. L. Fu, 'Analytical Study on Mechanism of Electrolysis and Plasma Polishing', *Adv. Mater. Res.*, vol. 472–475, pp. 350–353, Feb. 2012, doi: 10.4028/www.scientific.net/AMR.472-475.350.

[308] M. Cornelsen, C. Deutsch, and H. Seitz, 'Electrolytic Plasma Polishing of Pipe Inner Surfaces', *Metals*, vol. 8, no. 1, p. 12, Dec. 2017, doi: 10.3390/met8010012.

[309] Z. Xiang, C. Nie, and J. Hou, 'A Chemical Polish-etching of Optics Suface Based on the Marangoni Interface Effect', *J. Optoelectron. Laser*, vol. 18, no. 10, p. 1158, 2007.

[310] A. P. Volenko and O. V. Boychenko, 'Electrolyte-plasma treatment of metals', *Vector Nauki TGU*, no. 4, pp. 144–147, 2012.

[311] J. Wang, L. Suo, Y. Fu, and L. Guan, 'Study on material removal rate of electrolysis and plasma polishing', in *2012 IEEE International Conference on Information and Automation*, 2012, pp. 917–922.

[312] E. V. Parfenov and A. L. Erochin, 'Управление электролитноплазменными и электрохимическими технологическими процессами на основе контроля состояния объекта методом импедансной спектроскопии (Control of electrolytic-plasma and electrochemical processes based on control of condition of object by impedance spectroscopy)', presented at the XII ALL-RUSSIAN MEETING ON THE PROBLEMS OF MANAGEMENT OF THE 2014 VSPU, 2014, pp. 4348–4359. [Online]. Available: https://elibrary.ru/item.asp?id=22224568

[313] E. V. Parfenov, R. G. Farrakhov, V. R. Mukaeva, A. V. Gusarov, R. R. Nevyantseva, and A. Yerokhin, 'Electric field effect on surface layer removal during electrolytic plasma polishing', *Surf. Coat. Technol.*, vol. 307, pp. 1329–1340, Dec. 2016, doi: 10.1016/j.surfcoat.2016.08.066.

[314] N. P. Ivanova and Yu. V. Sinkevich, 'Механизм анодного растворения коррозионностойких и конструкц. углерод. сталей в условиях электроимпульсного полирования (The mechanism of anodic dissolution of corrosion-resistant and structural carbon steels under conditions of electropulse polishing)', *Nauka teh.*, 2013, [Online]. Available: https://cyberleninka.ru/article/n/mehanizm-anodnogo-rastvoreniya-korrozionnostoykih-i-konstruktsionnyh-uglerodistyh-staley-v-usloviyah-elektroimpulsnogo-polirovaniya

[315]   N. P. Ivanova and Yu. V. Sinkevich, 'Исследование морфологии и химического состава электроимпульсно полированной поверхности углеродистых и коррозионностойких сталей (Study of the morphology and chemical composition of electropulse polished surface of carbon and corrosion-resistant steels)', *Nauka teh.*, 2012, [Online]. Available: https://cyberleninka.ru/article/n/issledovanie-morfologii-i-himicheskogo-sostava-elektroimpulsno-polirovannoy-poverhnosti-uglerodistyh-i-korrozionnostoykih-staley

[316]   O. Kröning, H.-P. Schulze, C. Kranhold, M. Herzig, and H. Zeidler, 'Investigation of the ignition phase in electrolytic plasma polishing under different starting conditions', *Procedia CIRP*, vol. 95, pp. 993–998, 2020, doi: 10.1016/j.procir.2020.02.287.

[317]   C. Kranhold, O. Kröning, H.-P. Schulze, M. Herzig, and H. Zeidler, 'Investigation of stable boundary conditions for the Jet-electrolytic Plasma Polishing (Jet-ePP)', *Procedia CIRP*, vol. 95, pp. 987–992, 2020, doi: 10.1016/j.procir.2020.02.294.

[318]   Yumpu.com, 'Dektak 8 Advanced Development Profiler Manual', *yumpu.com*. https://www.yumpu.com/en/document/view/16730205/dektak-8-advanced-development-profiler-manual (accessed Nov. 15, 2022).

[319]   'Energy-dispersive X-ray spectroscopy', *Wikipedia*. Jul. 04, 2022. Accessed: Dec. 21, 2022. [Online]. Available: https://en.wikipedia.org/w/index.php?title=Energy-dispersive_X-ray_spectroscopy&oldid=1096403275

[320]   V. Palmieri and V. Rampazzo, 'Automated electropolishing', CARE, 2007.

[321]   E. Chyhyrynets, 'Chemical and electrochemical treatments for accelerating cavities', Master in surface treatments for industrial applications, Università degli Studi di Padova, 2017. [Online]. Available: https://surfacetreatments.infn.it/chemical-and-electrochemical-treatments-for-accelerating-cavities-master-thesis-eduard-chyhyrynets/

[322]   E. Chyhyrynets, 'Chemical and Electrochemical Treatment of Copper coating for Particle Accelerators', Master degree, National Technical University of Ukraine "Igor Sikorsky Kyiv Polytechnic Institute", 2018.

[323]   'italvibrasusa – italvibrasusa'. https://www.italvibrasusa.com/ (accessed Nov. 20, 2022).

[324]   'Technical data and guidelines for the choice'. https://www.elesa.com/en/CatalogoDatiTecniciCA/technical-data-and-guidelines-for-the-choice (accessed Nov. 20, 2022).

[325]   J. Domblesky, R. Evans, and V. Cariapa, 'Material removal model for vibratory finishing', *Int. J. Prod. Res.*, vol. 42, no. 5, pp. 1029–1041, 2004.

[326]   C. Pira, E. Chyhyrynets, and F. Stivanello, 'Green processing of cavities via vibro-tumbling', presented at the TTC 2019, Vancouver, Canada, Feb. 06, 2019. [Online]. Available: https://indico.desy.de/event/21337/contributions/42684/

[327]   I. A. Kostogrud, E. V. Boyko, P. E. Matochkin, and D. V. Sorokin, 'Comparing the methods of copper substrate polishing for CVD graphene synthesis', *J. Phys. Conf. Ser.*, vol. 2057, no. 1, p. 012121, Oct. 2021, doi: 10.1088/1742-6596/2057/1/012121.

[328]   A. Mayorov and A. Berkovich, 'Plasma-electrolytic polishing of metals products', US20100200424A1, Aug. 12, 2010 Accessed: Nov. 16, 2022. [Online]. Available: https://patents.google.com/patent/US20100200424A1

[329]   S. I. Bagaev and I. A. Kapustin, 'Method of plasma electrolyte   surface polishing of copper and/or copper alloys', BY11410, Dec. 30, 2008 [Online]. Available: https://bypatents.com/4-11410-sposob-plazmenno-elektrolitnogo-polirovaniya-poverhnosti-izdeliya-iz-medi-i-ili-ee-splavov.html

[330]   N. A. Amirkhanova, V. A. Belonogov, and G. U. Belonogova, 'Method of polishing copper and copper-base alloys', RU2127334C1, Mar. 10, 1999 Accessed: Nov. 16, 2022. [Online]. Available: https://patents.google.com/patent/RU2127334C1

[331]   V. K. Stanishevsky, A. E. Parshuto, and A. A. Kosobutsky, 'Electrochemical treatment method', a.c. 1314729 A1, May 27, 1985

[332]   V. L. Ermakov, L. A. Klimova, I. S. Kulikov, and Kamenev A.Y., 'Method for the electrochemical treatment of metal products, mainly copper and copper alloys, for electroplating', BY842413C1, Aug. 30, 2006 [Online]. Available:

https://bypatents.com/5-8424-sposob-elektrohimicheskojj-obrabotki-metallicheskih-izdelijj-preimushhestvenno-iz-medi-i-mednyh-splavov-pod-galvanicheskie-pokrytiya.html

[333] V. N. Duradji and D. E. Kaputkin, 'Method of electrolite-plasma processing of metal surface', RU2013129493A, Jan. 10, 2015 Accessed: Nov. 16, 2022. [Online]. Available: https://patents.google.com/patent/RU2013129493A/en

[334] E. Chyhyrynets, F. Stivanello, C. Pira, G. Keppel, and O. Azzolini, 'Soluzione chimica contenente acido solfammico e perossido di idrogeno adatta alla lucidatura del rame e delle sue leghe mediante elettrolucidatura al plasma (Chemical solution containing sulfamic acid and hydrogen peroxide suitable for polishing copper and its alloys by plasma electrolytic polishing)' , n° 102023000004173, 07/03/2023.

[335] E. Chyhyrynets, F. Stivanello, C. Pira, G. Keppel, and O. Azzolini, 'Soluzione chimica contenente fosforo adatta alla lucidatura del rame e delle sue leghe mediante elettrolucidatura al plasma (Chemical solution containing phosphates suitable for polishing copper and its alloys by plasma electrolytic polishing)', n° 102023000001221, 27/01/2023.

[336] Yu. G. Aliakseyeu, A. Yu. Korolyov, V. S. Niss, A. E. Parshuto, and A. S. Budnitskiy, 'ELECTROLYTE-PLASMA POLISHING OF TITANIUM AND NIOBIUM ALLOYS', *Sci. Tech.*, vol. 17, no. 3, pp. 211–219, May 2018, doi: 10.21122/2227-1031-2018-17-3-211-219.

[337] E. Chyhyrynets, F. Stivanello, C. Pira, G. Keppel, and O. Azzolini, 'Soluzione chimica adatta alla lucidatura del niobio e delle sue leghe mediante elettrolucidatura al plasma (Chemical solution suitable for polishing niobium and its alloys by plasma electrolytic polishing)', n° 102022000009899, 13/05/2022.

[338] E. Chyhyrynets *et al.*, 'Application of Plasma Electrolytic Polishing onto SRF Substrates', *Proc. 20th Int. Conf. RF Supercond.*, vol. SRF2021, p. 5 pages, 0.947 MB, 2022, doi: 10.18429/JACOW-SRF2021-SUPTEV002.

[339] E. Chyhyrynets, 'Recent advancements on Nb Plasma Electrolytic Polishing', presented at the The 10th International Workshop on 'Thin films and New Ideas for Pushing the Limits of RF Superconducting', Newport News, USA, Sep. 21, 2022. [Online]. Available: https://indico.jlab.org/event/535/timetable/?layout=room#4-recent-advancements-on-plasm

[340] 'About ARIES | ARIES'. https://aries.web.cern.ch/about-aries (accessed Jan. 01, 2023).

[341] 'About I.FAST | IFAST'. https://ifast-project.eu/about (accessed Jan. 01, 2023).

[342] O. Kugeler *et al.*, 'Evaluation of system 3 and SIS', CERN, DELIVERABLE: D15.3 ARIES-D15.3, Jun. 2020. [Online]. Available: https://edms.cern.ch/document/1820619/1.0

[343] E. Chyhyrynets *et al.*, 'Cu/Nb QPR Surface Preparation Protocol in the Framework of ARIES Project', *Proc. 20th Int. Conf. RF Supercond.*, vol. SRF2021, p. 3 pages, 0.638 MB, 2022, doi: 10.18429/JACOW-SRF2021-SUPTEV003.

List of figures

217

List of tables